NOVEL ANTIANGIOGENIC PEPTIDE TARGETED THERAPEUTIC NANOSYSTEM FOR NON-SMALL-CELL LUNG CARCINOMA

LINDOKUHLE MALIBONGWE NGEMA

A thesis submitted to the Faculty of Health Sciences, University of the Witwatersrand, in fulfilment of the requirements for the degree of
Doctor of Philosophy

Supervisors
Professor Yahya Essop Choonara
Associate Professor Thashree Marimuthu
Dr. Samson Adebawole Adeyemi

Department of Pharmacy and Pharmacology, Faculty of Health Sciences, University of the Witwatersrand, South Africa

Johannesburg
2023

DECLARATION

I, Lindokuhle Malibongwe Ngema, declare that this thesis is my own work. It has been submitted for the degree of Doctor of Philosophy in the Faculty of Health Sciences at the University of the Witwatersrand, Johannesburg. It has not been submitted before for any degree or examination at this or any other university.

Signed this 25th day of October 2023

ANIMAL ETHICS DECLARATION

I, Lindokuhle Malibongwe Ngema, hereby confirm that the study entitled “Novel Drug-Loaded Conjugated Linoleic Acid (CLA) Targeted Theragnostic Nanosystem for Non-Small-Cell Lung Carcinoma Treatment in the MF1-nu/nu Nude Mice Model” was approved by the Animal Ethics Screening Committee (AESC) of the University of the Witwatersrand with Ethics Clearance Number 2020/11/01/B.

Appendix B

PUBLICATIONS

Review Article

1. A Review on Engineered Magnetic Nanoparticles in Non-Small-Cell Lung Carcinoma Targeted Therapy. Lindokuhle M. Ngema, Samson A. Adeyemi, Thashree Marimuthu and Yahya E. Choonara. *International Journal of Pharmaceutics*, 606, 120870, 2021. Impact factor: 6.5

Appendix C1

Research Articles

2. Synthesis of Novel Conjugated Linoleic Acid (CLA)-Coated Superparamagnetic Iron Oxide Nanoparticles (SPIONs) for the Delivery of Paclitaxel with Enhanced *In Vitro* Anti-Proliferative Activity on A549 Lung Cancer Cells. Lindokuhle M. Ngema, Samson A. Adeyemi, Thashree Marimuthu, Philemon Ubanako, Daniel Wamwangi and Yahya E. Choonara. *Pharmaceutics*, 14, 8219, 2022. Impact factor: 5.4

Appendix C2

3. Surface Immobilization of Anti-VEGF Peptide on SPIONs for Anti-Angiogenic and Targeted Delivery of Paclitaxel in Non-Small-Cell Lung Carcinoma. Lindokuhle M. Ngema, Samson A. Adeyemi, Thashree Marimuthu, Philemon Ubanako, Wilfred Ngwa and Yahya E. Choonara. *ACS Applied Bio Materials*, 6, 2747, 2023. Impact factor: 4.7

Appendix C3

4. Short Anti-Angiogenic MMP-2 Peptide Decorated Nanoparticles for Targeted Paclitaxel Delivery in an A549 Cell Xenograft Mouse Tumor Model. Lindokuhle M. Ngema, Samson A. Adeyemi, Thashree Marimuthu, Philemon Ubanako, Wilfred Ngwa and Yahya E. Choonara. *Submitted for review: ACS Applied Nano Materials*

Appendix C4

RESEARCH OUTPUTS

Podium Presentations

1. Synthesis of Novel CLA-Coated SPIONs for the Delivery of Paclitaxel with Enhanced *In Vitro* Anti-Proliferative Activity on A549 Lung Cancer Cells. Lindokuhle M. Ngema, Samson A. Adeyemi, Philemon Ubanako, Thashree Marimuthu, and Yahya E. Choonara. *Annual Young Scientists Conference 2023*. University of Venda, Thohoyandou, South Africa, June 12 – 13, 2023.

   Appendix D1

2. Synthesis of Novel Conjugated Linoleic Acid (CLA)-Coated Superparamagnetic Iron Oxide Nanoparticles (SPIONs) for the Delivery of Paclitaxel with Enhanced *In Vitro* Anti-Proliferative Activity on A549 Lung Cancer Cells. Lindokuhle M. Ngema, Samson A. Adeyemi, Thashree Marimuthu, Philemon Ubanako, Daniel Wamwangi and Yahya E. Choonara. *13th WITS Cross Faculty Postgraduate Symposium*, University of the Witwatersrand, Johannesburg, South Africa, July 11 – 13, 2022.

   Appendix D2

3. Novel Conjugated Linoleic Acid (CLA)-Coated Superparamagnetic Iron Oxide Nanoparticles (SPIONs) for the Delivery of Paclitaxel with Superlative Anti-Proliferative Activity in Non-Small-Cell Lung Carcinoma. Lindokuhle M. Ngema, Samson A. Adeyemi, Thashree Marimuthu, Philemon Ubanako, Daniel Wamwangi and Yahya E. Choonara. *4th International Conference on Nanomedicine and Drug Delivery*. Virtual, June 06 – 07, 2022.

   Appendix D3

Poster Presentation

4. Enhanced Conjugated Linoleic Acid Paclitaxel-Loaded Superparamagnetic Iron Oxide Nanoparticles for Anti-Proliferative Activity in Non-Small-Cell Lung Carcinoma. Lindokuhle M. Ngema, Samson A. Adeyemi, Philemon Ubanako, Thashree Marimuthu, and Yahya E. Choonara. *American Association of Pharmaceutical Sciences (AAPS) PharmSci360*. Boston Convention and Exhibition Center, Boston, MA, United States of America, October 16 – 19, 2022.

   Appendix D4

Research Accolades

1. Fulbright Foreign Student Program Scholarship 2022 – 2023; Johns Hopkins University, School of Medicine, USA.
2. 71st Lindau Nobel Laureate Meeting (Chemistry) Attendee; Germany, 2022.
3. Philip V. Tobias Educational Bursary, University of the Witwatersrand, 2022.
4. National Research Foundation (NRF) - German Academic Exchange Services/ Deutscher Akademischer Austausch Dienst (NRF-DAAD) Joint In-Country Doctoral Scholarship, 2020 – 2022.
5. University of the Witwatersrand PhD Postgraduate Merit Award (PMA), 2020 – 2022.

ABSTRACT

Lung cancer is the leading cause of cancer deaths globally, with nearly 1.8 million deaths and 2.2 million incidences recorded annually. Primarily, non-small-cell lung carcinoma (NSCLC) is the most commonly diagnosed type of lung cancer, which makes up approximately 85% of all reported lung cancer cases. Currently, the management of NSCLC is a global challenge, and although, various treatment protocols are available, such as surgery, radiotherapy, and chemotherapy, the survival outcomes remain poor. Combination chemotherapy is the current first-line treatment for NSCLC, however, it presents with a myriad of drawbacks, including non-specificity, high dosage, and detrimental side effects, resulting in patients intolerability to the regimen. Consequently, a new therapeutic approach is greatly needed and warrants the design of biocompatible targeted drug delivery nanosystems that can halt tumor proliferation and metastasis by targeting key molecules and deliver drugs directly to tumors, with limited side effects and toxicity to healthy cells. Tumor targeted drug delivery nanosystems such as magnetic nanoparticles (MNPs) modified with biomolecules and functionalized with homing peptides are of great interest for potential application as a potent nanomedicine in NSCLC management. Accordingly, the present study set to develop novel targeted paclitaxel (PTX) delivery nanosystems from the amenable superparamagnetic iron oxide nanoparticles (SPIONs) coated with *trans*-10,*cis*-12 conjugated linoleic acid (10E, 12Z) and functionalized with either a vascular endothelial growth factor receptor (VEGFR) binding or a matrix metalloproteinase 2 (MMP-2) binding peptide, for specific delivery of PTX to VEGFR and MMP-2 expressing NSCLC tumors. A preceding nanosystem without the peptides (CLA-coated PTX-SPIONs) was originally fabricated as proof of concept for the application of 10E, 12Z CLA as a surface coating and drug partitioning biomolecule. CLA-coated PTX-SPIONs exhibited a spherical shape, with an average particle size and zeta potential of 96.5 ± 0.6 nm and −27.3 ± 1.9 mV, respectively. The nanosystem had a drug loading efficiency of 98.5% and demonstrated a sustained site-specific *in vitro* release of PTX over 24 h (i.e., 94% at pH 6.8 mimicking the tumor microenvironment). Enhanced anti-proliferative activity was also observed with the CLA-coated PTX-SPIONs against a lung adenocarcinoma (A549) cell line after 72 h, with a recorded cell viability of 17.1%. Thereafter, the fabricated nanosystem was optimised for direct tumor-targeting by functionalization with HRH or CTT peptides, to give CLA-coated PTX-SPIONs@HRH and CLA-coated PTX-SPIONs@CTT. A new design methodology was established for the tandem surface functionalization of CLA-coated PTX-SPIONs with the antiangiogenic peptides, via coupling reactions. A series of robust nanotechnological techniques were employed for pertinent physicochemical characterization, *in vitro* evaluation of drug release, anti-proliferative activity, and quantification of VEGF-A and MMP-2 levels. Meanwhile, *in vivo* testing was carried out on a lung tumor xenograft mouse model. Both nanosystems exhibited a marked cellular uptake and internalization by A549 cells, and CLA-coated PTX-SPIONs@HRH significantly reduced secretion levels of VEGF-A in human dermal microvascular endothelial cells (HMEC-1) from 46.9 pg/mL to 35.6 pg/mL, meanwhile CLA-coated PTX-SPIONs@CTT significantly inhibited MMP-2 secretion by almost 70% , indicating specific anti-MMP-2 activity. A 76.6% and 69.7 % tumor regression was observed in a lung tumor xenograft mouse model treated with CLA-coated PTX-SPIONS@HRH and CLA-coated PTX-SPIONs@CTT, respectively, demonstrating tumor targetability and angiogenesis inhibition. Lastly, the pharmacokinetics (PK) evaluation revealed that both nanosystems prolonged the half-life of PTX and circulation time *in vivo*. In essence, potent antiangiogenic tumor-targeted PTX delivery nanosystems were successfully fabricated, and the obtained results suggest potential application of CLA-coated PTX-SPIONs@HRH and CLA-coated PTX-SPIONs@CTT for effective management of NSCLC.

ACKNOWLEDGEMENTS

First and foremost, I would like to thank God Almighty for giving me the strength and courage to make it this far.

My profound gratitude also goes to my selfless supervisors, Prof. Y.E Choonara, Prof. T. Marimuthu, and Dr. S.A Adeyemi for their guidance and unwavering support throughout this Doctoral program. I am eternally grateful and it has been an absolute honour to work with them.

A special “thank you” to all my colleagues at the Wits Advanced Drug Delivery Platform (WADDP) Research Unit, particularly Dr. Philemon Ubanako, Ms. Divesha Essa, Mr. Ahmed Abdelgadar, and Mr. Leon Joseph Khoza, as well as all the technical staff in the Department of Pharmacy and Pharmacology. Their contribution to the success of this study is highly appreciated. To Dr. Kimberly Jardine, Ms. Lorraine Matjila, Ms. Amelia Rammekwa, and Mr. Patrick Selahle of the Wits Research Animal Facility (WRAF), I express my sincere gratitude and appreciation for their assistance during animal experimentation.

I also extend gratitude and appreciation to the National Research Foundation (NRF) of South Africa and the University of the Witwatersrand (Postgraduate Financial Aid and Scholarships Administration) for financial assistance. I thank the U.S Embassy and Consulates in South Africa, and the Institute of International Education (IIE) for the Fulbright Foreign Exchange Program scholarship. My sincere gratitude goes to Prof. Wilfred Ngwa and all the members of the Biomaterial Drones and Immuno-Radiotherapy Group at the Sydney Kimmel Comprehensive Cancer Centre, Johns Hopkins Medicine, for welcoming and hosting me during my Fulbright Program period.

Lastly, I would like to thank my family and friends for their love and support throughout this long and challenging, but yet rewarding journey. May the God Almighty bless them all!

DEDICATION

This work is dedicated to my beloved late maternal grandparents; Mr. Sindangenkosi Mnguni and Mrs. Gugulina “MaZulu” Mnguni, and also to my dearest parents; Mr. Lucky Thulani Ngema and Mrs. Siziwe Happiness Ngema. All that I am and hope to be, I owe to them.

TABLE OF CONTENTS

CHAPTER 1

INTRODUCTION AND BACKGROUND

CHAPTER 2

A REVIEW ON ENGINEERED MAGNETIC NANOPARTICLES IN NON-SMALL-CELL LUNG CARCINOMA TARGETED THERAPY

CHAPTER 3

SYNTHESIS OF NOVEL CONJUGATED LINOLEIC ACID (CLA)-COATED SUPERPARAMAGNETIC IRON OXIDE NANOPARTICLES (SPIONs) FOR THE DELIVERY OF PACLITAXEL WITH ENHANCED *IN VITRO* ANTI-PROLIFERATIVE ACTIVITY ON A549 LUNG CANCER CELLS

CHAPTER 4

FORMULATION AND *IN VITRO* CHARACTERIZATION OF PACLITAXEL-LOADED SPIONs FUNCTIONALIZED WITH ANTI-VEGF PEPTIDE FOR INHIBITION OF ANGIOGENESIS IN NON-SMALL-CELL LUNG CARCINOMA

CHAPTER 5

A TARGETED ANTIANGIOGENIC PEPTIDE-FUNCTIONALIZED PACLITAXEL DELIVERY NANOVECTOR OF SPIONs AND CONJUGATED LINOLEIC ACID FOR SELECTIVE INHIBITION OF MMP-2 SECRETION *IN VITRO*

CHAPTER 6

IN VIVO EVALUATION OF NOVEL ANTIANGIOGENIC PEPTIDE-FUNCTIONALIZED PACLITAXEL DELIVERY NANOSYSTEMS ON A LUNG TUMOR XENOGRAFT MOUSE MODEL

CHAPTER 7

CONCLUSIONS AND RECOMMENDATIONS

CHAPTER 8

FULBRIGHT FOREIGN STUDENT PROGRAM EXPERIENCE

APPENDICES

LIST OF FIGURES

LIST OF TABLES

LIST OF EQUATIONS

LIST OF ABBREVIATIONS

10E,12Z	*trans*-10,*cis*-12
A549	Lung adenocarcinoma cell line
AE	Adsorption Efficiency
AREC	Animal Research Ethics Committee
CLA	Conjugated Linoleic Acid
CTT	CTTHWGFTLC
DAPI	4′,6-diamidino-2-phenylindole
DLC	Drug Loading Capacity
DMEM	Dulbecco's Modified Eagle Medium
DMF	Dimethylformamide
DMSA	*meso*-2,3-Dimercaptosuccinic acid
DTX	Docetaxel
EDC	1-ethyl-3(3-dimethylaminopropyl) carbodiimide
ELISA	Enzyme-Linked Immunosorbent Assay
FBS	Foetal Bovine Serum
FITC	Fluorescein 5(6)-isothiocyanate
FTIR	Fourier Transform Infrared
HMEC-1	Human dermal microvascular endothelial cell line
HPLC	High Pressure Liquid Chromatography
HRH	HRHTKQRHTALH
MMPs	Matrix Metalloproteinases
MNPs	Magnetic Nanoparticles
MTT	3-(4,5-dimethylthiazole-2-yl)-2,5-diphenyl tetrazolium bromide
NaOH	Sodium hydroxide
NHS	N-hydroxysuccinimide
NSCLC	Non-Small-Cell Lung Carcinoma
PBS	Phosphate Buffered Saline
PDI	Polydispersity Index
PK	Pharmacokinetics
Powder XRD	Powder X-Ray Diffraction
PTX	Paclitaxel
SPIONs	Superparamagnetic Iron Oxide Nanoparticles
SEM	Scanning Electron Microscope
TEM	Transmission Electron Microscope

TGI	Tumor Growth Inhibition
VEGF	Vascular Endothelial Growth Factor
VEGFRs	Vascular Endothelial Growth Factor Receptors
VSM	Vibrating Sample Magnetometer

CHAPTER 1

INTRODUCTION AND BACKGROUND

1.1. Background of the Study

Cancer is one of the major causes of death worldwide. According to the World Health Organisation (WHO), nearly 10 million deaths are attributed to cancer, annually (Chhikara and Parang, 2022; World Health Organization, 2022). It is reported that approximately 70% of global cancer deaths, and more than 60% of the cases occur in developing countries. Africa alone accounted for 22.4% deaths and 19.4% cases in 2020 (Sharma et al., 2022). Consequently, cancer is currently the fifth leading cause of death in Africa, and South Africa ranks third as the most cancer-burdened country in the continent, after Egypt and Nigeria (ranking first and second, respectively) (Bray et al., 2022; Sharma et al., 2022). As it stands, the trajectory of cancer incidences and deaths is estimated to rise rapidly in Africa, with projected estimates of 2.1 million cases and 1.4 million deaths in 2040 (Sharma et al., 2022). Meanwhile, globally, more than 26 million cancer cases and 17 million annual deaths are projected by 2030 (Siegel et al., 2021).

Lung cancer is the leading cause of cancer deaths globally and in Southern Africa (Ferlay et al., 2021). Nearly 1.8 million lung cancer deaths and 2.2 million incidences were recorded in 2020, with an estimated increase of up to 67% deaths and 64% incident cases by 2040, according to the recent GLOBACON reports (Sung et al., 2021; Zhou et al., 2022). The global incidence and mortality rates of lung cancer remain comparatively higher in men than in women. Accordingly, lung cancer is the main cause of cancer deaths amongst men in 93 countries, and the most diagnosed cancer in men in 36 countries (Sung et al., 2021). Smoking, exposure to asbestos, and air pollution remain primary risk factors for lung cancer, and with nearly two-thirds of global lung cancer deaths attributed to smoking, the WHO has called for the implementation of effective interventions to reduce the demand of tobacco (Klebe et al., 2020; Sung et al., 2021). Approximately, only 16% of lung cancer cases are diagnosed at an early stage, thus contributing to the poor five-year survival rate (18 – 22%) (Luo et al., 2019; Zhou et al., 2022).

Primarily, lung cancer is differentiated into two types, namely; small-cell lung carcinoma (SCLC) and non-small-cell lung carcinoma (NSCLC) (Zamay et al., 2017). NSCLC is the most commonly diagnosed type of lung cancer, which makes up approximately 85% of all reported lung cancer cases (Zhou et al., 2021), meanwhile SCLC is a poorly differentiated neuroendocrine carcinoma, responsible for almost 15% of all lung cancer cases (Raso et al., 2021). NSCLC is typically characterised as a biologically aggressive form of lung cancer with rapid proliferation and metastasis, and is further divided into three sub-types;

adenocarcinoma, squamous cell carcinoma, and large-cell carcinoma (Zappa and Mousa, 2016; Zhou et al., 2021). Currently, the management of NSCLC is a global challenge, and although, various treatment protocols are available, such as surgery, radiotherapy, and chemotherapy, the survival outcomes remain poor. Combination chemotherapy is the current first-line treatment for NSCLC, however, it presents with a myriad of drawbacks, including non-specificity, high dosage, and detrimental side effects, resulting in patients intolerability to the regimen (Kydd et al., 2017; Ye et al., 2021; Zhang et al., 2019).

Consequently, alternative effective treatment modalities, such as targeted nanomedicine, are needed and provide a great promise in circumventing the drawbacks presented by conventional combination chemotherapy in NSCLC management (García-Fernández et al., 2020; Haider et al., 2022). Essentially, targeted nanomedicine allows direct and sustained delivery of anticancer drugs to target tumors, while exhibiting great efficacy and limited undesired cytotoxicity (Haider et al., 2022). As such, the advent of nanotechnology and the application of nanoparticles (NPs) in the development of efficacious anticancer nano-based therapeutics has gained enormous attention in translational lung cancer research (Cheng et al., 2021; Mohtar et al., 2021). Accordingly, magnetic nanoparticles (MNPs), particularly superparamagnetic iron oxide nanoparticles (SPIONs) are amongst the most promising nanoparticulates with suitable biomedical application as vehicles for the targeted delivery of anticancer drugs in NSCLC targeted nanotherapy (Wu et al., 2022a; Zhi et al., 2020). SPIONs offer unique merits for application in targeted nanomedicine, such as smaller size (<100 nm), high drug-loading capacity, and a flexible and biocompatible outer-shell which allows desired modifications with polymers and targeting moieties, for active tumor targeting and drug delivery (Reczyńska et al., 2020; Zhi et al., 2020).

Nevertheless, as foreign entities, SPIONs may be recognized by the immune system, and induce different immunological effects (Zhi et al., 2020). As such, surface coating of SPIONs with biocompatible polymers is deemed vital for their application as drug delivery vehicles, as it offers immunological safety, remarkable bioavailability and minimal cytotoxicity, while enabling efficient drug loading (Akhtar et al., 2022; Reczyńska et al., 2020). A suitable polymer will facilitate controlled release of the drug and enhances circulation time and the probability of SPIONs permeation into tumors (Zhi et al., 2020). Polymers derived from natural agents that possess anticancer benefits and high affinity for hydrophobic anticancer drugs are ideal for surface-coating of SPIONs with potential application in NSCLC targeted nanotherapy. As such, conjugated linoleic acid (CLA) has been identified as a suitable polymer and a fitting partitioning agent for hydrophobic anticancer drugs, such as paclitaxel. CLA is a natural fatty acid with two biologically active isomers, namely; *trans*-10,*cis*-12 CLA (t10,c12 CLA or 10E,12Z CLA) and *cis*-9,*trans*-11 CLA (c9,t11 CLA or 9Z, 11E CLA), with proven anticancer

benefits, having shown to halt the growth of various cancer cells such as hepatic, breast, stomach, colon, prostate, and colorectal cancer (Dachev et al., 2021; den Hartigh, 2019; Flowers and Thompson, 2009; Moreira et al., 2019).

Although the two isomers of CLA had normally been used in combination (50:50) in the past, emerging evidence shows that 10E,12Z CLA is more potent than 9Z,11E CLA (Pierre et al., 2013; Shahzad et al., 2018). The potency of *trans*-10,*cis*-12 CLA makes it an interesting isomer to explore and exploit as a superlative coating agent for SPIONs in application as therapeutic carriers in NSCLC management. Essentially, 10E,12Z CLA possess a distinguished mechanism of action involving limiting the uptake of lipids in adipocytes by blocking the activities of lipoprotein lipase and stearoyl-CoA desaturase (Zhang et al., 2018). It is reported that only 10E,12Z CLA, and not 9Z,11E CLA, exhibited fat-reducing properties and could affect lipid metabolism in human liver cancer (HepG2) cells *in vitro* (Siwiec et al., 2019). Since cancer cells require high energy supply to grow, and abnormal levels of lipids have been implicated in tumor proliferation and metastasis (Long et al., 2018), affecting lipid metabolism pathways in tumors may provide means to halt proliferation and metastasis.

The identification and evaluation of various biological pathways involved in carcinogenesis and tumor proliferation and metastasis have been pivotal in the development of many FDA-approved (U.S Food and Drug Administration) anticancer therapeutics (Wu et al., 2022b; Zhong et al., 2021). Angiogenesis has been identified as one of the prominent tumorigenic pathways which enables tumor growth and metastasis in NSCLC (Choi et al., 2022; Hanahan, 2022). In essence, angiogenesis is an intricate process of formation of new blood vessels from the pre-existing vasculature, which supply tumors with oxygen and essential nutrients to grow and migrate to other parts of the body (Aspriţoiu et al., 2021). Angiogenesis biomarkers, such as vascular endothelial growth factor and its receptors (VEGF/VEGFRs), as well as matrix metalloproteinases (MMPs) are over-expressed by tumors, and have been identified as potential therapeutic targets in NSCLC management (Daum et al., 2021; Olejarz et al., 2020; Quintero-Fabián et al., 2019). VEGF is a key angiogenesis biomarker which plays a crucial role in activation of angiogenesis pathway through binding to VEGFRs, and signalling of various cellular pathways which lead to a rampant tumor growth (Daum et al., 2021). Meanwhile, MMPs, particularly MMP-2, is involved in the regulation of angiogenesis by controlling the degradation of extracellular matrix (ECM), thus allowing tumors to proliferate and initiate metastasis (Quintero-Fabián et al., 2019).

Several selective targeting modalities such as antibodies, aptamers, proteins, and peptides, are currently being explored as potential inhibitors of biomarkers associated with angiogenesis (Hu et al., 2022; Huang et al., 2022; Karami Fath et al., 2022; Razlansari et al., 2022).

Interestingly, peptides have exhibited excellent antiangiogenic activity on certain cancers (Adeyemi and Choonara, 2022; Karami Fath et al., 2022), and presumably hold great promise for application in NSCLC targeted nanotherapy for inhibition of tumor angiogenesis. Essentially, peptides present with distinct characteristics, such as high target specificity and membrane permeability, which impart enhanced therapeutic potency, over proteins and other small molecules (Adeyemi et al., 2019; Wang et al., 2022). Accordingly, the functionalization of drug delivery nanosystems with peptide ligands that specifically target VEGF/VEGFRs and MMP-2 could aid achieve tumor targetability and allow anticancer drugs to be delivered directly to tumors for effective therapeutic action, while inhibiting angiogenesis.

Two particular short peptides; HRH (HRHTKQRHTALH) and CTT (CTTHWGFTLC) are of considerable interest as homing peptides in the development of tumor targeted nanotherapeutics for NSCLC management. HRH peptide is a novel 12-amino acid peptide isolated from a 12-mer phage display, in 2017, and shown to specifically bind to VEGFR (Zhang et al., 2017). The peptide exhibited remarkable antiangiogenic efficacy both *in vitro* and *in vivo*, as it was found to inhibit the proliferation (<50%) of human umbilical vein endothelial cells (HUVEC) and abnormal vascular development in chick embryo and rat corneal models (Chen et al., 2021; Zhang et al., 2017). Consequently, HRH peptide has been pronounced as a promising anti-VEGF peptide for the development of potential targeted antiangiogenic therapeutics (Chen et al., 2021). Meanwhile, CTT peptide is a selective MMP-2 inhibitor identified from the screening of phage display peptide libraries (Koivunen et al., 1999). The peptide has a well-defined, saddle-shaped circular form, and has been shown to inhibit the migration of ovarian carcinoma, melanoma, and fibrosarcoma cell lines at significant levels (Ndinguri et al., 2012). Due to its MMP-2 inhibitory potential, CTT peptide could be employed to selectively target tumors, since MMP-2 is over-expressed in the tumor vasculature.

1.2. Rationale and Motivation for the Study

The non-targeted delivery of conventional NSCLC therapeutics remains a major challenge in the effective management of the disease (Haider et al., 2022; Ye et al., 2021). Although, combinational chemotherapy and radiotherapy had been prominent treatment options for NSCLC, the lack of target specificity has hindered their therapeutic efficacy, resulting in poor treatment outcomes (Ye et al., 2021). Combinational chemotherapy, as first-line treatment for NSCLC, is currently riddled with intolerable challenges including undesired cytotoxicity to healthy cells and non-specific binding of the drugs to proteins and other biomolecules, owing to non-targeted delivery (Chen et al., 2022; Haider et al., 2022). Consequently, there is a high demand for the development of alternative efficacious treatment approaches such as smart

drug delivery nanosystems, which are surface-engineered to recognize specific targets on NSCLC tumors, and directly deliver therapeutic payloads at tumor sites.

Currently, there is a growing interest in targeted nanotherapy as a potentially viable modality for the treatment of various cancers, including NSCLC (Mohtar et al., 2021; Raguraman et al., 2022). In essence, the formulation of tumor-targeted nanoparticles with the capability to carry anticancer drugs directly to tumors may provide an alternative modality for the management of primary and advanced metastatic NSCLC tumors, with excellent therapeutic efficacy and limited undesired cytotoxicity (Raguraman et al., 2022). The attractive physicochemical properties of nanoparticles, such as size, shape, composition, and stability impart a wide variety of advantages for application as effective drug delivery vehicles (Chandrakala et al., 2022; Joudeh and Linke, 2022). Moreover, nanoparticles may complement both passive and active targeting strategies for high accumulation in tumors (Joudeh and Linke, 2022).

The remarkable size (10 – 100 nm), superparamagnetism, high drug loading capacity, and biocompatibility are excellent properties that have given rise to the application of SPIONs as drug delivery vehicles in cancer (Reczyńska et al., 2020; Zhi et al., 2020). The flexibility of SPIONs to be surface-modified and functionalized with polymers and targeting ligands, make these nanoparticulates ideal for the present study. Likewise, the reported anticancer merits of 10E,12Z CLA and its hydrophobic nature makes the natural fatty acid a suitable polymer for loading of a hydrophobic anticancer drug of choice, paclitaxel (PTX) (Dachev et al., 2021; Shahzad et al., 2018). PTX is an antimitotic agent used in combinational chemotherapy for NSCLC management, however, its therapeutic efficacy is short-lived owing to rapid clearance, poor solubility, non-specific protein binding, and non-selective toxicity (Ma et al., 2021). Therefore, a delivery system for PTX is necessary in order to enhance the therapeutic action of the drug and limit its non-selective toxicity.

Angiogenesis has been reported as one of the hallmarks in cancer (Hanahan, 2022), and therefore, targeting angiogenesis biomarkers (i.e., VEGF/VEGFR and MMPs) is a promising approach in cancer nanomedicine (Choi et al., 2022). The inhibition of VEGF/VEGFR binding and MMP-2 activity using short antiangiogenic peptides is a prospective strategy in NSCLC management, as such, the use of HRH and CTT peptides as targeting ligands in the development of tumor-targeted PTX delivery nanonsystems could yield a potent nanomedicine for NSCLC, with excellent therapeutic efficacy. Essentially, the functionalization of PTX delivery nanosystem with HRH and CTT peptides (as shown in **Figure 1.1**) would revolutionize NSCLC treatment, providing a nanomedicine capable of enhancing anticancer activity (antimitotic action) of PTX, with reduced non-selective toxicity, while concurrently inhibiting angiogenesis.

① Synthesis of SPIONs via co-precipitation method

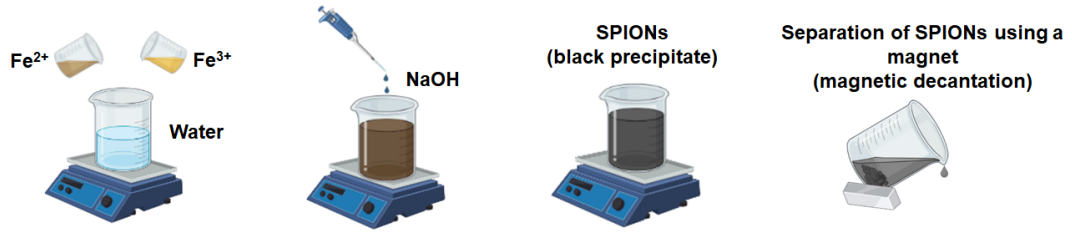

② Surface-coating of SPIONs with 10E,12Z CLA and PTX Loading

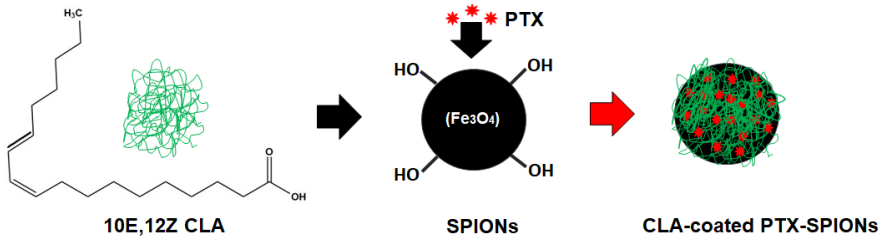

③ Surface-functionalization with HRH/CTT peptide

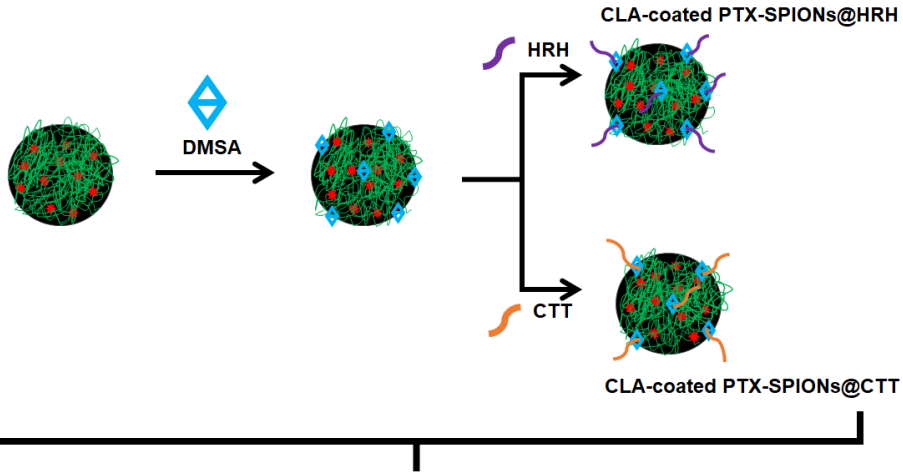

Physicochemical characterization

↓

***In vitro* analyses**

↓

***In vivo* antiangiogenic and antitumor analyses on a lung tumor xenograft mouse model**

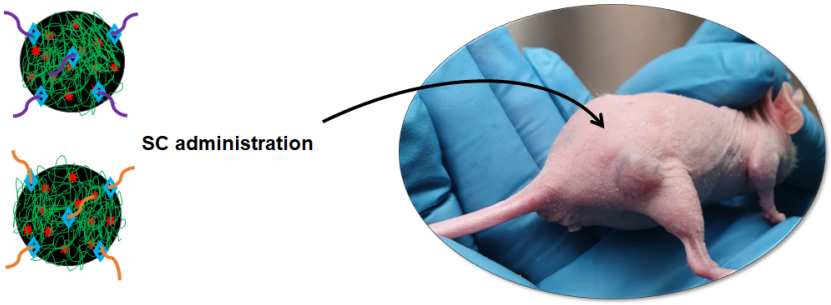

Figure 1.1. A schematic representation of the study design for the development of proposed novel peptide-functionalized, CLA-modified PTX-loaded SPIONs, as potential nanomedicine in NSCLC management.

1.3. Aim and Objectives

The aim of the study was to develop a novel targeted delivery nanosystem for PTX, employing SPIONs coated with 10E, 12Z CLA and functionalized with antiangiogenic peptides HRH or CTT, and carry out comprehensive *in vitro* and *in vivo* characterization. In order to achieve the aim, the following set objectives were carried out:

1. Fabricated 10E, 12Z CLA-coated SPIONs loaded with PTX, using co-precipitation, chemisorption, and self-assembly techniques, to serve as a novel PTX delivery vehicle.
2. Characterized the formulated PTX-loaded, 10E, 12Z-coated SPIONs for all pertinent physicochemical properties and evaluated *in vitro* anti-proliferative activity on lung adenocarcinoma cell line (A549) to establish a candidate formulation.
3. Surface-functionalized PTX-loaded, 10E, 12Z CLA-coated SPIONs with either HRH or CTT peptides to yield VEGFR and MMP-2 targeting nanosystems, respectively.
4. Characterized physicochemical properties and *in vitro* cellular behaviour of both peptide-functionalized nanosystems to examine their affinity and anti-proliferative activity on lung adenocarcinoma cells.
5. Assessed the secretion levels of VEGF-A and MMP-2 using ELISA, from endothelial cells treated with the nanosystems, in order to ascertain the targetability and antiangiogenic activity of the nanonosystems.
6. Evaluated *in vivo* tumor targetability and antitumor activity of both HRH and CTT-functionalized nanosystems on established lung tumor xenografts in Athymic nude mice to establish pre-clinical therapeutic efficacy.

1.4. Novelty of the Study

The following attributes signify the novelty of the study:

1. The study is the first to establish the application of 10E, 12Z CLA as an ideal partitioning agent for a hydrophobic anticancer drug, yielding PTX entrapment efficiency of 98.5%, while conferring additional anticancer benefits.
2. The study has evidently shown that a novel nanovector of SPIONs with 10E, 12Z CLA enhances the anticancer activity of PTX, and improves the drug's half-life *in vivo.*

3. The reported design and formulation of targeted drug delivery nanosystems using antiangiogenic peptides which exploit over-expressed angiogenesis biomarkers on tumors as targets to deliver PTX directly to tumors, and able to concurrently halt angiogenesis, is pioneering work in NSCLC management research.

1.5. Overview of the Thesis

The thesis is presented as multiple chapters, collated to provide a detailed comprehension of the design and development of the novel antiangiogenic anticancer drug delivery nanosystems for NSCLC management.

Chapter 1 gives a detailed introduction and background of the study, expounding on the rationale and motivation, aim and set objectives, as well as the perceived novelty of the study.

Chapter 2 explores the rationale behind the design and development of magnetic nanoparticles for application in targeted NSCLC therapy, and reviews the anticancer merits of CLA to provide concise insights and perspective into its possible application for the invention of surface-modified magnetic nanoparticles.

Chapter 3 describes the preliminary synthesis and pertinent characterization of a novel PTX delivery nanosystem comprising SPIONs and 10E, 12Z CLA. In this chapter, the evaluation of the physicochemical properties of the formulated nanosystem, including overall morphology, crystallinity, iron oxide core identity, CLA coating content, drug loading and release profile, as well as the overall magnetic behaviour, is discussed. Moreover the anti-proliferative activity of the nanosystem on A549 lung cancer cells is presented.

Chapter 4 details the fabrication of a targeted PTX delivery nanosystem functionalized with anti-VEGF peptide (HRH) for tumor vasculature targeting in NSCLC. In this chapter, a detailed fabrication methodology established to formulate a novel HRH-functionalized nanosystem that is safe by design, as well as the robust *in vitro* analyses carried out to ascertain the anticancer and antiangiogenic activity of the nanosystem, are described.

Chapter 5 details the fabrication and *in vitro* characterization of yet another potent targeted PTX delivery nanosystem functionalized with CTT peptide for specific MMP-2 targeting and inhibition of angiogenesis in NSCLC management. The efficiency of the established fabrication methodology to yield a desired CTT-functionalized PTX delivery nanosystem is outlined, and the relevant *in vitro* cellular analyses, including cellular uptake and internalization, MMP-2 binding affinity, and endothelial cell migration, are reported.

Chapter 6 delineates the pragmatically undertaken *in vivo* experimentation on a lung tumor xenograft mouse model, for assessing the antitumor activity of the formulated novel antiangiogenic peptide (HRH/CTT)-functionalized PTX delivery nanosystems. In this chapter, a comprehensive experimental design, including the development of a lung tumor xenograft mouse model, treatment of tumor-bearing mice, histopathological analysis of select tissues, and plasma pharmacokinetics of PTX, is outlined. This chapter further highlights the merits of a subcutaneous (SC) route for administration of chemotherapeutics, over the conventional intravenous (IV) route.

Chapter 7 summarizes the overall findings of the research study and provides proactive recommendations worth exploring in the future for further pre-clinical and clinical investigations on the formulated novel nanosystems.

Chapter 8 provides an overview of the Fulbright Exchange Program experiences. This chapter is considered an extension and further advancement of research related to this study and it briefly highlights my experiences as a Fulbright Visiting Student Researcher, at Johns Hopkins University, School of Medicine, United States of America. In this chapter, evidential accounts in regards to the abstracts emanating from co-authored outputs during the Fulbright Program tenure are presented.

1.6. References

Adeyemi, S.A., Choonara, Y.E., 2022. *In vitro* and *in vivo* evaluation of a cyclic LyP-1-modified nanosystem for targeted endostatin delivery in a KYSE-30 cell xenograft Athymic nude mice model. Pharmaceuticals 15, 353.

Adeyemi, S.A., Choonara, Y.E., Kumar, P., du Toit, L.C., Marimuthu, T., Kondiah, P.P.D., Pillay, V., 2019. Folate-decorated, endostatin-loaded, nanoparticles for anti-proliferative chemotherapy in esophaegeal squamous cell carcinoma. Biomed. Pharmacother. 119, 109450.

Akhtar, N., Mohammed, H.A., Yusuf, M., Al-Subaiyel, A., Sulaiman, G.M., Khan, R.A., 2022. SPIONs conjugate supported anticancer drug doxorubicin's delivery: Current status, challenges, and prospects. Nanomaterials (Basel) 12, 3686.

Aspriţoiu, V.M., Stoica, I., Bleotu, C., Diaconu, C.C., 2021. Epigenetic regulation of angiogenesis in development and tumors progression: Potential implications for cancer treatment. Front. Cell Dev. Biol. 9.

Bray, F., Parkin, D.M., Gnangnon, F., Tshisimogo, G., Peko, J.-F., Adoubi, I., Assefa, M., Bojang, L., Awuah, B., Koulibaly, M., Buziba, N., Korir, A., Dzamalala, C., Kamate, B., Manraj, S., Ferro, J., Lorenzoni, C., Hansen, R., Nouhou, H., Ogunbiyi, O., Igbinoba, F., Ekanem, I., Omonisi, A., Chirpaz, E., Uwinkindi, F., Finesse, A., Somdyala, N., Singh, E., Dlamini, X., Masalu, N.,

Serventi, F., Mrema, C., Wabinga, H., Ogwang, M., Chiwele, L., Borok, M., Chingonzoh, T., 2022. Cancer in sub-saharan africa in 2020: A review of current estimates of the national burden, data gaps, and future needs. Lancet Oncol. 23, 719-728.

Chandrakala, V., Aruna, V., Angajala, G., 2022. Review on metal nanoparticles as nanocarriers: Current challenges and perspectives in drug delivery systems. Emergent Mater. 5, 1593-1615.

Chen, Q., Zhang, Z., Li, X., Bu, L., 2022. Chemotherapy combined with immunotherapy as a first-line treatment brings benefits to patients with lung squamous cell carcinoma but different risks of adverse reactions: A systematic review and meta-analysis. Front. Pharmacol. 13.

Chen, Z., Mao, X., Ye, X., Li, S., Wu, T., Wang, Q., Zhang, J., Chen, L., Tang, N., He, H., Wang, Z., McAlinden, C., Wang, Q., Chen, S., Gao, R., Huang, J., 2021. A novel and biocompatible nanofiber of VEGF peptide for enhanced corneal neovascularization suppression. Chem. Eng. J. 416, 129081.

Cheng, Z., Li, M., Dey, R., Chen, Y., 2021. Nanomaterials for cancer therapy: Current progress and perspectives. J. Hematol. Oncol. 14, 85.

Chhikara, B.S., Parang, K., 2022. Global cancer statistics 2022: The trends projection analysis. Chem. Biol. Lett. 10, 451.

Choi, S.H., Yoo, S.S., Lee, S.Y., Park, J.Y., 2022. Anti-angiogenesis revisited: Reshaping the treatment landscape of advanced non-small cell lung cancer. Arch. Pharm. Res. 45, 263-279.

Dachev, M., Bryndová, J., Jakubek, M., Moučka, Z., Urban, M., 2021. The effects of conjugated linoleic acids on cancer. Processes 9, 454.

Daum, S., Hagen, H., Naismith, E., Wolf, D., Pircher, A., 2021. The role of anti-angiogenesis in the treatment landscape of non-small cell lung cancer: New combinational approaches and strategies of neovessel inhibition. Fron. Cell Dev. Biol. 8.

den Hartigh, L.J., 2019. Conjugated linoleic acid effects on cancer, obesity, and atherosclerosis: A review of pre-clinical and human trials with current perspectives. Nutrients 11, 370.

Ferlay, J., Colombet, M., Soerjomataram, I., Parkin, D.M., Piñeros, M., Znaor, A., Bray, F., 2021. Cancer statistics for the year 2020: An overview. Int. J. Cancer 149, 778-789.

Flowers, M., Thompson, P.A., 2009. T10c12 conjugated linoleic acid suppresses HER2 protein and enhances apoptosis in SKBr3 breast cancer cells: Possible role of COX2. PLoS One 4, e5342.

García-Fernández, C., Fornaguera, C., Borrós, S., 2020. Nanomedicine in non-small cell lung cancer: From conventional treatments to immunotherapy. Cancers (Basel) 12, 1609.

Haider, M., Elsherbeny, A., Pittalà, V., Consoli, V., Alghamdi, M.A., Hussain, Z., Khoder, G., Greish, K., 2022. Nanomedicine strategies for management of drug resistance in lung cancer. Int. J. Mol. Sci. 23, 1853.

Hanahan, D., 2022. Hallmarks of cancer: New dimensions. Cancer Discov. 12, 31-46.

Hu, X., Zhang, D., Zeng, Z., Huang, L., Lin, X., Hong, S., 2022. Aptamer-based probes for cancer diagnostics and treatment. Life 12, 1937.

Huang, M., Lin, Y., Wang, C., Deng, L., Chen, M., Assaraf, Y.G., Chen, Z. S., Ye, W., Zhang, D., 2022. New insights into antiangiogenic therapy resistance in cancer: Mechanisms and therapeutic aspects. Drug Resist. Updat. 64, 100849.

Joudeh, N., Linke, D., 2022. Nanoparticle classification, physicochemical properties, characterization, and applications: A comprehensive review for biologists. J. Nanobiotechnology 20, 262.

Karami Fath, M., Babakhaniyan, K., Zokaei, M., Yaghoubian, A., Akbari, S., Khorsandi, M., Soofi, A., Nabi-Afjadi, M., Zalpoor, H., Jalalifar, F., Azargoonjahromi, A., Payandeh, Z., Alagheband Bahrami, A., 2022. Anti-cancer peptide-based therapeutic strategies in solid tumors. Cell. Mol. Biol. Lett. 27, 33.

Klebe, S., Leigh, J., Henderson, D.W., Nurminen, M., 2020. Asbestos, smoking and lung cancer: An update. Int. J. Environ. Res. Public Health 17, 258.

Koivunen, E., Arap, W., Valtanen, H., Rainisalo, A., Medina, O.P., Heikkilä, P., Kantor, C., Gahmberg, C.G., Salo, T., Konttinen, Y.T., Sorsa, T., Ruoslahti, E., Pasqualini, R., 1999. Tumor targeting with a selective gelatinase inhibitor. Nat. Biotechnol. 17, 768-774.

Kydd, J., Jadia, R., Velpurisiva, P., Gad, A., Paliwal, S., Rai, P., 2017. Targeting strategies for the combination treatment of cancer using drug delivery systems. Pharmaceutics 9, 46.

Long, J., Zhang, C. J., Zhu, N., Du, K., Yin, Y. F., Tan, X., Liao, D. F., Qin, L., 2018. Lipid metabolism and carcinogenesis, cancer development. Am. J. Cancer Res. 8, 778-791.

Luo, Y. H., Luo, L., Wampfler, J.A., Wang, Y., Liu, D., Chen, Y. M., Adjei, A.A., Midthun, D.E., Yang, P., 2019. 5-year overall survival in patients with lung cancer eligible or ineligible for screening according to US preventive services task force criteria: A prospective, observational cohort study. Lancet Oncol. 20, 1098-1108.

Ma, Y., Yu, S., Ni, S., Zhang, B., Kung, A.C.F., Gao, J., Lu, A., Zhang, G., 2021. Targeting strategies for enhancing paclitaxel specificity in chemotherapy. Front. Cell Dev. Biol. 9.

Mohtar, N., Parumasivam, T., Gazzali, A.M., Tan, C.S., Tan, M.L., Othman, R., Fazalul Rahiman, S.S., Wahab, H.A., 2021. Advanced nanoparticle-based drug delivery systems and their cellular evaluation for non-small cell lung cancer treatment. Cancers (Basel) 13, 3539.

Moreira, T.G., Horta, L.S., Gomes-Santos, A.C., Oliveira, R.P., Queiroz, N.M.G.P., Mangani, D., Daniel, B., Vieira, A.T., Liu, S., Rodrigues, A.M., Gomes, D.A., Gabriely, G., Ferreira, E., Weiner, H.L., Rezende, R.M., Nagy, L., Faria, A.M.C., 2019. CLA-supplemented diet accelerates experimental colorectal cancer by inducing TGF-β-producing macrophages and T cells. Mucosal Immunol. 12, 188-199.

Ndinguri, M.W., Bhowmick, M., Tokmina-Roszyk, D., Robichaud, T.K., Fields, G.B., 2012. Peptide-based selective inhibitors of matrix metalloproteinase-mediated activities. Molecules 17, 14230-14248.

Olejarz, W., Kubiak-Tomaszewska, G., Chrzanowska, A., Lorenc, T., 2020. Exosomes in angiogenesis and anti-angiogenic therapy in cancers. Int. J. Mol. Sci. 21, 5840.

Pierre, A.-S., Minville-Walz, M., Fèvre, C., Hichami, A., Gresti, J., Pichon, L., Bellenger, S., Bellenger, J., Ghiringhelli, F., Narce, M., Rialland, M., 2013. *Trans*-10, *cis*-12 conjugated linoleic acid induced cell death in human colon cancer cells through reactive oxygen species-mediated ER stress. Biochim. Biophys. Acta - Mol. Cell Biol. Lipids 1831, 759-768.

Quintero-Fabián, S., Arreola, R., Becerril-Villanueva, E., Torres-Romero, J.C., Arana-Argáez, V., Lara-Riegos, J., Ramírez-Camacho, M.A., Alvarez-Sánchez, M.E., 2019. Role of matrix metalloproteinases in angiogenesis and cancer. Front. Oncol. 9, 1370-1370.

Raguraman, R., Shanmugarama, S., Mehta, M., Elle Peterson, J., Zhao, Y.D., Munshi, A., Ramesh, R., 2022. Drug delivery approaches for HuR-targeted therapy for lung cancer. Adv. Drug Del. Rev. 180, 114068.

Raso, M.G., Bota-Rabassedas, N., Wistuba, I.I., 2021. Pathology and classification of SCLC. Cancers (Basel) 13, 820.

Razlansari, M., Jafarinejad, S., rahdar, A., Shirvaliloo, M., Arshad, R., Fathi-Karkan, S., Mirinejad, S., Sargazi, S., Sheervalilou, R., Ajalli, N., Pandey, S., 2022. Development and classification of RNA aptamers for therapeutic purposes: An updated review with emphasis on cancer. Mol. Cell. Biochem.

Reczyńska, K., Marszałek, M., Zarzycki, A., Reczyński, W., Kornaus, K., Pamuła, E., Chrzanowski, W., 2020. Superparamagnetic iron oxide nanoparticles modified with silica layers as potential agents for lung cancer treatment. Nanomaterials (Basel) 10, 1076.

Shahzad, M.M.K., Felder, M., Ludwig, K., Van Galder, H.R., Anderson, M.L., Kim, J., Cook, M.E., Kapur, A.K., Patankar, M.S., 2018. *Trans*-10,*cis*-12 conjugated linoleic acid inhibits proliferation and migration of ovarian cancer cells by inducing ER stress, autophagy, and modulation of SRC. PLoS One 13, e0189524.

Sharma, R., Aashima, Nanda, M., Fronterre, C., Sewagudde, P., Ssentongo, A.E., Yenney, K., Arhin, N.D., Oh, J., Amponsah-Manu, F., Ssentongo, P., 2022. Mapping cancer in africa: A comprehensive and comparable characterization of 34 cancer types using estimates from Globocan 2020. Front. Public Health 10.

Siegel, R.L., Miller, K.D., Fuchs, H.E., Jemal, A., 2021. Cancer statistics, 2021. CA Cancer J. Clin. 71, 7-33.

Siwiec, E., Szynkowska, A., Milkiewicz, M., Marlicz, W., Stachowska, E., 2019. Diverse inhibition of forkhead box O1 activity by linoleic acid isomers: Potential role in lipid metabolism in HepG2 cells and livers of C57BL/6J mice. J. Physiol. Pharmacol. 70.

Sung, H., Ferlay, J., Siegel, R.L., Laversanne, M., Soerjomataram, I., Jemal, A., Bray, F., 2021. Global cancer statistics 2020: Globocan estimates of incidence and mortality worldwide for 36 cancers in 185 countries. CA Cancer J. Clin. 71, 209-249.

Wang, L., Wang, N., Zhang, W., Cheng, X., Yan, Z., Shao, G., Wang, X., Wang, R., Fu, C., 2022. Therapeutic peptides: Current applications and future directions. Signal. Transduct. Target. Ther. 7, 48.

World Health Organization, 2022. Cancer. https://www.who.int/news-room/fact-sheets/detail/cancer. Accessed Jan 21, 2022.

Wu, L., Wang, C., Li, Y., 2022a. Iron oxide nanoparticle targeting mechanism and its application in tumor magnetic resonance imaging and therapy. Nanomedicine 1, 12.

Wu, Q., Qian, W., Sun, X., Jiang, S., 2022b. Small-molecule inhibitors, immune checkpoint inhibitors, and more: FDA-approved novel therapeutic drugs for solid tumors from 1991 to 2021. J. Hematol. Oncol. 15, 143.

Ye, Z., Huang, Y., Ke, J., Zhu, X., Leng, S., Luo, H., 2021. Breakthrough in targeted therapy for non-small cell lung cancer. Biomed. Pharmacother. 133, 111079.

Zamay, T.N., Zamay, G.S., Kolovskaya, O.S., Zukov, R.A., Petrova, M.M., Gargaun, A., Berezovski, M.V., Kichkailo, A.S., 2017. Current and prospective protein biomarkers of lung cancer. Cancers 9, 11.

Zappa, C., Mousa, S.A., 2016. Non-small cell lung cancer: Current treatment and future advances. Transl. Lung Cancer Res. 5, 288-300.

Zhang, C., Leighl, N.B., Wu, Y.-L., Zhong, W.-Z., 2019. Emerging therapies for non-small cell lung cancer. J. Hematol. Oncol. 12, 45.

Zhang, T.Y., Huang, J.T., Tian, H.B., Ma, Y., Chen, Z., Wang, J.J., Shi, H.P., Luo, J., 2018. *Trans*-10,*cis*-12 conjugated linoleic acid alters lipid metabolism of goat mammary epithelial cells by regulation of *de novo* synthesis and the AMPK signaling pathway. J. Dairy Sci. 101, 5571-5581.

Zhang, Y., He, B., Liu, K., Ning, L., Luo, D., Xu, K., Zhu, W., Wu, Z., Huang, J., Xu, X., 2017. A novel peptide specifically binding to VEGF receptor suppresses angiogenesis *in vitro* and *in vivo*. Signal. Transduct. Target. Ther. 2, 17010.

Zhi, D., Yang, T., Yang, J., Fu, S., Zhang, S., 2020. Targeting strategies for superparamagnetic iron oxide nanoparticles in cancer therapy. Acta Biomater. 102, 13-34.

Zhong, L., Li, Y., Xiong, L., Wang, W., Wu, M., Yuan, T., Yang, W., Tian, C., Miao, Z., Wang, T., Yang, S., 2021. Small molecules in targeted cancer therapy: Advances, challenges, and future perspectives. Signal. Transduct. Target. Ther. 6, 201.

Zhou, B., Zang, R., Zhang, M., Song, P., Liu, L., Bie, F., Peng, Y., Bai, G., Gao, S., 2022. Worldwide burden and epidemiological trends of tracheal, bronchus, and lung cancer: A population-based study. eBioMedicine 78, 103951.

Zhou, Y.J., Zheng, W., Zeng, Q. H., Ye, Y., Wang, C., Fang, C., Liu, C. J., Niu, L., Wu, L.M., 2021. Targeted exome sequencing identifies mutational landscape in a cohort of 1500 Chinese patients with non-small cell lung carcinoma (NSCLC). Hum. Genomics 15, 21.

CHAPTER 2

A REVIEW ON ENGINEERED MAGNETIC NANOPARTICLES IN NON-SMALL-CELL LUNG CARCINOMA TARGETED THERAPY

2.1. Introduction

Lung cancer treatment has been an open problem for over a decade (Thun et al., 2010), and lung cancer currently ranks first as the contributor to global cancer deaths (Barta et al., 2019). Moreover, the global mortality rate associated with lung cancer, inclusive of all genders, surpasses combined records for patients with breast, colon, and pancreatic cancer (Zappa and Mousa, 2016). Lung cancer has poor prognostic factors and a low (17.8%) five (5)-year survival rate (Siegel et al., 2014). Non-small cell lung carcinoma (NSCLC) and small cell lung carcinoma (SCLC) represent the two foremost classes of lung cancer with NSCLC being more prevalent (Molina et al., 2008). Primarily, NSCLC comprises three sub-types, namely; adenocarcinoma, squamous-cell, and large-cell carcinoma, which are classified based on their histological origins (Zappa and Mousa, 2016). Accordingly, adenocarcinoma originates from abnormal lung cells, squamous-cell starts in the bronchi, and large-cell carcinoma are peripheral lying tumors. Importantly, these sub-types behave and respond to treatment in a similar manner (Zappa and Mousa, 2016).

Adenocarcinoma is the leading and most recognized NSCLC sub-type. It constitutes about 40% of all NSCLC, and is mostly common in both male and female smokers, regardless of their age (Couraud et al., 2012; Noguchi et al., 1995). Adenocarcinoma emerges from type II alveolar cells in the small airway epithelial, and mostly manifests throughout the periphery of the lungs (Zappa and Mousa, 2016). Squamous-cell and large-cell carcinoma comprise about 30% and 10% of NSCLC, respectively. Squamous-cell carcinoma generally occurs in the lung bronchial tubes, arising from the premature squamous cells in the airway epithelium (Kenfield et al., 2008). Meanwhile, large-cell carcinoma usually locates on the outer regions of the lungs and tends to metastasize more quickly than other forms of NSCLC (Popper, 2016).

Although uncertainty still remains on what causes each case of NSCLC, there is a multitude of risk factors like lifestyle, occupational, and environmental exposure which have been shown to contribute in the etiology of NSCLC (Barta et al., 2019). The roles these risk factors play vary and are dependent on various aspects such as race, gender, genetic predisposition, and geographic location. Smoking is the common primary risk factor implicated in NSCLC development, and at least 80% and 50% of NSCLC cases in men and women, respectively, can be attributed to smoking (Didkowska et al., 2016). Although nicotine itself is not carcinogenic, polycyclic aromatic hydrocarbons (PAHs) are amongst the substances present in cigarette which present with carcinogenic properties (Brawley et al., 2014).

Exposure to asbestos is another prominent occupational risk factor linked to increased lung cancer incidence (Villeneuve et al., 2012). Expectedly, workers in construction, textile and insulation, automobile repair, and shipbuilding, are highly exposed to asbestos and are at the highest risk of developing NSCLC (Markowitz et al., 2013). Moreover, the exposure to arsenic compounds (insecticides, antifungal, herbicides), use of beryllium oxide (radiation technology and X-ray), as well as inhalation of chemical substances such as silica, chromium compounds, nickel compounds, cadmium, vinyl chloride, chloromethyl esters, mustard gas, and coal products are amongst other occupational exposures that could result in increased lung cancer incidents (Spyratos et al., 2013; Zappa and Mousa, 2016).

Researchers have leveraged results of Genome-wide association studies (GWAS) for studying the genetic predisposition of lung cancer. Reports on GWAS that have been undertaken on various populations to assess the impact of genetics in susceptibility to lung cancer have been reviewed elsewhere (Yang et al., 2013). These reports depicted that the relative risk was increased for NSCLC amongst siblings and offspring of lung cancer patients (Cote et al., 2012). Likewise, the carriers of tumor protein 53 *(TP53)* germline sequence variations are reportedly highly susceptible to lung cancer, with a 3-fold lung cancer likelihood for carriers who are cigarette smokers (Molina et al., 2008; Olivier et al., 2010; Zappa and Mousa, 2016). Additionally, some genetic evaluations have identified a link between lung cancer and chromosome 15 marker. The risk of lung cancer is approximately 30% and 70% higher for people with one and two copies of the marker, respectively (Amos et al., 2008; Molina et al., 2008).

The treatment protocol for NSCLC is mainly advocated by the degree at which the cancer has progressed (stage I-IV), and the treatment is aimed at slowing down further progression and possibly increase the overall survival (Bareschino et al., 2011). Patients that present with stage I, II and IIIA NSCLC mostly undergo tumour removal surgery, whereas stage IIA, IIB, and IIIB patients typically receive platinum-based drugs such as carboplatin or cisplatin (Amini et al., 2014; Bareschino et al., 2011; Howington et al., 2013). Stage IV NSCLC patients receive cytotoxic combination chemotherapy, a regimen of a platinum (carboplatin or cisplatin) combined with standard therapeutic agents (i.e., paclitaxel, gemcitabine, docetaxel, vinorelbine, pemetrexed, or irinotecan) (Masters et al., 2015). Combination chemotherapy represents first-line treatment modality for advanced NSCLC, and is particularly a preferred option for patients with no comorbidities and presenting with high performance status (Gridelli et al., 2010).

Early diagnosis and effective management of NSCLC remains a challenge, and surgery or radiation therapy alone are not effective (Huang et al., 2017). Consequently, combination chemotherapy is the main therapeutic intervention for NSCLC management (Gridelli et al., 2010; Huang et al., 2017). However, the platinum-based doublet (augmented) chemotherapy is coupled with cytotoxic side effects and the drug combination is adversely intolerable to most patients (Babu et al., 2013). The majority of the chemotherapeutics are hydrophobic in nature and therefore present with poor water solubility which hinders their administration at high doses (Naderinezhad et al., 2017). Moreover, conventional administration of chemotherapeutics has been challenged with non-specificity of action (resulting in cytotoxicity to normal cells), rapid clearance , and poor tumor penetration (Kydd et al., 2017).

The advent of targeted nanosystems such as functionalized magnetic nanoparticles (MNPs) has provided great promise for targeted drug delivery platform interventions for NSCLC (Lombardo et al., 2019). Targeted MNPs enable the precision of chemotherapeutics, resulting in enhanced pharmacological action and low cytotoxicity levels (Aslan et al., 2013; Lombardo et al., 2019), and offer desirable advantages as drug delivery vectors, such as enhanced drug stability, drug solubility, and high drug-loading capacity (Ganapathe et al., 2020). MNPs have been functionalized with targeting moieties including peptides to achieve targeted drug delivery (Li et al., 2021; Liang et al., 2020; Nosrati et al., 2019), and polymers to enhance biocompatibility (Liu et al., 2020a). A possible cancer treatment modality has been reported for tumor-associated blood vasculature targeting by directing nanoparticle-based therapeutics towards biomarkers of angiogenesis like receptors of vascular endothelial growth factor (VEGF) or integrin (Barr et al., 2015; Chen et al., 2015; Liu et al., 2016). Some nanoparticle-based therapies, such as albumin-bound paclitaxel nanoformulations (Abraxane®) have been explored for metastatic NSCLC treatment, however their translation into clinical success has been a challenge (Yuan et al., 2012).

The current focus in cancer research is to develop chemotherapeutics that target key molecules to halt tumor growth, metastasis, and proliferation, while exhibiting minimal toxicity or side effects (Lombardo et al., 2019; Schirrmacher, 2019). Experimental evidence suggests that combining natural compounds that possess anticancer properties with antitumoral drugs can potentially attenuate cancer resistance against therapy and elicit chemoprotective actions (Lin et al., 2020). Natural compounds have been, for many years, a source of anticancer compounds, and their cancer preventive or protective activities can be attributed to their effects on cellular defences (antioxidant enzyme systems) in combination with the antitumor responses, such as apoptosis, triggered by specific targeting of significant transcription factors (Aravindaram and Yang, 2010; Huang et al., 2017).

Conjugated linoleic acid (CLA), a natural essential fatty acid is known to bear anticancer properties (De la Torre et al., 2005; Slowikowski et al., 2020). Structurally, CLA comprises of at least 28 isomers, and of these, *trans*-10,*cis*-12 (t10,c12-CLA) and *cis*-9,*trans*-11 (c9,t11-CLA) are the most abundant (Shahzad et al., 2018), and have shown to suppress tumor proliferation in animal and cell models (Beppu et al., 2006; Flowers and Thompson, 2009; Ip et al., 2002; Kelley et al., 2007; Yamasaki et al., 2002). Moreover, literature supports the increasing prevalence of CLA as a potential inhibitor of angiogenesis by suppression of VEGF and basic fibroblast growth factor (bFGF), and lowering of the VEGF receptor affinity and fetal liver kinase-1 expression (Ke et al., 2010; Moon et al., 2003; Wang et al., 2005). Recent advancements in cancer nanotherapy have culminated in the exploration of magnetic nanoplatforms for targeted treatment of NSCLC. This review focuses on this aspect, and considering the antitumor and anti-proliferative effects of CLA, the potential use of CLA as an antitumor agent in the development of functionalized magnetic nanosystems for NSCLC targeted therapy is discussed. In addition, to further substantiate for the use of nanosystems, current nanoparticle-based targeted chemotherapies focusing on targeting angiogenesis biomarkers in NSCLC are also explored.

2.2. Combining Chemotherapeutics as NSCLC First-Line Regimens

Although NSCLC patients receive platinum-based combination protocols as a first-line regimen, there is a sense that the conventional platinum-based combination chemotherapeutics are now at their therapeutic plateau (Le Chevalier, 2011; Scheff and Schneider, 2013). The two-drug combination, comprising either carboplatin or cisplatin with an additional third-generation cytotoxic agent, is the first-line systemic therapy administered once or twice in a cycle (Vasconcellos et al., 2020). Classes of common cytotoxic agents (distinguished by their mechanisms of action) used in platinum doublets for treatment of NSCLC are listed in **Table 2.1**. While clinical data suggest that cisplatin doublets present with considerable superior clinical outcomes over carboplatin doublets, cisplatin may, however, confer intolerable toxicity and for patients under palliative care their quality of life is compromised (Ardizzoni et al., 2007; Scheff and Schneider, 2013). Cisplatin also presents with increased levels of nausea, renal toxicity, peripheral neuropathy, and ototoxicity (Oun et al., 2018).

Table 2.1. Classes of common cytotoxic agents used in platinum-based combination chemotherapy for treatment of NSCLC

Class	Mechanism of Action	Cytotoxic Agents	Ref.
Antimetabolites	Block nucleic acid synthesis by limiting deoxyribonucleoside triphosphates (dNTPs) availability.	Pemetrexed Gemcitabine	(Olaussen and Postel-Vinay, 2016)
Spindle poisons	Interfere with mitotic spindle microtubule polymerisation/depolymerisation.	Paclitaxel Vinorelbine Docetaxel	(Huang et al., 2017)
Topoisomerase inhibitors	Suppress the enzymes (topoisomerase I or II) responsible for relaxing DNA supercoiling.	Topetecan Etoposide	(Huang et al., 2017; Olaussen and Postel-Vinay, 2016)

The adverse side effects of conventional combination chemotherapy such as myelosuppression, alopecia, mucositis, and weight loss, as well as high levels of toxicity to normal cells impede the effective use of conventional platinum-based regimens (Nurgali et al., 2018), and consequently necessitate the development of alternative safer treatment modalities. Non-platinum-containing therapeutics have since been studied and proposed as acceptable therapeutic alternatives for treatment of patients who cannot tolerate platinum-based therapy, however, they have no major clinical advantage over platinum-based combinations (Jiang et al., 2013). Additionally, combination chemotherapy with more than two agents may presumably enhance the tumor response rate, however, there is no evidence of the ameliorative effects of this approach, meanwhile, its application outside clinical trials is limited by the additive toxicity. (Di Maio et al., 2009).

Conventional administration of combinational chemotherapeutics has often been associated with poor tumor penetration and susceptibility to rapid clearance by the immune system, resulting in inconsistent *in vivo* pharmacokinetics and bio-distribution profiles (Hu et al., 2016). Limited solubility of selected drugs used in combination chemotherapy that require high surfactant concentrations to dissolve, limit their administration at highly effective doses, of which can subsequently compromise the effectiveness of the treatment and render it inefficient (Narvekar et al., 2014; Zhang et al., 2016). Moreover, non-specific action synonymous with

conventional administration of chemotherapeutics severely threatens the optimal success of combination chemotherapy as an effective treatment strategy for NSCLC.

The incorporation of targeting ligands into platinum-based doublets for NSCLC treatment has been clinically evaluated and reportedly demonstrate no additional benefits (Le Chevalier, 2011). Despite the increased response rates observed, no clinically meaningful survival benefit is demonstrated, except for bevacizumab, a monoclonal antibody that targets VEGF (Sandler et al., 2006). Thus, there is still a great demand for alternative tumor-targeted chemotherapeutic approaches for the treatment of NSCLC that will achieve high drug efficacy, confer no toxicity to normal tissues, and demonstrate significant survival benefit. One such alternative that has been explored is the use of the essential fatty acid, CLA (Slowikowski et al., 2020). CLA is primarily sourced from animal products like meat or dairy (Visioli et al., 2012) and in respective animal models and *in vitro* cell models has exhibited anti-tumor and anti-proliferative activity (Cunningham et al., 1997; Maggiora et al., 2004; Tanmahasamut et al., 2004). Merging CLA with magnetic nanoparticles has the potential to provide an alternative efficacious approach to the chemotherapy of NSCLC.

2.3. Conjugated Linoleic Acid: A Prospective Antitumor Agent

The reported mechanisms involved in anti-proliferative activity of CLA include inhibition of DNA synthesis, modulation of lipid peroxidation, inhibition of VEGF and matrix metalloproteinases (MMPs), and induction of apoptosis (Lee et al., 2005). An overview of these mechanisms is presented in **Table 2.2**. Research conducted on CLA to date, employing both *in vitro* and *in vivo* models has garnered significant insight on the role of CLA as a prospective anticancer agent (Evans et al., 2010; Moreira et al., 2019; Ochoa et al., 2004; Rakib et al., 2013). CLA comprises numerous positional and geometric isomers that are identified based on the position (i.e., 7-,9-; 8-,10-; 9-,11-; 10-,12-; 11-,13-; 12-,14-) and geometry (*trans* or *cis*) of the double bonds on the linoleic acid chain (Lee et al., 2005). The *trans*-10,*cis*-12 CLA and *cis*-9,*trans*-11 CLA are the two most biologically active isomers and have been widely explored (Kennedy et al., 2010). Studies involving the mixture of both isomers have revealed that CLA suppresses proliferation of colon (Evans et al., 2010; Shiraishi et al., 2010), breast (Rakib et al., 2013; Tanmahasamut et al., 2004), colorectal (Moreira et al., 2019), stomach (Ha et al., 1990), and prostate cancer cells (Cesano et al., 1998; Ochoa et al., 2004).

Table 2.2. Mechanisms reportedly involved in anti-proliferative activities of CLA

Mechanism	Description	Anti-proliferative Activity Example(s)	Ref.
Inhibition of DNA Synthesis	CLA interferes with the biosynthesis of nucleotides and proteins involved in DNA synthesis.	Significant inhibition of [^{3}H] leucine, [^{3}H] thymidine and [^{3}H] uridine incorporation into the DNA of MFC-7 cancer cells observed, when CLA added.	(Cunningham et al., 1997; desBordes and Lea, 1995; Lee et al., 2005; Rossi et al., 2012)
Modulation of Lipid Peroxidation	CLA induces lipid peroxidation through formation of cytotoxic lipid oxidation products, enabled by the susceptibility of conjugated double bond system to oxidation.	Notable increase in lipid peroxidation levels in human lung carcinoma cells (A549, A427, SK-LU-1), resulted in reduced proliferation.	(Belury, 2002; Cunningham et al., 1997; Lee et al., 2005; Schønberg and Krokan, 1995; Shultz et al., 1992)
Inhibition of VEGF and MMPs	CLA affects the binding of VEGF to its receptor Flk-1. CLA suppresses MMP-2 and MMP-9 activities.	Results showed effective dose-dependent inhibition of angiogenesis in mammary glands in mice. Rapid induction of apoptosis led to the collapse of the tumor vasculature and suppressed proliferation.	(Harris et al., 2001; Lee et al., 2005; Masso-Welch et al., 2002; Masso-Welch et al., 2004; Quintero-Fabián et al., 2019; Teleanu et al., 2019)
Induction of Apoptosis	CLA downregulates ErbB3 signalling and the PI3K/Akt pathway.	Significant inhibition of growth in human colorectal cancer cell via induction of apoptosis. Enhanced anti-proliferative activity reported in dRLh-84 rat hepatoma cells.	(Cho et al., 2003; Lee et al., 2005; Yamasaki et al., 2002)

For a while, the beneficial effects of individual isomers of CLA in cancer had not been conclusive, until the late 2000s when purified CLA isomers emerged and were studied for anticancer activity (Kelley et al., 2007; Pierre et al., 2013). Initially it was found that the *cis*-9,*trans*-11 CLA isomer displayed a higher potency relative to the *trans*-10,*cis*-12 isomer (Khanal, 2004), until more evidence surfaced showing that the *trans*-10,*cis*-12 isomer is equally or even more beneficial than *cis*-9,*trans*-11 CLA isomer (Cho et al., 2006; Cho et al., 2009; Pierre et al., 2013; Shahzad et al., 2018).

2.4. Inhibition of Angiogenesis: A Prospective Management Approach to NSCLC

Angiogenesis is a controlled series of steps in which blood vessel formation occurs from existing vasculature **(Figure 2.1)**. It is one of the hallmarks in cancer responsible for providing essential nutrients and oxygen which enable the tumor to grow and metastasize (Mashreghi et al., 2018). Over the years, mechanisms of tumor angiogenesis have been investigated as key targets in cancer therapy, including NSCLC (Hall et al., 2015). Tumor growth is essentially reliant on the efficient angiogenesis (Rajabi and Mousa, 2017) , and accordingly, exploitation of tumor vasculature could be a lucrative therapeutic intervention for cancer management (Mumtaz et al., 2020).

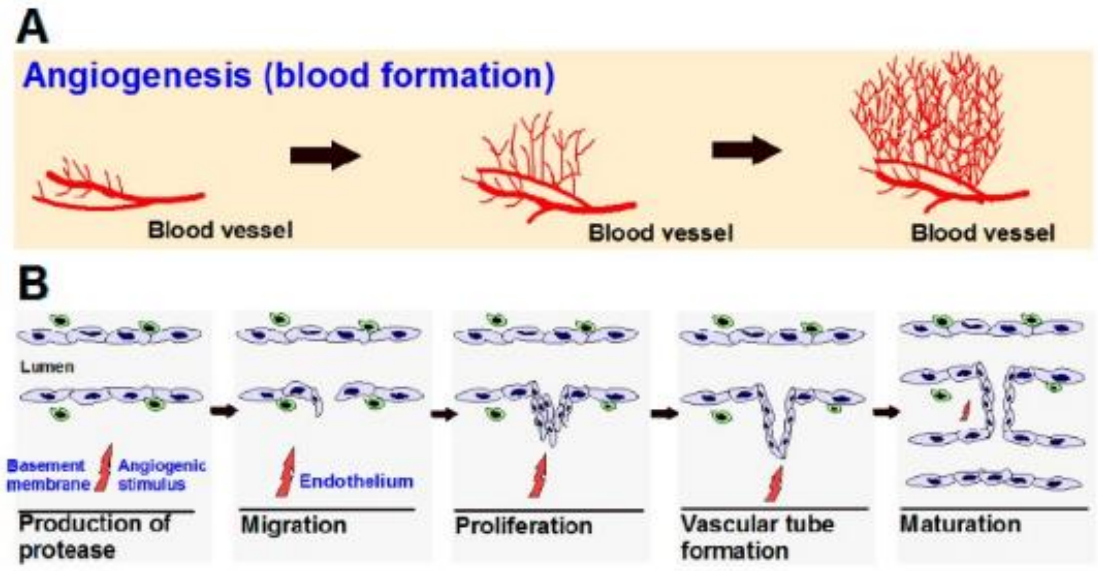

Figure 2.1. A graphical depiction of angiogenesis. **(A)** Endothelial cells from pre-existing blood vessels sprout to form new network of blood vessels; **(B)** Steps involved in the process of angiogenesis comprise production of protease, migration and proliferation of endothelial cells, formation of vascular tubes, and vessel maturation (i.e., new basement membrane formation, and myocytes/pericytes incorporation). Reprinted under Creative Common License from Ref. (Rajabi and Mousa, 2017).

New blood vessel formation (neo-angiogenesis) is a very complex process, and yet provides numerous potential targets for inhibiting tumor proliferation (Mumtaz et al., 2020). In NSCLC, these targets include growth factors (i.e., VEGF and epidermal growth factor), MMPs, and integrins (Brock and Lee, 2002; Teleanu et al., 2019), and could potentially be targeted using CLA-derived magnetic nanoparticles. **Table 2.3** provides an overview of VEGF and MMPs as targets of interest for inhibition of angiogenesis in NSCLC. VEGF and MMPs are common key regulators of angiogenesis (Quintero-Fabián et al., 2019), and consequently considered the main targets for the advancement of anti-angiogenic therapeutics (Teleanu et al., 2019).

Table 2.3. Overview of VEGF and MMPs as anti-angiogenic therapeutic targets in NSCLC

Target	Description	Implication in NSCLC	Ref.
VEGF	Dimeric protein belonging to the family of growth factors comprising VEGF-F, VEGF-E, VEGF-D, VEGF-C, VEGF-B, and placenta growth factor (PIGF). Key role player in the endothelial cell proliferation and migration.	Commonly expressed in lung cancer, with approximately 75% expression in NSCLC cases. Promoted angiogenesis in NSCLC through binding to VEGFR-2.	(Alevizakos et al., 2013; Fallah et al., 2019; Ferrara, 2010; Ferrara et al., 2003; Wheatley-Price and Shepherd, 2008)
MMPs	Members of a large family (24 known MMPs in humans) of calcium- and zinc-dependent enzymes which degrade extracellular matrix (ECM) proteins.	Primarily involved in lung tumorigenesis by forming the complex microenvironment, enabling invasion of lung tissue.	(Blanco-Prieto et al., 2017; Egeblad and Werb, 2002; Foley et al., 2014; Kim et al., 2012; Nagase and Woessner, 1999)

VEGFR-2; vascular endothelial growth factor receptor-2

Anti-angiogenic therapies in NSCLC have been exploited, with the aim to inhibit tumor angiogenesis, through two primary approaches; (i) use of monoclonal antibodies that block binding of VEGF to VEGFRs, and (ii) use of tyrosine kinase inhibitors (TKIs) that halt VEGFR-mediated downstream signalling (Imai and Takaoka, 2006). As per the U.S Food and Drug Administration (FDA) standards, bevacizumab and ramucirumab are currently available FDA-approved monoclonal antibodies for application in NSCLC (Hall et al., 2015). Bevacizumab became the first market available anti-VEGF monoclonal antibody for NSCLC after proving

efficacy in all tested endpoints, in particular the overall survival rate (OS), doubling of response rates (RR), coupled with progression-free survival (PFS) (Sandler et al., 2006). Small molecule TKIs, such as sorafenib, sunitinib, cediranib, stableorafenib, axitinib and pazopanib have been evaluated, mostly in combination with chemotherapy, but show little success due to increased toxicity (Hall et al., 2015; Scagliotti and Govindan, 2010).

2.4.1. Peptide-based antiangiogenic approach: Specific targeting of VEGF and MMPs with peptide ligands

Although major developments have been made in antiangiogenic therapies over the years, specificity remains a huge drawback in developing new effective angiogenesis inhibiting systems (Jászai and Schmidt, 2019). Currently, the majority of angiogenic inhibitors available for clinical application are primarily small molecules and proteins (Ferrara and Adamis, 2016). Small molecule-derived systems may present with poor target selectivity due to their miniature size, while proteins may exhibit poor membrane permeability, low bioavailability and metabolic instability (Craik et al., 2013). Alternatively, peptide-based targeting therapeutics such as peptide-functionalized superparamagnetic iron oxide nanoparticles (SPIONs), may allow mitigation of these shortcomings. Particularly, peptides present with high target specificity, high membrane permeability, high potency, as well as low cost (Adebowale et al., 2015; Sun and Xu, 2015). It has been demonstrated that endostatin (antiangiogenic peptide) could elicit anti-proliferative activity as an angiogenesis inhibitor in esophageal cancer (Adeyemi et al., 2019; Adeyemi et al., 2017).

VEGF promotes tumor angiogenesis as it binds to VEGFR-2 to facilitate downstream signal transduction which mediates formation of new vasculature, endothelial differentiation, coupled with migration of tumor cells (Alevizakos et al., 2013). Zhang et al., 2017, isolated a VEGF-selective peptide that was shown to specifically bind to VEGFRs to suppress angiogenesis (Zhang et al., 2017). The peptide with a sequence HRHTKQRHTALH (peptide HRH) was tested on human umbilical vein endothelial cells (HUVEC), and was found to halt HUVEC proliferation by inhibiting VEGF binding, through VEGFR 2 domain blockade (Zhang et al., 2017). The peptide currently holds great promise for future advancements in the design of potential anti-VEGF systems. Before that, Michaloski et al., 2016 had also identified and characterized small 6-mer peptides capable of specifically targeting the extracellular binding domain of VEGFRs (VEGR 1-3), thus preventing VEGF-VEGFR binding and downstream signalling (Michaloski et al., 2016).

The involvement of MMPs in lung carcinogenesis make these endopeptidases attractive as potential markers of NSCLC and therapeutic targets for its management. MMPs promote initial

stages of tumor growth, where they mediate signalling pathways that regulate cell differentiation, proliferation, migration, as well as angiogenesis (Hadler-Olsen et al., 2013; Mumtaz et al., 2020). Multitude of MMP-mediated activities such as proliferation and invasion can be inhibited by selective MMP binding peptides (Ndinguri et al., 2012).

Koivunen *et al.,* 1999 successfully identified selective MMP-2 and MMP-9 inhibiting peptides using phage display peptide libraries (Koivunen et al., 1999). A range of peptide libraries were screened, and two cyclic peptides with sequences CRRHWGFEFC and CTTHWGFTLC, consisting of a HWGF motif, showed to inhibit MMP-9 and MMP-2, respectively. The mechanisms of these peptides in MMP inhibition have been extensively explored and reported elsewhere (Ndinguri et al., 2012). Primarily, CTT selectively binds MMP-2 and blocks the endothelial cells from degrading and remodelling the adjacent extracellular matrix, leading to the disruption of neovascularization and ultimately tumor growth regression (Ndinguri et al., 2012). Additionally, Bhowmick et al., 2017, recently reported on triple helical peptide inhibitors (THPIs) that effectively inhibit MMPs (Bhowmick et al., 2017). The specific binding of these peptides to the MMPs is facilitated by their triple helical structure (Bhowmick et al., 2017). These THPIs hold great promise as MMP-targeting ligands, with their excellent stability and favourable *in vivo* properties.

2.5. Application of Nanosystems for Targeted Delivery of Chemotherapeutics in NSCLC

Nanotechnology is a broad research field involving the application of novel nano-devices and nanomaterials, as well as different types of nanoparticles (NPs) in various areas of interest including cancer therapeutics (Nana et al., 2019; Woodman et al., 2020). There is a large interest in studying the application of nanotechnology in medicine for the treatment of lung cancer due to its potential to elicit site-specific action without causing harmful side effects (Babu et al., 2013; García-Fernández et al., 2020). Evidently, the use of NPs has rapidly increased in importance in lung cancer chemotherapy due to their potential to increase drug solubility, improve drug stability and half-life, concentrate drugs at target sites, and minimize off target effects (Ediriwickrema and Saltzman, 2015; Sukumar et al., 2013). Essentially, the size and composition of NPs are part of the physicochemical properties that determine their bioavailability in the body, with smaller-sized NPs being able to penetrate through challenging biological barriers (García-Fernández et al., 2020). **Figure 2.2** shows various types of NPs available for lung cancer chemotherapy with the focus on the magnetic NPs, particularly SPIONs as targeted nanosystem for NSCLC therapy.

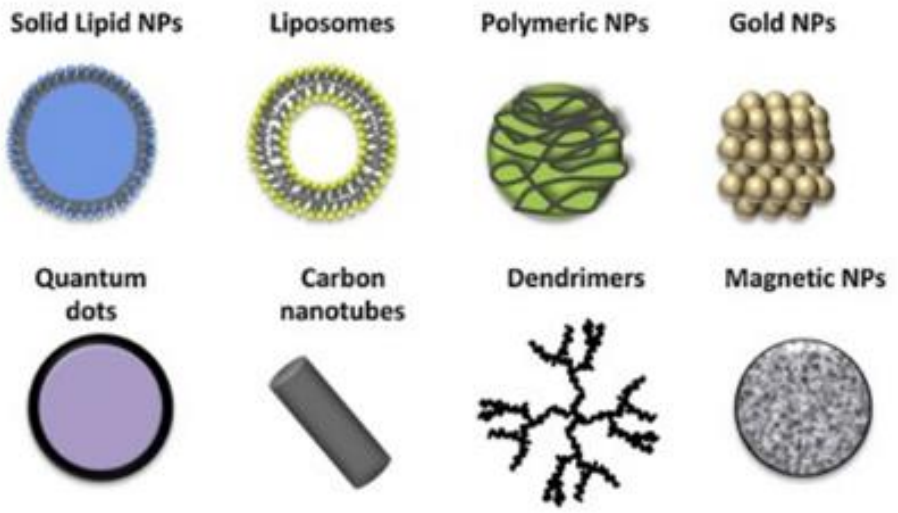

Figure 2.2. Various forms of nanoparticles for application in lung cancer nanotherapy. The NPs vary in chemical composition, shape, and size, and may be modified accordingly to overcome biological barriers and elicit desired action in lung cancer therapy. Image adapted from Ref (Woodman et al., 2020) with permission. Copyright Elsevier 2020.

2.5.1. Magnetic nanoparticles

Magnetic nanoparticles (MNPs) are fabricated from pure metals (i.e., Fe, Ni, Co), with an increasing application in various biomedical fields including bioimaging (Fathi Karkan et al., 2017; Khizar et al., 2021) and lung cancer therapy (Babincová et al., 2014; Farzin et al., 2020; Li et al., 2019; Munaweera et al., 2015; Yokoyama et al., 2011; Yu et al., 2018; Zhang et al., 2019). Summarized in **Table 2.4** are selected significant studies that have explored the application of MNPs in NSCLC targeted therapy in the last decade. MNPs traditionally comprise magnetic metal oxides with one or two alloys, as well as iron oxide NPs (Veiseh et al., 2010), and the latter include maghemite (γ-Fe_2O_3) and magnetite (Fe_3O_4) (Wu and Huang, 2017). Iron oxides are characterized by less sensitivity to oxidation, thus able to yield a steady magnetic response, and are also relatively easier to functionalize with polymers (i.e., polyethylene glycol (PEG), dextran, polyvinyl alcohol (PVA)) or functional groups (i.e., carboxyl, amines, thiols) which make them more effective for lung cancer theranostic platforms (Liu et al., 2020a; Sukumar et al., 2013).

Table 2.4. Notable studies on the application of magnetic nanoparticles in NSCLC targeted therapy over the last decade

Magnetic Nanoparticle System	Results / Significance	Year	Ref.
Dox and Cet -loaded dextran-coated iron oxide (Fe_3O_4) NPs (Dox-NPs-Cet).	Dox-NPs-Cet notably suppressed proliferation of A549 cells. Dox-NPs-Cet demonstrated a great promise as a candidate for targeting NSCLC.	2019	(Zhang et al., 2019)
Paclitaxel-loaded core-shell-MNPs with cold atmospheric plasma (CAP).	PTX- MNPs and CAP showed synergistic inhibition of A549 cell growth. Combination of PTX-loaded MNPs and CAP could be an effective NSCLC treatment system.	2018	(Yu et al., 2018)
Actein (AT) conjugated iron oxide (Fe_3O_4) magnetic nanoparticles (AT-MNPs)	AT-MNPs induced apoptosis and suppressed NSCLC growth. AT-MNPs demonstrated potential clinical value in suppressing NSCLC progression.	2017	(Wang et al., 2017)
Platinum (II) drug (cisplatin, carboplatin, oxaliplatin)-loaded holmium iron garnet magnetic nanoparticles (HoIG-Pt MNPs).	HoIG-Pt inhibited tumor growth compared to untreated controls	2015	(Munaweera et al., 2015)
EGFR-targeted superparamagnetic nanoparticles (EGFR-SPIONs).	EGFR-SPIONs significantly inhibited lung tumor growth *in vivo.* EGFR targeting enhanced tumor retention of SPIONs.	2013	(Sadhukha et al., 2013)
Iron oxide (Fe_3O_4) magnetic nanoparticles.	Fe_3O_4 NPs suppressed the growth of lung cancer cells (A549), but had no negative effects on the normal cells (IMR-90). Fe_3O_4 NPs selectively killed cancerous cells.	2012	(Khan et al., 2012)
EGFR-targeted hybrid plasmonic magnetic nanoparticles (EGFR-C225 MNPs).	Selective uptake of EGFR-C225 MNPs by EGFR-expressing NSCLC cells was reported. EGFR-C225 MNPs induced apoptosis and demonstrated increased antitumor activity.	2011	(Yokoyama et al., 2011)

EGFR; Epidermal growth factor receptor, Dox; doxorubicin, Cet; cetuximab, PTX; paclitaxel

Particularly, MNPs have gained significant interest over non-magnetic nanomaterials (i.e., liposomes, polymer based drug carriers) in cancer theranostic bestowed by their inherent magnetism, nanoscale size, and large specific surface area (Albinali et al., 2019; Khizar et al., 2021). MNPs are excellent contrast agents for bioimaging (magnetic resonance imaging) in cancer diagnosis (Yigit et al., 2012), and their inherent magnetism allows for magnetic drug delivery which concentrates drugs at the target site, an offers magnetic hyperthermia as an alternative cancer treatment modality (Liu et al., 2020b). Moreover, the relatively smaller particle size of MNPs, such as SPIONs (<100nm), make them superior over their counterparts as they present with longer half-life, while the larger surface area imparts high drug-loading capacity (Ganapathe et al., 2020). Generally, an MNP bears a magnetic core surrounded by a shell structure onto which imaging reporters and targeting moieties are anchored, and therapeutic agents may be embedded or chemically bonded on its surface (**Figure 2.3A**) (Albinali et al., 2019). Magnetic behaviour, chemical composition, size, morphology, and geometry are the most crucial criteria that underpin the application of MNPs in lung cancer therapy (Fathi Karkan et al., 2017). These are essentially significant in ensuring that the MNPs can stay longer in circulation. MNPs with the diameter size of 10 - 100 nm [less than spleen cut off (200 nm)] can penetrate into large tumors, and with hydrophilic coatings like PEG, the nanoparticles can evade the reticuloendothelial system (RES), which consists of cells that are capable of engulfing foreign materials and particles (Davis et al., 2008; Tran and Webster, 2010).

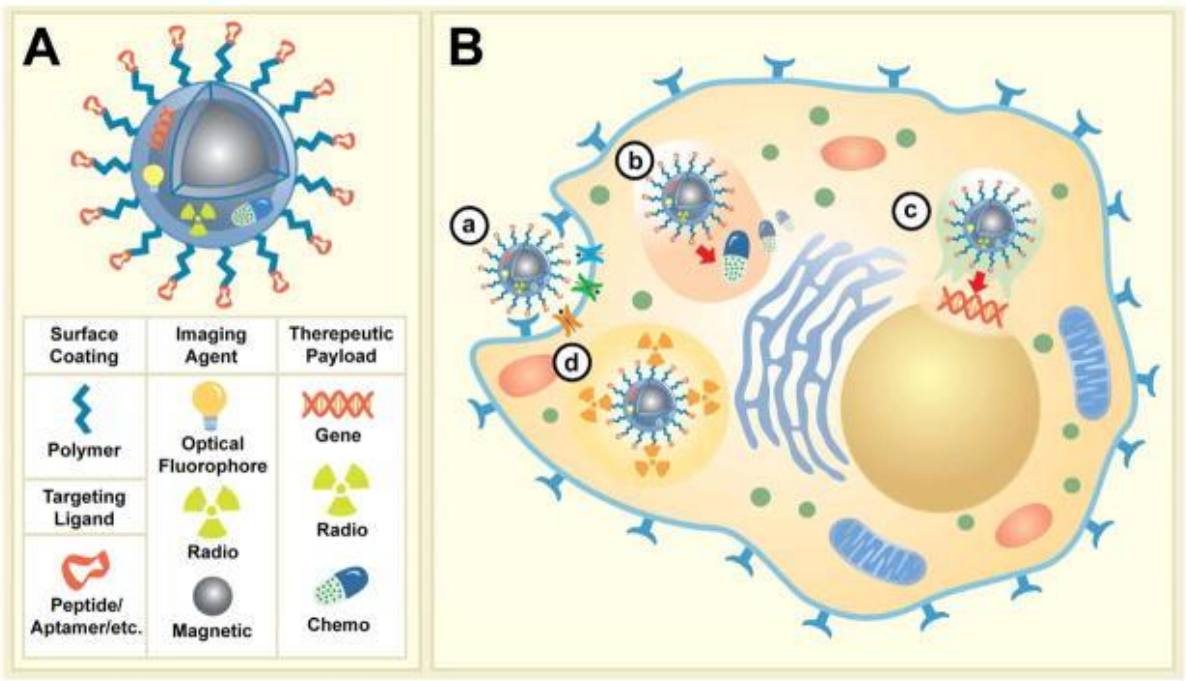

Figure 2.3. Schematic representation of the concept of MNP application in anticancer drug targeting and *in vivo* imaging, and potential mechanisms of action for different therapeutic agents. **(A)** An MNP may be coated with polymers, loaded with therapeutic payloads and imaging agents, and surface functionalized with targeting ligands. **(B)** Therapeutic payloads may elicit therapeutic effects through; **(a)** cellular internalization of an MNP through specific cell-receptor binding; **(b)** controlled release; **(c)** direct nucleus targeting; **(d)** intracellular decomposition. Reproduced from Ref. (Veiseh et al., 2010) with permission, Copyright, Elsevier 2010.

Tumor specificity of nanoparticles is very crucial in NSCLC targeted therapy since non-specific cell binding can potentially harm healthy tissue (Babu et al., 2013), and to limit such, the MNPs must be designed to possess affinity for lung tumors (Huang et al., 2016). Ideally, the delivery of MNPs to the tumor site in NSCLC targeted therapy can be achieved through magnetic, passive and active mechanisms (Garbuzenko et al., 2019; Tietze et al., 2015). Magnetic drug targeting employs external magnetic systems to focus and deliver MNPs to lung tumors (Saadat et al., 2020), while passive targeting involves exploitation of the physiological nature of tumor cells by MNPs, such as through the enhanced permeation and retention (EPR) effect, where high-molecular weight particles accumulate in the tumor (Bazak et al., 2014; Wei and Zhao, 2014). Meanwhile, active targeting occurs via engineering of the nanoparticle surface with targeting groups stemming from peptides, aptamers to antibodies, and small molecules complementary to unique receptors expressed on NSCLC cells (Alhajj et al., 2018; Goel et al., 2013). The specific receptor binding facilitates cellular internalization of the MNPs, and once inside the tumor, the therapeutics are released from the MNPs to elicit a therapeutic effect **(Figure 2.3B)**.

2.5.2. Methods to synthesize MNPs for targeted drug delivery in NSCLC

The fabrication of MNPs with desirable shape, particle size, morphology and distribution is the fundamental aspect for the application of these nanomaterials in lung cancer nanotherapy (Woodman et al., 2020). Reproducibility and predictability of the synthesis and fabrication processes are equally critical for the application of MNPs in cancer targeted therapy (Farzin et al., 2020). Essentially, MNPs have been fabricated with a diverse composition using different fabrication methodologies, like co-precipitation, microemulsion, hydrothermal synthesis, and temperature decomposition (Khizar et al., 2021; Lu et al., 2007). A more detailed account of these conventional methods are published elsewhere (Lu et al., 2007; Majidi et al., 2016). Meanwhile, co-precipitation and microemulsion methods are evidently superior when it comes to the synthesis of MNPs suitable for application in NSCLC targeted

therapy (Munaweera et al., 2015; Nejati-Koshki et al., 2014; Sadhukha et al., 2013; Yokoyama et al., 2011; Zhang et al., 2019).

2.5.2.1. Co-precipitation

Co-precipitation has been ranked as a facile fabrication method for iron oxides (i.e., γ-Fe_2O_4 and Fe_3O_4) from aqueous solutions of Iron(II)/Iron(III) treated with a base under controlled air-free conditions, at varying temperature (normally 20-90°C) (Akilo et al., 2016; Mascolo et al., 2013; Munaweera et al., 2015). Several factors like type of precursor salt, Fe^{2+}/Fe^{3+} ratio, conductivity and pH levels of the reaction media, as well as the reaction temperature directs the composition, geometry and dimensions of the MNPs (Gawali et al., 2019). Nejati-Koshki et al., 2014, adapted co-precipitation for the preparation of cisplatin-loaded Fe_3O_4 MNPs modified with poly (lactic-co-glycolic acid) (PLGA) and poly (ethylene glycol) (PEG_{600}) for targeted delivery of cisplatin into A549 lung cancer cells. The method yielded spherical, well-dispersed NPs which facilitated a robust and efficient uptake of cisplatin into tumor cells (Nejati-Koshki et al., 2014). Yokoyama *et al*., 2011, also reported on co-precipitation synthesis of EGFR-C225 MNPs which selectively targeted and killed EGFR-expressing NSCLC cells (Yokoyama et al., 2011). Monodispersed magnetite NPs of varying sizes can be fabricated by co-precipitation using organic additives as reducing agents and stabilizers (Majidi et al., 2016), and moreover, the method allows the use of any other substances, such as CLA, that may render the MNPs biocompatible and more appropriate for *in vivo* application, such as in NSCLC targeted therapy.

2.5.2.2. Microemulsion

Microemulsions are thermodynamically favoured dispersions of two immiscible liquids with surfactant-stabilized microdomains (Gradzielski et al., 2021). Microemulsions of aqueous phase within oil phase are generally employed in the fabrication of MNPs where the microemulsion is used as a reactor for nanoparticle formation (Capek, 2004). Accordingly, Sadhuka *et al*., 2013 evaluated the application of SPIONs in NSCLC targeted therapy and employed a microemulsion approach to synthesize the SPIONs (Sadhukha et al., 2013). Generally, the mixing of two immiscible liquids containing desired reactants leads to continuous collision, coalescence, and breaking of microdroplets, finally resulting in the formation of a precipitate in the micelles (Gradzielski et al., 2021). The precipitate may then be isolated by filtration or centrifugation (Malik et al., 2012). Using a microemulsion method, MNPs are synthesized in a controlled manner with desirable particle size and shapes (Lu et al., 2007), allowing for surface modifications with polymers and biocompatible materials, such as CLA which confers additional anticancer benefits.

2.5.3. Design considerations of MNPs for the delivery of chemotherapeutics in NSCLC

There are principal design elements such as shape, size, and surface property that need to be thoroughly controlled when designing MNPs for application in lung cancer targeted therapy (Babu et al., 2013; Woodman et al., 2020). These factors need to be optimized in the initial stages of MNPs design to achieve biocompatibility and increased probability of the nanoparticles to be able to navigate the body and reach lung tumors (Babu et al., 2013). Essentially, if neglected, these factors can drastically change the desired outcome of the nanosystem (Kudr et al., 2017). Practically, the desired therapeutic outcomes can be severely hampered by various biological barriers (both physical and cellular) that the nanosystem is likely to encounter while navigating the highly complex system of the body in search of the tumor and after the tumor is reached (Babu et al., 2013; Khalid et al., 2017).

2.5.3.1. Particle size

The size of MNPs significantly influences their bioavailability (Wahajuddin and Arora, 2012) and determines their permeability out of the vasculature (Senapati et al., 2018). Typically, MNPs with dimensions < 10 nm are prone to elimination by renal clearance, meanwhile MNPs with dimensions >200 nm bioaccumulate in the spleen or undergo phagocytosis, consequently resulting in decreased plasma concentrations (Hoshyar et al., 2016). In the lung, NPs of more than 100 nm are cleared by alveolar macrophages (Lee et al., 2014). MNPs ranging from 10-100 nm may be considered ideal for targeted lung cancer drug delivery because of their ability to escape the RES in the body, resulting in longer circulation times (Edis et al., 2021) and evade clearance by alveolar macrophages. These MNPs also possess the ability to traverse very small capillaries. Small sized MNPs such as SPIONs can highly accumulate in the tumor microenvironment owing to the EPR effect (Wan et al., 2016; Woodman et al., 2020). However, SPIONs <2 nm are deemed inappropriate for cancer nanotherapy due to potential diffusion through cell membranes, which may lead to the compromise of intracellular organelles. Ideally, appropriate surface modification method, such as CLA coating, can help control the size, avoid agglomeration and achieve biocompatibility of MNPs for application in NSCLC targeted therapy.

2.5.3.2. Shape

Factors such as the choice of chemicals and the reaction conditions applied in the fabrication of MNPs can largely influence their morphology (Lee et al., 2015). The influence of shape on the NPs behaviour *in vivo* has been evaluated, suggesting that the shape of NPs could influence their biodistribution, biocompatibility, and clearance (Huang et al., 2011). In the case of NSCLC targeted therapy, studies demonstrate that the particle shape is commonly spherical

(Li et al., 2019; Munaweera et al., 2015; Nejati-Koshki et al., 2014; Yokoyama et al., 2011; Zhang et al., 2019), owing to the fabrication methods employed (i.e., co-precipitation and microemulsion) which preferably yield spherical NPs due to thermodynamic favourability (Cooley et al., 2018). Interestingly, a CLA and paclitaxel (CLA-PTX) conjugate has been shown to self-assemble to form spherical NPs with high drug-loading capacity and enhanced antitumor activity against cancerous cells. The spherical shape of the NPs had a direct effect on cell toxicity and promoted cellular uptake in the cell lines studied (Zhong et al., 2016).

2.5.3.3. Surface properties

The chemical and physical nature of the MNPs surface determines their biodistribution (Khizar et al., 2021), and can potentially influence their internalization into lung tumors (Woodman et al., 2020). MNP surface charge and magnetism can significantly influence their biodistribution by either enhancing or impeding interactions of MNPs with the extracellular matrices, non-target cells, and plasma proteins (Davis, 2002). Magnetism is also important to consider in the application of MNPs when an external magnetic force is to be employed (Akilo et al., 2016; Kudr et al., 2017). MNPs tend to lose their magnetic properties when oxidized, and thus surface coating is vital for enhancing their stability by preventing oxidation (Mosayebi et al., 2017). The accumulation of NPs in the lungs may be influenced by the surface charge, with positively charged NPs being more favoured. This is most likely directed by positively charged NPs to form aggregates which can be entrapped into the lungs (Ishiwata et al., 2000; Zein et al., 2020). Additionally, positively charged NPs can easily penetrate into tumors due to high binding affinity between the NPs and tumor cells (Lee et al., 2015). Surface modification of MNPs presents another important aspect in their application in NSCLC targeted therapy, to limit phagocytosis by macrophages and increase circulation time. CLA has been used to functionalize SPIONs for improved dispersity and anticancer potential (Muzio et al., 2017). Moreover, tumor cells are known to take up essential fatty acids as energy sources and biochemical precursors (Jaracz et al., 2005).

2.6. Superparamagnetic Iron Oxide Nanoparticles (SPIONs)

The development of targeted NPs for effective delivery of anticancer drugs to the lungs offers great potential for successful treatment of NSCLC over current conventional chemotherapies (García-Fernández et al., 2020). Targeted NPs can directly deliver drugs to target tumors at a sustained rate and reduced dosage frequency (Hossen et al., 2019; Morales-Cruz et al., 2019), thus offering great efficacy and limited unwanted cytotoxicity for the treatment of NSCLC. Fundamentally, targeted NPs allow resolving the drawbacks of conventional cancer therapies, such as nonspecific drug distribution, low availability, rapid clearance, and toxicity

to normal cells (García-Fernández et al., 2020; Hossen et al., 2019; Lombardo et al., 2019). Consequently, for NSCLC management, targeted NPs may be a solution for providing prolonged disease control and potentially enhance long-term survival in NSCLC patients.

Over the years, researchers have conducted various studies on SPIONs platforms in lung cancer therapy (Branca et al., 2010; Reczyńska et al., 2020a; Reczyńska et al., 2020b; Sadhukha et al., 2013; Yoo et al., 2012). The reported attributes that make SPIONs most suitable and interesting drug transporters for NSCLC targeted therapy include their simplistic synthetic approaches, effective biocompatibility, and unique magnetic behaviour (Palanisamy and Wang, 2019). Typically, SPIONs have characteristic small size (< 100 nm), large surface area, and have iron oxide nanoparticle cores with a biocompatible outer-shell which permits functionalization with desired moieties (i.e., therapeutic agents, targeting ligands) into one particle for lung tumor-specific drug delivery (Reczyńska et al., 2020a; Reczyńska et al., 2020b; Sadhukha et al., 2013). Owing to the large surface area-to-volume ratio, SPIONs offer high drug-loading capacity and surface modification with targeting moieties (Revia and Zhang, 2016). Conventional anticancer agents like doxorubicin, methotrexate, and paclitaxel showed enhanced drug bioavailability and target specificity when loaded into SPIONs (Reczyńska et al., 2020a; Wahajuddin and Arora, 2012).

Drug loading is a critical step in the manipulation of SPIONs as drug transporters in lung cancer therapy and should always be carried out in a manner that does not compromise the functionality of the drug, and with assurance that the drug-loaded SPIONs release the drug at the desired rate upon reaching lung tumor cells (Mansouri et al., 2017; Reczyńska et al., 2020a). Essentially, drug loading into SPIONs is achieved either by conjugating the drug onto the NPs surface or co-encapsulation within the coating material (Gholami et al., 2020). Conjugation occurs through; (i) physical interactions (coupling of nanoparticles and the drug via hydrophilic/hydrophobic, electrostatic, or affinity interactions) or (ii) direct covalent linkage of the particles with the drug via the surface functional groups (i.e., hydroxyl or amino groups) (Hoang Thi et al., 2019). Generally, co-encapsulation is the preferred drug-loading technique, since it offers high drug entrapment efficiency and bioavailability (Mehnath et al., 2018).

Meanwhile, surface-coating of SPIONs is fundamental in preventing aggregation while shielding their surfaces from oxidation and providing a site for drug loading and attachment of targeting ligands (Reczyńska et al., 2020b). This also increases SPIONs blood circulation by escaping the RES and minimizing non-specificity (Mahmoudi et al., 2011). The (3-aminopropyl)trimethoxysilane surface-modified SPIONs loaded with methotrexate, tagged with folate receptor-binding ligands reportedly demonstrated an increased selective uptake of SPIONs by human cervical (HeLa) and human breast (MCF-7) cancer cells (Kohler et al.,

2005). Muzio *et al*., 2017 also investigated innovative SPIONs capped with CLA for enhanced antitumor activity, which selectively killed mouse breast (4T1) cells (Muzio et al., 2017). Studies on CLA-modified SPIONs for application in NSCLC targeted therapy are still needed as this approach could potentially be a breakthrough in NSCLC management.

2.7. Concluding Remarks

The high prevalence of NSCLC globally remains a major concern. Conventional chemotherapeutic options available for NSCLC have been faced with numerous limitations, resulting in a need for more effective, better-tolerated treatment modalities. Considerable advancements towards nascent platforms of targeted chemotherapies such as functionalized MNPs show much promise as effective nanomedicine for targeted cancer chemotherapy with application in NSCLC. Application of MNPs in lung cancer therapy offers a plethora of benefits including improved drug stability and half-life, site-specificity, minimized toxicity to healthy cells, and reduced dosage frequency, over conventional chemotherapy. The variety of MNP systems have been engineered for NSCLC therapy, and *in vitro* and *in vivo* studies of such nanosystems demonstrate exclusive anti-proliferative activity of engineered MNPs.

Through surface-coating and functionalization with targeting ligands, drug-loaded magnetic nanosystems could selectively target lung cancer cells (A549), induce apoptosis, and suppress tumor proliferation. Moreover, natural-based alternative agents with anticancer properties such as CLA are also captivating as prospective antitumor agents for the development of anticancer nanomedicines. The anti-proliferative activities associated with CLA may be of special interest for incorporation of this fatty acid into developing surface-modified nanoparticles to achieve enhanced chemotherapeutic delivery in NSCLC with minimal cytotoxicity. In addition, the on-going research on peptide-based angiogenic inhibitors in cancer therapy is yielding positive outcomes, demonstrating the ability of antiangiogenic peptides to effectively supress angiogenesis biomarkers (i.e., VEGF, MMP) and halt angiogenesis, hence a growing interest in the application of these biomolecules as targeting ligands for angiogenesis inhibition in lung cancer.

In essence, the development and leveraging of tumor targeted nanosystems, such as functionalized SPIONs could present a promising approach towards effective management of NSCLC. Ideally, the engineered SPIONs (magnetite, Fe_3O_4) would have to be of appropriate size for lung tumor penetration (~100 nm), have high drug-loading capacity, and be modified with CLA for enhanced biocompatibility and anticancer properties. Functionalization of SPIONs with either VEGF or MMP-targeting peptide ligands would ensure the specificity of the nanosystem to achieve targeted drug delivery and angiogenesis inhibition.

2.8. References

Adebowale, A.S., Choonara, Y.E., Kumar, P., du Toit, L.C., Pillay, V., 2015. Functionalized nanocarriers for enhanced bioactive delivery to squamous cell carcinomas: Targeting approaches and related biopharmaceutical aspects. Curr. Pharm. Des. 21, 3167-3180.

Adeyemi, S.A., Choonara, Y.E., Kumar, P., du Toit, L.C., Marimuthu, T., Kondiah, P.P.D., Pillay, V., 2019. Folate-decorated, endostatin-loaded, nanoparticles for anti-proliferative chemotherapy in esophaegeal squamous cell carcinoma. Biomed. Pharmacother. 119, 109450.

Adeyemi, S.A., Choonara, Y.E., Kumar, P., du Toit, L.C., Pillay, V., 2017. Design and characterization of endostatin-loaded nanoparticles for in vitro antiangiogenesis in squamous cell carcinoma. J. Nanomater. 2017, 2539065.

Akilo, O.D., Choonara, Y.E., Strydom, A.M., du Toit, L.C., Kumar, P., Modi, G., Pillay, V., 2016. An *in vitro* evaluation of a carmustine-loaded nano-co-plex for potential magnetic-targeted intranasal delivery to the brain. Int. J. Pharm. 500, 196-209.

Albinali, K.E., Zagho, M.M., Deng, Y., Elzatahry, A.A., 2019. A perspective on magnetic core-shell carriers for responsive and targeted drug delivery systems. Int. J. Nanomed. 14, 1707-1723.

Alevizakos, M., Kaltsas, S., Syrigos, K.N., 2013. The VEGF pathway in lung cancer. Cancer Chemother. Pharmacol. 72, 1169-1181.

Alhajj, N., Chee, C.F., Wong, T.W., Rahman, N.A., Abu Kasim, N.H., Colombo, P., 2018. Lung cancer: Active therapeutic targeting and inhalational nanoproduct design. Expert Opin. Drug Deliv. 15, 1223-1247.

Amini, A., Yeh, N., Gaspar, L.E., Kavanagh, B., Karam, S.D., 2014. Stereotactic body radiation therapy (SBRT) for lung cancer patients previously treated with conventional radiotherapy: A review. Radiat. Oncol. 9, 210.

Amos, C.I., Wu, X., Broderick, P., Gorlov, I.P., Gu, J., Eisen, T., Dong, Q., Zhang, Q., Gu, X., Vijayakrishnan, J., Sullivan, K., Matakidou, A., Wang, Y., Mills, G., Doheny, K., Tsai, Y.Y., Chen, W.V., Shete, S., Spitz, M.R., Houlston, R.S., 2008. Genome-wide association scan of tag SNPs identifies a susceptibility locus for lung cancer at 15q25.1. Nat. Genet. 40, 616-622.

Aravindaram, K., Yang, N.S., 2010. Anti-inflammatory plant natural products for cancer therapy. Planta Med. 76, 1103-1117.

Ardizzoni, A., Boni, L., Tiseo, M., Fossella, F.V., Schiller, J.H., Paesmans, M., Radosavljevic, D., Paccagnella, A., Zatloukal, P., Mazzanti, P., Bisset, D., Rosell, R., 2007. Cisplatin- versus carboplatin-based chemotherapy in first-line treatment of advanced non-small-cell lung cancer: An individual patient data meta-analysis. J. Natl. Cancer Inst. 99, 847-857.

Aslan, B., Ozpolat, B., Sood, A.K., Lopez-Berestein, G., 2013. Nanotechnology in cancer therapy. J. Drug Target. 21, 904-913.

Babincová, M., Kontrisova, K., Durdík, S., Bergemann, C., Sourivong, P., 2014. Radiation enhanced efficiency of combined electromagnetic hyperthermia and chemotherapy of lung carcinoma using cisplatin functionalized magnetic nanoparticles. Pharmazie 69, 128-131.

Babu, A., Templeton, A.K., Munshi, A., Ramesh, R., 2013. Nanoparticle-based drug delivery for therapy of lung cancer: Progress and challenges. J. Nanomater. 2013, 863951.

Bareschino, M.A., Schettino, C., Rossi, A., Maione, P., Sacco, P.C., Zeppa, R., Gridelli, C., 2011. Treatment of advanced non small cell lung cancer. J. Thorac. Dis. 3, 122-133.

Barr, M.P., O'Byrne, K.J., Al-Sarraf, N., Gray, S.G., 2015. VEGF-mediated cell survival in non-small-cell lung cancer: Implications for epigenetic targeting of VEGF receptors as a therapeutic approach. Epigenomics 7, 897-910.

Barta, J.A., Powell, C.A., Wisnivesky, J.P., 2019. Global epidemiology of lung cancer. Ann. Glob. Health 85, 8.

Bazak, R., Houri, M., Achy, S.E., Hussein, W., Refaat, T., 2014. Passive targeting of nanoparticles to cancer: A comprehensive review of the literature. Mol. Clin. Oncol. 2, 904-908.

Belury, M.A., 2002. Inhibition of carcinogenesis by conjugated linoleic acid: Potential mechanisms of action. J. Nutr. 132, 2995-2998.

Beppu, F., Hosokawa, M., Tanaka, L., Kohno, H., Tanaka, T., Miyashita, K., 2006. Potent inhibitory effect of trans9, trans11 isomer of conjugated linoleic acid on the growth of human colon cancer cells. J. Nutr. Biochem. 17, 830-836.

Bhowmick, M., Tokmina-Roszyk, D., Onwuha-Ekpete, L., Harmon, K., Robichaud, T., Fuerst, R., Stawikowska, R., Steffensen, B., Roush, W., Wong, H.R., Fields, G.B., 2017. Second generation triple-helical peptide inhibitors of matrix metalloproteinases. J. Med. Chem. 60, 3814-3827.

Blanco-Prieto, S., Barcia-Castro, L., Páez de la Cadena, M., Rodríguez-Berrocal, F.J., Vázquez-Iglesias, L., Botana-Rial, M.I., Fernández-Villar, A., De Chiara, L., 2017. Relevance of matrix metalloproteases in non-small cell lung cancer diagnosis. BMC Cancer 17, 823-823.

Branca, R.T., Cleveland, Z.I., Fubara, B., Kumar, C.S.S.R., Maronpot, R.R., Leuschner, C., Warren, W.S., Driehuys, B., 2010. Molecular MRI for sensitive and specific detection of lung metastases. PNAS. 107, 3693.

Brawley, O.W., Glynn, T.J., Khuri, F.R., Wender, R.C., Seffrin, J.R., 2014. The first Surgeon General's report on smoking and health: The 50th anniversary. CA Cancer J. Clin. 64, 5-8.

Brock, C.S., Lee, S.M., 2002. Anti-angiogenic strategies and vascular targeting in the treatment of lung cancer. Eur. Respir. J. 19, 557-570.

Capek, I., 2004. Preparation of metal nanoparticles in water-in-oil (w/o) microemulsions. Adv. Colloid Interface Sci. 110, 49-74.

Cesano, A., Visonneau, S., Scimeca, J.A., Kritchevsky, D., Santoli, D., 1998. Opposite effects of linoleic acid and conjugated linoleic acid on human prostatic cancer in SCID mice. Anticancer Res. 18, 1429-1434.

Chen, Y., Wang, X., Liu, T., Zhang, D.S., Wang, Y., Gu, H., Di, W., 2015. Highly effective antiangiogenesis via magnetic mesoporous silica-based siRNA vehicle targeting the VEGF gene for orthotopic ovarian cancer therapy. Int. J. Nanomed. 10, 2579-2594.

Cho, H.J., Kim, E.J., Lim, S.S., Kim, M.K., Sung, M.K., Kim, J.S., Park, J.H., 2006. Trans-10,cis-12, not cis-9,trans-11, conjugated linoleic acid inhibits G1-S progression in HT-29 human colon cancer cells. J. Nutr. 136, 893-898.

Cho, H.J., Kim, W.K., Kim, E.J., Jung, K.C., Park, S., Lee, H.S., Tyner, A.L., Park, J.H., 2003. Conjugated linoleic acid inhibits cell proliferation and ErbB3 signaling in HT-29 human colon cell line. Am. J. Physiol. Gastrointest. Liver Physiol. 284, G996-1005.

Cho, H.J., Kwon, G.T., Park, J.H., 2009. Trans-10,cis-12 conjugated linoleic acid induces depolarization of mitochondrial membranes in HT-29 human colon cancer cells: A possible mechanism for induction of apoptosis. J. Med. Food 12, 952-958.

Cooley, M., Sarode, A., Hoore, M., Fedosov, D.A., Mitragotri, S., Sen Gupta, A., 2018. Influence of particle size and shape on their margination and wall-adhesion: Implications in drug delivery vehicle design across nano-to-micro scale. Nanoscale 10, 15350-15364.

Cote, M.L., Liu, M., Bonassi, S., Neri, M., Schwartz, A.G., Christiani, D.C., Spitz, M.R., Muscat, J.E., Rennert, G., Aben, K.K., Andrew, A.S., Bencko, V., Bickeboller, H., Boffetta, P., Brennan, P., Brenner, H., Duell, E.J., Fabianova, E., Field, J.K., Foretova, L., Friis, S., Harris, C.C., Holcatova, I., Hong, Y.C., Isla, D., Janout, V., Kiemeney, L.A., Kiyohara, C., Lan, Q., Lazarus, P., Lissowska, J., Le Marchand, L., Mates, D., Matsuo, K., Mayordomo, J.I., McLaughlin, J.R., Morgenstern, H., Mueller, H., Orlow, I., Park, B.J., Pinchev, M., Raji, O.Y., Rennert, H.S., Rudnai, P., Seow, A., Stucker, I., Szeszenia-Dabrowska, N., Dawn Teare, M., Tjonnelan, A., Ugolini, D., van der Heijden, H.F., Wichmann, E., Wiencke, J.K., Woll, P.J., Yang, P., Zaridze, D., Zhang, Z.F., Etzel, C.J., Hung, R.J., 2012. Increased risk of lung cancer in individuals with a family history of the disease: A pooled analysis from the international lung cancer consortium. Eur. J. Cancer 48, 1957-1968.

Couraud, S., Zalcman, G., Milleron, B., Morin, F., Souquet, P.J., 2012. Lung cancer in never smokers-a review. Eur. J. Cancer 48, 1299-1311.

Craik, D.J., Fairlie, D.P., Liras, S., Price, D., 2013. The future of peptide-based drugs. Chem. Biol. Drug Des. 81, 136-147.

Cunningham, D.C., Harrison, L., Shultz, T., 1997. Proliferative responses of normal human mammary and MCF-7 breast cancer cells to linoleic acid, conjugated linoleic acid and eicosanoid synthesis inhibitors in culture. Anticancer Res. 17, 197-203.

Davis, M.E., 2002. Non-viral gene delivery systems. Curr. Opin. Biotechnol. 13, 128-131.

Davis, M.E., Chen, Z., Shin, D.M., 2008. Nanoparticle therapeutics: An emerging treatment modality for cancer. Nat. Rev. Drug Discov. 7, 771-782.

De la Torre, A., Debiton, E., Durand, D., Chardigny, J.M., Berdeaux, O., Loreau, O., Barthomeuf, C., Bauchart, D., Gruffat, D., 2005. Conjugated linoleic acid isomers and their conjugated derivatives inhibit growth of human cancer cell lines. Anticancer Res. 25, 3943-3949.

desBordes, C., Lea, M.A., 1995. Effects of C18 fatty acid isomers on DNA synthesis in hepatoma and breast cancer cells. Anticancer Res. 15, 2017-2021.

Di Maio, M., Chiodini, P., Georgoulias, V., Hatzidaki, D., Takeda, K., Wachters, F.M., Gebbia, V., Smit, E.F., Morabito, A., Gallo, C., Perrone, F., Gridelli, C., 2009. Meta-analysis of single-agent chemotherapy compared with combination chemotherapy as second-line treatment of advanced non-small-cell lung cancer. J. Clin. Oncol. 27, 1836-1843.

Didkowska, J., Wojciechowska, U., Mańczuk, M., Łobaszewski, J., 2016. Lung cancer epidemiology: Contemporary and future challenges worldwide. Ann. Transl. Med. 4, 150-150.

Ediriwickrema, A., Saltzman, W.M., 2015. Nanotherapy for cancer: Targeting and multifunctionality in the future of cancer therapies. ACS Biomater. Sci. Eng. 1, 64-78.

Edis, Z., Wang, J., Waqas, M.K., Ijaz, M., Ijaz, M., 2021. Nanocarriers-mediated drug delivery systems for anticancer agents: An overview and perspectives. Int. J. Nanomed. 16, 1313-1330.

Egeblad, M., Werb, Z., 2002. New functions for the matrix metalloproteinases in cancer progression. Nat. Rev. Cancer 2, 161-174.

Evans, N.P., Misyak, S.A., Schmelz, E.M., Guri, A.J., Hontecillas, R., Bassaganya-Riera, J., 2010. Conjugated linoleic acid ameliorates inflammation-induced colorectal cancer in mice through activation of PPARgamma. J. Nutr. 140, 515-521.

Fallah, A., Sadeghinia, A., Kahroba, H., Samadi, A., Heidari, H.R., Bradaran, B., Zeinali, S., Molavi, O., 2019. Therapeutic targeting of angiogenesis molecular pathways in angiogenesis-dependent diseases. Biomed. Pharmacother. 110, 775-785.

Farzin, A., Etesami, S.A., Quint, J., Memic, A., Tamayol, A., 2020. Magnetic nanoparticles in cancer therapy and diagnosis. Adv. Healthc. Mater. 9, 1901058.

Fathi Karkan, S., Mohammadhosseini, M., Panahi, Y., Milani, M., Zarghami, N., Akbarzadeh, A., Abasi, E., Hosseini, A., Davaran, S., 2017. Magnetic nanoparticles in cancer diagnosis and treatment: A review. Artif. Cells Nanomed. Biotechnol. 45, 1-5.

Ferrara, N., 2010. Pathways mediating VEGF-independent tumor angiogenesis. Cytokine Growth Factor Rev. 21, 21-26.

Ferrara, N., Adamis, A.P., 2016. Ten years of anti-vascular endothelial growth factor therapy. Nat. Rev. Drug Discov. 15, 385-403.

Ferrara, N., Gerber, H.P., LeCouter, J., 2003. The biology of VEGF and its receptors. Nat. Med. 9, 669-676.

Flowers, M., Thompson, P.A., 2009. T10c12 conjugated linoleic acid suppresses HER2 protein and enhances apoptosis in SKBr3 breast cancer cells: Possible role of cox2. PLoS One 4, e5342.

Foley, C.J., Fanjul-Fernández, M., Bohm, A., Nguyen, N., Agarwal, A., Austin, K., Koukos, G., Covic, L., López-Otín, C., Kuliopulos, A., 2014. Matrix metalloprotease 1a deficiency suppresses tumor growth and angiogenesis. Oncogene 33, 2264-2272.

Ganapathe, L.S., Mohamed, M.A., Mohamad Yunus, R., Berhanuddin, D.D., 2020. Magnetite (fe3o4) nanoparticles in biomedical application: From synthesis to surface functionalisation. Magnetochemistry 6, 68.

Garbuzenko, O.B., Kuzmov, A., Taratula, O., Pine, S.R., Minko, T., 2019. Strategy to enhance lung cancer treatment by five essential elements: Inhalation delivery, nanotechnology, tumor-receptor targeting, chemo- and gene therapy. Theranostics 9, 8362-8376.

García-Fernández, C., Fornaguera, C., Borrós, S., 2020. Nanomedicine in non-small cell lung cancer: From conventional treatments to immunotherapy. Cancers (Basel) 12, 1609.

Gawali, S.L., Barick, K.C., Shetake, N.G., Rajan, V., Pandey, B.N., Kumar, N.N., Priyadarsini, K.I., Hassan, P.A., 2019. pH-labile magnetic nanocarriers for intracellular drug delivery to tumor cells. ACS Omega 4, 11728-11736.

Gholami, A., Mousavi, S.M., Hashemi, S.A., Ghasemi, Y., Chiang, W.-H., Parvin, N., 2020. Current trends in chemical modifications of magnetic nanoparticles for targeted drug delivery in cancer chemotherapy. Drug Metab. Rev. 52, 205-224.

Goel, A., Baboota, S., Sahni, J.K., Ali, J., 2013. Exploring targeted pulmonary delivery for treatment of lung cancer. Int. J. Pharm. Invest. 3, 8-14.

Gradzielski, M., Duvail, M., de Molina, P.M., Simon, M., Talmon, Y., Zemb, T., 2021. Using microemulsions: Formulation based on knowledge of their mesostructure. Chem. Rev. 121, 5671-5740.

Gridelli, C., Ardizzoni, A., Douillard, J.Y., Hanna, N., Manegold, C., Perrone, F., Pirker, R., Rosell, R., Shepherd, F.A., De Petris, L., Di Maio, M., de Marinis, F., 2010. Recent issues in first-line treatment of advanced non-small-cell lung cancer: Results of an international expert panel meeting of the italian association of thoracic oncology. Lung Cancer 68, 319-331.

Ha, Y.L., Storkson, J., Pariza, M.W., 1990. Inhibition of benzo(a)pyrene-induced mouse forestomach neoplasia by conjugated dienoic derivatives of linoleic acid. Cancer Res. 50, 1097-1101.

Hadler-Olsen, E., Winberg, J.O., Uhlin-Hansen, L., 2013. Matrix metalloproteinases in cancer: Their value as diagnostic and prognostic markers and therapeutic targets. Tumour Biol. 34, 2041-2051.

Hall, R.D., Le, T.M., Haggstrom, D.E., Gentzler, R.D., 2015. Angiogenesis inhibition as a therapeutic strategy in non-small cell lung cancer (NSCLC). Transl. Lung Cancer Res. 4, 515-523.

Harris, M.A., Hansen, R.A., Vidsudhiphan, P., Koslo, J.L., Thomas, J.B., Watkins, B.A., Allen, K.G., 2001. Effects of conjugated linoleic acids and docosahexaenoic acid on rat liver and

reproductive tissue fatty acids, prostaglandins and matrix metalloproteinase production. Leukot. Essent. Fatty Acids 65, 23-29.

Hoang Thi, T.T., Nguyen Tran, D.-H., Bach, L.G., Vu-Quang, H., Nguyen, D.C., Park, K.D., Nguyen, D.H., 2019. Functional magnetic core-shell system-based iron oxide nanoparticle coated with biocompatible copolymer for anticancer drug delivery. Pharmaceutics 11, 120.

Hoshyar, N., Gray, S., Han, H., Bao, G., 2016. The effect of nanoparticle size on in vivo pharmacokinetics and cellular interaction. Nanomedicine (London, England) 11, 673-692.

Hossen, S., Hossain, M.K., Basher, M.K., Mia, M.N.H., Rahman, M.T., Uddin, M.J., 2019. Smart nanocarrier-based drug delivery systems for cancer therapy and toxicity studies: A review. J. Adv. Res. 15, 1-18.

Howington, J.A., Blum, M.G., Chang, A.C., Balekian, A.A., Murthy, S.C., 2013. Treatment of stage I and II non-small cell lung cancer: Diagnosis and management of lung cancer, 3rd ed: American college of chest physicians evidence-based clinical practice guidelines. Chest 143, e278S-e313S.

Hu, Q., Sun, W., Wang, C., Gu, Z., 2016. Recent advances of cocktail chemotherapy by combination drug delivery systems. Adv. Drug Del. Rev. 98, 19-34.

Huang, C.-Y., Ju, D.-T., Chang, C.-F., Muralidhar Reddy, P., Velmurugan, B.K., 2017. A review on the effects of current chemotherapy drugs and natural agents in treating non-small cell lung cancer. Biomedicine 7, 23-23.

Huang, J., Li, Y., Orza, A., Lu, Q., Guo, P., Wang, L., Yang, L., Mao, H., 2016. Magnetic nanoparticle facilitated drug delivery for cancer therapy with targeted and image-guided approaches. Adv. Funct. Mater. 26, 3818-3836.

Huang, X., Li, L., Liu, T., Hao, N., Liu, H., Chen, D., Tang, F., 2011. The shape effect of mesoporous silica nanoparticles on biodistribution, clearance, and biocompatibility in vivo. ACS Nano 5, 5390-5399.

Imai, K., Takaoka, A., 2006. Comparing antibody and small-molecule therapies for cancer. Nat. Rev. Cancer 6, 714-727.

Ip, C., Dong, Y., Ip, M.M., Banni, S., Carta, G., Angioni, E., Murru, E., Spada, S., Melis, M.P., Saebo, A., 2002. Conjugated linoleic acid isomers and mammary cancer prevention. Nutr. Cancer 43, 52-58.

Ishiwata, H., Suzuki, N., Ando, S., Kikuchi, H., Kitagawa, T., 2000. Characteristics and biodistribution of cationic liposomes and their DNA complexes. J. Control. Release 69, 139-148.

Jaracz, S., Chen, J., Kuznetsova, L.V., Ojima, I., 2005. Recent advances in tumor-targeting anticancer drug conjugates. Bioorg. Med. Chem. 13, 5043-5054.

Jászai, J., Schmidt, M.H.H., 2019. Trends and challenges in tumor anti-angiogenic therapies. Cells 8, 1102.

Jiang, J., Liang, X., Zhou, X., Huang, R., Chu, Z., Zhan, Q., 2013. Non-platinum doublets were as effective as platinum-based doublets for chemotherapy-naïve advanced non-small-cell lung cancer in the era of third-generation agents. J. Cancer Res. Clin. Oncol. 139, 25-38.

Ke, X.Y., Zhao, B.J., Zhao, X., Wang, Y., Huang, Y., Chen, X.M., Zhao, B.X., Zhao, S.S., Zhang, X., Zhang, Q., 2010. The therapeutic efficacy of conjugated linoleic acid - paclitaxel on glioma in the rat. Biomaterials 31, 5855-5864.

Kelley, N.S., Hubbard, N.E., Erickson, K.L., 2007. Conjugated linoleic acid isomers and cancer. J. Nutr. 137, 2599-2607.

Kenfield, S.A., Wei, E.K., Stampfer, M.J., Rosner, B.A., Colditz, G.A., 2008. Comparison of aspects of smoking among the four histological types of lung cancer. Tob. Control 17, 198-204.

Kennedy, A., Martinez, K., Schmidt, S., Mandrup, S., LaPoint, K., McIntosh, M., 2010. Antiobesity mechanisms of action of conjugated linoleic acid. J. Nutr. Biochem. 21, 171-179.

Khalid, A., Persano, S., Shen, H., Zhao, Y., Blanco, E., Ferrari, M., Wolfram, J., 2017. Strategies for improving drug delivery: Nanocarriers and microenvironmental priming. Expert Opin. Drug Deliv. 14, 865-877.

Khan, M.I., Mohammad, A., Patil, G., Naqvi, S.A.H., Chauhan, L.K.S., Ahmad, I., 2012. Induction of ROS, mitochondrial damage and autophagy in lung epithelial cancer cells by iron oxide nanoparticles. Biomaterials 33, 1477-1488.

Khanal, R.C., 2004. Potential health benefits of conjugated linoleic acid (CLA): A review. Asian-Australas J. Anim. Sci. 17, 1315-1328.

Khizar, S., Ahmad, N.M., Zine, N., Jaffrezic-Renault, N., Errachid-el-salhi, A., Elaissari, A., 2021. Magnetic nanoparticles: From synthesis to theranostic applications. ACS Appl. Nano Mater. 4, 4284-4306.

Kim, E.J., Lee, S.Y., Woo, M.K., Choi, S.I., Kim, T.R., Kim, M.J., Kim, K.C., Cho, E.W., Kim, I.G., 2012. Fibulin-3 promoter methylation alters the invasive behavior of non-small cell lung cancer cell lines via MMP-7 and MMP-2 regulation. Int. J. Oncol. 40, 402-408.

Kohler, N., Sun, C., Wang, J., Zhang, M., 2005. Methotrexate-modified superparamagnetic nanoparticles and their intracellular uptake into human cancer cells. Langmuir 21, 8858-8864.

Koivunen, E., Arap, W., Valtanen, H., Rainisalo, A., Medina, O.P., Heikkilä, P., Kantor, C., Gahmberg, C.G., Salo, T., Konttinen, Y.T., Sorsa, T., Ruoslahti, E., Pasqualini, R., 1999. Tumor targeting with a selective gelatinase inhibitor. Nat. Biotechnol. 17, 768-774.

Kudr, J., Haddad, Y., Richtera, L., Heger, Z., Cernak, M., Adam, V., Zitka, O., 2017. Magnetic nanoparticles: From design and synthesis to real world applications. Nanomaterials (Basel, Switzerland) 7, 243.

Kydd, J., Jadia, R., Velpurisiva, P., Gad, A., Paliwal, S., Rai, P., 2017. Targeting strategies for the combination treatment of cancer using drug delivery systems. Pharmaceutics 9, 46.

Le Chevalier, T., 2011. Non-small cell lung cancer: The challenges of the next decade. Front. Oncol. 1, 29.

Lee, K.W., Lee, H.J., Cho, H.Y., Kim, Y.J., 2005. Role of the conjugated linoleic acid in the prevention of cancer. Crit. Rev. Food Sci. Nutr. 45, 135-144.

Lee, W. H., Loo, C. Y., Traini, D., Young, P.M., 2015. Inhalation of nanoparticle-based drug for lung cancer treatment: Advantages and challenges. Asian J. Pharm. 10, 481-489.

Lee, W. H., Loo, C. Y., Young, P.M., Traini, D., Mason, R.S., Rohanizadeh, R., 2014. Recent advances in curcumin nanoformulation for cancer therapy. Expert Opin. Drug Deliv. 11, 1183-1201.

Li, R. N., Da, X. H., Li, X., Lu, Y.-S., Gu, F. F., Liu, Y., 2021. Functionalized magnetic nanoparticles for drug delivery in tumor therapy. Chin. Phys. B 30, 017502.

Li, W., Yu, H., Ding, D., Chen, Z., Wang, Y., Wang, S., Li, X., Keidar, M., Zhang, W., 2019. Cold atmospheric plasma and iron oxide-based magnetic nanoparticles for synergetic lung cancer therapy. Free Radic. Biol. Med. 130, 71-81.

Liang, N., Liu, L., Li, P., Xu, Y., Hou, Y., Peng, J., Song, Y., Bing, Z., Wang, Y., Wang, Y., Jia, Z., Yang, X., Li, D., Xu, H., Yu, Q., Li, S., Hu, Z., Yang, Y., 2020. Efficient isolation and quantification of circulating tumor cells in non-small cell lung cancer patients using peptide-functionalized magnetic nanoparticles. J. Thorac. Dis. 12, 4262-4273.

Lin, S. R., Chang, C. H., Hsu, C. F., Tsai, M. J., Cheng, H., Leong, M.K., Sung, P. J., Chen, J. C., Weng, C. F., 2020. Natural compounds as potential adjuvants to cancer therapy: Preclinical evidence. Br. J. Pharmacol. 177, 1409-1423.

Liu, S., Yu, B., Wang, S., Shen, Y., Cong, H., 2020a. Preparation, surface functionalization and application of Fe3O4 magnetic nanoparticles. Adv. Colloid Interface Sci. 281, 102165, 10.1016/j.cis.2020.102165.

Liu, T., Wu, H.J., Liang, Y., Liang, X.J., Huang, H.C., Zhao, Y.Z., Liao, Q.C., Chen, Y.Q., Leng, A.M., Yuan, W.J., Zhang, G.Y., Peng, J., Chen, Y.H., 2016. Tumor-specific expression of shVEGF and suicide gene as a novel strategy for esophageal cancer therapy. World J. Gastroenterol. 22, 5342-5352.

Liu, X., Zhang, Y., Wang, Y., Zhu, W., Li, G., Ma, X., Zhang, Y., Chen, S., Tiwari, S., Shi, K., Zhang, S., Fan, H.M., Zhao, Y.X., Liang, X.-J., 2020b. Comprehensive understanding of magnetic hyperthermia for improving antitumor therapeutic efficacy. Theranostics 10, 3793-3815.

Lombardo, D., Kiselev, M.A., Caccamo, M.T., 2019. Smart nanoparticles for drug delivery application: Development of versatile nanocarrier platforms in biotechnology and nanomedicine. J. Nanomater. 2019, 3702518.

Lu, A.-H., Salabas, E.L., Schüth, F., 2007. Magnetic nanoparticles: Synthesis, protection, functionalization, and application. Angew. Chem. Int. Ed. 46, 1222-1244.

Maggiora, M., Bologna, M., Cerù, M.P., Possati, L., Angelucci, A., Cimini, A., Miglietta, A., Bozzo, F., Margiotta, C., Muzio, G., 2004. An overview of the effect of linoleic and conjugated-linoleic acids on the growth of several human tumor cell lines. Int. J. Cancer 112, 909-919.

Mahmoudi, M., Sant, S., Wang, B., Laurent, S., Sen, T., 2011. Superparamagnetic iron oxide nanoparticles (SPIONs): Development, surface modification and applications in chemotherapy. Adv. Drug Deliv. Rev. 63, 24-46.

Majidi, S., Zeinali Sehrig, F., Farkhani, S.M., Soleymani Goloujeh, M., Akbarzadeh, A., 2016. Current methods for synthesis of magnetic nanoparticles. Artif. Cells Nanomed. Biotechnol. 44, 722-734.

Malik, M.A., Wani, M.Y., Hashim, M.A., 2012. Microemulsion method: A novel route to synthesize organic and inorganic nanomaterials: 1st nano update. Arab. J. Chem. 5, 397-417.

Mansouri, M., Nazarpak, M.H., Solouk, A., Akbari, S., Hasani-Sadrabadi, M.M., 2017. Magnetic responsive of paclitaxel delivery system based on SPION and palmitoyl chitosan. J. Magn. Magn. Mater. 421, 316-325.

Markowitz, S.B., Levin, S.M., Miller, A., Morabia, A., 2013. Asbestos, asbestosis, smoking, and lung cancer. New findings from the North American insulator cohort. Am. J. Respir. Crit. Care Med. 188, 90-96.

Mascolo, M.C., Pei, Y., Ring, T.A., 2013. Room temperature co-precipitation synthesis of magnetite nanoparticles in a large pH window with different bases. Materials (Basel, Switzerland) 6, 5549-5567.

Mashreghi, M., Azarpara, H., Bazaz, M.R., Jafari, A., Masoudifar, A., Mirzaei, H., 2018. Angiogenesis biomarkers and their targeting ligands as potential targets for tumor angiogenesis. J. Cell. Physiol. 233, 2949-2965.

Masso-Welch, P.A., Zangani, D., Ip, C., Vaughan, M.M., Shoemaker, S., Ramirez, R.A., Ip, M.M., 2002. Inhibition of angiogenesis by the cancer chemopreventive agent conjugated linoleic acid. Cancer Res. 62, 4383-4389.

Masso-Welch, P.A., Zangani, D., Ip, C., Vaughan, M.M., Shoemaker, S.F., McGee, S.O., Ip, M.M., 2004. Isomers of conjugated linoleic acid differ in their effects on angiogenesis and survival of mouse mammary adipose vasculature. J. Nutr. 134, 299-307.

Masters, G.A., Temin, S., Azzoli, C.G., Giaccone, G., Baker, S., Jr., Brahmer, J.R., Ellis, P.M., Gajra, A., Rackear, N., Schiller, J.H., Smith, T.J., Strawn, J.R., Trent, D., Johnson, D.H., 2015. Systemic therapy for stage IV non-small-cell lung cancer: American society of clinical oncology clinical practice guideline update. J. Clin. Oncol. 33, 3488-3515.

Mehnath, S., Arjama, M., Rajan, M., Annamalai, G., Jeyaraj, M., 2018. Co-encapsulation of dual drug loaded in MLNPs: Implication on sustained drug release and effectively inducing apoptosis in oral carcinoma cells. Biomed. Pharmacother. 104, 661-671.

Michaloski, J.S., Redondo, A.R., Magalhães, L.S., Cambui, C.C., Giordano, R.J., 2016. Discovery of pan-VEGF inhibitory peptides directed to the extracellular ligand-binding domains of the VEGF receptors. Sci. Adv. 2, e1600611-e1600611.

Molina, J.R., Yang, P., Cassivi, S.D., Schild, S.E., Adjei, A.A., 2008. Non-small cell lung cancer: Epidemiology, risk factors, treatment, and survivorship. Mayo Clin. Proc. 83, 584-594.

Moon, E.J., Lee, Y.M., Kim, K.W., 2003. Anti-angiogenic activity of conjugated linoleic acid on basic fibroblast growth factor-induced angiogenesis. Oncol. Rep. 10, 617-621.

Morales-Cruz, M., Delgado, Y., Castillo, B., Figueroa, C.M., Molina, A.M., Torres, A., Milián, M., Griebenow, K., 2019. Smart targeting to improve cancer therapeutics. Drug Des. Devel. Ther. 13, 3753-3772.

Moreira, T.G., Horta, L.S., Gomes-Santos, A.C., Oliveira, R.P., Queiroz, N.M.G.P., Mangani, D., Daniel, B., Vieira, A.T., Liu, S., Rodrigues, A.M., Gomes, D.A., Gabriely, G., Ferreira, E., Weiner, H.L., Rezende, R.M., Nagy, L., Faria, A.M.C., 2019. CLA-supplemented diet accelerates experimental colorectal cancer by inducing TGF-β-producing macrophages and t cells. Mucosal Immunol. 12, 188-199.

Mosayebi, J., Kiyasatfar, M., Laurent, S., 2017. Synthesis, functionalization, and design of magnetic nanoparticles for theranostic applications. Adv. Healthc. Mater. 6, 1700306.

Mumtaz, T., Qindeel, M., Asim.ur.Rehman, Tarhini, M., Ahmed, N., Elaissari, A., 2020. Exploiting proteases for cancer theranostic through molecular imaging and drug delivery. Int. J. Pharm. 587, 119712.

Munaweera, I., Shi, Y., Koneru, B., Saez, R., Aliev, A., Di Pasqua, A.J., Balkus, K.J., 2015. Chemoradiotherapeutic magnetic nanoparticles for targeted treatment of nonsmall cell lung cancer. Mol. Pharm. 12, 3588-3596.

Muzio, G., Miola, M., Ferraris, S., Maggiora, M., Bertone, E., Puccinelli, M.P., Ricci, M., Borroni, E., Canuto, R.A., Verné, E., Follenzi, A., 2017. Innovative superparamagnetic iron-oxide nanoparticles coated with silica and conjugated with linoleic acid: Effect on tumor cell growth and viability. Mater. Sci. Eng. C 76, 439-447.

Naderinezhad, S., Amoabediny, G., Haghiralsadat, F., 2017. Co-delivery of hydrophilic and hydrophobic anticancer drugs using biocompatible pH-sensitive lipid-based nano-carriers for multidrug-resistant cancers. RSC Advances 7, 30008-30019.

Nagase, H., Woessner, J.F., Jr., 1999. Matrix metalloproteinases. J. Biol. Chem. 274, 21491-21494.

Nana, A.B.A., Marimuthu, T., Kondiah, P.P.D., Choonara, Y.E., Du Toit, L.C., Pillay, V., 2019. Multifunctional magnetic nanowires: Design, fabrication, and future prospects as cancer therapeutics. Cancers (Basel) 11, 1956.

Narvekar, M., Xue, H.Y., Eoh, J.Y., Wong, H.L., 2014. Nanocarrier for poorly water-soluble anticancer drugs—barriers of translation and solutions. AAPS PharmSciTech 15, 822-833.

Ndinguri, M.W., Bhowmick, M., Tokmina-Roszyk, D., Robichaud, T.K., Fields, G.B., 2012. Peptide-based selective inhibitors of matrix metalloproteinase-mediated activities. Molecules 17, 14230-14248.

Nejati-Koshki, K., Mesgari, M., Ebrahimi, E., Abbasalizadeh, F., Fekri Aval, S., Khandaghi, A.A., Abasi, M., Akbarzadeh, A., 2014. Synthesis and in vitro study of cisplatin-loaded Fe3O4 nanoparticles modified with PLGA-PEG6000 copolymers in treatment of lung cancer. J. Microencapsul. 31, 815-823.

Noguchi, M., Morikawa, A., Kawasaki, M., Matsuno, Y., Yamada, T., Hirohashi, S., Kondo, H., Shimosato, Y., 1995. Small adenocarcinoma of the lung. Histologic characteristics and prognosis. Cancer 75, 2844-2852.

Nosrati, H., Tarantash, M., Bochani, S., Charmi, J., Bagheri, Z., Fridoni, M., Abdollahifar, M.-A., Davaran, S., Danafar, H., Kheiri Manjili, H., 2019. Glutathione (GSH) peptide conjugated magnetic nanoparticles as blood–brain barrier shuttle for mri-monitored brain delivery of paclitaxel. ACS Biomater. Sci. Eng. 5, 1677-1685.

Nurgali, K., Jagoe, R.T., Abalo, R., 2018. Editorial: Adverse effects of cancer chemotherapy: Anything new to improve tolerance and reduce sequelae? Front. Pharmacol. 9, 245-245.

Ochoa, J.J., Farquharson, A.J., Grant, I., Moffat, L.E., Heys, S.D., Wahle, K.W., 2004. Conjugated linoleic acids (CLAs) decrease prostate cancer cell proliferation: Different molecular mechanisms for cis-9, trans-11 and *trans*-10, *cis*-12 isomers. Carcinogenesis 25, 1185-1191.

Olaussen, K.A., Postel-Vinay, S., 2016. Predictors of chemotherapy efficacy in non-small-cell lung cancer: A challenging landscape. Ann. Oncol. 27, 2004-2016.

Olivier, M., Hollstein, M., Hainaut, P., 2010. Tp53 mutations in human cancers: Origins, consequences, and clinical use. Cold Spring Harb. Perspect. Biol. 2, a001008-a001008.

Oun, R., Moussa, Y.E., Wheate, N.J., 2018. The side effects of platinum-based chemotherapy drugs: A review for chemists. Dalton Trans. 47, 6645-6653.

Palanisamy, S., Wang, Y.-M., 2019. Superparamagnetic iron oxide nanoparticulate system: Synthesis, targeting, drug delivery and therapy in cancer. Dalton Trans. 48, 9490-9515.

Pierre, A.-S., Minville-Walz, M., Fèvre, C., Hichami, A., Gresti, J., Pichon, L., Bellenger, S., Bellenger, J., Ghiringhelli, F., Narce, M., Rialland, M., 2013. *Trans*-10, *cis*-12 conjugated linoleic acid induced cell death in human colon cancer cells through reactive oxygen species-mediated ER stress. BBA Mol. Cell Biol. Lipids 1831, 759-768.

Popper, H.H., 2016. Progression and metastasis of lung cancer. Cancer Metastasis Rev. 35, 75-91.

Quintero-Fabián, S., Arreola, R., Becerril-Villanueva, E., Torres-Romero, J.C., Arana-Argáez, V., Lara-Riegos, J., Ramírez-Camacho, M.A., Alvarez-Sánchez, M.E., 2019. Role of matrix metalloproteinases in angiogenesis and cancer. Front. Oncol. 9, 1370-1370.

Rajabi, M., Mousa, S.A., 2017. The role of angiogenesis in cancer treatment. Biomedicines 5, 34.

Rakib, M.A., Lee, W.S., Kim, G.S., Han, J.H., Kim, J.O., Ha, Y.L., 2013. Antiproliferative action of conjugated linoleic acid on human mcf-7 breast cancer cells mediated by enhancement of gap junctional intercellular communication through inactivation of NF-κB. Evid. Based Complement. Alternat. Med. 2013, 429393.

Reczyńska, K., Marchwica, P., Khanal, D., Borowik, T., Langner, M., Pamuła, E., Chrzanowski, W., 2020a. Stimuli-sensitive fatty acid-based microparticles for the treatment of lung cancer. Mater. Sci. Eng. C 111, 110801.

Reczyńska, K., Marszałek, M., Zarzycki, A., Reczyński, W., Kornaus, K., Pamuła, E., Chrzanowski, W., 2020b. Superparamagnetic iron oxide nanoparticles modified with silica layers as potential agents for lung cancer treatment. Nanomaterials 10, 1076.

Revia, R.A., Zhang, M., 2016. Magnetite nanoparticles for cancer diagnosis, treatment, and treatment monitoring: Recent advances. Mater. Today (Kidlington, England) 19, 157-168.

Rossi, E., Della Casa, L., Piana, S., Iannone, A., 2012. Conjugated linoleic acid isomers modulate protein expression profile in rat hepatocytes. Genes Nutr. 7, 511-527.

Saadat, M., Manshadi, M.K.D., Mohammadi, M., Zare, M.J., Zarei, M., Kamali, R., Sanati-Nezhad, A., 2020. Magnetic particle targeting for diagnosis and therapy of lung cancers. J. Control. Release 328, 776-791.

Sadhukha, T., Wiedmann, T.S., Panyam, J., 2013. Inhalable magnetic nanoparticles for targeted hyperthermia in lung cancer therapy. Biomaterials 34, 5163-5171.

Sandler, A., Gray, R., Perry, M.C., Brahmer, J., Schiller, J.H., Dowlati, A., Lilenbaum, R., Johnson, D.H., 2006. Paclitaxel-carboplatin alone or with bevacizumab for non-small-cell lung cancer. N. Engl. J. Med. 355, 2542-2550.

Scagliotti, G., Govindan, R., 2010. Targeting angiogenesis with multitargeted tyrosine kinase inhibitors in the treatment of non-small cell lung cancer. Oncologist 15, 436-446.

Scheff, R.J., Schneider, B.J., 2013. Non-small-cell lung cancer: Treatment of late stage disease: Chemotherapeutics and new frontiers. Semin. Intervent. Radiol. 30, 191-198.

Schirrmacher, V., 2019. From chemotherapy to biological therapy: A review of novel concepts to reduce the side effects of systemic cancer treatment. Int. J. Oncol. 54, 407-419.

Schønberg, S., Krokan, H.E., 1995. The inhibitory effect of conjugated dienoic derivatives (CLA) of linoleic acid on the growth of human tumor cell lines is in part due to increased lipid peroxidation. Anticancer Res. 15, 1241-1246.

Senapati, S., Mahanta, A.K., Kumar, S., Maiti, P., 2018. Controlled drug delivery vehicles for cancer treatment and their performance. Signal Transduct. Target. Ther. 3, 7.

Shahzad, M.M.K., Felder, M., Ludwig, K., Van Galder, H.R., Anderson, M.L., Kim, J., Cook, M.E., Kapur, A.K., Patankar, M.S., 2018. Trans10,cis12 conjugated linoleic acid inhibits proliferation and migration of ovarian cancer cells by inducing ER stress, autophagy, and modulation of src. PLoS One 13, e0189524.

Shiraishi, R., Iwakiri, R., Fujise, T., Kuroki, T., Kakimoto, T., Takashima, T., Sakata, Y., Tsunada, S., Nakashima, Y., Yanagita, T., Fujimoto, K., 2010. Conjugated linoleic acid suppresses colon carcinogenesis in azoxymethane-pretreated rats with long-term feeding of diet containing beef tallow. J. Gastroenterol. 45, 625-635.

Shultz, T.D., Chew, B.P., Seaman, W.R., Luedecke, L.O., 1992. Inhibitory effect of conjugated dienoic derivatives of linoleic acid and beta-carotene on the in vitro growth of human cancer cells. Cancer Lett. 63, 125-133.

Siegel, R., Ma, J., Zou, Z., Jemal, A., 2014. Cancer statistics, 2014. CA Cancer J. Clin. 64, 9-29.

Slowikowski, B.K., Drzewiecka, H., Malesza, M., Madry, I., Sterzynska, K., Jagodzinski, P.P., 2020. The influence of conjugated linoleic acid on the expression of peroxisome proliferator-activated receptor-gamma and selected apoptotic genes in non-small cell lung cancer. Mol. Cell. Biochem. 466, 65-82.

Spyratos, D., Zarogoulidis, P., Porpodis, K., Tsakiridis, K., Machairiotis, N., Katsikogiannis, N., Kougioumtzi, I., Dryllis, G., Kallianos, A., Rapti, A., Li, C., Zarogoulidis, K., 2013. Occupational exposure and lung cancer. J. Thorac. Dis. 5 Suppl 4, S440-445.

Sukumar, U.K., Bhushan, B., Dubey, P., Matai, I., Sachdev, A., Packirisamy, G., 2013. Emerging applications of nanoparticles for lung cancer diagnosis and therapy. Int. Nano Lett. 3, 45.

Sun, Q., Xu, X., 2015. A promising future for peptides in ophthalmology: Work effectively and smartly. Curr. Med. Chem. 22, 1030-1040.

Tanmahasamut, P., Liu, J., Hendry, L.B., Sidell, N., 2004. Conjugated linoleic acid blocks estrogen signaling in human breast cancer cells. J. Nutr. 134, 674-680.

Teleanu, R.I., Chircov, C., Grumezescu, A.M., Teleanu, D.M., 2019. Tumor angiogenesis and anti-angiogenic strategies for cancer treatment. J. Clin. Med. 9, 84.

Thun, M.J., DeLancey, J.O., Center, M.M., Jemal, A., Ward, E.M., 2010. The global burden of cancer: Priorities for prevention. Carcinogenesis 31, 100-110.

Tietze, R., Zaloga, J., Unterweger, H., Lyer, S., Friedrich, R.P., Janko, C., Pöttler, M., Dürr, S., Alexiou, C., 2015. Magnetic nanoparticle-based drug delivery for cancer therapy. Biochem. Biophys. Res. Commun. 468, 463-470.

Tran, N., Webster, T., 2010. Magnetic nanoparticles: Biomedical applications and challenges. J. Mater. Chem. 20, 8760-8767.

Vasconcellos, V.F., Marta, G.N., da Silva, E.M., Gois, A.F., de Castria, T.B., Riera, R., 2020. Cisplatin versus carboplatin in combination with third-generation drugs for advanced non-small cell lung cancer. Cochrane Database Syst. Rev. 1, 1.

Veiseh, O., Gunn, J.W., Zhang, M., 2010. Design and fabrication of magnetic nanoparticles for targeted drug delivery and imaging. Adv. Drug Del. Rev. 62, 284-304.

Villeneuve, P.J., Parent, M.-É., Harris, S.A., Johnson, K.C., Canadian Cancer Registries Epidemiology Research, G., 2012. Occupational exposure to asbestos and lung cancer in

men: Evidence from a population-based case-control study in eight canadian provinces. BMC Cancer 12, 595-595.

Visioli, F., Giordano, E., Nicod, N.M., Dávalos, A., 2012. Molecular targets of omega 3 and conjugated linoleic fatty acids - "micromanaging" cellular response. Front. Physiol. 3, 42-42.

Wahajuddin, Arora, S., 2012. Superparamagnetic iron oxide nanoparticles: Magnetic nanoplatforms as drug carriers. Int. J. Nanomed. 7, 3445-3471.

Wan, X., Song, Y., Song, N., Li, J., Yang, L., Li, Y., Tan, H., 2016. The preliminary study of immune superparamagnetic iron oxide nanoparticles for the detection of lung cancer in magnetic resonance imaging. Carbohydr. Res. 419, 33-40.

Wang, L.S., Huang, Y.W., Sugimoto, Y., Liu, S., Chang, H.L., Ye, W., Shu, S., Lin, Y.C., 2005. Effects of human breast stromal cells on conjugated linoleic acid (CLA) modulated vascular endothelial growth factor-A (VEGF-A) expression in MFC-7 cells. Anticancer Res. 25, 4061-4068.

Wang, M. S., Chen, L., Xiong, Y. Q., Xu, J., Wang, J. P., Meng, Z. L., 2017. Iron oxide magnetic nanoparticles combined with actein suppress non-small-cell lung cancer growth in a p53-dependent manner. Int. J. Nanomed. 12, 7627-7651.

Wei, Y., Zhao, L., 2014. Passive lung-targeted drug delivery systems via intravenous administration. Pharm. Dev. Technol. 19, 129-136.

Wheatley-Price, P., Shepherd, F.A., 2008. Targeting angiogenesis in the treatment of lung cancer. J. Thorac. Oncol. 3, 1173-1184.

Woodman, C., Vundu, G., George, A., Wilson, C.M., 2020. Applications and strategies in nanodiagnosis and nanotherapy in lung cancer. Semin. Cancer Biol. 69, 349-364.

Wu, M., Huang, S., 2017. Magnetic nanoparticles in cancer diagnosis, drug delivery and treatment. Mol. Clin. Oncol. 7, 738-746.

Yamasaki, M., Chujo, H., Koga, Y., Oishi, A., Rikimaru, T., Shimada, M., Sugimachi, K., Tachibana, H., Yamada, K., 2002. Potent cytotoxic effect of the trans10, cis12 isomer of conjugated linoleic acid on rat hepatoma dRLh-84 cells. Cancer Lett. 188, 171-180.

Yang, I.A., Holloway, J.W., Fong, K.M., 2013. Genetic susceptibility to lung cancer and co-morbidities. J. Thorac. Dis. 5 Suppl 5, S454-S462.

Yigit, M.V., Moore, A., Medarova, Z., 2012. Magnetic nanoparticles for cancer diagnosis and therapy. Pharm. Res. 29, 1180-1188.

Yokoyama, T., Tam, J., Kuroda, S., Scott, A.W., Aaron, J., Larson, T., Shanker, M., Correa, A.M., Kondo, S., Roth, J.A., Sokolov, K., Ramesh, R., 2011. EGFR-targeted hybrid plasmonic magnetic nanoparticles synergistically induce autophagy and apoptosis in non-small cell lung cancer cells. PLoS One 6, e25507.

Yoo, M. K., Park, I. K., Lim, H. T., Lee, S. J., Jiang, H. L., Kim, Y. K., Choi, Y. J., Cho, M. H., Cho, C. S., 2012. Folate-PEG-superparamagnetic iron oxide nanoparticles for lung cancer imaging. Acta Biomater. 8, 3005-3013.

Yu, H., Wang, Y., Wang, S., Li, X., Li, W., Ding, D., Gong, X., Keidar, M., Zhang, W., 2018. Paclitaxel-loaded core–shell magnetic nanoparticles and cold atmospheric plasma inhibit non-small cell lung cancer growth. ACS Appl. Mater. Interfaces 10, 43462-43471.

Yuan, D.M., Lv, Y.L., Yao, Y.W., Miao, X.H., Wang, Q., Xiao, X.W., Yin, J., Shi, Y., Shi, M.Q., Zhang, X.W., Song, Y., 2012. Efficacy and safety of abraxane in treatment of progressive and recurrent non-small cell lung cancer patients: A retrospective clinical study. Thorac. Cancer 3, 341-347.

Zappa, C., Mousa, S.A., 2016. Non-small cell lung cancer: Current treatment and future advances. Transl. Lung Cancer Res. 5, 288-300.

Zein, R., Sharrouf, W., Selting, K., 2020. Physical properties of nanoparticles that result in improved cancer targeting. J. Oncol. 2020, 5194780.

Zhang, Q., Liu, Q., Du, M., Vermorken, A., Cui, Y., Zhang, L., Guo, L., Ma, L., Chen, M., 2019. Cetuximab and doxorubicin loaded dextran-coated Fe3O4 magnetic nanoparticles as novel targeted nanocarriers for non-small cell lung cancer. J. Magn. Magn. Mater. 481, 122-128.

Zhang, R.X., Wong, H.L., Xue, H.Y., Eoh, J.Y., Wu, X.Y., 2016. Nanomedicine of synergistic drug combinations for cancer therapy – strategies and perspectives. J. Control. Release 240, 489-503.

Zhang, Y., He, B., Liu, K., Ning, L., Luo, D., Xu, K., Zhu, W., Wu, Z., Huang, J., Xu, X., 2017. A novel peptide specifically binding to vegf receptor suppresses angiogenesis in vitro and in vivo. Signal Transduct. Target. Ther. 2, 17010.

Zhong, T., Yao, X., Zhang, S., Guo, Y., Duan, X. C., Ren, W., Dan, H., Yin, Y. F., Zhang, X., 2016. A self-assembling nanomedicine of conjugated linoleic acid-paclitaxel conjugate (CLA-PTX) with higher drug loading and carrier-free characteristic. Sci. Rep. 6, 36614.

CHAPTER 3

SYNTHESIS OF NOVEL CONJUGATED LINOLEIC ACID (CLA)-COATED SUPERPARAMAGNETIC IRON OXIDE NANOPARTICLES (SPIONs) FOR THE DELIVERY OF PACLITAXEL WITH ENHANCED *IN VITRO* ANTI-PROLIFERATIVE ACTIVITY ON A549 LUNG CANCER CELLS

3.1. Introduction

The notable success in the application of magnetic nanoparticles (MNPs) in non-small-cell lung carcinoma (NSCLC) therapy, as well as the anticancer merits of conjugated linoleic acid (CLA) discussed in the previous chapter allow for the exploitation of these materials in the design of potent drug delivery nanosystems for the management of NSCLC. As such, this chapter describes the innovative design of a novel paclitaxel (PTX) delivery nanosystem comprising superparamagnetic iron oxide nanoparticles and CLA as a potential nanomedicine in NSCLC therapy. NSCLC is the most prevalent type of lung cancer affecting millions of people worldwide, with almost 85% of diagnosed lung cancer cases being NSCLC (Zhou et al., 2021). The treatment of NSCLC continues to be a daunting challenge, with combinational chemotherapy as first-line treatment reportedly at its therapeutic plateau (Ngema et al., 2021).

Intolerable toxicity due to high doses and non-specificity are key hindrances in the effective use of combinational chemotherapy (Genova et al., 2020; Nana et al., 2019; Salgia et al., 2021; Ye et al., 2021). PTX is a first-line anticancer drug used in platinum-based combination chemotherapy for advanced NSCLC (Chen et al., 2017; Gui et al., 2021). PTX shows adequate efficacy at the onset of treatment, however, subsequent side effects (i.e., neutropenia, myalgia, allergic reactions) and resistance (caused by alterations in drug metabolism) are major setbacks for effective NSCLC treatment (Paz-Ares et al., 2018). Consequently, numerous studies have proposed the use of targeted nano-enabled drug delivery systems, including nanoparticles and nanoemulsions, as an approach to enhance the efficacy of PTX in NSCLC therapy (Cheng et al., 2021; Crintea et al., 2021; García-Fernández et al., 2020; Mohtar et al., 2021; Salehi et al., 2020; Zhou et al., 2021).

Particularly, the use of SPIONs as anticancer drug delivery vectors has shown enormous success over the years (Ansari et al., 2018; El-Sherbiny et al., 2020; Zhi et al., 2020; Zhuang et al., 2020). SPIONs offer desirable features as drug transporters for NSCLC therapy, such as high drug-loading capacity, small size (<100 nm) to allow penetration into lung tumor, and a biocompatible outer-shell that can be functionalized with targeting ligands to achieve active targeted drug delivery (Reczyńska et al., 2020a; Reczyńska et al., 2020b; Sadhukha et al., 2013). Studies have shown that anticancer drugs loaded into SPIONs present with high

bioavailability (Reczyńska et al., 2020a; Senapati et al., 2018; Wahajuddin and Arora, 2012), and coating prevents particle aggregation and extends the systemic circulation time of SPIONs (Dulińska-Litewka et al., 2019; Nelson et al., 2020). In addition, coating of SPIONs with naturally derived anticancer compounds, such as conjugated linoleic acid, could render them as excellent nanovectors for targeted NSCLC therapy.

CLA has been previously explored to have potential anticancer activity and comprises of ~28 isomers (Dachev et al., 2021; den Hartigh, 2019). CLA has been shown to suppress proliferation in breast (Rakib et al., 2013), colon (Shiraishi et al., 2010), stomach (Ha et al., 1990), colorectal (Moreira et al., 2019), and prostate cancer cells (Ochoa et al., 2004). The *trans*-10,*cis*-12 CLA isomer (10E, 12Z CLA) is one of two biologically active isomers of CLA. The 10E, 12Z CLA reportedly acts on adipocytes where it limits lipid uptake by blocking stearoyl-CoA desaturase and lipoprotein lipase activity and affects lipid metabolism in cancer cells, which subsequently halts cell growth and metastasis (Masso-Welch et al., 2004; Zhang et al., 2018). Tumor cells require high energy supply to proliferate and metastasize, hence affecting lipid metabolism pathways, which halts their growth and metastasis (Fernández et al., 2020; Long et al., 2018). In addition, the hydrophobic nature of CLA is suitable for partitioning hydrophobic drugs such as PTX, thus allowing higher drug loading capacity and encapsulation into nanostructures.

Accordingly, in this study, we describe the novel inclusion of CLA as a surface directing agent for efficient drug loading on SPIONS for potential targeted therapy in NSCLC. The combination of PTX and SPIONs with a natural fatty acid such as CLA (with potential anticancer activity) could yield a more efficacious nanomedicine for NSCLC chemotherapy with enhanced anti-proliferative activity and biocompatibility. To investigate the effect of CLA functionalization of SPIONs, a nanosystem comprising 10E, 12Z CLA surface-coated SPIONs with self-assembly of PTX (termed CLA-coated PTX-SPIONs) was synthesized and characterized for all pertinent physiochemical, pharmaceutical (including anti-proliferative activity on an A549 lung cancer cell line), and superparamagnetic properties.

3.2. Materials and Methods

3.2.1. Materials

Iron (III) chloride hexahydrate ($FeCl_3 \cdot 6H_2O$), iron (II) chloride tetrahydrate ($FeCl_2 \cdot 4H_2O$), sodium hydroxide (NaOH) pellets, conjugated linoleic acid (10E,12Z CLA) solution in ethanol, paclitaxel (PTX), and all consumables, ie., tween 80, phosphate buffered saline tablets, magnetite standard, SnakeSkin™ dialysis membrane, 3500 MWCO, Foetal Bovine Serum

(FBS), penicillin-streptomycin antibiotics, dimethyl sulfoxide (DMSO), and acid-isopropanol solubilizing agent were procured from Sigma-Aldrich (St. Louis, MO, USA). All solvents employed were of analytical grade, and were used as received.

3.2.2. Fabrication of the CLA-Coated, PXT-Loaded SPIONs (CLA-PTX-SPIONs)

3.2.2.1. Synthesis of the SPIONs

To ensure high yield, a co-precipitation method was adopted for the preparation of SPIONs (Akilo et al., 2016). Briefly, an aqueous solution of $FeCl_2 \cdot 4H_2O$ (0.3 mol) and $FeCl_3 \cdot 6H_2O$ (0.6 mol) was prepared in 60 mL N_2-purged deionized water to attain 1:2 M ratio of Fe^{2+} and Fe^{3+}. Thereafter, 0.4 M NaOH (pH = 13) was added drop-wise into the solution under continuous stirring (300 rpm) at 75°C until dark precipitates of SPIONs formed. This was executed under N_2 gas to eliminate oxygen and control the size of SPIONs produced. The formed SPIONs were centrifuged at 5000 rpm (Eppendorf Centrifuge 5804, Hamburg, Germany) for 30 min at room temperature (25°C) to eliminate any unreacted material. The precipitate (SPIONs) was washed twice with N_2-purged deionized water and separated by magnetic decantation and air dried.

3.2.2.2. Coating of the SPIONs with trans-10 cis-12 (10E, 12Z) conjugated linoleic acid

Coating of the SPIONs was carried out in a single-step reaction. Forty microliters (40 μL) from a 100 mg/mL 10E, 12Z CLA solution in ethanol was added drop-wise into a 1.5 mL suspension of SPIONs (20 mg SPIONs in 1.5 mL ethanol) in a sonication bath (Sientech Ultrasonic cleaner, Labotec, Midrand, South Africa) kept at 80°C and low frequency for 30 min. A magnet was used to precipitate the coated SPIONs. The supernatant was withdrawn, and the precipitate washed twice with deionized water and ethanol, respectively. The CLA-coated SPIONs (10E, 12Z CLA-SPIONs) were vacuum dried at 80°C for 24 h (Muzio et al., 2017; Sawisai et al., 2019). The quantity of CLA on SPIONs was then determined by thermogravimetric analysis (TGA).

3.2.2.3. Self-assembled loading of PTX into 10E, 12Z CLA-SPIONs

In order to exploit SPIONs as an anticancer drug carrier, paclitaxel (PTX) was self-assembled on the hydrophobic tails of CLA coated on SPIONs surface. To achieve this, a superlative method by Dilnawaz et al. (Dilnawaz et al., 2010) was employed, with modifications. Accordingly, 10% (*w*/*w*) PTX was used for loading into 100% (*w*/*w*) CLA-coated SPIONs. A total of 15 mg CLA-coated SPIONs was dispersed in 1.5 mL methanol and sonicated for 2

min. PTX (1.5 mg) was dissolved in 70% methanol (150 µL) and added drop-wise to the CLA-coated SPIONs suspension under continuous gradual stirring at 200 rpm (Magnetic Stirrer MSH10, Labcon, Johannesburg, South Africa) overnight to allow for the adsorption of PTX onto the hydrophobic CLA on the surface of the SPIONs. The particle suspension was centrifuged at 13,800 rpm (TC-MiniSpin Centrifuge, TopScien, Ningbo, China) for 10 min at 10°C, with subsequent washing (three times distilled water) to separate free drug. The supernatant (with free drug) was collected for quantifying the PTX loading capacity and adsorption efficiency via UV spectrophotometry (Cary™ 50, Varian Inc., Palo Alto, CA, USA). The PTX-loaded CLA-coated SPIONs subsequently lyophilized (FreeZone-50C Benchtop Freeze Dryer, Labconco, Kansas City, MO, USA) to attain free-flowing powdered CLA-coated PTX-SPIONs.

3.2.3. Physicochemical characterization of the synthesized CLA-Coated PTX-SPIONs

3.2.3.1. Analysis of chemical structure integrity and transitions

Fourier transform infrared (FTIR) spectroscopy (Spectrum 100, PerkinElmer Inc., Waltham, MA, USA) was appropriately used to comparatively analyze vibrational transitions in the chemical structures of the individual and combined components of the CLA-coated PTX-SPIONs. Samples of pristine SPIONs, CLA, PTX, and CLA-coated PTX-SPIONs were analyzed at 120 psi pressure in a range of 4000–550 cm^{-1} over 20 scans to obtain relevant spectra.

3.2.3.2. Determination of particle size, zeta potential, and overall morphology

Dynamic light scattering and phase-analysis light scattering analyses were implemented to obtain the average hydrodynamic diameter and zeta potential, respectively, of the synthesized CLA-coated PTX-SPIONs on a ZetaSizer instrument (NanoZS, Malvern Panalytical, Malvern, UK). Dried samples (10 µg; BM Series Micro Analytical Balance, BM-22, A&D Company, Ltd., Boulevard, USA) of pristine SPIONs and CLA-coated PTX-SPIONs were suspended in 1 mL distilled water followed by sonication for 10 min (Sonics Vibra Cell, Newtown, CT, USA). Samples were transferred into disposable cuvettes for hydrodynamic size and polydispersity index (PDI) analysis, thereafter into zeta potential cuvettes (DTS 1070) for surface charge analysis at 25°C. A sample of CLA-coated PTX-SPIONs was also analyzed for morphology using Scanning Electron Microscopy (SEM) (ZEISS Electron Microscopy, Carl Zeiss Microscopy Ltd., Cambridge, UK). An aliquot was carefully placed on an aluminium specimen stub and air dried before coating (×2) with gold palladium (AuPd). The sample was viewed and captured under a low (82.34 KX) and high (314.84 KX) magnification.

3.2.3.3. Determination of CLA content on CLA-Coated SPIONs

The amount of 10E, 12Z CLA coated onto SPIONs was determined using thermogravimetric analysis (TGA) (TGA 4000, PerkinElmer Inc., Waltham, MA, USA). Pristine SPIONs and CLA-coated SPIONs were analyzed (mass change as function of temperature over time) under set TGA conditions: 30–900°C, continuous nitrogen flow, and heat rate of 10°C/min.

3.2.3.4. Analysis of the crystallographic structure of the CLA-Coated PTX-SPIONs

X-ray diffractometry (XRD) (RIGAKU MiniFlex, RIGAKU Inc., Tokyo, Japan) was employed to analyze the crystallinity of the SPIONs before and after modifications. Dried samples of pristine SPIONs and the CLA-coated PTX-SPIONs were mounted on aluminium sample holders and analyzed to obtain diffractograms. The following measurement conditions were set for the analysis: 2θ range of 5°–90°, scan rate at 10 deg/min, current and voltage were 15 mA and 40 kV, respectively.

3.2.3.5. Iron oxide core mapping of the SPIONs

Raman spectroscopy (SENTERRA II, BRUKER, Bremen, Germany) was employed as a precise method to characterize the magnetite nature of the iron oxide core of the SPIONs before and after the CLA-coating enhancement process (Lee et al., 2015; Sawisai et al., 2019). Samples were prepared on glass slides and analyzed with a beam diameter of 1μm at a laser power of 0.04 mV at 25°C. A magnetite standard (Sigma-Aldrich, Saint Louis, MO, USA) was used as reference.

3.2.3.6. Analysis of the magnetic properties of the CLA-Coated PTX-SPIONs

The paramagnetic properties of the synthesized SPIONs and the CLA-coated PTX-SPIONs were analyzed using a vibrating sample magnetometer (VSM) (12T Physical Property Measurement System, PPMS® DynaCool™, Quantum Design, San Diego, CA,USA), at room temperature. The PPMS® DynaCool™ measurement temperature was fixed at 300 K with the magnetic field span of −8000 to 8000 Oe.

3.2.3.7. Determination of PTX-loading capacity and adsorption efficiency within the CLA-coated SPIONs

A standard calibration curve with serial concentrations (5 – 25 μg/mL) was prepared for PTX loading using UV spectrophotometry (Cary™ 50, Varian Inc., Palo Alto, CA, USA). The concentrations were prepared in a 70:30 methanol: water co-solvent system. The Adsorption Efficiency (%AE) and Drug (PTX) Loading Capacity (%DLC) were defined by quantification of

free PTX in the supernatant following the loading procedure. Briefly, the PTX-loaded CLA-coated SPIONs were centrifuged (13,800 rpm, 10 min, 10°C) with subsequent washing, thrice with distilled water, and the supernatant was withdrawn. The concentration of PTX in the supernatant was determined by recording the absorbance of the samples (n = 3) at 227 nm, and the %AE as well as %DLC were computed by application of Equations (3.1) and (3.2), respectively.

$$\%AE = \frac{D_l - D_s}{D_l} \times 100 \quad \text{(Equation 3.1)}$$

$$\%DLC = \frac{D_l - D_s}{W_f} \times 100 \quad \text{(Equation 3.2)}$$

where D_l is the amount of drug loaded, D_s is the amount of unloaded drug in supernatant, and W_f is the total weight of formulation, in mg.

3.2.3.8. Evaluation of in vitro release of PTX from the CLA-Coated SPIONs

The drug release profile was evaluated for CLA-coated PTX-SPIONs at pH 6.8 and pH 7.4, for 24 h at 37°C, mimicking tumor microenvironment (TME) and physiological pH, respectively (Adeyemi et al., 2019; Dilnawaz et al., 2010). Lyophilized CLA-coated PTX-SPIONs (3 mg) were dispersed in 2 mL of prepared 0.1 M PBS (pH: 6.8 and, 7.4) containing 0.1% *v*/*v* Tween. The samples were then loaded into a dialysis membrane (SnakeSkin™, 3500 MWCO) and submerged into the relevant drug release buffer (30 mL) of corresponding pH and incubated in an orbital shaking incubator (YIHDER LM-530, YIHDER Co., Ltd., Taipei, Taiwan). The dialysis membrane was used to facilitate the diffusion of only PTX into the release medium for quantification. Sampling (2 mL) was undertaken at different time intervals (t = 1, 2, 4, 8, 12, and 24 h) and the UV absorbance readings were recorded at 227 nm for PTX. The release medium was constantly replenished with the equivalent volume of PBS, after each sampling point to maintain sink conditions.

3.2.4. *In vitro* evaluation of the anti-proliferative activity of the CLA-Coated PTX-SPIONs using MTT Assay

The model lung adenocarcinoma cell line (A549) (Cellonex, Johannesburg, South Africa) was employed for the cell viability study. Cells were cultured in Dulbecco's Modified Eagle's Medium (DMEM) supplemented with Foetal Bovine Serum (FBS, 10% *v*/*v*) and 1% (*v*/*v*) penicillin-streptomycin antibiotic, and incubated at 37°C and 5% CO_2 saturation, under humidity, in a T-25 cell culture flask. Cells were allowed to grow, and when a 90% confluence was reached, the cells seeded in a 96-well plate, at a seeding density of 2.5×10^4. To each well, a cell suspension of 90 µL was added followed by incubation at 37°C, 5% CO_2 for 24 h

to allow adequate cell adherence. The experimental cells were then treated in triplicate (n = 3) with 10 µL of SPIONs, CLA, and CLA-coated PTX-SPIONs corresponding to treatment concentrations of 3.125, 6.25, 12.5, 25, 50, and 100 µg/mL in PBS (0.2% DMSO). Pristine PTX was used as a positive control at varying treatment concentrations of 0.156, 0.312, 0.625, 1.25, 2.5, 5, and 10 µg/mL, corresponding to 10% of PTX concentration in CLA-coated PTX-SPIONs (matching 9.8% drug loading capacity). The cells were subjected to incubation for 72 h prior to the commencement of the cell viability assay. The MTT assay was performed after 72 h using the MTT Cell Proliferation Kit I (Roche, Basel, Switzerland). MTT solution (10 µL; 5 mg/mL) was introduced into each well, followed by 4-h incubation of the plate (37°C, 5% CO_2, humid conditions). Thereafter, 100 µL of the solubilizing agent (acid-isopropanol; 0.04 N HCl in isopropanol) was added to dissolve formed formazan crystals, followed by overnight incubation at 37°C and 5% CO_2. Wells containing only solubilizing agent and growth medium were used as a blank. The absorbance was measured with a multimodal microplate reader (Victor X3, PerkinElmer, Waltham, MA, USA) at 570 nm with a reference wavelength of 620 nm. The absorbance measurements were computed (mean ± standard deviation) and used to calculate % cell viability via Equation 3.3.

$$\% \text{ Cell viability} = \frac{A_{test} - A_{blank}}{A_{control} - A_{blank}} \times 100 \qquad \text{(Equation 3.3)}$$

where A_{test} is test absorbance, A_{blank} is blank absorbance, and $A_{control}$ is control absorbance in nm.

The AAT Bioquest IC_{50} calculator (ATT Bioquest, Inc., Sunnyvale, CA, USA) was used to compute IC_{50} values (Lin et al., 2019).

3.2.5. Statistical analysis

The results were analyzed using a two-tailed Student's unpaired t-test on GraphPad prism version 9 (GraphPad Software, Inc., San Diego, CA, USA). Two groups were analyzed at a time at 95% confidence interval, with $p < 0.05$ deemed statistically significant. All data are expressed as mean ± standard deviation of analyses in triplicate (n = 3).

3.3. Results and Discussion

3.3.1. Assessment of the CLA-Coated PTX-SPIONs synthesized in terms of particle size and morphology

Amongst several reported methods of synthesizing magnetic nanoparticles (MNPs), co-precipitation was selected as the most suitable as it is undertaken in an inert atmosphere with controlled pH and temperature to avoid oxidation, and to control particle size, distribution, and

morphology (Palanisamy and Wang, 2019; Slimani et al., 2021). In the present study, SPIONs were successfully synthesized as a black colored powder (characteristic of pure Fe_3O_4 nanoparticles). Essentially pure magnetite Fe_3O_4 exhibit a black color and once oxidized transitions to a brownish/red color (Wallyn et al., 2019). Performing the precipitation in an inert environment (N_2) evidently prevented oxidation/reduction of the iron II/III salts and the deterioration of the SPIONs. Furthermore, coating of the synthesized SPIONs with a suitable polymer was crucial in order to limit particle agglomeration and prevent oxidation (Sawisai et al., 2019).

In this study, 10E, 12Z CLA was used to coat the SPIONs mainly due to its previously reported anticancer benefits and excellent reactivity owing to the inherent carboxyl group (Sawisai et al., 2019). Additionally, its hydrophobicity (for partition of hydrophobic drugs), and excellent crosslinking activity were other attractive features (Fan et al., 2014; Sawisai et al., 2019). The successful coating of 10E, 12Z CLA onto the SPIONs surface occurred through chemisorption via the carboxyl group of 10E, 12Z CLA and the oxygen coordinated at the surface of the SPIONs. A similar mechanism was reported for SPIONs coated with oleic acid and glycerol monooleate, both containing carboxyl groups (Dilnawaz et al., 2010; Muzio et al., 2017; Sawisai et al., 2019). The hydrophobicity of 10E, 12Z CLA further allowed efficient loading of PTX (hydrophobic drug) onto the 10E, 12Z CLA-coated SPIONs via spontaneous hydrophobic interactions. PTX was adsorbed on the 10E, 12Z CLA hydrophobic ends surrounding the SPIONs core to form the CLA-coated PTX-SPIONs (Luchini et al., 2017; Luchini and Vitiello, 2019).

The average hydrodynamic particle size and zeta potential of pristine SPIONs was found to be 51.0 ± 1.3 nm and −24.3 ± 1.3 mV, respectively, meanwhile CLA-coated SPIONs exhibited average size of 62.7 ± 5.6 nm and zeta potential of −26.3 ± 0.5 mV. The CLA-coated PTX-SPIONs had a hydrodynamic size of 96.5 ± 0.6 nm and a zeta potential of −27.3 ± 1.9 mV (**Figure 3.1a, b**). The synthesized SPIONs were therefore in a desirable range for potential targeted PTX delivery in NSCLC. Essentially, previous studies have shown that conventional MNPs in a 10 – 100 nm range can penetrate lung tumors, while particles <10 nm are subject to renal clearance, and those >100 nm accumulate in the spleen or are removed by alveolar macrophages in the lungs (Hoshyar et al., 2016; Lee et al., 2014). The recorded particle size for SPIONs produced in this study is attributed to the co-precipitation method of synthesis and the processing parameters that were maintained as constant (i.e., 75°C temperature and inert atmosphere). Processing factors such as pH, reaction temperature, and media are known to significantly influence the particle size (Gawali et al., 2019; Kondiah et al., 2018).

Interestingly, the pristine SPIONs had a PDI value of 0.4 ± 0.1, while that of CLA-coated PTX-SPIONs was found to be 0.1 ± 0.02. This indicated that the CLA-coating reduced aggregation and imparted a more colloidal stability to the particles. These results, together with the zeta potential values recorded for the CLA-coated PTX-SPIONs, reveal that this synthesis strategy provides superior dispersion and aqueous stability to the nanosystem, suggesting its suitability as nano-enabled drug delivery system. Modified SPIONs in a similar size range and zeta potential values have been previously reported by Goncalves et al. (Gonçalves et al., 2017). The overall morphology of the free-flowing powdered CLA-coated PTX-SPIONs (**Figure 3.1c**), as confirmed by SEM, further revealed that the CLA-coated PTX-SPIONs were spherical in shape and had a relatively rugged surface with a mean particle size of <100 nm (**Figure 3.1d, e**). This correlates with previous studies that have reported that co-precipitation yield spherical nanoparticles (Akilo et al., 2016; Cooley et al., 2018), which when employed in cancer nanomedicine studies, resulted in enhanced biodistribution and cellular uptake (Huang et al., 2011; Zhong et al., 2016).

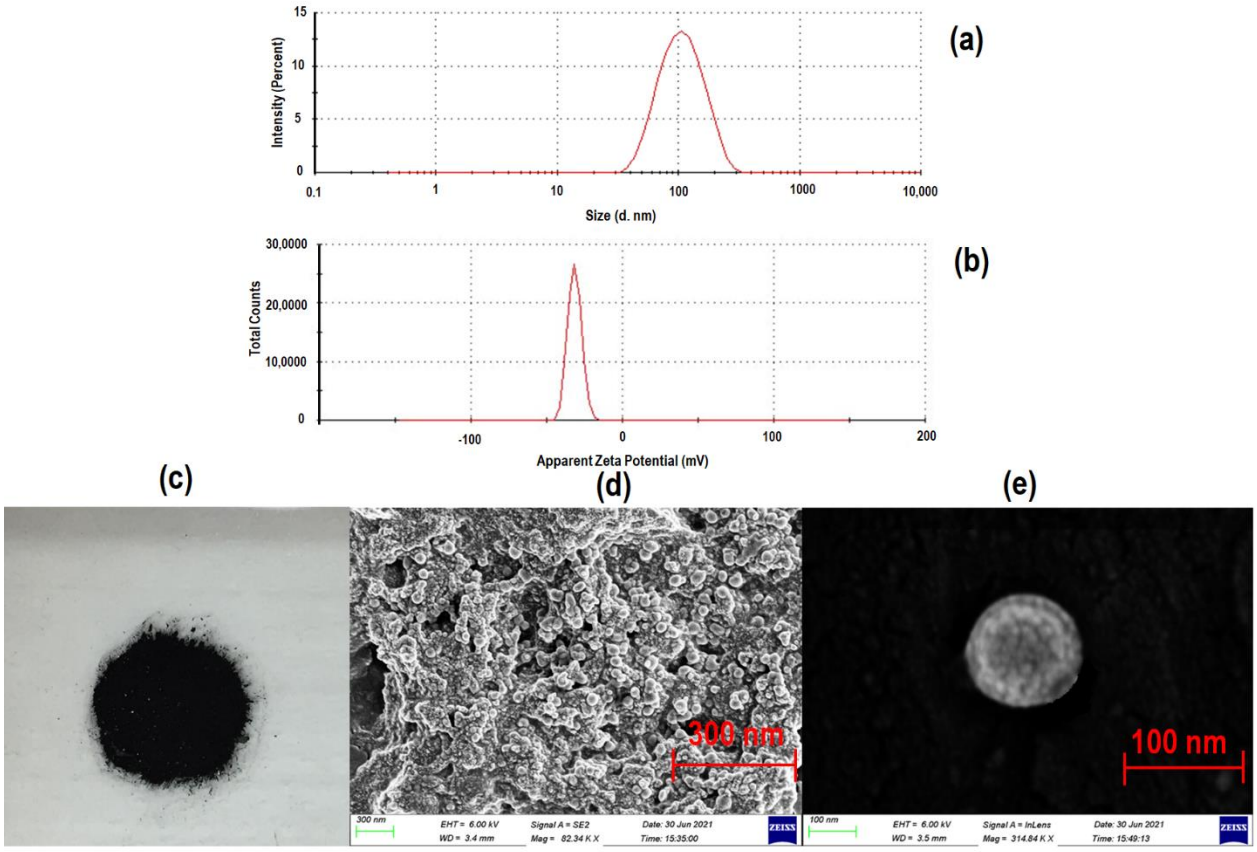

Figure 3.1. A visualization of the morphological attributes of the CLA-coated PTX-SPIONs, showing (**a**) average hydrodynamic particle size of 96.5 ± 0.6 nm (PDI = 0.1 ± 0.02), (**b**) zeta potential of – 27.3 ± 1.9 mV, and (**c**) a lyophilized sample with corresponding SEM images

showing overall morphology (**d**) at 300 nm scale (82.34 KX magnification) and (**e**) 100 nm scale (314.84 KX) (isolated particle), showing a particle size of <100 nm.

3.3.2. Assessment of the chemical stability and functional transformation of the CLA-coated PTX-SPIONs

The FTIR spectra of pristine SPIONs, 10E, 12Z CLA, and PTX as well as the drug-free and drug-loaded CLA-coated SPIONs are presented in **Figure 3.2a–e**. Two bands were observed on the spectrum of pristine (uncoated) SPIONs (**Figure 3.2a**) at around 3420 cm^{-1} and 570–580 cm^{-1}, which was ascribed to the respective molecular stretch and bending of hydroxyl groups (OH) on magnetite SPIONs surface and Fe-O bonds, respectively (Akilo et al., 2016; Sawisai et al., 2019). The two sharp peaks observed for pristine 10E, 12Z CLA (**Figure 3.2b**) at around 2922 cm^{-1} and 2852 cm^{-1} belonged to the symmetrical and asymmetrical CH_2 group stretching (Muzio et al., 2017). Another sharp peak at around 1710 cm^{-1} was attributed to C=O of the carboxyl group, and that at around 1408 cm^{-1} to the CH_3 group bending (Muzio et al., 2017; Yang et al., 2010). There was no significant distinction in the spectrum of the CLA-coated SPIONs (**Figure 3.2c**) and those of pristine 10E, 12Z CLA and SPIONs, except that the band at 3420 cm^{-1} initially present in the absorption spectrum of the uncoated SPIONs attributed to surface OH groups disappeared with the CLA-coated SPIONs, due to chemisorption of 10E, 12Z CLA to the surface of the SPIONs (**Figure 3.2f**). Characteristic peaks of PTX (**Figure 3.2d**) were observed at around 3500, 3479, 2976–2885, 1731, and 1244 cm^{-1}, assigned to the OH, N-H, and CH_2 vibrations, C=O, and ester groups, respectively (Dilnawaz et al., 2010; Zhao et al., 2015). Similar peaks were present in the spectrum of the CLA-coated PTX-SPIONs (**Figure 3.2e**), indicating that PTX was successfully adsorbed onto the surface of the CLA-coated SPIONs and the partitioning did not alter the chemical structure of PTX.

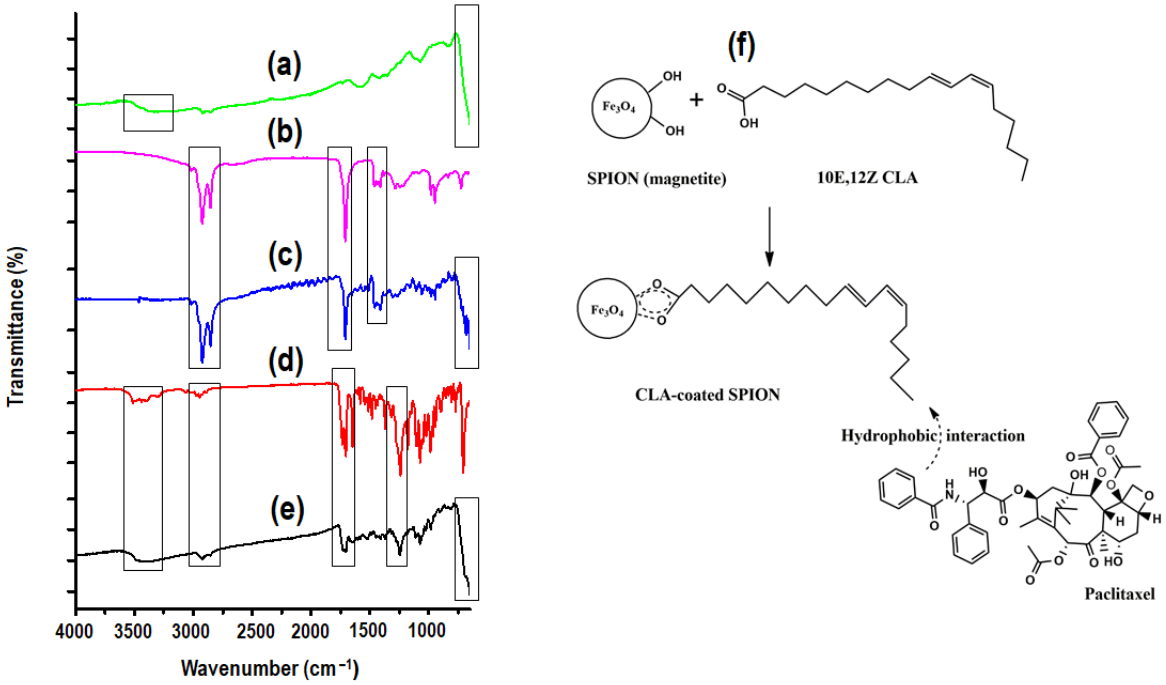

Figure 3.2. FTIR spectra of (**a**) pristine SPIONs, (**b**) 10E, 12 CLA, (**c**) CLA-coated SPIONs, (**d**) pristine PTX, (**e**) CLA-coated PTX-SPIONs, and (**f**) schematic representation of 10E, 12Z CLA chemisorption onto SPIONs and CLA-PTX hydrophobic interaction.

3.3.3. Quantification of CLA content on CLA-Coated SPIONs

The amount of CLA coated onto SPIONs was ascertained by TGA. **Figure 3.3** presents TGA data showing % weight loss as function of temperature, for pristine SPIONs (**Figure 3.3a**) and CLA-coated SPIONs (**Figure 3b**). Pristine SPIONs demonstrated an initial weight loss at below 200 °C, which is attributed to the evaporation of adsorbed water on the surface (Akilo et al., 2016; Sawisai et al., 2019). The total weight loss of 5.7% was thus recorded for pristine SPIONs. Meanwhile, CLA-coated SPIONs exhibited a two-step weight loss pattern. The initial weight loss was observed at below 200 °C, complementary to pristine SPIONs (water desorption), and the second weight loss was observed between 200 – 450 °C, which is attributed to the removal of CLA layer from SPIONs surface. The content of CLA on SPIONs could therefore be estimated from 200 – 450°C and was found to be 10.3%. Previous studies have reported fatty acid contents in the range of 10 – 14%, when fatty acids such as linoleic acid and palmitic acid were coated onto SPIONs and analyzed by TGA (Dilnawaz et al., 2010; Sawisai et al., 2019). The TGA results correlate with VSM data, which demonstrated a slight reduction in saturation magnetization of CLA-coated PTX-SPIONs (60 emu/g) compared to pristine SPIONs (65 emu/g) due to the presence of CLA on magnetite.

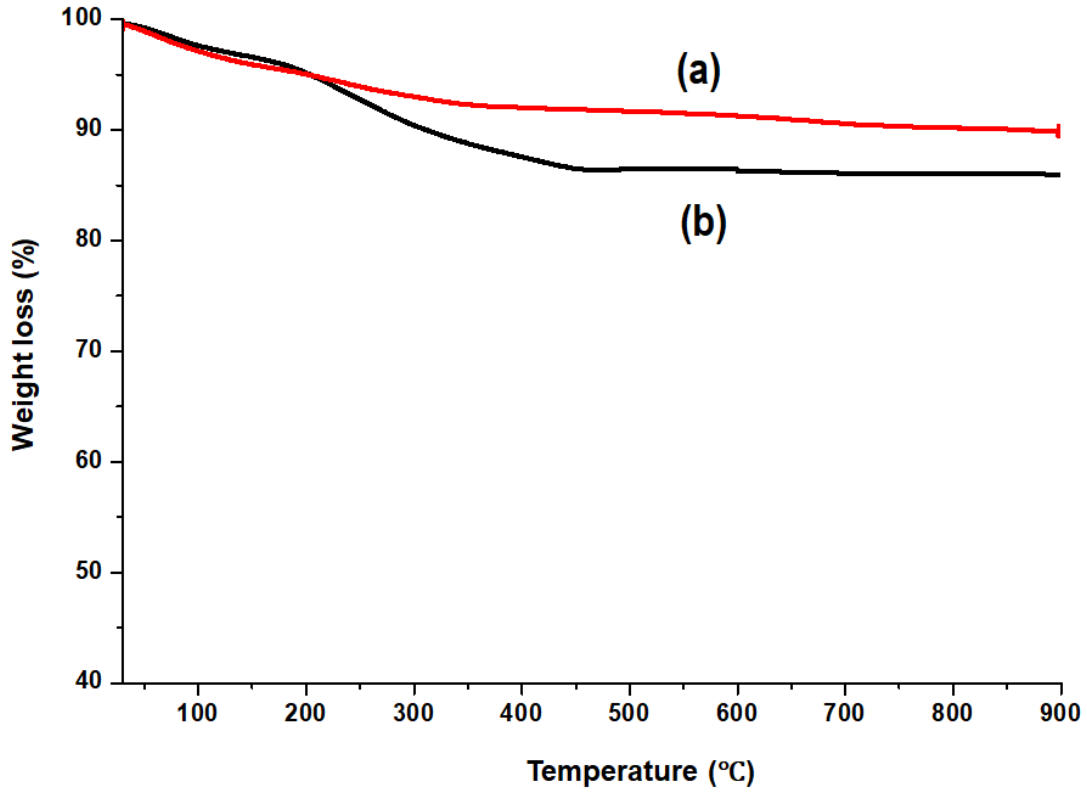

Figure 3.3. TGA thermograms of (**a**) pristine SPIONs and (**b**) CLA-coated SPIONs demonstrating weight loss (%) over a temperature range of 30 – 900°C.

3.3.4. Determination of the structural crystallinity of the CLA-Coated PTX-SPIONs

The diffraction patterns presented in **Figure 3.4** show the crystalline nature of the SPIONs before (**Figure 3.4a**) and after CLA coating (**Figure 3.4b**) and PTX loading (**Figure 3.4c**) (CLA-coated PTX-SPIONs). The obtained XRD patterns show similar diffraction peaks (2θ) at 30.5°, 35.8°, 43.5°, 57.3°, and 63.1°, for all samples, characteristic of magnetite origin (Akilo et al., 2016; Sawisai et al., 2019), indicating that pristine SPIONs and the CLA-coated PTX-SPIONs were purely magnetite (Fe_3O_4) and crystalline in nature. This correlates with the Raman spectroscopy analysis and further ascertains that CLA did not affect the crystallinity of the SPIONs. These results agree well with existing studies reported by Sawisai et al. (2019), for SPIONs coated with linoleic acid (Sawisai et al., 2019). The difference in peak intensity between SPIONs and the CLA-coated SPIONs was attributed to the CLA coating process that reduced the peak intensity. Meanwhile, the diffractogram for CLA-coated PTX-SPIONs showed additional diffraction peaks (2θ) at 22.4° and 25.1° corresponding to PTX crystallinity (Christodoulou et al., 2019; Tang et al., 2016). This indicated the presence of PTX in the formulation in its crystalline form.

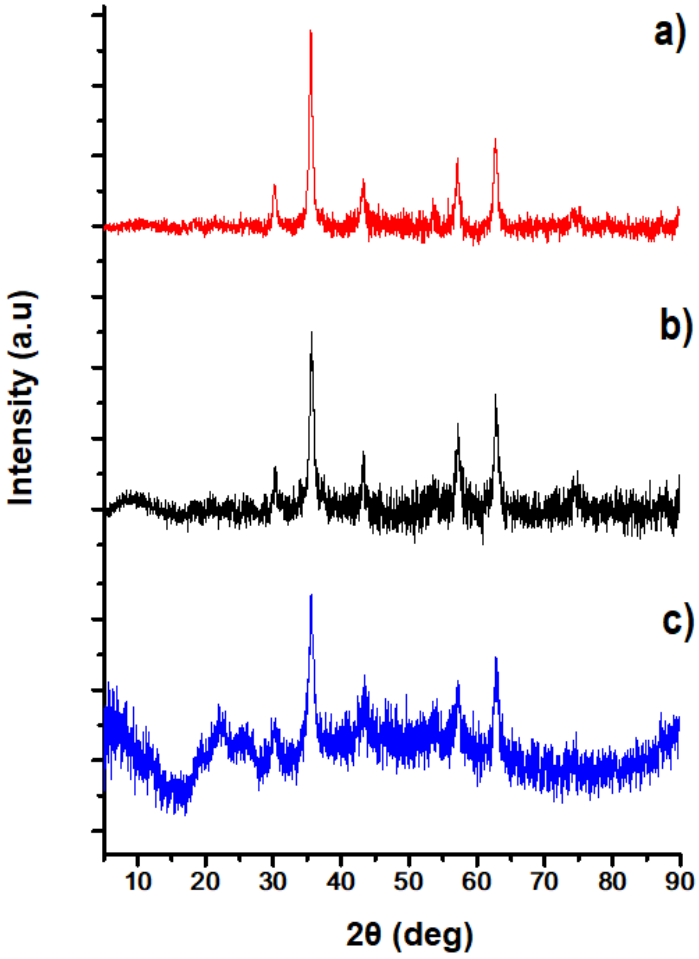

Figure 3.4. XRD spectra of (**a**) pristine SPIONs, (**b**) CLA-coated SPIONs, and (**c**) CLA-coated PTX-SPIONs showing the crystalline nature of the SPIONs before and after the CLA coating and PTX loading.

3.3.5. Evaluation of the iron oxide core integrity of the SPIONs

Figure 3.5 presents Raman spectra of (**a**) pristine SPIONs and (**b**) the CLA-coated PTX-SPIONs. Both spectra show a single prominent band at 670 cm^{-1} representing magnetite (Fe_3O_4) origin, attributed to the A_{1g} photon mode (Sawisai et al., 2019). A similar observation was made for CLA-coated SPIONs. The single peak observed provides evidence that the synthesized SPIONs were purely magnetite, and there was no phase transition after the CLA coating process. Previously published literature has reported that the phase transition of magnetite to maghemite (γ-Fe_2O_3) mainly occurs at higher temperatures (200 – 600 °C) (Gao et al., 2011).

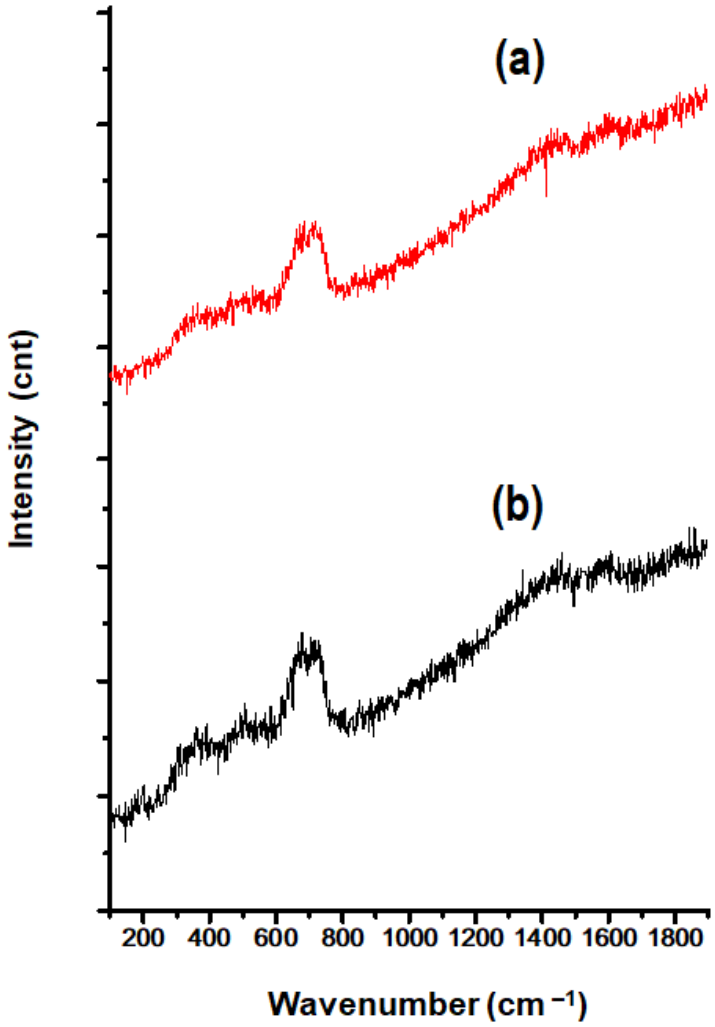

Figure 3.5. Raman spectra of (**a**) pristine SPIONs and (**b**) the CLA-coated PTX-SPIONs depicting the presence and integrity of the magnetite.

3.3.6. Assessment of the magnetic properties of the CLA-Coated PTX-SPIONs

The magnetization analysis was conducted to further confirm superparamagnetism of the synthesized SPIONs prior and post modification with the CLA coating and the adsorption of PTX (CLA-coated PTX-SPIONs). Shown in **Figure 3.6a, b** are pristine SPIONs and CLA-coated PTX-SPIONs localized by a magnet, indicative of inherent magnetism. Magnetization hysteresis loops for pristine SPIONs and the CLA-coated PTX-SPIONs are depicted **in Figure 3.6c, d**, with corresponding saturation magnetization and coercivity values presented in **Table 3.1**. Both samples were confirmed to be superparamagnetic as evidenced by the S-type behavior and nearly no remanence in the hysteresis. However, CLA-coated PTX-SPIONs

exhibited a slightly reduced magnetic saturation compared to the pristine SPIONs, which is attributed to the CLA coating process resulting in slight reduction of exposed Fe_3O_4 content and reduced effect of the magnetic field. Moreover, the coercivity values of the samples varied, but were both <100 Oe, thus further demonstrating superparamagnetism and suitability for biomedical application (Maldonado-Camargo et al., 2017; Zhang et al., 2016). In essence, the CLA-coated PTX-SPIONs maintained the superparamagnetic behavior and met the criteria for biomedical applications.

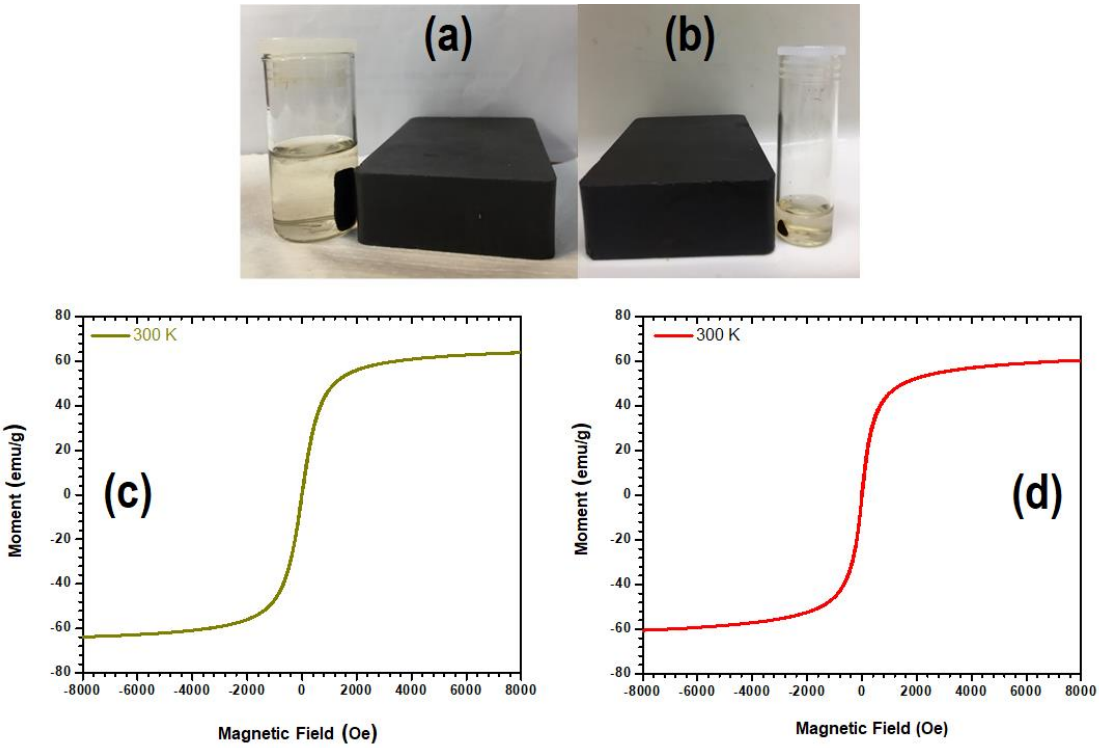

Figure 3.6. A depiction of (**a**) pristine SPIONs and (**b**) CLA-coated PTX-SPIONs localized by a magnet, and magnetization hysteresis loops of (**c**) pristine SPIONs and (**d**) CLA-coated PTX-SPIONs at 300 K and magnetic field range of – 8000 to 8000 Oe.

Table 3.1. Saturation magnetization and coercivity of pristine SPIONs and the CLA-coated PTX-SPIONs as determined by VSM analysis

Sample	Saturation Magnetization (emu/g)	Coercivity (Oe)
Pristine SPIONs	65	50
CLA-coated PTX-SPIONs	60	29

3.3.7. Assessment of the PTX adsorption efficiency and *in vitro* release from the CLA-Coated PTX-SPIONs

PTX loading onto the SPIONs is a crucial step in their application as an anticancer nanomedicine for potential subcutaneous injection. Essentially, the drug should be loaded in a way that does not compromise its functionality, while ensuring adequate release from the nanosystem upon reaching the target site (Reczyńska et al., 2020a). In the present study, PTX was successfully loaded onto the CLA-coated SPIONs, achieving an Adsorption Efficiency (%AE) of 98.5% and %DLC of 9.8%. Conventionally, it is challenging to encapsulate hydrophobic drugs and to achieve controlled drug release (Ghosh and Banerjee, 2021). However, in the present study, PTX was preferentially adsorbed (98.5%) onto the CLA coating due to the hydrophobicity of 10E, 12Z CLA, which facilitated adsorption and sustained release over time from the SPIONs architype. The efficient drug loading achieved validates the strategy of CLA-coating process over classical conjugation for hydrophobic drugs such as PTX. Dilnawaz *et al*., 2010, reportedly achieved ~95% loading efficiency for PTX and rapamycin in glycerol monooleate (GMO)-coated SPIONs, where drugs were co-encapsulated in the hydrophobic GMO crust (Dilnawaz et al., 2010).

The *in vitro* drug release study was conducted to quantify the amount of PTX released from the CLA-coated SPIONs at pH 7.4 and 6.8, representative of physiological pH and a tumor microenvironment (TME), respectively (Adeyemi et al., 2019). The PTX release over 24 h is presented in **Figure 3.7**. Evidently, the release of PTX was relatively higher at pH 6.8 than pH 7.4. A maximum cumulative release of 94% was obtained over 12 h at pH 6.8, indicating sufficient sustained release of PTX from the CLA coating, which is attributed to the disruption of the CLA-PTX hydrophobic interaction at a relatively acidic pH of 6.8 over time, resulting in PTX release. A similar observation was reported with PTX-loaded SPIONs coated with GMO (Dilnawaz et al., 2010; Wulandari et al., 2019). The cumulative drug release at pH 7.4 was <18%, implying that the CLA-coated PTX-SPIONs has the potential to control the release of PTX to lung cancer tumors (as indicated by the higher PTX release at pH 6.8) while having minimal cytotoxicity to healthy cells (evidenced by lower drug release at physiological pH of 7.4). Furthermore, shielding of PTX at pH 7.4 shows the potential of the nanosystem to enhance the bioavailability of PTX.

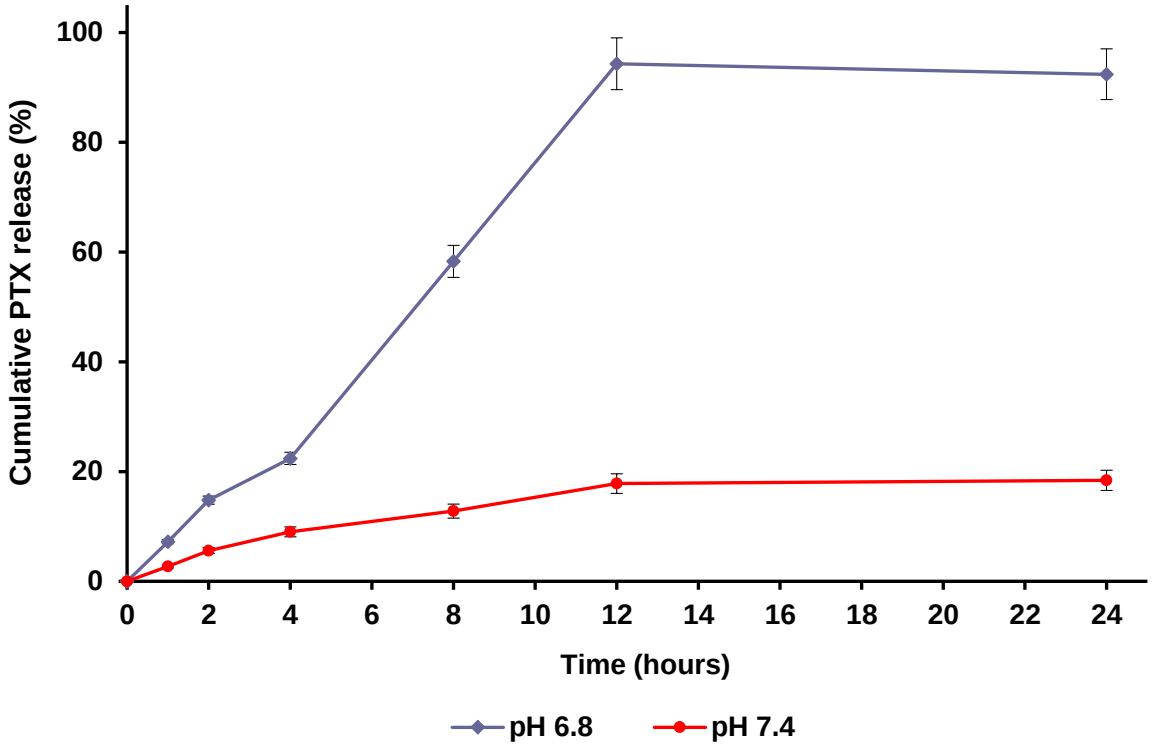

Figure 3.7. *In vitro* PTX release profiles from the CLA-coated PTX-SPIONs at pH 6.8 and pH 7.4. Data from experiments are presented as the mean ± SD, *n* = 3.

3.3.8. Evaluation of the anti-proliferative activity of the CLA-Coated PTX-SPIONs on A549 cancer cells

The MTT assay was used to evaluate the cytotoxicity of the CLA-coated PTX-SPIONs in a lung adenocarcinoma cell line (A549) by measuring cell viability after 72 h of treatment. Cells were treated with varying concentrations (3.215 – 100 µg/mL) of pristine SPIONs, 10E, 12Z CLA, and CLA-coated PTX-SPIONs, while pristine PTX was used as a positive control (**Figure 3.8**). The % cell viability for cells treated with pristine SPIONs was comparatively higher after 72 h, with 95.5% and 91.3% obtained at the lowest and highest treatment concentration, respectively. This indicated that the pristine SPIONs did not have significant cytotoxicity on A549 cells. This further validated the use of SPIONs as bio-imaging agents in cancer diagnosis, since they do not confer any significant harm to cells. Generally, SPIONs are applied in magnetic resonance imaging (MRI) for bio-imaging because of their excellent image contrasting properties attributed to their inherent magnetism (Khizar et al., 2021). The anti-proliferative activity of pristine 10E, 12Z CLA was observed, with recorded 69.8% cell viability of A549 cells at highest treatment concentration (100 µg/mL) after 72 h. This showed that 10E, 12Z CLA resulted in 30.2% inhibition of lung adenocarcinoma cells, and adds to previous

works which have demonstrated that 10E, 12Z CLA suppresses cancer proliferation (Flowers and Thompson, 2009; Ochoa et al., 2004; Zhang et al., 2018).

Treatment with the CLA-coated PTX-SPIONs highly suppressed A549 cell proliferation after 72 h in a dose-dependent manner (**Figure 3.8a**). Treatment at highest concentration (100 µg/mL) resulted in only 17.1% cell viability and treatment with the lowest concentration (3.125 µg/mL) resulted in 24.2% viability. Interestingly, when compared to the pristine PTX (**Figure 3.8b**), treatment with lower concentrations of CLA-coated PTX-SPIONs, 3.125 and 6.25 µg/mL, yielded a % cell viability of 24.2% and 21.6%, respectively. This demonstrated the enhanced anti-proliferative activity than recorded from the highest concentration of pristine PTX (10 µg/mL), which resulted in a cell viability of 25.3%. Essentially, this showed that a smaller dose of the CLA-coated PTX-SPIONs would be sufficient to elicit equivalent anti-proliferative activity as exerted by a ~3-fold dose of pristine PTX. The results then suggest that the CLA-coated PTX-SPIONs enhance the efficacy of PTX in suppressing A549 cell proliferation. The IC_{50} of PTX and the CLA-coated PTX-SPIONs were measured to be 0.7 and 0.3 µg/mL, respectively. This substantiates the comparatively higher anti-proliferative activity of the CLA-coated PTX-SPIONs as evidenced by the lower % cell viability compared to pristine PTX. An IC_{50} of 0.9 µg/mL for pristine PTX in A549 cells has been reported previously by Jiang et al. (Jiang et al., 2013), thus demonstrating that pristine PTX employed in this study had comparable cytotoxicity.

The enhanced anti-proliferative activity of the CLA-coated PTX-SPIONs observed is attributed to the presence of the CLA coating onto the SPIONs. The two biologically active isomers of CLA (10E, 12Z and 9Z,11E CLA) have been previously reported to confer anticancer activity, with studies suggesting that in combination they may suppress tumor growth via inhibition of DNA synthesis and modulation of lipid peroxidation, amongst other mechanisms (Evans et al., 2010; Lee et al., 2005; Moreira et al., 2019; Rakib et al., 2013). As such, it is presumed that, in addition to acting as a surface coating agent that allowed maximal partitioning of PTX onto the SPIONs, 10E, 12Z CLA imparted additional anticancer action in tandem with PTX, thus resulting in the observed enhanced anti-proliferative activity on A549 cells. Additionally, the sustained release of PTX observed from the CLA-coated PTX-SPIONs (**Figure 3.7**) is directly linked to the outcome of the cell viability study, demonstrating that the prolonged release of PTX over time results in enhanced cytotoxicity.

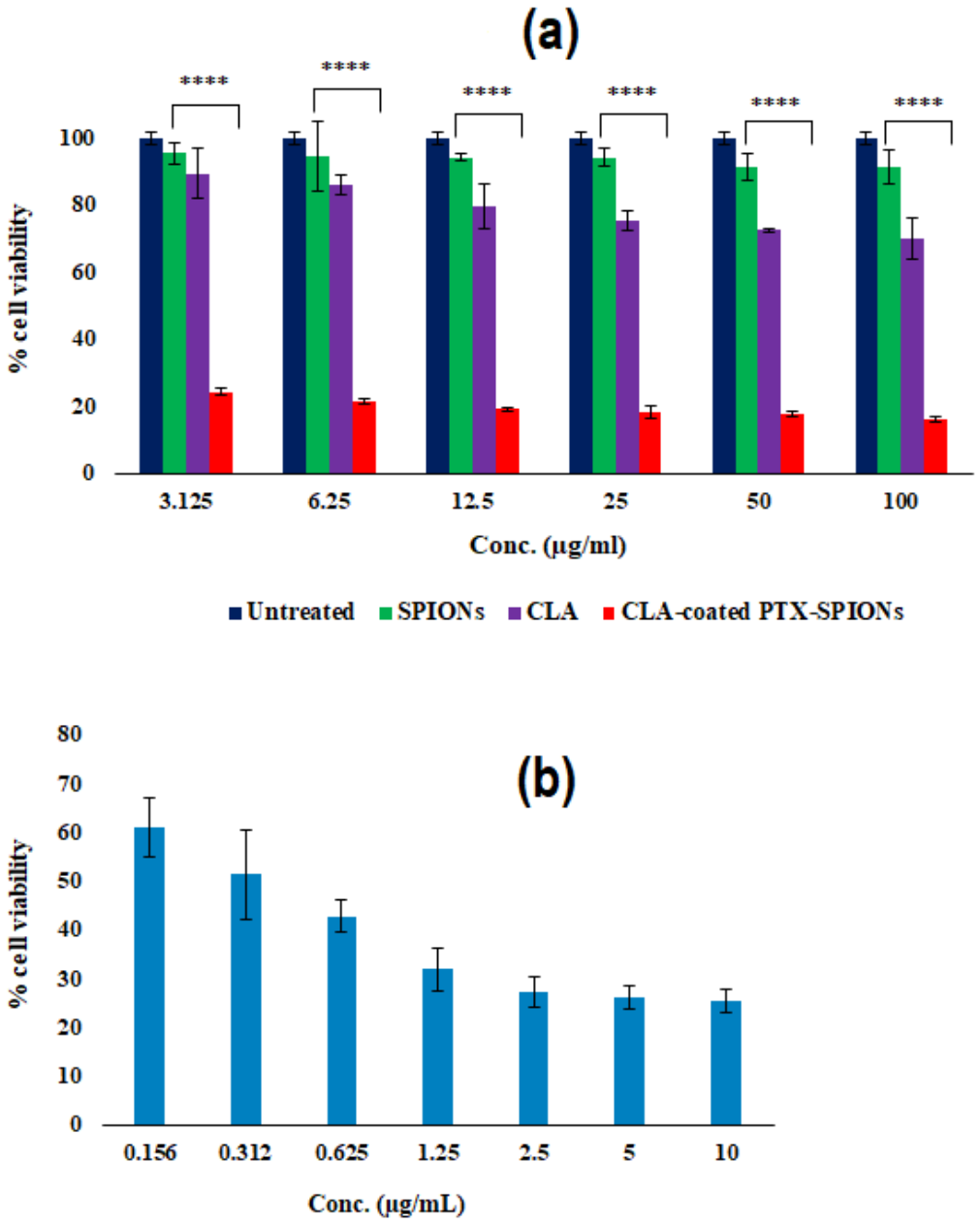

Figure 3.8. Profiles showing % cell viability of lung adenocarcinoma cells (A549) treated with varying concentrations of (**a**) pristine SPIONs (*negative control*) and the CLA-coated PTX-SPIONs, and (**b**) pristine PTX (equivalent to 10% PTX in the nanosystem, corresponding to ~10% DLC) (*positive control*) after 72 h. Concentrations of pristine PTX correspond to 10% DLC (match the actual amount of PTX loaded onto CLA-coated SPIONs). Data presented as mean ± SD, $n = 3$ (**** denotes $p < 0.0001$, when CLA-coated PTX-SPIONs is compared to SPIONs and CLA at the same concentrations).

3.4. Concluding Remarks

Essentially, the aim of the work presented in this chapter was to fabricate novel CLA-coated PTX-SPIONs and carry out preliminary physicochemical characterization and assessment of *in vitro* anti-proliferative activity on A549 cells to establish the viability of the nanosystem as a potential candidate for the effective delivery of PTX in NSCLC management. Accordingly, SPIONs, which are purely magnetite (Fe_3O_4), were successfully synthesized, coated with 10E, 12Z CLA, and loaded with PTX to formulate CLA-coated PTX-SPIONs with an desired particle size of <100 nm. The surface coating of SPIONs with 10E, 12Z CLA facilitated enhanced and efficient PTX adsorption (98.5%) via hydrophobic interactions. PTX was partitioned onto the CLA surrounding the SPIONs as confirmed by physicochemical characterization. Sustained release of PTX was achieved up to 94% in a simulated TME at pH 6.8 after 24 h with a significantly reduced release at pH 7.4 (physiological milieu). Thus, the fabrication method was found to be apt in terms of controlled and robust synthesis of the desired nanosystem.

The A549 cells treated with CLA-coated PTX-SPIONs showed a comparatively lower viability compared to cells treated with pristine PTX, confirming the potential enhancement of the anticancer activity of PTX when loaded into the superparamagnetic nanosystem. Importantly, the superparamagnetic nature of the SPIONs was maintained throughout the formulation of CLA-coated PTX-SPIONs, which presents the nanosystem for consideration as a potential cancer theranostic tool (i.e., MRI imaging and PTX delivery). Primarily, the results from this work validate the proof-of-concept of using CLA as a coating agent onto SPIONs to enhance the activity of hydrophobic anticancer drugs with future optimization that could provide more active targeting in NSCLC. The functionalization of CLA-coated PTX-SPIONs with homing antiangiogenic peptides could optimize the nanosystem for active targeted delivery of PTX and inhibition of tumor angiogenesis. As such, the next chapter reports on a detailed fabrication methodology for surface-functionalization of CLA-coated PTX-SPIONs with an anti-vascular endothelial growth factor (VEGF) peptide, for active VEGF receptor targeting and inhibition of angiogenesis in NSCLC.

3.5. References

Adeyemi, S.A., Choonara, Y.E., Kumar, P., du Toit, L.C., Marimuthu, T., Kondiah, P.P.D., Pillay, V., 2019. Folate-decorated, endostatin-loaded, nanoparticles for anti-proliferative chemotherapy in esophaegeal squamous cell carcinoma. Biomed. Pharmacother. 119, 109450.

Akilo, O.D., Choonara, Y.E., Strydom, A.M., du Toit, L.C., Kumar, P., Modi, G., Pillay, V., 2016. An *in vitro* evaluation of a carmustine-loaded nano-co-plex for potential magnetic-targeted intranasal delivery to the brain. Int. J. Pharm. 500, 196-209.

Ansari, M.O., Ahmad, M.F., Shadab, G.G.H.A., Siddique, H.R., 2018. Superparamagnetic iron oxide nanoparticles based cancer theranostics: A double edge sword to fight against cancer. J. Drug Deliv. Sci. Technol. 45, 177-183.

Chen, Y., Li, J., Chen, S., Zhang, Y., Hu, Y., Zhang, G., Yan, X., Jiao, S., 2017. Nab-paclitaxel in combination with cisplatin versus docetaxel plus cisplatin as first-line therapy in non-small cell lung cancer. Sci. Rep. 7, 10760.

Cheng, Z., Li, M., Dey, R., Chen, Y., 2021. Nanomaterials for cancer therapy: Current progress and perspectives. J. Hematol. Oncol. 14, 85.

Christodoulou, E., Nerantzaki, M., Nanaki, S., Barmpalexis, P., Giannousi, K., Dendrinou-Samara, C., Angelakeris, M., Gounari, E., Anastasiou, A.D., Bikiaris, D.N., 2019. Paclitaxel magnetic core–shell nanoparticles based on poly(lactic acid) semitelechelic novel block copolymers for combined hyperthermia and chemotherapy treatment of cancer. Pharmaceutics 11, 213.

Cooley, M., Sarode, A., Hoore, M., Fedosov, D.A., Mitragotri, S., Sen Gupta, A., 2018. Influence of particle size and shape on their margination and wall-adhesion: Implications in drug delivery vehicle design across nano-to-micro scale. Nanoscale 10, 15350-15364.

Crintea, A., Dutu, A.G., Samasca, G., Florian, I.A., Lupan, I., Craciun, A.M., 2021. The nanosystems involved in treating lung cancer. Life 11, 682.

Dachev, M., Bryndová, J., Jakubek, M., Moučka, Z., Urban, M., 2021. The effects of conjugated linoleic acids on cancer. processes 9, 454.

den Hartigh, L.J., 2019. conjugated linoleic acid effects on cancer, obesity, and atherosclerosis: A review of pre-clinical and human trials with current perspectives. Nutrients 11, 370.

Dilnawaz, F., Singh, A., Mohanty, C., Sahoo, S.K., 2010. Dual drug loaded superparamagnetic iron oxide nanoparticles for targeted cancer therapy. Biomaterials 31, 3694-3706.

Dulińska-Litewka, J., Łazarczyk, A., Hałubiec, P., Szafrański, O., Karnas, K., Karewicz, A., 2019. Superparamagnetic iron oxide nanoparticles: Current and prospective medical applications. Materials (Basel) 12, 617.

El-Sherbiny, I.M., El-Sayed, M., Reda, A., 2020. Superparamagnetic iron oxide nanoparticles (SPIONs) as multifunctional cancer theranostics, in: Sharma, S.K., Javed, Y. (Eds.), Magnetic nanoheterostructures: Diagnostic, imaging and treatment. Springer International Publishing, Cham, pp. 223-241.

Evans, N.P., Misyak, S.A., Schmelz, E.M., Guri, A.J., Hontecillas, R., Bassaganya-Riera, J., 2010. Conjugated linoleic acid ameliorates inflammation-induced colorectal cancer in mice through activation of PPARgamma. J. Nutr. 140, 515-521.

Fan, Y., Fang, Y., Ma, L., 2014. The self-crosslinked ufasome of conjugated linoleic acid: Investigation of morphology, bilayer membrane and stability. Colloids Surf. B. Biointerfaces 123, 8-14.

Fernández, L.P., Gómez de Cedrón, M., Ramírez de Molina, A., 2020. Alterations of lipid metabolism in cancer: Implications in prognosis and treatment. Front. Oncol. 10.

Flowers, M., Thompson, P.A., 2009. T10c12 conjugated linoleic acid suppresses HER2 protein and enhances apoptosis in SKBr3 breast cancer cells: possible role of COX2. PLoS One 4, e5342.

Gao, M., Li, W., Dong, J., Zhang, Z., Yang, B., 2011. Synthesis and characterization of superparamagnetic Fe_3O_4@SiO_2 core-shell composite nanoparticles. World J. Condens. Matter Phys. 1, 49-54.

García-Fernández, C., Fornaguera, C., Borrós, S., 2020. Nanomedicine in non-small cell lung cancer: From conventional treatments to immunotherapy. Cancers (Basel) 12, 1609.

Gawali, S.L., Barick, K.C., Shetake, N.G., Rajan, V., Pandey, B.N., Kumar, N.N., Priyadarsini, K.I., Hassan, P.A., 2019. pH-labile magnetic nanocarriers for intracellular drug delivery to tumor cells. ACS Omega 4, 11728-11736.

Genova, C., Rossi, G., Tagliamento, M., Rijavec, E., Biello, F., Cerbone, L., Zullo, L., Grossi, F., 2020. Targeted therapy of oncogenic-driven advanced non-small cell lung cancer: Recent advances and new perspectives. Expert Rev. Respir. Med. 14, 367-383.

Ghosh, S., Banerjee, M., 2021. A smart viral vector for targeted delivery of hydrophobic drugs. Sci. Rep. 11, 7030.

Gonçalves, L.C., Seabra, A.B., Pelegrino, M.T., de Araujo, D.R., Bernardes, J.S., Haddad, P.S., 2017. Superparamagnetic iron oxide nanoparticles dispersed in pluronic F127 hydrogel: Potential uses in topical applications. RSC Advances 7, 14496-14503.

Gui, G., Fan, Z., Ning, Y., Yuan, C., Zhang, B., Xu, Q., 2021. Optimization, characterization and *in vivo* evaluation of paclitaxel-loaded folate-conjugated superparamagnetic iron oxide nanoparticles. Int. J. Nanomed. 16, 2283-2295.

Ha, Y.L., Storkson, J., Pariza, M.W., 1990. Inhibition of benzo(a)pyrene-induced mouse forestomach neoplasia by conjugated dienoic derivatives of linoleic acid. Cancer Res. 50, 1097-1101.

Hoshyar, N., Gray, S., Han, H., Bao, G., 2016. The effect of nanoparticle size on *in vivo* pharmacokinetics and cellular interaction. Nanomedicine (Lond.) 11, 673-692.

Huang, X., Li, L., Liu, T., Hao, N., Liu, H., Chen, D., Tang, F., 2011. The shape effect of mesoporous silica nanoparticles on biodistribution, clearance, and biocompatibility *in vivo*. ACS Nano 5, 5390-5399.

Jiang, L., Li, X., Liu, L., Zhang, Q., 2013. Thiolated chitosan-modified PLA-PCL-TPGS nanoparticles for oral chemotherapy of lung cancer. Nanoscale Res. Lett. 8, 66-66.

Khizar, S., Ahmad, N.M., Zine, N., Jaffrezic-Renault, N., Errachid-el-salhi, A., Elaissari, A., 2021. Magnetic nanoparticles: From synthesis to theranostic applications. ACS Appl. Nano Mater. 4, 4284-4306.

Kondiah, P.P.D., Choonara, Y.E., Kondiah, P.J., Marimuthu, T., Kumar, P., du Toit, L.C., Modi, G., Pillay, V., 2018. 17 - Nanocomposites for therapeutic application in multiple sclerosis, in: Inamuddin, Asiri, A.M., Mohammad, A. (Eds.), Applications of nanocomposite materials in drug delivery. Woodhead Publishing, pp. 391-408.

Lee, K.W., Lee, H.J., Cho, H.Y., Kim, Y.J., 2005. Role of the conjugated linoleic acid in the prevention of cancer. Crit. Rev. Food Sci. Nutr. 45, 135-144.

Lee, N., Schuck, P.J., Nico, P.S., Gilbert, B., 2015. Surface enhanced Raman spectroscopy of organic molecules on magnetite (Fe_3O_4) nanoparticles. J. Phys. Chem. Lett. 6, 970-974.

Lee, W. H., Loo, C. Y., Young, P.M., Traini, D., Mason, R.S., Rohanizadeh, R., 2014. Recent advances in curcumin nanoformulation for cancer therapy. Expert Opin. Drug Deliv. 11, 1183-1201.

Lin, Z.J., Bies, J., Johnson, S.S., Gorden, J.D., Strickland, J.F., Frazier, M., Meyers, J.M., Shelton, K.L., 2019. Synthesis and anti-proliferative activity of N,N′-bis-substituted 1,2,4-triazolium salts against breast cancer and prostate cancer cell lines. J. Heterocycl. Chem. 56, 533-538.

Long, J., Zhang, C. J., Zhu, N., Du, K., Yin, Y. F., Tan, X., Liao, D. F., Qin, L., 2018. Lipid metabolism and carcinogenesis, cancer development. Am. J. Cancer Res. 8, 778-791.

Luchini, A., Gerelli, Y., Fragneto, G., Nylander, T., Pálsson, G.K., Appavou, M.-S., Paduano, L., 2017. Neutron reflectometry reveals the interaction between functionalized SPIONs and the surface of lipid bilayers. Colloids Surf. B. Biointerfaces 151, 76-87.

Luchini, A., Vitiello, G., 2019. Understanding the nano-bio interfaces: Lipid-coatings for inorganic nanoparticles as promising strategy for biomedical applications. Front. Chem. 7.

Maldonado-Camargo, L., Unni, M., Rinaldi, C., 2017. Magnetic characterization of iron oxide nanoparticles for biomedical applications. Methods Mol. Bio (Clifton, N.J.) 1570, 47-71.

Masso-Welch, P.A., Zangani, D., Ip, C., Vaughan, M.M., Shoemaker, S.F., McGee, S.O., Ip, M.M., 2004. Isomers of conjugated linoleic acid differ in their effects on angiogenesis and survival of mouse mammary adipose vasculature. J. Nutr. 134, 299-307.

Mohtar, N., Parumasivam, T., Gazzali, A.M., Tan, C.S., Tan, M.L., Othman, R., Fazalul Rahiman, S.S., Wahab, H.A., 2021. Advanced nanoparticle-based drug delivery systems and their cellular evaluation for non-small cell lung cancer treatment. Cancers (Basel) 13, 3539.

Moreira, T.G., Horta, L.S., Gomes-Santos, A.C., Oliveira, R.P., Queiroz, N.M.G.P., Mangani, D., Daniel, B., Vieira, A.T., Liu, S., Rodrigues, A.M., Gomes, D.A., Gabriely, G., Ferreira, E., Weiner, H.L., Rezende, R.M., Nagy, L., Faria, A.M.C., 2019. CLA-supplemented diet accelerates experimental colorectal cancer by inducing TGF-β-producing macrophages and T cells. Mucosal Immunol. 12, 188-199.

Muzio, G., Miola, M., Ferraris, S., Maggiora, M., Bertone, E., Puccinelli, M.P., Ricci, M., Borroni, E., Canuto, R.A., Verné, E., Follenzi, A., 2017. Innovative superparamagnetic iron-oxide

nanoparticles coated with silica and conjugated with linoleic acid: Effect on tumor cell growth and viability. Mater. Sci. Eng: C 76, 439-447.

Nana, A.B.A., Marimuthu, T., Kondiah, P.P.D., Choonara, Y.E., Du Toit, L.C., Pillay, V., 2019. Multifunctional magnetic nanowires: Design, fabrication, and future prospects as cancer therapeutics. Cancers (Basel) 11, 1956.

Nelson, N.R., Port, J.D., Pandey, M.K., 2020. Use of superparamagnetic iron oxide nanoparticles (SPIONs) via multiple imaging modalities and modifications to reduce cytotoxicity: An educational review. J. Nanotheranostics 1, 105-135.

Ngema, L.M., Adeyemi, S.A., Marimuthu, T., Choonara, Y.E., 2021. A review on engineered magnetic nanoparticles in non-small-cell lung carcinoma targeted therapy. Int. J. Pharm. 606, 120870.

Ochoa, J.J., Farquharson, A.J., Grant, I., Moffat, L.E., Heys, S.D., Wahle, K.W., 2004. Conjugated linoleic acids (CLAs) decrease prostate cancer cell proliferation: Different molecular mechanisms for cis-9, trans-11 and trans-10, cis-12 isomers. Carcinogenesis 25, 1185-1191.

Palanisamy, S., Wang, Y.-M., 2019. Superparamagnetic iron oxide nanoparticulate system: Synthesis, targeting, drug delivery and therapy in cancer. Dalton Trans. 48, 9490-9515.

Paz-Ares, L., Luft, A., Vicente, D., Tafreshi, A., Gümüş, M., Mazières, J., Hermes, B., Çay Şenler, F., Csőszi, T., Fülöp, A., Rodríguez-Cid, J., Wilson, J., Sugawara, S., Kato, T., Lee, K.H., Cheng, Y., Novello, S., Halmos, B., Li, X., Lubiniecki, G.M., Piperdi, B., Kowalski, D.M., 2018. Pembrolizumab plus chemotherapy for squamous non–small-cell lung cancer. N. Engl. J. Med. 379, 2040-2051.

Rakib, M.A., Lee, W.S., Kim, G.S., Han, J.H., Kim, J.O., Ha, Y.L., 2013. Antiproliferative action of conjugated linoleic acid on human MCF-7 breast cancer cells mediated by enhancement of gap junctional intercellular communication through inactivation of NF-κB. Evid. Based Complement. Alternat. Med. 2013, 429393.

Reczyńska, K., Marchwica, P., Khanal, D., Borowik, T., Langner, M., Pamuła, E., Chrzanowski, W., 2020a. Stimuli-sensitive fatty acid-based microparticles for the treatment of lung cancer. Mater. Sci. Eng: C 111, 110801.

Reczyńska, K., Marszałek, M., Zarzycki, A., Reczyński, W., Kornaus, K., Pamuła, E., Chrzanowski, W., 2020b. Superparamagnetic iron oxide nanoparticles modified with silica layers as potential agents for lung cancer treatment. Nanomaterials (Basel) 10, 1076.

Sadhukha, T., Wiedmann, T.S., Panyam, J., 2013. Inhalable magnetic nanoparticles for targeted hyperthermia in lung cancer therapy. Biomaterials 34, 5163-5171.

Salehi, M., Movahedpour, A., Tayarani, A., Shabaninejad, Z., Pourhanifeh, M.H., Mortezapour, E., Nickdasti, A., Mottaghi, R., Davoodabadi, A., Khan, H., Savardashtaki, A., Mirzaei, H., 2020. Therapeutic potentials of curcumin in the treatment of non-small-cell lung carcinoma. Phytother. Res. 34, 2557-2576.

Salgia, R., Pharaon, R., Mambetsariev, I., Nam, A., Sattler, M., 2021. The improbable targeted therapy: KRAS as an emerging target in non-small cell lung cancer (NSCLC). Cell Rep. Med. 2, 100186.

Sawisai, R., Wanchanthuek, R., Radchatawedchakoon, W., Sakee, U., 2019. Simple continuous flow synthesis of linoleic and palmitic acid-coated magnetite nanoparticles. Surf. Interfaces 17, 100344.

Senapati, S., Mahanta, A.K., Kumar, S., Maiti, P., 2018. Controlled drug delivery vehicles for cancer treatment and their performance. Signal Transduct. Target. Ther. 3, 7-7.

Shiraishi, R., Iwakiri, R., Fujise, T., Kuroki, T., Kakimoto, T., Takashima, T., Sakata, Y., Tsunada, S., Nakashima, Y., Yanagita, T., Fujimoto, K., 2010. Conjugated linoleic acid suppresses colon carcinogenesis in azoxymethane-pretreated rats with long-term feeding of diet containing beef tallow. J. Gastroenterol. 45, 625-635.

Slimani, S., Meneghini, C., Abdolrahimi, M., Talone, A., Murillo, J.P.M., Barucca, G., Yaacoub, N., Imperatori, P., Illés, E., Smari, M., Dhahri, E., Peddis, D., 2021. Spinel iron oxide by the co-precipitation method: Effect of the reaction atmosphere. Appl. Sci. 11, 5433.

Tang, X.-l., Lin, B.-l., Cui, S., Zhang, X., Zhong, Y., Wu, Q., Shen, X.-d., Wang, T.-w., 2016. Paclitaxel modified Fe_3O_4 loaded albumin nanoparticles as drug delivery vehicles by self-assembly. RSC advances 6, 43284-43292.

Wahajuddin, Arora, S., 2012. Superparamagnetic iron oxide nanoparticles: Magnetic nanoplatforms as drug carriers. Int. J. Nanomed. 7, 3445-3471.

Wallyn, J., Anton, N., Vandamme, T.F., 2019. Synthesis, Principles, and properties of magnetite nanoparticles for *in vivo* imaging applications: A Review. Pharmaceutics 11, 601.

Wulandari, I.O., Sulistyarti, H., Safitri, A., Santjojo, D., Sabarudin, A., 2019. Development of synthesis method of magnetic nanoparticles modified by oleic acid and chitosan as a candidate for drug delivery agent. Development 9.

Yang, K., Peng, H., Wen, Y., Li, N., 2010. Re-examination of characteristic FTIR spectrum of secondary layer in bilayer oleic acid-coated Fe_3O_4 nanoparticles. Appl. Surf. Sci. 256, 3093-3097.

Ye, Z., Huang, Y., Ke, J., Zhu, X., Leng, S., Luo, H., 2021. Breakthrough in targeted therapy for non-small cell lung cancer. Biomed. Pharmacother. 133, 111079.

Zhang, L., Shao, H. P., Zheng, H., Lin, T., Guo, Z.-m., 2016. Synthesis and characterization of Fe_3O_4@SiO_2 magnetic composite nanoparticles by a one-pot process. Int. J. Miner. Metall. Mater. 23, 1112-1118.

Zhang, T.Y., Huang, J.T., Tian, H.B., Ma, Y., Chen, Z., Wang, J.J., Shi, H.P., Luo, J., 2018. Trans-10,cis-12 conjugated linoleic acid alters lipid metabolism of goat mammary epithelial cells by regulation of de novo synthesis and the AMPK signaling pathway. J. Dairy Sci. 101, 5571-5581.

Zhao, Z., Li, Y., Zhang, Y., 2015. Preparation and characterization of paclitaxel loaded SF/PLLA-PEG-PLLA nanoparticles via solution-enhanced dispersion by supercritical CO_2. J. Nanomater. 2015, 913254.

Zhi, D., Yang, T., Yang, J., Fu, S., Zhang, S., 2020. Targeting strategies for superparamagnetic iron oxide nanoparticles in cancer therapy. Acta Biomater. 102, 13-34.

Zhong, T., Yao, X., Zhang, S., Guo, Y., Duan, X.-C., Ren, W., Dan, H., Yin, Y.-F., Zhang, X., 2016. A self-assembling nanomedicine of conjugated linoleic acid-paclitaxel conjugate (CLA-PTX) with higher drug loading and carrier-free characteristic. Sci. Rep. 6, 36614.

Zhou, Y. J., Zheng, W., Zeng, Q. H., Ye, Y., Wang, C., Fang, C., Liu, C. J., Niu, L., Wu, L. M., 2021. Targeted exome sequencing identifies mutational landscape in a cohort of 1500 Chinese patients with non-small cell lung carcinoma (NSCLC). Hum. Genomics 15, 21.

Zhuang, M., Chen, X., Du, D., Shi, J., Deng, M., Long, Q., Yin, X., Wang, Y., Rao, L., 2020. SPION decorated exosome delivery of TNF-α to cancer cell membranes through magnetism. Nanoscale 12, 173-188.

CHAPTER 4

FORMULATION AND *IN VITRO* CHARACTERIZATION OF PACLITAXEL-LOADED SPIONs FUNCTIONALIZED WITH ANTI-VEGF PEPTIDE FOR INHIBITION OF ANGIOGENESIS IN NON-SMALL-CELL LUNG CARCINOMA

4.1. Introduction

The development of a targeted therapeutic modality with the ability to selectively target cancer biomarkers and deliver anticancer therapeutics to tumors is a coveted goal for effective management of non-small-cell lung carcinoma (NSCLC) (Salehi et al., 2020; Zhou et al., 2021). Following the successful fabrication of a novel paclitaxel (PTX) delivery nanosystem with desirable physicochemical merits and a promising *in vitro* anti-proliferative action on lung adenocarcinoma cells (as presented in **Chapter 3**), in this chapter, a comprehensive design methodology is presented for the formulation of the antiangiogenic peptide-functionalized targeted PTX delivery nanosystem for targeting vascular endothelial growth factor receptors (VEGFRs) and inhibition of angiogenesis in NSCLC. Additionally, the relevant physicochemical characterization and *in vitro* cellular analyses are aptly presented.

Over the years, conventional treatment modalities for NSCLC, including combinational chemotherapy, have been shown to be riddled with exigent shortcomings such as non-specificity, high dosages, and intolerable side effects, which have culminated to their therapeutic plateau (Ngema et al., 2021; Ye et al., 2021). Particularly, PTX, as a first-line chemotherapeutic drug prescribed to NSCLC patients is challenged with poor solubility, short half-life, and undesired binding to tissue-proteins (Ye et al., 2021). Consequently, effective delivery strategies are needed to address these shortcomings. The approach of targeted nanomedicine presents a promising avenue which allows specific targeting of key tumor biomarkers and the delivery of drugs directly to target tumors (Raju et al., 2022).

Angiogenesis is one of the crucial pathways in tumor growth, responsible for the provision of oxygen and key nutrients, promoting tumor vascularization and metastasis (Lugano et al., 2020; Mashreghi et al., 2018). Therefore, the inhibition of angiogenesis through targeting of its biomarkers can potentially halt tumor proliferation and metastasis in NSCLC (Shukla et al., 2020). Vascular endothelial growth factor, encompassing VEGF A – D, is a vital biomarker and regulator of angiogenesis involved in the stimulation of new blood vessel formation through binding to vascular endothelial growth receptors (VEGFR 1 – 3) (Lugano et al., 2020; Zirlik and Duyster, 2018). As such, antiangiogenic therapy has emerged as an effective therapeutic modality in the management of NSCLC through either blocking of VEGF/VEGFRs

binding or supressing VEGFR-mediated downstream signalling through tyrosine kinase inhibitors (Daum et al., 2021; Hu et al., 2022; Yuan et al., 2019).

The peptide HRH (HRHTKQRHTALH) was first identified by Zhang *et al*., in 2017, and demonstrated high affinity for VEFGRs, both *in vitro* and *in vivo* (Zhang et al., 2017). The novel peptide was identified using VEGFR-Fc fusion protein from the Ph.D-12 phage library screening, and assessed for antiangiogenic activity on human umbilical vein endothelial cells, and alkali-burnt and suture-induced rat corneal models. HRH was found to be a mimotope that mimicked the binding sites of VEGF on VEGFRs, thus competitively inhibiting the binding of VEGF A, B, C to VEGFR 1 and 2, and subsequently halting angiogenesis (Zhang et al., 2017). Later, Chen *et al*., 2021, explored a chemically functionalized derivative of HRH to enable fabrication of nanofibers. The nanofibers demonstrated excellent *in vitro* and *in vivo* antiangiogenic activity relative to HRH administered at the same conditions (Chen et al., 2021) Ideally, the incorporation of HRH, as a homing peptide, onto a drug delivery nanosystem could yield an efficacious targeted nanomedicine, with the ability to target tumors (highly expressing VEGFRs) to block angiogenesis while releasing the anticancer drug, thus halting tumor growth and metastasis.

In **Chapter 3**, we have reported on the formulation of novel *trans*-10,*cis*-12 conjugated linoleic acid (CLA)-coated superparamagnetic iron oxide nanoparticles (SPIONs) loaded with paclitaxel (PTX), designated CLA-coated PTX-SPIONs, as a potential nanomedicine with enhanced anti-proliferative activity for NSCLC intervention (Ngema et al., 2022). Essentially, SPIONs are favourable drug vehicles, presenting with high drug-loading capacity, compatibility, and smaller size (suitable for lung tumor penetration) (Reczyńska et al., 2020; Senapati et al., 2018). Interestingly, *trans*-10,*cis*-12 conjugated linoleic acid (10E, 12Z CLA) is a natural fatty acid exhibiting anticancer properties, shown to disrupt lipid uptake and metabolism in cancerous cells, resulting in suppression of cell growth (Dachev et al., 2021; den Hartigh, 2019; Zhang et al., 2018).

Moreover, 10E, 12Z CLA is an excellent coating agent, allowing maximal partitioning of PTX, a hydrophobic anticancer drug, owing to its poor aqueous solubility (Anzai et al., 2017; Luo et al., 2010; Ngema et al., 2022). SPIONs coated with conjugated linoleic acid (CLA) have demonstrated enhanced antitumor activity against mouse breast cancer cells (4T1) (Muzio et al., 2017). Meanwhile, peptides generally exhibit high selectivity and good efficacy for biomedical application (Adeyemi and Choonara, 2022; Chen et al., 2021). This study reports on a holistic fabrication approach in achieving a targeted nanosystem that is safe by design, through the formulation of HRH-functionalized CLA-coated PTX-SPIONs (CLA-coated PTX-SPIONs@HRH), and its *in vitro* evaluation.

4.2. Materials and Methods

4.2.1. Materials

Iron (II) chloride tetrahydrate ($FeCl_2 \cdot 4H_2O$), iron (III) chloride hexahydrate ($FeCl_3 \cdot 6H_2O$), sodium hydroxide (NaOH) pellets, conjugated (10E, 12Z)-linoleic acid solution in ethanol, Taxol®, *meso*-2,3-Dimercaptosuccinic acid (DMSA), 1-ethyl-3(3-dimethylaminopropyl) carbodiimide (EDC), *N*-hydroxysuccinimide (NHS), phosphate buffered saline (PBS) tablets, dimethylformamide (DMF), 4′,6-diamidino-2-phenylindole (DAPI), and fluorescein 5(6)-isothiocyanate (FITC), were procured from Sigma-Aldrich Corp. (St. Louis, MO, USA). Pristine PTX was sourced from DLD-Scientific (Durban, South Africa) The HRH peptide was purchased from Peptron Inc. (South Korea). All solvents were of analytical grade and were utilized as received.

4.2.2. Methodology

4.2.2.1. Fabrication of CLA-coated PTX-SPIONs

The fabrication of CLA-coated PTX-SPIONs was achieved through a three-step process, as previously described in **Chapter 3.2.2**. Accordingly, SPIONs were fabricated by co-precipitation method using $FeCl_3 \cdot 6H_2O$ and $FeCl_2 \cdot 4H_2O$, 0.6mol and 0.3mol respectively, under inert atmosphere. Subsequently, SPIONs were coated with 10E, 12Z CLA, exploiting the carboxylic functionality of CLA, allowing chemisorption onto SPIONs surface. PTX self-assembled loading was achieved, with PTX adsorbing onto CLA hydrophobic ends through spontaneous hydrophobic-hydrophobic interaction. A 10% (*w/w*) PTX was added into 100% CLA-coated SPIONs suspension for loading. PTX adsorption efficiency (%AE) and drug loading capacity (%DLC) were quantified using UV spectrophotometry (Cary™ 50, Varian Inc., Palo Alto, CA, USA), meanwhile, thermogravimetric analysis (TGA 4000, PerkinElmer Inc., Waltham, MA, USA) was employed to quantify CLA content (Ngema et al., 2022).

4.2.2.2. Carboxylic acid functionalization of CLA-coated PTX-SPIONs

CLA-coated PTX-SPIONs were further functionalized with carboxylic acid (-COOH) groups to allow HRH peptide conjugation, employing optimized methods by (Martins et al., 2021) and (Dilnawaz et al., 2010), with modifications. Briefly, 1.6 M DMSA was prepared in DMF, and 20 mg CLA-coated PTX-SPIONs was added into 450 µL DMSA solution. The mixture was kept under continuous stirring at 300 rpm (Magnetic Stirrer MSH10, Labcon, Johannesburg, SA) for 24 h to allow thorough functionalization, and thereafter centrifuged for 20 min at 13 800 rpm, 10°C (TC-MiniSpin Centrifuge, TopScien, Ningbo, China) with three subsequent washes

with ethanol. The functionalized sample was lyophilized, and analyzed by Fourier Transform Infrared (FTIR) spectroscopy (Spectrum 100, PerkinElmer Inc., Waltham, MA, USA) and double titration method to confirm functionalization and determine acid number, respectively.

4.2.2.3. Free carboxylic acid groups quantification

The amount of free –COOH on the surface of CLA-coated PTX-SPIONs, following DMSA coupling, was determined using a double titration method (Dilnawaz et al., 2010; Garkhal et al., 2007). This was done to ascertain the presence of –COOH groups and estimate the concentration of EDC/NHS needed for optimal HRH conjugation. A 15 mg lyophilized sample of CLA-coated PTX-SPIONs-DMSA was suspended in 5 mL 1*N* NaOH to generate free COOH ends, for 30 min. The nanoparticles were washed three times by centrifugation at 13 800 rpm (TC-MiniSpin Centrifuge, TopScien, Ningbo, China) for 20 min at 10°C with deionized water, then lyophilized. The sample was collected into 5 mL deionized water and titrated to an endpoint with oxalic acid standardized solution of NaOH. The acid number (*A*) was computed using equation 4.1:

$$A = \frac{V_t \times N \times Mw}{w} \qquad \text{(Equation 4.1)}$$

where V_t is the required titration volume (mL), *N* is NaOH normality, *Mw* is the molecular weight of NaOH, and *w* is the weight of the nanoparticles (g).

4.2.2.4. HRH peptide conjugation to CLA-coated PTX-SPIONs

HRH was conjugated to COOH-functionalized CLA-coated PTX-SPIONs by employing the chemistry of EDC and NHS (Adeyemi et al., 2019; Dilnawaz et al., 2010; Pugliese and Gelain, 2020). Briefly, EDC in conjunction with NHS allows for 2-step coupling of peptides, where EDC activates carboxyl groups and couples NHS to carboxyls, forming a stable NHS ester which favours efficient peptide conjugation. A sample of functionalized CLA-coated PTX-SPIONs (10 mg) was added to 5 mL of 0.01 M PBS, pH 7.4. Solutions of NHS and EDC (15 mM each) were timely prepared, and 250 µL of each solution was added into the sample. The concentration of EDC/NHS was fixed at 1:0.5 molar ratio to free –COOH (as per calculated acid numbers). The mixture was then stirred at 200 rpm (Magnetic Stirrer MSH10, Labcon, Johannesburg, SA) at room temperature for 4 h. A magnetic decantation was performed to remove the supernatant, followed by addition of 3 mL 0.01 M PBS (pH 7.4) and 300 µL HRH (1 mg/mL) into the pellet. This was acclimatized at room temperature (2 h) prior to overnight incubation at 4 °C. Subsequently, the sample was precipitated using a permanent magnet, washed with PBS (3 times) to remove unbound peptide, and the supernatant was collected to determine %HRH conjugation. The sample was air dried at room temperature and the attained

CLA-coated PTX-SPIONs@HRH were further characterized. The % HRH conjugation was determined using a prepared standard plot of HRH concentrations (5 – 30 µg/mL) on a UV spectrophotometer (Cary™ 50, Varian Inc., Palo Alto, CA, USA) at 280 nm, using the formula in equation 4.2:

$$\%\ HRH\ conjugation = \frac{P_t - P_s}{P_t} \times 100 \qquad \text{(Equation 4.2)}$$

where P_t is the total amount of peptide added and P_s is the amount of unbound peptide in the supernatant, in mg.

4.2.3. Physicochemical characterization of CLA-coated PTX-SPIONs@HRH

4.2.3.1. Assessment of chemical functionality and functional transformations

Chemical composition of individual materials and functional transformations in the combined components of CLA-coated PTX-SPIONs@HRH were assessed using the Fourier Transform Infrared (FTIR) spectroscopy (Spectrum 100, PerkinElmer Inc., Waltham, MA, USA). The analysis was conducted with the set conditions in place; 4000 – 550 cm^{-1}, 120 psi, and 20 scans (Ngema et al., 2022).

4.2.3.2. Analysis of particle hydrodynamic size, polydispersity index and zeta potential

The average hydrodynamic size, polydispersity index (PDI) and zeta potential (surface charge) of CLA-coated PTX-SPIONs@HRH were ascertained using a dynamic ZetaSizer instrument (NanoZS, Malvern Panalytical, Malvern, UK). Dynamic light scattering measurements were recorded from a sample (10 µg suspended in 1 mL distilled water) to confirm the particle size and PDI, while phase-analysis light scattering measurements confirmed the zeta potential. The analyses were conducted at 25°C using a disposable cuvette and a DTS 1070 cuvette, for size/PDI and zeta potential, respectively. The sample was first sonicated (Sonics Vibra Cell, Newtown, CT, USA) for 10 min prior analyses.

4.2.3.3. Assessment of overall morphology

Scanning Electron Microscopy (SEM) and Transmission Electron Microscopy (TEM) were employed to assess the overall morphology of CLA-coated PTX-SPIONs@HRH. An aliquot was withdrawn from the sample that was previously measured for hydrodynamic size, and was allowed to dry on a specimen stub and coated twice with gold palladium (AuPd) for SEM analysis (ZEISS Electron Microscopy, Carl Zeiss Microscopy Ltd., Cambridge, UK). Meanwhile, preparation for TEM analysis involved dipping a carbon-coated 200-mesh copper

grid into a sample suspension and dried overnight before analysis (FEI™ Tecnai T12 120 kV, FEI Technologies Inc., Hillsboro, OR, USA).

4.2.4. *In vitro* analyses of CLA-coated PTX-SPIONs@HRH

4.2.4.1. In vitro PTX release from CLA-coated PTX-SPIONs@HRH

The release of PTX from CLA-coated PTX-SPIONs@HRH was evaluated at physiological pH (7.4) as well as tumor microenvironment-mimicking pH (6.8) (Adeyemi et al., 2019). A 3 mg sample of CLA-coated PTX-SPIONs@HRH was dispersed in 2.5 mL of each prepared 0.1 M buffer (pH 6.8 and 7.4) conditioned with 0.1% v/v tween, in a dialysis membrane (SnakeSkin™, 3 500 MWCO). The membrane only permitted the release of PTX into the release buffer over 24 h in a 37°C orbital shaker (YIHDER LM-530, YIHDER Co., Lt., Taipei, Taiwan). The amount of PTX released at t = 1, 2, 4, 8, 12, 16, and 24 h was calculated against the standard curve at 227 nm (Cary™ 50, Varian Inc., Palo Alto, CA, USA). Medium replenishment with equivalent sampling volume (2 mL) after each sampling point was carried out at all sampling points.

4.2.4.2. Anti-proliferative activity assessment on lung adenocarcinoma

Lung adenocarcinoma (A549) cell line (Cellonex, Johannesburg, South Africa) was employed to assess the viability of the cells post-treatment with CLA-coated PTX-SPIONs@HRH, over 72 h. A standard 3-(4,5-dimethylthiazole-2-yl)-2,5-diphenyl tetrazolium bromide (MTT) Cell Proliferation Kit I protocol was followed (Roche, Basel, Switzerland). A549 cells were cultured in Dulbecco's Modified Eagle Medium (DMEM) supplemented with 10% *v/v* Foetal Bovine Serum (FBS) and penicillin-streptomycin antibiotic (1% *v/v*) in a T-25 culture flask. The cells were incubated at 37°C, 5% CO_2 saturation, and humid environment until reaching a confluence of 90%. Cells were then seeded (2.5×10^4 cells/ml) in a 96-well plate, with each well containing 90 µL cell suspension, and incubated for 24 h (37°C, 5% CO_2) for optimal cellular adherence. Treatment concentrations of 25, 50, and 100 µg/mL CLA-coated PTX-SPIONs and CLA-coated PTX-SPIONs@HRH were prepared in PBS and experimental cells treated (n=*3*) with 10 µL while control cells were left untreated. The cells were incubated for 72 h (37°C, 5% CO_2, humidity) before the viability assay could be carried out. Accordingly, after 72 h incubation, 10 µL of MTT solution (5 mg/mL) was added into wells and the plate incubated for 4 h as before. Thereafter, formed formazan crystals were dissolved with acid-isopropanol solubilizing agent (100 µL) overnight under incubation. The plate was then analyzed using a multimodal microplate reader (Victor X3, PerkinElmer, Waltham, MA, USA) by measuring the absorbance at 570 nm. Plate wells with only growth medium and solubilizing

agent were sampled as a blank. The % cell viability (CV) was calculated from the absorbance readings (mean±standard deviation) using the formula (equation 4.3):

$$\% \text{ CV} = \frac{A_{test} - A_{blank}}{A_{control} - A_{blank}} \times 100 \qquad \text{(Equation 4.3)}$$

where A_{test}, $A_{control}$, and A_{blank} are test absorbance, control absorbance, and blank absorbance, respectively, in nm (620 nm reference wavelength).

4.2.4.3. Evaluation of cellular uptake and internalization by lung adenocarcinoma cells

FITC-labelled CLA-coated PTX-SPIONs@HRH were prepared using a modified encapsulation method described by Kumar and Srivastava (2018) (Kumar and Srivastava, 2018). Briefly, FITC (1 mg) was dissolved in 1 mL dichloromethane and methanol (50:50), and the solution was added dropwise into a nanoformulation suspension (2.5 mg in 5 mL distilled water). The sample was stirred at 300 rpm for 15 min (Magnetic Stirrer MSH10, Labcon, Johannesburg, SA) in the dark and at room temperature to evaporate the solvent. The sample was then centrifuged three times at 14 000 rpm for 20 min, 10°C (TC-MiniSpin Centrifuge, TopScien, Ningbo, China), with subsequent washing (distilled water) to remove unbound FITC. The FITC-labelled nanoformulation was collected and stored away from light.

The model A549 cell line was cultured as described above (*4.2.4.2*) and employed for the uptake and internalization study. Cells were seeded (5×10^4 cells/mL) on presterilized cover slips in a 6-well plate, with each well containing 800 µL cell suspension, and incubated for 24 h at 37°C and 5% CO_2. After incubation, experimental cells were treated with 200 µL of FITC-labelled nanoformulation (1 mg/mL in PBS) and further incubated for another 24 h, while control cells were not treated. After 24 h, all wells were spiked with 500 µL of 4% paraformaldehyde (PFA) for 2 min to acclimatise the cells to the fixation solution. Thereafter, the media was decanted and cells were fixed with 1 mL 4% PFA for 20 min. The cells were washed 4 times with 2 mL 1X PBS, and stained with DAPI (300 µL; 300 nM) followed by incubation for 5 min in the dark at room temperature. The stained cells on cover slips were further washed 4 times with 1X PBS, and then cover slips mounted on glass slides with 80% *v/v* cooled glycerol, and allowed to dry before microscopy analysis. A compound fluorescent microscope (Olympus IX51, Olympus Corporation, Tokyo, Japan) was used to view and capture images of the cells at 517 nm green fluorescence excitation (FITC) and 461 nm blue fluorescence excitation (DAPI) using the super 40X objective lens.

4.2.4.4. Assessment of VEGFR targeting using Enzyme-linked Immunosorbent Assay (ELISA)

A human dermal microvascular endothelial cell line (HMEC-1) (Separation Scientific SA Pty. Ltd, Johannesburg, South Africa) was employed for the evaluation of VEGFR targeting by CLA-coated PTX-SPIONs@HRH, using a direct Human VEGF-A ELISA Kit (Invitrogen, Thermo Fisher Scientific Corporation, Waltham, MA, USA). HMEC-1 cells were cultured in a special MCDB 131 medium supplemented with 10 ng/mL human EGF recombinant protein, 1 µg/mL hydrocortisone, 10 nM L-glutamine, and 10% *v/v* FBS. The cells were incubated in a T-25 culture flask at 37°C, 5% CO_2 saturation, and humid environment. At 90% confluence, cells were seeded (5×10^4 density) in two 6-well plates, with each well containing 800 µL cell suspension, and incubated for 24 h to attach. Thereafter, cells were treated in triplicate with 200 µL of 50 µg/mL CLA-coated PTX-SPIONs@HRH and CLA-coated PTX-SPIONs for 24 h under incubation. The control cells were not treated. After 24 h of incubation, 1 mL of cell media supernatant was collected, placed on ice, and centrifuged at 13 000 rpm, 4°C for 20 min (Eppendorf™ Centrifuge 5415R, Merck, Darmstadt, Germany). The supernatant was then used for VEGF-A ELISA analysis as per the manufacturer's protocol, with the absorbance recorded at 450 nm using a multimodal microplate reader (Victor X3, PerkinElmer, Waltham, MA, USA).

4.2.5. Statistical analysis

A two-tailed Student's *t*-test was applied to statistically analyze the data on GraphPad prism 9 (GraphPad Software, Inc., San Diego, CA, USA), with $p < 0.05$ deemed statistically significant. Data are reported as mean values of biological triplicates ($n=3$) ± standard deviation.

4.3. Results and Discussion

4.3.1. Fabrication of CLA-coated PTX-SPIONs@HRH

A CLA-coated PTX-SPIONs@HRH nanosystem was successfully fabricated from black powdered, purely magnetite SPIONs (Fe_3O_4) synthesized from iron chloride salts, coated with a hydrophobic 10E, 12Z CLA isomer, partitioned with hydrophobic PTX, and functionalized with HRH peptide via a DMSA-aided EDC/NHS chemistry conjugation (**Figure 4.1**). Essentially, surface modification is key in the application of SPIONs as anticancer drug vehicles as it allows customization of SPIONs according to tumor specificity (Reczyńska et al., 2020). Primarily, SPIONs synthesized via co-precipitation method have excess surface OH^- groups that can be manipulated to achieve desired surface modifications, via chemisorption

chemistry (Dilnawaz et al., 2010; Ngema et al., 2022). Accordingly, the active carboxyl group and inherent crosslinking activity of 10E, 12Z CLA was exploited for chemisorption onto the SPIONs for surface coating, while the hydrophobicity of the isomer allowed adsorption of hydrophobic PTX.

Fundamentally, the understanding of the coating material (polymer), as well as the loading technique are very critical in drug loading, in order to maximize drug entrapment, ensure that the functionality of the drug is not comprised, and achieve sustained release of the drug at the target site (Adepu and Ramakrishna, 2021). The content of 10E, 12Z CLA coated onto SPIONs was found to be 10.3%, which resulted in PTX adsorption efficiency of 98.5% and 9.8% DLC (amount of PTX per unit mass of nanoformulation). The %AE and %DLC (98.5 and 9.8%, respectively) indicated the superiority of 10E, 12Z CLA as a suited partitioning agent for PTX, and arguably for other hydrophobic anticancer drugs, and supports the concept that SPIONs offer high drug loading capacity (Kovrigina et al., 2022; Ngema et al., 2021). Moreover, the latter could be confirmed from the present study, considering that 10% (*w/w*) PTX was applied in the loading process, and 9.8% was found to be successfully loaded onto CLA-coated SPIONs.

Carboxylic acid functionalization by DMSA was a crucial step in the fabrication of CLA-coated PTX-SPIONs@HRH, which required the use of a polar aprotic solvent DMF to enable DMSA grafting (via hydrogen bonding) onto SPIONs. Ideally, a polar aprotic solvent allows the coupling reaction to occur without it partaking in hydrogen bonding with the nucleophile (Bucholz and Loo, 2008). The number of free –COOH was ascertained to be 63.7 per gram of CLA-coated PTX-SPIONs which could be expected from 1.6 M of DMSA. Dilnawaz et al., 2010 previously reported acid numbers from 8 per gram of glycerol monooleate (GMO)-coated Fe_3O_4 when 0.2 M DMSA was used, up to 130 acid number with increase in DMSA concentration, however noted that once binding saturation is reached, even the increase in DMSA concentration does not significantly alter acid numbers (Dilnawaz et al., 2010). Another study by Garkhal et al., reported acid number of 44.4 for conjugation of P-15 peptide on poly(L-lactide-co-ε-caprolactone) modified microspheres (Garkhal et al., 2007). The molar ratio of EDC/NHS to free –COOH was fixed at 1:0.5 to allow adequate activation of the –COOH groups and conjugation of HRH peptide. The methodology exhibited high efficacy with a recorded %HRH conjugation of 66.6%. The successful conjugation of HRH peptide was also evident from the qualitative FTIR analysis (**Figure 4.2e**).

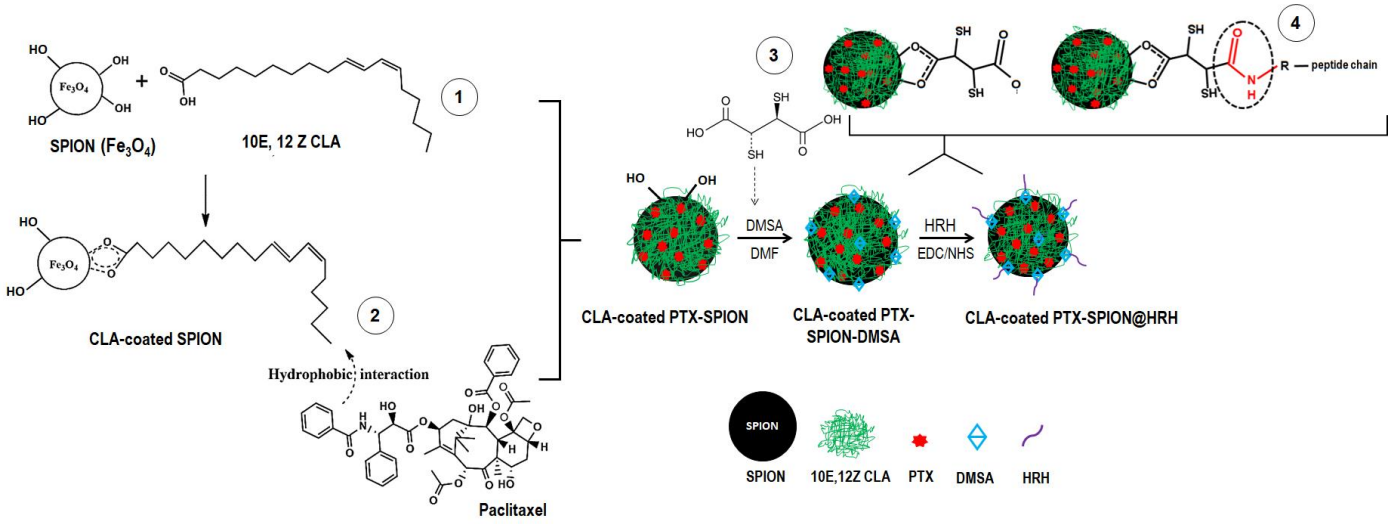

Figure 4.1. Schematic representation of the fabrication methodology of CLA-coated PTX-SPIONs@HRH (*not drawn to actual scale*). The coating of SPIONs with 10E, 12Z is through chemisorption via –COOH of CLA and –OH on SPIONs surface (**1**). PTX loading onto CLA-coated SPIONs is via a spontaneous hydrophobic-hydrophobic interaction between CLA and PTX (**2**). The physical functionalization of the SPIONs surface with DMSA was carried out in DMF to favour the formation of hydrogen bonding between the –COOH groups in DMSA and available adsorbed –OH groups on SPIONs surface (**3**) (Galli et al., 2017; Walter et al., 2015). Subsequently, the HRH peptide has a reactive $–NH_2$ terminal which enabled conjugation to surface bound $–COO^-$ groups on SPIONs after EDC/NHS activation (**4**).

4.3.2. Particle size and overall morphological analysis of CLA-coated PTX-SPIONs@HRH

The average hydrodynamic size and zeta potential of formulated CLA-coated PTX-SPIONs@HRH was found to be 108.5 ± 3.5 nm and -30.4 ± 2.3 mV, respectively (**Figure 4.2a, b**), with a polydispersity index (PDI) of 0.2 ± 0.01. The zeta potential and PDI revealed that CLA-coated PTX-SPIONs@HRH exhibited colloidal stability with reduced aggregation in aqueous media, which fits the criteria for biomedical application (Marins et al., 2018). Interestingly, the particle size obtained is relatively smaller compared to other reported ligand-functionalized targeted nanosystems for NSCLC, such as tumor homing peptide LYP-1 functionalized liposome nanoparticles (*tLYP-1-PEG-NPs*; 188 nm) by Jin et al., (Jin et al., 2018) and an antibody modified targeted nanostructured carrier (*Flk-1-DSPE-PEG-NH_2-NLC*; 168 nm) by Liu et al., (Liu et al., 2011) amongst others. Essentially, the smaller particle size is ideal for lung tumor penetration (Wang et al., 2022). The overall morphology, as examined by SEM and TEM (**Figure 4.2c, d**), revealed a quasi-spherical shape for CLA-coated PTX-SPIONs@HRH, with a slightly rugged surface, and nm size range. The quasi-spherical shape

could be attributed to surface modification by DMSA, with short chains of DMSA around the spherical iron oxide imparting the quasi-spherical conformation, as mostly reported for DMSA-modified iron oxide nanoparticles (Song et al., 2017; Sun et al., 2015).

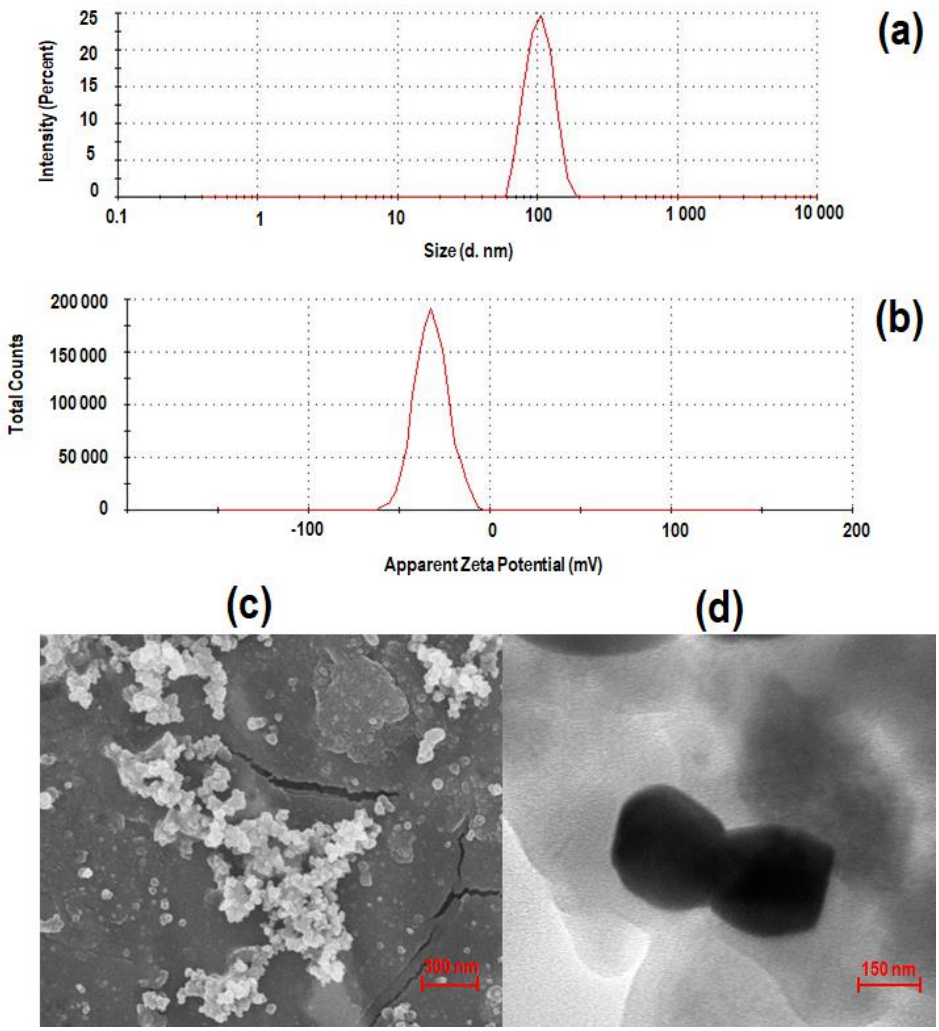

Figure 4.2. A graphical representation of (**a**) average hydrodynamic size and (**b**) zeta potential of CLA-coated PTX-SPIONs@HRH, with corresponding morphological depiction by (**c**) SEM viewed at 300 nm (magnification = 81.75 KX) and (**d**) TEM viewed at 150 nm scale (magnification = 73000 X). Captured micrographs show quasi-spherical shaped nanoparticles in the nm size range, and within the specified average size, as shown by the scale bars.

4.3.3. Assessment of chemical composition and functional transformations of CLA-coated PTX-SPIONs@HRH

The chemical composition of CLA-coated PTX-SPIONs, DMSA, and HRH, as well as functional transformations towards the formation of CLA-coated PTX-SPIONs@HRH were ascertained by FTIR spectroscopy. Essentially, FTIR spectroscopy has proven to be a robust

technique for immediate identification of functional groups in compounds, and characterization of bond formations (Galli et al., 2017). The FTIR spectra obtained in the present study are shown in **Figure 4.3a-e**. The spectrum for CLA-coated PTX-SPIONs (**Figure 4.3a**) exhibited characteristic PTX peaks at 3479 cm^{-1} and 1244 cm^{-1} (belonging to –OH and ester groups, respectively), characteristic 10E, 12Z CLA peaks around 2922 – 2852 cm^{-1} belonging to symmetric and asymmetric $–CH_2$ stretch vibrations, and 1608 cm^{-1} belonging to a CH_3 bending, as well as an iron oxide (Fe-O) peak at around 580 cm^{-1} (Akilo et al., 2016; Muzio et al., 2017; Zhao et al., 2015). Characteristic peaks of DMSA (**Figure 4.3b**) were observed at 2561 cm^{-1} and 1685 cm^{-1} attributed to the thiol (–SH) and C=O of the carboxyl groups, respectively (Çitoğlu et al., 2021).

In a spectrum of CLA-coated PTX-SPIONs-DMSA (**Figure 4.3c**), a split in the C=O peak of DMSA to 1685 cm^{-1} and 1647 cm^{-1} was observed, presumably belonging to the stretching vibrations of the carboxylate (COO^-) ions due to DMSA linkage onto SPIONs surface via the carboxyl group (**Figure 4.1**) (Çitoğlu et al., 2021; Tsoukalas et al., 2018). A spectrum of pure HRH peptide (**Figure 4.3d**) exhibited characteristic peaks at around 3276 cm^{-1}, 1654 - 1619 cm^{-1}, and 1261 - 1255 cm^{-1} attributed to the terminus primary amine ($–NH_2$), C=O stretch, and peptide bond (C-N) stretch, respectively (Rinawati et al., 2015; Sebben and Pendleton, 2014). Meanwhile, CLA-coated PTX-SPIONs@HRH (**Figure 4.3e**) exhibited major characteristic peaks of all starting materials (red rectangle), with overlapping bands at ~1652 cm^{-1} and 1570 cm^{-1} attributed to amide I and II, respectively (Ji et al., 2020). Particularly, the amide II [R'C(=O)NHR] band could be associated with HRH conjugation via $–NH_2$ onto activated COO^- afforded by DMSA (**Figure 4.1**). Moreover, a new broad band at 3302 cm^{-1} was identified (red circle), attributed to N-H stretching resulting from HRH conjugation, meanwhile a shift in C-N stretch (~1028 cm^{-1}) could be associated with increasing peptide bonds, owing to new amide II bond formation. This qualitatively confirmed the conjugation of HRH peptide onto the nanosystem, and together with the plausible %HRH conjugation obtained supports the effectiveness of the method for binding of HRH peptide onto the surface of CLA-coated PTX-SPIONs.

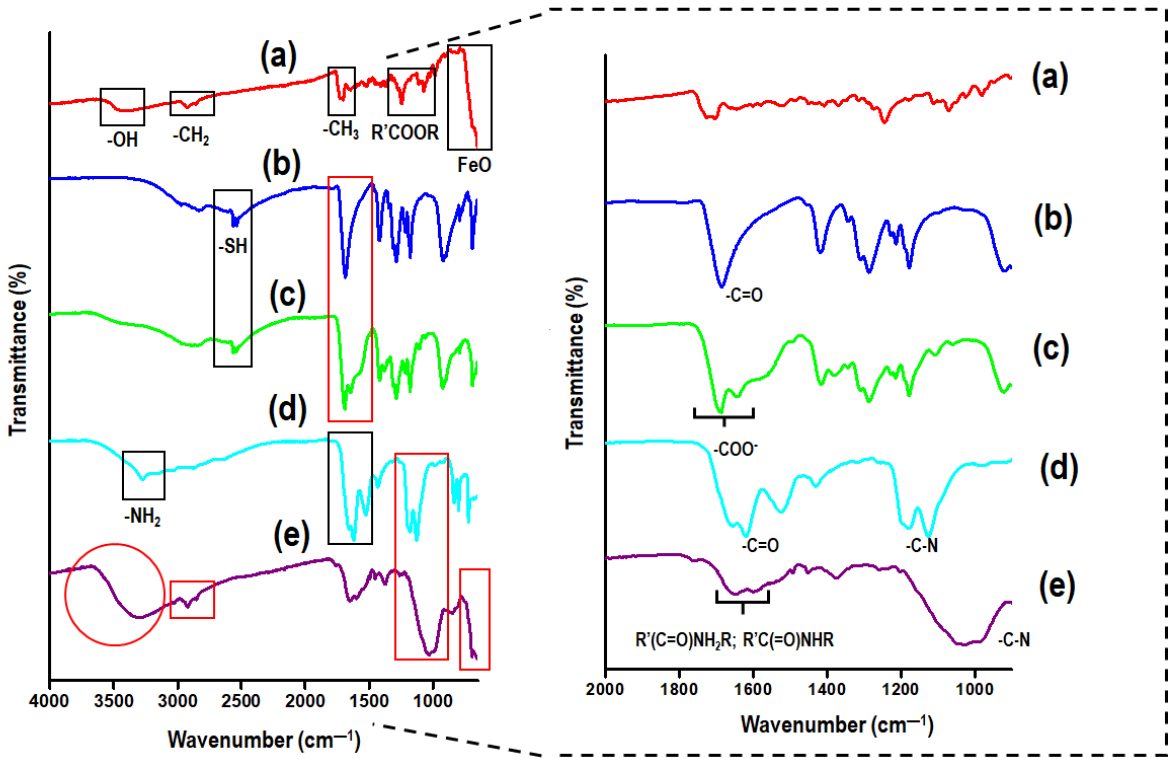

Figure 4.3. Functional group mapping by FTIR spectroscopy showing identified characteristic functionality of (**a**) CLA-coated PTX-SPIONs, (**b**) DMSA, (**c**) CLA-coated PTX-SPIONs-DMSA, (**d**) HRH, and (**e**) CLA-coated PTX-SPIONs@HRH. On the right is the pan image at 2000 – 1000 cm^{-1}.

4.3.4. *In vitro* PTX release kinetics from CLA-coated PTX-SPIONs@HRH

The *in vitro* release profile of PTX from CLA-coated PTX-SPIONs@HRH over 24 h is presented in **Figure 4.4**. The fabricated nanosystem exhibited a sustained PTX release at pH 6.8, with maximal cumulative release of 99.4% recorded at 16 h. The sustained PTX release at acidic pH is consistent with previous studies which have reported a similar release behaviour when PTX is loaded onto fatty acids such as oleic acid and its derivatives (Wulandari et al., 2019; Zhang et al., 2021). The high and sustained release of PTX at pH 6.8 could be attributed to the weakening of the hydrophobic-hydrophobic strength between CLA~PTX at relatively acidic pH, thus allowing PTX to detach from CLA ends and is released over time (Ngema et al., 2022). Meanwhile, the PTX release was comparatively lower at physiological pH 7.4, with only 19.6% of PTX released in over 24 h. This low cumulative release rate relates to the stability of the hydrophobic CLA~PTX interaction at physiological pH, keeping PTX intact over time. The initial release at the first hour was 11.4%, and only 19.6% of PTX was released at 24 h, which is even lower than the release in the first h (25.9%)

at pH 6.8. Primarily, the overall *in vitro* release data suggest that the release of PTX from the CLA-coated PTX-SPIONs@HRH nanosystem is site-specific.

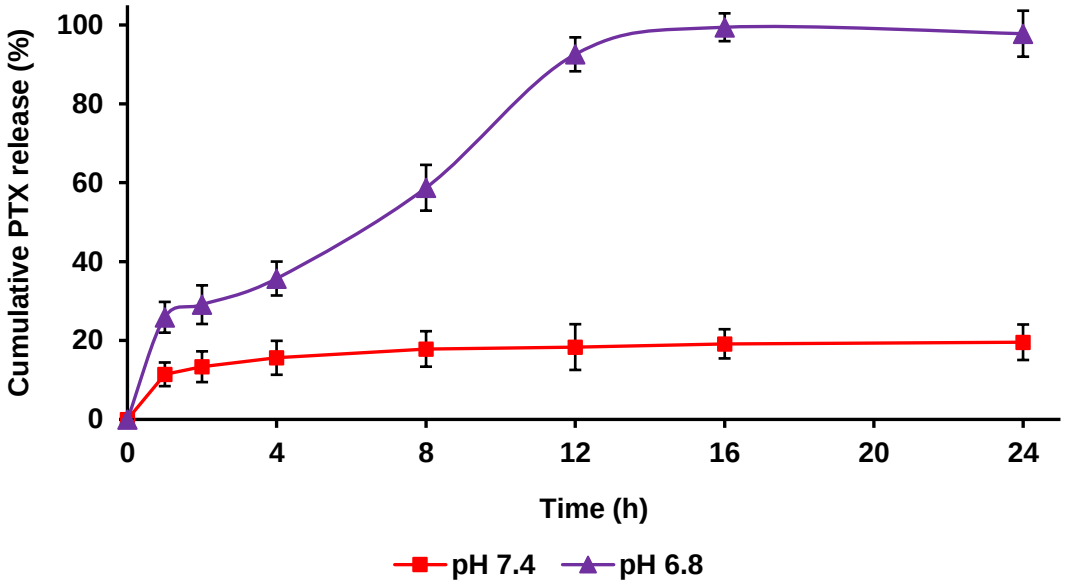

Figure 4.4. *In vitro* cumulative release of PTX at pH 6.8 and pH 7.4 over 24 h. Data presented as mean ± SD of three sample analyses (*n=3*) per time point.

4.3.5. Anti-proliferative activity of CLA-coated PTX-SPIONs@HRH on A549 lung adenocarcinoma cells

The anti-proliferative activity of CLA-coated PTX-SPIONs@HRH was assessed on A549 lung adenocarcinoma cells, and the treatment response (% cell viability) was recorded and is presented in **Figure 4.5**. The anti-proliferative activity was found to be concentration dependent, with a decrease in % cell viability as the concentration increased. The highest treatment concentration (100 µg/mL) with CLA-coated PTX-SPIONs@HRH and CLA-coated PTX-SPIONs yielded a % cell viability of 12.8% and 17.1%, respectively. Meanwhile, the cells treated with the lowest concentration (25 µg/mL) of CLA-coated PTX-SPIONs@HRH and CLA-coated PTX-SPIONs had a % cell viability of 17.8% and 19.3%, respectively. This showed that both formulations comparatively supressed A549 cell proliferation over 72 h, however, CLA-coated PTX-SPIONs@HRH resulted in an enhanced suppression of A549 cells, which is attributed to the effect of HRH peptide on cancer cell proliferation. There is already compelling evidence in literature that HRH peptide suppresses cancer cell proliferation *in vitro* by halting angiogenesis (Zhang et al., 2017). Moreover, the results obtained support our previous findings in **Chapter 3** which showed that CLA-coated PTX-SPIONs confer

enhanced anti-proliferative activity against A549 cells owing to additional anticancer activity of 10E, 12Z CLA in synergy with PTX.

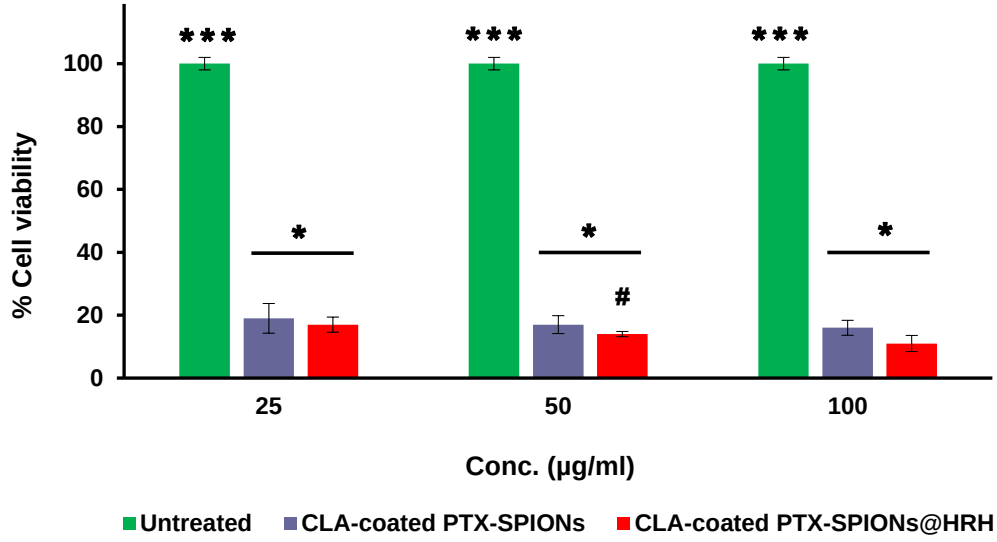

Figure 4.5. Cell viability (%) profile of A549 cells following treatment with varying concentrations of CLA-coated PTX-SPIONs and CLA-coated PTX-SPIONs over 72 h. The treatment concentrations were based on the concentrations that could yield distinguishable outcome between the HRH-functionalized and non-functionalized nanosystem, to discern the effect of the peptide. Data computed as mean ± SD, *n=3* (*** denotes $p < 0.001$ compared to treatment groups at each concentration, * denotes $p < 0.05$ amongst all concentrations, and # depicts $p < 0.05$ against CLA-coated PTX-SPIONs at a specified concentration).

4.3.6. Cellular uptake and internalization of CLA-coated PTX-SPIONs@HRH

A high uptake of CLA-coated PTX-SPIONs@HRH, sufficient to cause detrimental nuclei damage was observed in model A549 lung adenocarcinoma cells (**Figure 4.6**). The DAPI staining (blue fluorescence) was solely employed to visualize the nuclei of untreated cells (**Figure 4.6a**) and treated cells (**Figure 4.6c**). Meanwhile, FITC (green fluorescence) was used to visualize the nanoformulation (**Figure 4.6b**) and track the cellular uptake, as shown on the superimposed (DAPI+FITC) micrograph in (**Figure 4.6d**). The proximity of the green fluorescence to the blue fluorescence (**Figure 4.6d**) compellingly showed that the nanoformulation was internalized and reached the nuclei of the cells. CLA-coated PTX-SPIONs@HRH could be visualized within the cells, engulfing the nuclei and rupturing the nuclei architecture (red boxes), subsequently resulting in presumed cell death. This revelation compliments and further explains the superlative anti-proliferative activity exhibited by CLA-coated PTX-SPIONs@HRH, as recorded on the MTT assay. Essentially, the high uptake of

CLA-coated PTX-SPIONs@HRH observed could be attributed to the preferential binding of HRH onto VEGF receptors on the cellular surface, thus facilitating a receptor-mediated internalization by A549 cells. Moreover, the presence of 10E, 12Z could be assumed to have played a role in increasing the affinity of A549 cells for CLA-coated PTX-SPIONs@HRH, as cancer cells normally take up essential fatty acids as energy source (Currie et al., 2013). Similarly, the smaller size of the nanoparticles could have favoured the uptake by the cells (Shang et al., 2014).

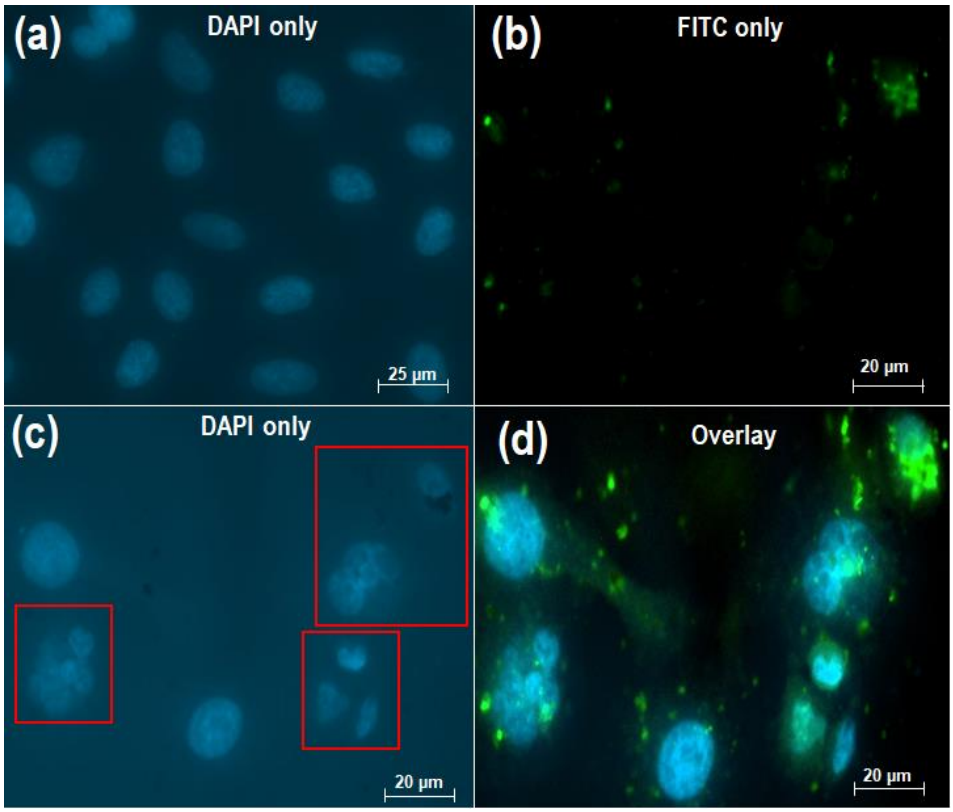

Figure 4.6. Fluorescent micrographs from a CLSM, showing (**a**) intact nuclei of untreated control cells, (**b**) visualization of FITC-labelled CLA-coated PTX-SPIONs@HRH on treated cells, (**c**) ruptured nuclei of treated cells, and (**d**) overlay of DAPI and FITC showing the uptake of CLA-coated PTX-SPIONs@HRH by A549 lung adenocarcinoma cells. The ruptured nuclei architecture of treated cells (red boxes) could be distinguished from the normal nuclei architecture of untreated cells.

4.3.7. Quantification of VEGF-A levels via ELISA

VEGF-A predominantly regulates angiogenesis and its levels are perfectly maintained in endothelial cells, such that even a slight change may result in lethality (Abhinand et al., 2016). Herein, the levels of VEGF-A were quantified from endothelial cells (HMEC-1) treated with

nanoformulations (with and without HRH peptide) as a measure of antiangiogenic activity through VEGFR blockage. The VEGF-A ELISA concentration plot is presented in **Figure 4.7**. The levels of secreted VEGF-A varied amongst the groups after 24 h, ranging from 35.6 – 53.1 pg/mL. This range could be expected from the endothelial cells as a marker of physiological angiogenesis rather than a pathological angiogenesis (i.e., in cancer and other diseases). It is reported that the over expression of VEGF in cancerous cells could be quantified at much elevated levels of about 310 pg/mL and above (Kut et al., 2007; Truelsen et al., 2021).

The level of VEGF-A from untreated cells was 46.9 pg/mL while that from cells treated with CLA-coated PTX-SPIONs and CLA-coated PTX-SPIONs@HRH was 53.1 pg/mL and 35.6 pg/mL, respectively. A significant decline in VEGF-A levels in cells treated with CLA-coated PTX-SPIONs@HRH compared to untreated cells is indicative of a possible disruption in normal VEGF-A/VEGFR signalling. Fundamentally, growing cells continuously secrete VEGF-A which binds to VEGFR 2 for further growth and migration, since VEGFR 1 has minimal kinase activity (Shibuya, 2011). Since VEGF-A/VEGFR 2 downstream signalling regulates angiogenesis and stimulates endothelial proliferation, a decline observed in VEGF-A levels could be explained as limited cell proliferation due to inhibition of angiogenesis by VEGFR blockage. Herein, it is presumed that CLA-coated PTX-SPIONs@HRH bind VEGFR 2 and block the binding of VEGF-A, thus preventing further vascular development and epithelial proliferation.

Meanwhile, cells treated with CLA-coated PTX-SPIONs showed comparatively increased levels of VEGF-A, indicative of continuous epithelial proliferation. This could hypothetically be the response of HMEC-1 in trying to overcome the exogenous agent by secreting more growth factors to stimulate further proliferation. Moreover, HMEC-1 are known to retain most of the primary angiogenic features and possess stability over time (Muñoz-Vega et al., 2018; Prigozhina et al., 2011). Interestingly, the observation could suggest that even though CLA-coated PTX-SPIONs exhibit cancer anti-proliferative activity, its mechanism of action is different from that of CLA-coated PTX-SPIONs@HRH, and does not involve angiogenesis inhibition.

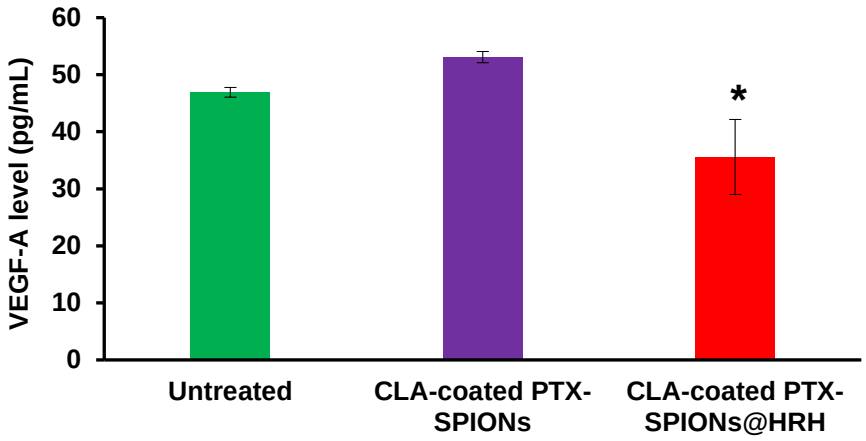

Figure 4.7. VEGF-A levels from HMEC-1 after 24 h. Data presented as mean ± SD (* denotes $p < 0.05$, statistically significant compared to untreated and CLA-coated PTX-SPIONs groups).

The diminishing levels of VEGF-A recorded from HMEC-1 treated with CLA-coated PTX-SPIONs@HRH agreed with the proposed notion that CLA-coated PTX-SPIONs@HRH could halt angiogenesis through selective binding of the nanosystem to VEGFRs, and could explain the marked cellular uptake and anti-proliferative activity of CLA-coated PTX-SPIONs@HRH. VEGF-A predominantly regulates angiogenesis (vascular development) (Peach et al., 2018; Shibuya, 2011), and its action and expression may also be controlled by different proteins which are able to bind and sequester it, including VEGFRs (Eichmann and Simons, 2012). VEGF/VEGFR 2 binding is responsible for vascular development, while VEGFR 1 is recognised as a decoy receptor because of its poor kinase activity (Peach et al., 2018). Accordingly, it is believed that the low levels of VEGF-A recorded could be the results of the blockage of VEGFR 2 (bound by CLA-coated PTX-SPIONs@HRH) which prevented VEGF-A downstream signalling and subsequently halted angiogenesis.

4.4. Concluding Remarks

Primarily, the work presented in this chapter aimed to optimize the initially fabricated CLA-coated PTX-SPIONs by surface-functionalization with an anti-VEGF peptide HRH, using robust coupling reactions, to afford VEGFR targetability while maintaining the desired physicochemical properties. Accordingly, an efficient fabrication methodology was successfully established to formulate a targeted drug delivery nanosystem, capable of selectively binding to VEGFRs and block the binding of VEGF-A responsible for angiogenesis. The methodology was efficient in immobilizing sufficient HRH on the surface of CLA-coated PTX-SPIONs, with the aid of DMSA, to elicit marked VEGFRs targetability and cellular uptake. Moreover, the estimation of acid numbers worked well in determining the appropriate

concentrations of EDC and NHS for a favourable coupling reaction, meanwhile, the use of FTIR was preferable for the confirmation of the overall formation of the desired nanosystem.

In essence, the formulated CLA-coated PTX-SPIONs@HRH is safe-by-design and presents with high PTX loading capacity and a sustained, site-specific release. The stimuli-responsiveness of 10E, 12Z CLA to acidic pH 6.8 (mimicking tumor microenvironment) imparted a crucial aspect to the nanosystem, enabling site-specific release of PTX, which was evident from the high *in vitro* anti-proliferative activity recorded against A549 cells. Moreover, the nanosystem exhibited a remarkable uptake and internalization by lung adenocarcinoma cells. Consequently, CLA-coated PTX-SPIONs@HRH present a potentially viable targeted nanomedicine for NSCLC management, with specific angiogenesis targeting and direct drug delivery at tumor sites. Nonetheless, the investigation of other angiogenesis biomarkers as potential targets in NSCLC therapy still needs to be considered. In this regard, in the next chapter, another prominent biomarker of angiogenesis, matrix metalloproteinase-2 (MMP-2), is targeted *in vitro* using optimized CLA-coated PTX-SPIONs, surface functionalized with anti-MMP-2 peptide CTT to yield a selective MMP-2 targeting nanosystem.

4.5. References

Abhinand, C.S., Raju, R., Soumya, S.J., Arya, P.S., Sudhakaran, P.R., 2016. VEGF-A/VEGFR2 signaling network in endothelial cells relevant to angiogenesis. J. Cell Commun. Signal. 10, 347-354.

Adepu, S., Ramakrishna, S., 2021. Controlled drug delivery systems: Current status and future directions. Molecules 26, 5905.

Adeyemi, S.A., Choonara, Y.E., 2022. *In vitro* and *in vivo* evaluation of a cyclic LyP-1-modified nanosystem for targeted endostatin delivery in a KYSE-30 cell xenograft athymic nude mice model. Pharmaceuticals 15, 353.

Adeyemi, S.A., Choonara, Y.E., Kumar, P., du Toit, L.C., Marimuthu, T., Kondiah, P.P.D., Pillay, V., 2019. Folate-decorated, endostatin-loaded, nanoparticles for anti-proliferative chemotherapy in esophaegeal squamous cell carcinoma. Biomed. Pharmacother. 119, 109450.

Akilo, O.D., Choonara, Y.E., Strydom, A.M., du Toit, L.C., Kumar, P., Modi, G., Pillay, V., 2016. An *in vitro* evaluation of a carmustine-loaded nano-co-plex for potential magnetic-targeted intranasal delivery to the brain. Int. J. Pharm. 500, 196-209.

Anzai, M., Morikawa, M., Okuno, T., Umeda, Y., Demura, Y., Sonoda, T., Yamaguchi, M., Kanno, K., Shiozaki, K., Ameshima, S., Akai, M., Ishizuka, T., 2017. Efficacy and safety of nanoparticle albumin-bound paclitaxel monotherapy as second-line therapy of cytotoxic anticancer drugs in patients with advanced non-small cell lung cancer. Medicine 96.

Bucholz, T.L., Loo, Y. L., 2008. Polar aprotic solvents disrupt interblock hydrogen bonding and induce microphase separation in double hydrophilic block copolymers of PEGMA and PAAMPSA. Macromolecules 41, 4069-4070.

Chen, Z., Mao, X., Ye, X., Li, S., Wu, T., Wang, Q., Zhang, J., Chen, L., Tang, N., He, H., Wang, Z., McAlinden, C., Wang, Q., Chen, S., Gao, R., Huang, J., 2021. A novel and biocompatible nanofiber of VEGF peptide for enhanced corneal neovascularization suppression. Chem. Eng. J. 416, 129081.

Çitoğlu, S., Coşkun, Ö.D., Tung, L.D., Onur, M.A., Thanh, N.T.K., 2021. DMSA-coated cubic iron oxide nanoparticles as potential therapeutic agents. Nanomedicine 16, 925-941.

Currie, E., Schulze, A., Zechner, R., Walther, Tobias C., Farese, Robert V., Jr., 2013. Cellular fatty acid metabolism and cancer. Cell Metab. 18, 153-161.

Dachev, M., Bryndová, J., Jakubek, M., Moučka, Z., Urban, M., 2021. The effects of conjugated linoleic acids on cancer. Processes 9, 454.

Daum, S., Hagen, H., Naismith, E., Wolf, D., Pircher, A., 2021. The role of anti-angiogenesis in the treatment landscape of non-small cell lung cancer: New combinational approaches and strategies of neovessel inhibition. Front. Cell Dev. Biol. 8.

den Hartigh, L.J., 2019. Conjugated linoleic acid effects on cancer, obesity, and atherosclerosis: A review of pre-clinical and human trials with current perspectives. Nutrients 11, 370.

Dilnawaz, F., Singh, A., Mohanty, C., Sahoo, S.K., 2010. Dual drug loaded superparamagnetic iron oxide nanoparticles for targeted cancer therapy. Biomaterials 31, 3694-3706.

Eichmann, A., Simons, M., 2012. VEGF signaling inside vascular endothelial cells and beyond. Curr. Opin. Cell Biol. 24, 188-193.

Galli, M., Guerrini, A., Cauteruccio, S., Thakare, P., Dova, D., Orsini, F., Arosio, P., Carrara, C., Sangregorio, C., Lascialfari, A., Maggioni, D., Licandro, E., 2017. Superparamagnetic iron oxide nanoparticles functionalized by peptide nucleic acids. RSC Advances 7, 15500-15512.

Garkhal, K., Verma, S., Tikoo, K., Kumar, N., 2007. Surface modified poly(l-lactide-co-epsilon-caprolactone) microspheres as scaffold for tissue engineering. J. Biomed. Mater. Res. A 82, 747-756.

Hu, H., Chen, Y., Tan, S., Wu, S., Huang, Y., Fu, S., Luo, F., He, J., 2022. The research progress of antiangiogenic therapy, immune therapy and tumor microenvironment. Front. Immunol. 13.

Ji, Y., Yang, X., Ji, Z., Zhu, L., Ma, N., Chen, D., Jia, X., Tang, J., Cao, Y., 2020. DFT-calculated IR spectrum amide I, II, and III band contributions of N-methylacetamide fine components. ACS Omega 5, 8572-8578.

Jin, X., Zhou, J., Zhang, Z., Lv, H., 2018. The combined administration of parthenolide and ginsenoside CK in long circulation liposomes with targeted tLyP-1 ligand induce mitochondria-mediated lung cancer apoptosis. Artif. Cells Nanomed. Biotechnol. 46, S931-S942.

Kovrigina, E., Chubarov, A., Dmitrienko, E., 2022. High drug capacity doxorubicin-loaded iron oxide nanocomposites for cancer therapy. Magnetochemistry 8, 54.

Kumar, P., Srivastava, R., 2018. FITC conjugated polycaprolactone-glycol-chitosan nanoparticles containing the longwave emitting fluorophore IR820 for *in vitro* tracking of hyperthermia-induced cell death. bioRxiv, 273748.

Kut, C., Mac Gabhann, F., Popel, A.S., 2007. Where is VEGF in the body? A meta-analysis of VEGF distribution in cancer. Br. J. Cancer 97, 978-985.

Liu, D., Liu, F., Liu, Z., Wang, L., Zhang, N., 2011. Tumor specific delivery and therapy by double-targeted nanostructured lipid carriers with anti-VEGFR-2 antibody. Mol. Pharm. 8, 2291-2301.

Lugano, R., Ramachandran, M., Dimberg, A., 2020. Tumor angiogenesis: Causes, consequences, challenges and opportunities. Cell. Mol. Life Sci. 77, 1745-1770.

Luo, J., Xiao, K., Li, Y., Lee, J.S., Shi, L., Tan, Y. H., Xing, L., Holland Cheng, R., Liu, G. Y., Lam, K.S., 2010. Well-defined, size-tunable, multifunctional micelles for efficient paclitaxel delivery for cancer treatment. Bioconjug. Chem. 21, 1216-1224.

Marins, J.A., Montagnon, T., Ezzaier, H., Hurel, C., Sandre, O., Baltrunas, D., Mazeika, K., Petrov, A., Kuzhir, P., 2018. Colloidal stability of aqueous suspensions of polymer-coated iron oxide nanorods: Implications for biomedical applications. ACS Appl. Nano Mater. 1, 6760-6772.

Martins, E.S., Espindola, A., Britos, T.N., Chagas, C., Barbosa, E., Castro, C.E., Fonseca, F.L.A., Haddad, P.S., 2021. Potential use of DMSA-containing iron oxide nanoparticles as magnetic vehicles against the covid-19 disease. ChemistrySelect 6, 7931-7935.

Mashreghi, M., Azarpara, H., Bazaz, M.R., Jafari, A., Masoudifar, A., Mirzaei, H., 2018. Angiogenesis biomarkers and their targeting ligands as potential targets for tumor angiogenesis. J. Cell. Physiol. 233, 2949-2965.

Muñoz-Vega, M., Massó, F., Páez, A., Carreón-Torres, E., Cabrera-Fuentes, H.A., Fragoso, J.M., Pérez-Hernández, N., Martinez, L.O., Najib, S., Vargas-Alarcón, G., Pérez-Méndez, Ó., 2018. Characterization of immortalized human dermal microvascular endothelial cells (HMEC-1) for the study of HDL functionality. Lipids Health Dis. 17, 44.

Muzio, G., Miola, M., Ferraris, S., Maggiora, M., Bertone, E., Puccinelli, M.P., Ricci, M., Borroni, E., Canuto, R.A., Verné, E., Follenzi, A., 2017. Innovative superparamagnetic iron-oxide nanoparticles coated with silica and conjugated with linoleic acid: Effect on tumor cell growth and viability. Mater. Sci. Eng: C 76, 439-447.

Ngema, L.M., Adeyemi, S.A., Marimuthu, T., Choonara, Y.E., 2021. A review on engineered magnetic nanoparticles in non-small-cell lung carcinoma targeted therapy. Int. J. Pharm. 606, 120870.

Ngema, L.M., Adeyemi, S.A., Marimuthu, T., Ubanako, P., Wamwangi, D., Choonara, Y.E., 2022. Synthesis of novel conjugated linoleic acid (CLA)-coated superparamagnetic iron oxide nanoparticles (SPIONs) for the delivery of paclitaxel with enhanced *in vitro* anti-proliferative activity on A549 lung cancer cells. Pharmaceutics 14, 829.

Peach, C.J., Mignone, V.W., Arruda, M.A., Alcobia, D.C., Hill, S.J., Kilpatrick, L.E., Woolard, J., 2018. Molecular pharmacology of VEGF-A isoforms: Binding and signalling at VEGFR2. Int. J. Mol. Sci. 19, 1264.

Prigozhina, N.L., Heisel, A., Wei, K., Noberini, R., Hunter, E.A., Calzolari, D., Seldeen, J.R., Pasquale, E.B., Ruiz-Lozano, P., Mercola, M., Price, J.H., 2011. Characterization of a novel angiogenic model based on stable, fluorescently labelled endothelial cell lines amenable to scale-up for high content screening. Biol. Cell 103, 467-481.

Pugliese, R., Gelain, F., 2020. Cross-linked self-assembling peptides and their post-assembly functionalization via one-pot and in situ gelation system. Int. J. Mol. Sci. 21, 4261.

Raju, G.S.R., Pavitra, E., Varaprasad, G.L., Bandaru, S.S., Nagaraju, G.P., Farran, B., Huh, Y.S., Han, Y.-K., 2022. Nanoparticles mediated tumor microenvironment modulation: Current advances and applications. J. Nanobiotechnology 20, 274.

Reczyńska, K., Marszałek, M., Zarzycki, A., Reczyński, W., Kornaus, K., Pamuła, E., Chrzanowski, W., 2020. Superparamagnetic iron oxide nanoparticles modified with silica layers as potential agents for lung cancer treatment. Nanomaterials (Basel) 10, 1076.

Rinawati, L., Nugraha, R.E., Mahdia, R., Munifa, I., Chasanah, U., Wahyuningsih, S., Ramelan, A., 2015. Increasing the effectiveness of pesticides based urea nanofertilizer encapsulated nanosilica with addition of rice husk TiO_2 additive substances. J. Chem. Pharm. Res. 2015, 85-89.

Salehi, M., Movahedpour, A., Tayarani, A., Shabaninejad, Z., Pourhanifeh, M.H., Mortezapour, E., Nickdasti, A., Mottaghi, R., Davoodabadi, A., Khan, H., Savardashtaki, A., Mirzaei, H., 2020. Therapeutic potentials of curcumin in the treatment of non-small-cell lung carcinoma. Phytother. Res. 34, 2557-2576.

Sebben, D., Pendleton, P., 2014. Infrared spectrum analysis of the dissociated states of simple amino acids. Spectrochim. Acta A: Mol. Biomol. Spectrosc. 132, 706-712.

Senapati, S., Mahanta, A.K., Kumar, S., Maiti, P., 2018. Controlled drug delivery vehicles for cancer treatment and their performance. Signal Transduct. Target. Ther. 3, 7-7.

Shang, L., Nienhaus, K., Nienhaus, G.U., 2014. Engineered nanoparticles interacting with cells: Size matters. J. Nanobiotechnology 12, 5.

Shibuya, M., 2011. Vascular endothelial growth factor (VEGF) and its receptor (VEGFR) signaling in angiogenesis: A crucial target for anti- and pro-angiogenic therapies. Genes Cancer 2, 1097-1105.

Shukla, N.A., Yan, M.N., Hanna, N., 2020. The story of angiogenesis inhibitors in non–small-cell lung cancer: The past, present, and future. Clin. Lung Cancer 21, 308-313.

Song, L.N., Gu, N., Zhang, Y., 2017. A moderate method for preparation DMSA coated Fe_3O_4 nanoparticles. IOP Conf. Ser.: Mater. Sci. Eng. 164, 012026.

Sun, M., Wang, J., Lu, Q., Xia, G., Zhang, Y., Song, L., Fang, Y., 2015. Novel synthesizing method of Ph-dependent doxorubicin-loaded anti-CD22-labelled drug delivery nanosystem. Drug Des. Devel. Ther. 9, 5123-5133.

Truelsen, S.L.B., Mousavi, N., Wei, H., Harvey, L., Stausholm, R., Spillum, E., Hagel, G., Qvortrup, K., Thastrup, O., Harling, H., Mellor, H., Thastrup, J., 2021. The cancer angiogenesis co-culture assay: *In vitro* quantification of the angiogenic potential of tumoroids. PLoS One 16, e0253258.

Tsoukalas, C., Psimadas, D., Kastis, G.A., Koutoulidis, V., Harris, A.L., Paravatou-Petsotas, M., Karageorgou, M., Furenlid, L.R., Moulopoulos, L.A., Stamopoulos, D., Bouziotis, P., 2018. A novel metal-based imaging probe for targeted dual-modality SPECT/MR imaging of angiogenesis. Front. Chem. 6.

Walter, A., Garofalo, A., Parat, A., Martinez, H., Felder-Flesch, D., Begin-Colin, S., 2015. Functionalization strategies and dendronization of iron oxide nanoparticles. Nanotechnol. Rev. 4, 581-593.

Wang, J., Zhou, T., Liu, Y., Chen, S., Yu, Z., 2022. Application of nanoparticles in the treatment of lung cancer with emphasis on receptors. Front. Pharmacol. 12.

Wulandari, I.O., Sulistyarti, H., Safitri, A., Santjojo, D., Sabarudin, A., 2019. Development of synthesis method of magnetic nanoparticles modified by oleic acid and chitosan as a candidate for drug delivery agent. Development 9.

Ye, Z., Huang, Y., Ke, J., Zhu, X., Leng, S., Luo, H., 2021. Breakthrough in targeted therapy for non-small cell lung cancer. Biomed. Pharmacother. 133, 111079.

Yuan, M., Huang, L. L., Chen, J. H., Wu, J., Xu, Q., 2019. The emerging treatment landscape of targeted therapy in non-small-cell lung cancer. Signal Transduct. Target. Ther. 4, 61.

Zhang, T.Y., Huang, J.T., Tian, H.B., Ma, Y., Chen, Z., Wang, J.J., Shi, H.P., Luo, J., 2018. *Trans*-10,*cis*-12 conjugated linoleic acid alters lipid metabolism of goat mammary epithelial cells by regulation of *de novo* synthesis and the AMPK signaling pathway. J. Dairy Sci. 101, 5571-5581.

Zhang, Y., Cui, H., Zhang, R., Zhang, H., Huang, W., 2021. Nanoparticulation of prodrug into medicines for cancer therapy. Adv. Sci. 8, 2101454.

Zhang, Y., He, B., Liu, K., Ning, L., Luo, D., Xu, K., Zhu, W., Wu, Z., Huang, J., Xu, X., 2017. A novel peptide specifically binding to VEGF receptor suppresses angiogenesis *in vitro* and *in vivo*. Signal Transduct. Target. Ther. 2, 17010-17010.

Zhao, Z., Li, Y., Zhang, Y., 2015. Preparation and characterization of paclitaxel loaded SF/PLLA-PEG-PLLA nanoparticles via solution-enhanced dispersion by supercritical CO_2. J. Nanomater. 2015, 913254.

Zhou, Y. J., Zheng, W., Zeng, Q. H., Ye, Y., Wang, C., Fang, C., Liu, C. J., Niu, L., Wu, L. M., 2021. Targeted exome sequencing identifies mutational landscape in a cohort of 1500 Chinese patients with non-small cell lung carcinoma (NSCLC). Hum. Genomics 15, 21.

Zirlik, K., Duyster, J., 2018. Anti-angiogenics: Current situation and future perspectives. Oncol. Res. Treat. 41, 166-171.

CHAPTER 5

A TARGETED ANTIANGIOGENIC PEPTIDE-FUNCTIONALIZED PACLITAXEL DELIVERY NANOVECTOR OF SPIONs AND CONJUGATED LINOLEIC ACID FOR SELECTIVE INHIBITION OF MMP-2 SECRETION *IN VITRO*

5.1. Introduction

New therapeutic interventions for non-small-cell lung carcinoma (NSCLC) are being devised and the focus is currently on targeted nanomedicines with high specificity, minimal side effects, and smaller size for tumor penetration (Genova et al., 2020; Salgia et al., 2021; Ye et al., 2021). Having established a working methodology for the formulation of a targeted paclitaxel (PTX) delivery nanosystem via immobilization of an antiangiogenic peptide onto surface-modified, PTX-loaded superparamagnetic iron oxide nanoparticles (SPIONs), described in **Chapter 4**, this chapter delineates the formulation of another targeted PTX nanosystem functionalized with a distinct selective angiogenesis inhibitory peptide.

Interestingly, angiogenesis targeting presents a potentially viable therapeutic intervention for NSCLC (Hall et al., 2015; Shukla et al., 2020; Zhang et al., 2020). Angiogenesis plays a fundamental role in the growth and metastasis of tumor cells as a key provider of nutrients and oxygen (Lugano et al., 2020; Mashreghi et al., 2018). Hence, the inhibition of tumor angiogenesis pathways is a prospective therapeutic approach for NSCLC (Salehi et al., 2020; Zhou et al., 2021). Synthetic and natural angiogenesis inhibitors which block new blood vessel formation have been explored for tumor therapy (Adeyemi et al., 2017; Bałan et al., 2017) , and some peptide-based inhibitors have demonstrated promising antiangiogenic activity (Adeyemi and Choonara, 2022; Adeyemi et al., 2019; Aloisio et al., 2021; Lu et al., 2019; Rosca et al., 2011).

Matrix metalloproteinase 2 (MMP-2) is an important member of enzymes much implicated in lung cancer angiogenesis regulation and tumor metastasis (Han et al., 2020; Quintero-Fabián et al., 2019). MMP-2 expression is linked to tumor-induced angiogenesis, where it plays a vital role in degrading the extracellular matrix (ECM) and releasing stored angiogenic factors (i.e., basic fibroblast growth factor and vascular endothelial growth factor) which promote angiogenesis, tumor differentiation and metastasis (Gonzalez-Avila et al., 2019; Winkler et al., 2020). Thus, targeting MMP-2 and down-regulating its expression could halt tumor angiogenesis and suppress proliferation and metastasis. CTT peptide (CTTHWGFTLC) is an MMP-2 selective inhibitory peptide with promising antiangiogenic activity (Wang et al., 2020; Wang et al., 2014). CTT is a cyclic peptide (~1.17 kDa) shown to suppress MMP-2 and

significantly blocks angiogenesis and migration of various cancer cell lines and endothelial cells (Ndinguri et al., 2012; Webb et al., 2017).

Previously, we have formulated and characterized a nanosystem comprising superparamagnetic iron oxide nanoparticles (SPIONs) coated with *trans*-10,*cis*-12 conjugated linoleic acid (10E, 12Z CLA) and loaded (self-assemble) with paclitaxel (PTX) to yield CLA-coated PTX-SPIONs which exhibited enhanced anti-proliferative activity in lung adenocarcinoma cell lines (reported in **Chapter 3**). SPIONs are excellent nanovectors with desirable smaller size (<100 nm) and are easy to functionalize. Meanwhile, 10E, 12Z CLA is a natural fatty acid with proven anticancer benefits (Dachev et al., 2021; den Hartigh, 2019; Zhang et al., 2018), and allows partitioning of hydrophobic anticancer drugs like PTX for enhanced bioavailability and anti-proliferative activity (Ngema et al., 2022). As such, in the present study, we functionalized CLA-coated PTX-SPIONs with CTT peptide to yield CLA-coated PTX-SPIONs@CTT, and conducted *in vitro* analyses to show antiangiogenic activity in endothelial cells, for potential management of NSCLC tumor proliferation.

5.2. Materials and Methods

5.2.1. Materials

Iron (II) chloride tetrahydrate ($FeCl_2 \cdot 4H_2O$), iron (III) chloride hexahydrate ($FeCl_3 \cdot 6H_2O$), sodium hydroxide (NaOH) pellets, conjugated (10E, 12Z)-linoleic acid solution in ethanol, paclitaxel (Taxol®), *meso*-2,3-Dimercaptosuccinic acid (DMSA), dimethylformamide (DMF), 1-ethyl-3(3-dimethylaminopropyl) carbodiimide (EDC), *N*-hydroxysuccinimide (NHS), phosphate buffered saline (PBS) tablets, fluorescein 5(6)-isothiocyanate (FITC), 4′,6-diamidino-2-phenylindole (DAPI) and sodium hydroxide (NaOH) pellets were procured from Sigma-Aldrich Corp. (St. Louis, MO, USA). CTT peptide was purchased from Peptron Inc. (Daejeon, South Korea). All solvents were of analytical grade and were utilized as received.

5.2.2. Methodology

5.2.2.1. Formulation of CLA-coated PTX-SPIONs

CLA-PTX-SPIONs were formulated using an established method described in **Chapter 3** and **Chapter 4**. Briefly, SPIONs were synthesized via co-precipitation method from an aqueous solution of $FeCl_2 \cdot 4H_2O$ (0.3mol) and $FeCl_3 \cdot 6H_2O$ (0.6mol), under inert (N_2) atmosphere. SPIONs were then coated with 10E, 12Z CLA in a single-step reaction, and CLA content on SPIONs was quantified by thermogravimetric analysis (TGA 4000, PerkinElmer Inc., Waltham, MA, USA) (Ngema et al., 2022). PTX was efficiently loaded by self-assembling onto CLA via

spontaneous CLA~PTX hydrophobic interaction, facilitating PTX adsorption on CLA hydrophobic ends. The amount of PTX used for loading was fixed at 10% (*w/w*) of CLA-coated SPIONs. The adsorption efficiency (%AE) of PTX and the drug loading capacity (%DLC) of the nanosystem was determined using UV spectrophotometry (Cary™ 50, Varian Inc., Palo Alto, CA, USA). Briefly, following an established direct method (Adekiya et al., 2022), the nanosystem was completely air dried and vigorously ruptured by probe sonication (Sonics Vibra Cell, Newtown, CT, USA), in 5 mL 70% methanol and filtered for UV quantification at 227 nm. The %AE and %DLC were then computed, using equation (5.1) and (5.2), respectively (Adekiya et al., 2022; Ngema et al., 2022):

$$\%AE = \frac{D_q}{D_l} \times 100 \qquad \text{(Equation 5.1)}$$

$$\%DLC = \frac{D_q}{W_f} \times 100 \qquad \text{(Equation 5.2)}$$

where, D_q denotes the amount of drug as quantified by UV spectrophotometry, D_l is the amount of the drug initially loaded, and W_f is the total weight of formulation, in mg.

5.2.2.2. Functionalization of CLA-coated PTX-SPIONs with carboxylic acid groups

A superlative optimized method by Dilnawaz et al., (Dilnawaz et al., 2010) was adapted, with modifications, to surface-functionalize CLA-coated PTX-SPIONs with carboxylic acid (COOH) groups to aid the conjugation of CTT peptide. Accordingly, 15 mg CLA-coated PTX-SPIONs was added to 450 µL of 1.6 M DMSA prepared in DMF, and was kept under continuous stirring (Magnetic Stirrer MSH10, Labcon, Johannesburg, SA) for 24 h. The formulation was centrifuged at 13 800 rpm, 10°C (TC-MiniSpin Centrifuge, TopScien, Ningbo, China) for 20 min and washed three times with ethanol. The resultant pellet was lyophilized and examined with Fourier Transform Infrared (FTIR) spectroscopy (Spectrum 100, PerkinElmer Inc., Waltham, MA, USA) to confirm functionalization, and double titration was performed to determine acid numbers (Dilnawaz et al., 2010).

5.2.2.3. Conjugation of CTT to CLA-coated PTX-SPIONs

CTT peptide was conjugated to carboxylic acid-functionalized CLA-coated PTX-SPIONs using EDC and NHS (EDC/NHS chemistry) (Adeyemi et al., 2019; Dilnawaz et al., 2010; Pugliese and Gelain, 2020). COOH-functionalized CLA-coated PTX-SPIONs (10 mg) were added to 5 mL of 0.01 M PBS, pH 7.4. EDC and NHS solutions (1mg/mL in PBS, pH 7.4) were prepared

and 250 µL of each added into the sample (COOH-functionalized-CLA-coated PTX-SPIONs in PBS). The mixture was kept stirring at 200 rpm (Magnetic Stirrer MSH10, Labcon, Johannesburg, SA) at room temperature for 4 h, and precipitated with a permanent magnet. A supernatant was decanted, and 3 mL 0.01 M PBS (pH 7.4) and 300 µL CTT (1 mg/mL) added into the pellet. This was left for 2 h at room temperature before overnight incubation at 4 °C. Thereafter, the supernatant was decanted with a magnet, and the pellet subsequently washed three times with PBS to remove unbound peptide and determine. The resultant CLA-coated PTX-SPIONs@CTT was air-dried at room temperature and CTT conjugation confirmed by FTIR spectroscopy.

5.2.3. Characterization of CLA-coated PTX-SPIONs@CTT

5.2.3.1. Analysis of chemical structural transformations

The analysis of structural integrity and functional transformations on the components of CLA-coated PTX-SPIONs@CTT was conducted to confirm the formation of the nanosystem, using Fourier Transform Infrared (FTIR) spectroscopy (Spectrum 100, PerkinElmer Inc., Waltham, MA, USA). FTIR spectra of CLA-coated PTX-SPIONs, DMSA, CTT, and CLA-coated PTX-SPIONS@CTT were acquired over 20 scans at 120 psi pressure and wavenumber range of 4000 – 550 cm^{-1}.

5.2.3.2. Determination of size, surface charge and overall morphology of CLA-coated PTX-SPIONs@CTT

The hydrodynamic size and zeta potential of CLA-coated PTX-SPIONs@CTT were confirmed by ZetaSizer (NanoZS, Malvern Panalytical, Malvern, UK), using a dried sample (10 µg) suspended in distilled water (1 mL). The suspension was sonicated for 10 min (Sonics Vibra Cell, Newtown, CT, USA) before analysis at 25°C. The average hydrodynamic size and polydispersity index (PDI) was recorded using a disposable cuvette, and zeta potential attained using a special DTS 1070 cuvette. The same sample was used (aliquot) to ascertain the overall morphology of CLA-coated PTX-SPIONs@CTT using Transmission Electron Microscopy (TEM) (FEI™ Tecnai T12 120 kV, FEI Technologies Inc., Hillsboro, OR, USA). A carbon-coated 200-mesh copper grid was dipped in a sample and allowed to dry for TEM analysis.

5.2.3.3. In vitro analysis of PTX release from CLA-coated PTX-SPIONs@CTT

In vitro release of PTX from CLA-coated PTX-SPIONs@CTT was investigated over 24 h at pH 6.8 and 7.4, mimicking tumor microenvironment and physiological pH, respectively (Adeyemi et al., 2019). Dried samples (3 mg) were dispersed in 2.5 mL of corresponding buffer solutions (0.1 M; 0.1% v/v tween) in a dialysis membrane (SnakeSkin™, 3 500 MWCO) and submerged into 30 mL of respective release buffer (pH 6.8 and 7.4). The samples were incubated in an orbital shaker (YIHDER LM-530, YIHDER Co., Lt., Taipei, Taiwan) at 37°C, with sampling done over 24 h interval at t = 1, 2, 4, 8, 12, 16, and 24 h. Sampled volume (2 mL) was analysed with UV spectrophotometer (Cary™ 50, Varian Inc., Palo Alto, CA, USA) at 227 nm (PTX absorbance), and the medium replenished with 2 mL after each sampling.

5.2.4. *In vitro* cellular analyses of CLA-coated PTX-SPIONs@CTT on lung adenocarcinoma and endothelial cells

5.2.4.1. Evaluation of anti-proliferative activity on A549 cancer cells

A typical cell culture protocol was adopted to culture lung adenocarcinoma (A549) cells for the study (Ngema et al., 2022). Accordingly, a growth medium comprising Dulbecco's Modified Eagle Medium (DMEM), Foetal Bovine Serum (FBS, 10% *v/v*), and 1% *v/v* penicillin-streptomycin antibiotic was prepared for growing the cells in T-25 culture flask at 37°C and 5% CO_2 in a humidified incubator. Cells were allowed to grow to 90% confluence and then seeded (2.5×10^4 cells/mL, 90 µL each well) in a 96-well plate and adhered under incubation over 24 h. Subsequently, experimental cells were treated with 10 µL of varying concentrations (i.e., 25, 50, 100 µg/mL) of CLA-coated PTX-SPIONs@CTT, in triplicates. Thereafter, cells were in incubation for 72 h for cell viability assessment using a 3-(4,5-dimethylthiazole-2-yl)-2,5-diphenyl tetrazolium bromide (MTT) assay (MTT Cell Proliferation Kit I, Roche, Basel, Switzerland). As per a standard MTT protocol, each well was filled with 10 µL MTT solution (5 mg/mL) and the plate further incubated at 37°C, 5% CO_2 for 4 h. Formed formazan crystals were dissolved by adding 100 µL of acid-isopropanol solubilizing agent and incubating the plate overnight at 37°C and 5% CO_2. The results were recorded on a multimodal plate reader (Victor X3, PerkinElmer, Waltham, MA, USA) at 570 nm and 620 nm reference wavelength. The absorbance readings (mean±standard deviation) were used to determine % cell viability (CV) via equation 5.3. Blank wells only contained growth medium and solubilizing agent.

$$\% \text{ CV} = \frac{A_{test} - A_{blank}}{A_{control} - A_{blank}} \times 100 \qquad \text{(Equation 5.3)}$$

where A_{test}, $A_{control}$, and A_{blank} are absorbance from test, control, and blank wells in nm.

5.2.4.2. Assessment on uptake and internalization by A549 cells

The cellular uptake and internalization of CLA-coated PTX-SPIONs@CTT was evaluated using an FITC-labelled nanoformulation. FITC labelling was achieved through a method described by Kumar and Srivastava (2018) (Kumar and Srivastava, 2018), with modifications. Accordingly, 1 mg FITC was dissolved 1 mL methanol: dichloromethane (50:50), and added, while stirring (300 rpm for 15 min (Magnetic Stirrer MSH10, Labcon, Johannesburg, SA), in a suspension of CLA-coated PTX-SPIONs@CTT in distilled water (2.5 mg in 5 mL). The sample was allowed to continuously stir and evaporate the solvent in the dark for 20 min at room temperature. Subsequently, the sample was washed by centrifugation (×3 distilled water) at 14 000 rpm, 10°C, for 20 min (TC-MiniSpin Centrifuge, TopScien, Ningbo, China). FTIC-CLA-coated PTX-SPIONs@CTT was collected for cell work.

Following a standard cell culture protocol (*5.2.4.1*), A549 cells were cultured and seeded in a 6-well plate, at 5×10^4 cells/mL seeding density. The wells were fitted with presterilized cover slips, and each well contained 800 µL of cell suspension. The cells were incubated for 24 h and thereafter treated with FITC-CLA-coated PTX-SPIONs@CTT (200 µL of 1 mg/mL in PBS), followed by a further 24 h incubation at 37°C and 5% CO_2. Subsequently, the cells were spiked with 500 µL 4% paraformaldehyde (PFA) for 2 min for cell acclimatization. Thereafter, the well contents were aspirated, a further 1 mL 4% PFA was added per well, and the cells were incubated for 20 mins for cell fixation. The fixed cells were washed with 1XPBS (2 mL, 4 times) before staining with 300 µL DAPI (300 nM) and incubating in the dark at room temperature for 5 min. Further 4 washes with 1XPBS were done before the cover slips were removed and mounted on glass slides, using cooled glycerol (80% *v/v*) and allowed to dry overnight. The slides were then analysed on a compound fluorescent microscope (Olympus IX51, Olympus Corporation, Tokyo, Japan), with images captured at 517 nm green fluorescence excitation for FITC and 416 nm for DAPI (blue fluorescence) on a super 40X objective lens.

5.2.4.3. Evaluation of MMP-2 targeting activity

A human MMP-2 ELISA Kit (Invitrogen, Thermo Fisher Scientific Corporation, Waltham, MA, USA) was employed in assessing the binding ability of CLA-coated PTX-SPIONs@CTT onto MMP-2 on human dermal microvascular endothelial cells (HMEC-1) (Separation Scientific SA Pty. Ltd, Johannesburg, South Africa). A typical MCDB 131 medium with special supplements of 10% *v/v* FBS, 1 µg/mL hydrocortisone, 10 ng/mL human EGF recombinant protein, and 10

nM L-glutamine, was used to culture HMEC-1 cells in a T-25 flask. The cells were cultured at 37°C, 5% CO_2 until 90% confluence, and 800 µL of cell suspension were seeded in two 6-well plates at a seeding density of 5×10^4 cells/mL and allowed 24 h to adequately adhere. A concentration of 50 µg/mL CLA-coated PTX-SPIONs@CTT, CLA-coated PTX-SPIONs, and pristine CTT, were used to treat experimental cells for 24 h. Post 24 h incubation, cell culture supernatant was collected and immediately centrifuged at 13 000 rpm for 20 min at 4°C (Eppendorf™ Centrifuge 5415R, Merck, Darmstadt, Germany). The ELISA analysis was conducted using the supernatant, following the manufacturer's protocol. A multimodal microplate reader (Victor X3, PerkinElmer, Waltham, MA, USA) was used to read the absorbance at 450 nm.

5.2.4.4. Evaluation of inhibition of cell migration by CLA-coated PTX-SPIONs@CTT

Migration of HMEC-1 endothelial cells was assessed following treatment with CLA-coated PTX-SPIONs@CTT, using a Modified Boyden Chamber Assay (Corning Inc., Corning, NY, USA). The assay measures the ability of the cells to migrate towards a chemical gradient. Thus it was carried out to ascertain the inhibition of MMP-2 activity, since MMP-2 is responsible for the migration of endothelial cells through degradation of extracellular matrix components, to promote angiogenesis and cell invasion (Quintero-Fabián et al., 2019). Briefly, 200 µL of 5×10^4 HMEC-1 cells in growth medium was added to the upper chamber, and treated with 200 µL of 50 µg/mL CLA-coated PTX-SPIONs or CLA-coated PTX-SPIONs@CTT, while control cells were left untreated. A volume of 0.4 mL of 10% FBS-containing medium was then added to the lower chamber as a chemoattractant. Cells were incubated for 8 hours at 37°C, and non-migrating cells (dead/loss of MMP-2 activity) on the upper surface of the membrane, were then scraped off with cotton swabs. A 1 mL Alamar blue reagent was added to the cells that migrated to the bottom of the membrane, and after 4 hours, cells were quantified at maximum emission and excitation wavelengths of 535 nm and 595 nm, respectively on a microplate reader (Victor X3, PerkinElmer, Waltham, MA, USA). The % cell migration was determined using equation 5.4:

$$\%\text{Cell migration} = \frac{Viable\ migrated\ cells}{Initial\ seeded\ cells} \times 100 \qquad \text{(Equation 5.4)}$$

5.2.5. Statistical analysis

GraphPad prism 9 (GraphPad Software, Inc., San Diego, CA, USA) two-tailed Student's *t*-test was used for data analysis, with $p < 0.05$ deemed statistically significant. Data are presented as mean values of biological triplicates ($n=3$) ± standard deviation.

5.3. Results and Discussion

5.3.1. Formulation of CLA-coated PTX-SPIONs@CTT

The SPIONs, as the core of the nanosystem were efficiently synthesized using a co-precipitation method, yielding black Fe_3O_4 nanoparticles with average hydrodynamic size of ~51 nm. The working conditions involved in co-precipitation method, including inert atmosphere and high temperature were instrumental in attaining the desired smaller size, morphology and distribution of the particles, while limiting oxidation (Ngema et al., 2022; Slimani et al., 2021). The overall formulation scheme of CLA-coated PTX-SPIONs@CTT is depicted in **Figure 5.1** (*step 1 – 4*). The coating of the SPIONs surface with 10E, 12Z CLA was successfully achieved, owing to the availability of the hydroxyl (-OH) groups on SPIONs, and the carboxyl group (-COOH) on 10E, 12Z CLA, allowing chemisorption. The chemisorption of fatty acids such as oleic acid, linoleic acid, palmitic acid, and glycerol monooleate onto SPIONs is an appreciated phenomenon that has been widely reported (Dilnawaz et al., 2010; Muzio et al., 2017; Sawisai et al., 2019).

Accordingly, about 10.3% of 10E, 12 CLA was found to be coated onto SPIONs. A range of 10 – 14% fatty acid content on SPIONs has been reported from previous studies, employing TGA (Dilnawaz et al., 2010; Ngema et al., 2022; Sawisai et al., 2019). The presence of 10E, 12Z CLA allowed maximal partitioning of PTX, with %AE = 98.5% and %DLC = 9.8% obtained. The high %AE obtained is attributed to the hydrophobicity of 10E, 12Z CLA complementing the hydrophobic nature of PTX, allowing spontaneous hydrophobic-hydrophobic interaction. Meanwhile, the 9.8% DLC is attributed to the large surface area of SPIONs, and is favourable considering that 10% (*w/w*) PTX was applied in the formulation. The loading of hydrophobic drugs is generally challenging (Chen et al., 2021), however, in the present study, the choice of 10E, 12Z CLA circumvented the problem. The excessive –OH groups on SPIONs were further exploited to functionalize the nanoformulation with –COOH groups (DMSA) for CTT conjugation. Normally, SPIONs synthesized via co-precipitation present with excessive –OH groups (Dilnawaz et al., 2010). A total of 64 per gram free –COOH groups were present on the surface from 1.6 M DMSA used. The proportion of free –COOH obtained correlate to the concentration of DMSA employed. A related study has reported free –COOH numbers of nearly 8 per gram of the sample when 0.2 M DMSA was employed, and noted that acid numbers increase when DMSA concentration is increased, until binding saturation is reached (Dilnawaz et al., 2010). The –COOH functionalization step was successful, and FTIR spectroscopy analysis (**Figure 5.3**) confirmed the conjugation of CTT, yielding CLA-coated PTX-SPIONs@CTT.

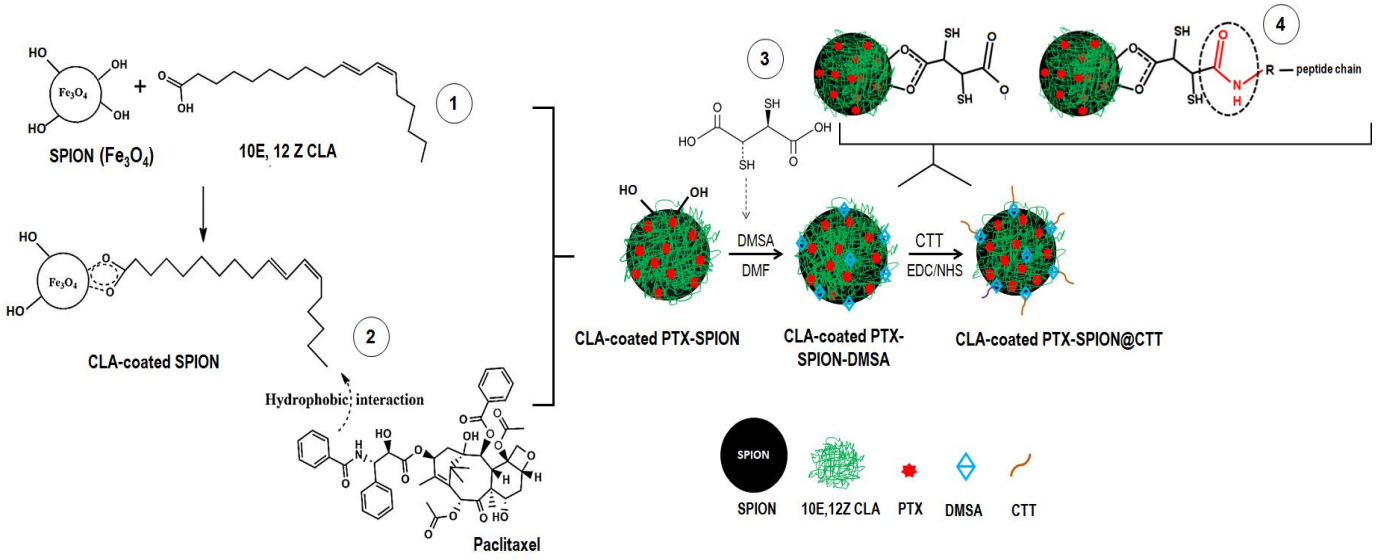

Figure 5.1. Step-wise synthesis of CLA-coated PTX-SPIONs@CTT (not drawn to actual scale). ***Step 1*** is the coating of SPIONs with 10E, 12Z CLA via chemisorption. ***Step 2*** is self-assembled loading of PTX via spontaneous hydrophobic interaction with 10E, 12Z CLA ends. ***Step 3*** is –COOH functionalization using DMSA (DMF facilitates the reaction between SPIONs –OH and DMSA, through hydrogen bonding). ***Step 4*** is the finally conjugated CTT onto activated $–COO^-$, via its terminal $–NH_2$ group, facilitated by EDC/NHS. The conjugation of CTT results in amide II bond formation and a growing peptide chain.

5.3.2. Overall morphological assessment of CLA-coated PTX-SPIONs@CTT.

The surface charge, average particles size, and particle dispersion were all ascertained through dynamic and phase-light scattering, and the results are presented in **Table 5.1**. TEM further confirmed the overall morphology of CLA-coated PTX-SPIONs@CTT (**Figure 5.2**). A zeta potential of -31.8 ± 0.5 mV and PDI of 0.2 ± 0.01 indicated the colloidal stability and reduced aggregation of CLA-coated PTX-SPIONs@CTT in aqueous media. Moreover, the PDI recorded was lower than that of pure SPIONs (0.4 ± 0.1) previously reported (**Chapter 3**), indicating the effect of surface coating with 10E, 12Z CLA. Essentially, SPIONs tend to aggregate due to their magnetic behaviour, and therefore, require to be surface-modified to limit aggregation (Gonçalves et al., 2017). Various surface-coating agents, including related fatty acids, such as oleic and linoleic acids have been employed to circumvent SPIONs aggregation (Muzio et al., 2017; Sawisai et al., 2019).

The average hydrodynamic size recorded for CLA-coated PTX-SPIONs@CTT was 99.4 ± 2.0 nm (**Figure 5.2a**), which is an ideal size for application in NSCLC. It is reported that nanocarriers with a size range of 10 – 100 nm are ideal for lung tumor penetration, meanwhile carriers above 100 nm may be subject to removal by alveolar macrophages (Hoshyar et al., 2016). As such, maintaining the size closer to 100 nm was crucial in the present study. SEM and TEM analysis further confirmed the size, and revealed that CLA-coated PTX-SPIONs@CTT exhibited a quasi-spherical shape (**Figure 5.2b, c**). The shape could be associated to carboxylic functionalization with DMSA, through which the DMSA short chains impart a quasi-spherical conformation on iron oxides (Song et al., 2017; Sun et al., 2015). Generally, spherical nanoparticles have been linked to enhanced cellular uptake and biodistribution (Li et al., 2019; Zhang et al., 2019; Zhong et al., 2016), and although, CLA-coated PTX-SPIONs@CTT is not entirely spherical, a comparable behaviour may be envisaged.

Table 5.1. Recorded average size, zeta potential, and PDI of CLA-coated PTX-SPIONs@CTT and pristine SPIONs

	Average hydrodynamic size (nm)	**Zeta potential (mV)**	**Polydispersity index (PDI)**
CLA-coated PTX-SPIONs@CTT	99.4 ± 2.0	-31.8 ± 0.5	0.2 ± 0.1
SPIONs (before modifications)	51.0 ± 1.3	-24.3 ± 1.3	0.4 ± 0.1

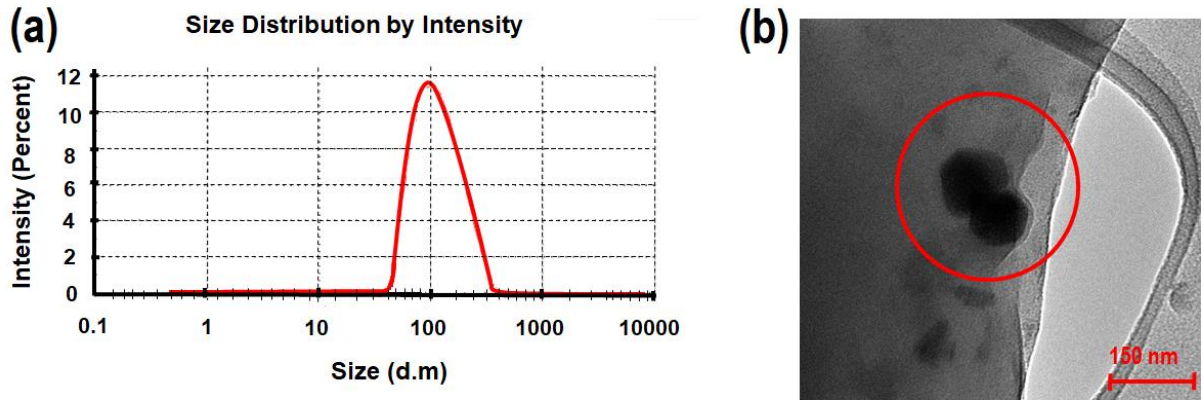

Figure 5.2. A representation of characteristic physical attributes of CLA-coated PTX-SPIONs@CTT, showing (**a**) average hydrodynamic size distribution from DLS measurement and (**b**) TEM micrograph on a scale bar of 150 nm (magnification = 7000 X) showing a quasi-spherical shape of formulated CLA-coated PTX-SPIONs@CTT (red circle).

5.3.3. Evaluation of chemical functionality and transformations towards formulation of CLA-coated PTX-SPIONs@CTT

The evaluation of chemical functionality of the constituents of CLA-coated PTX-SPIONs@CTT, and transformations thereof was crucial in ascertaining the successful formation of the desired CLA-coated PTX-SPIONs@CTT. Accordingly, the spectra from the FTIR spectroscopy analysis are presented in **Figure 5.3a-e**. Characteristic peaks of PTX (1244 cm^{-1} and 3479 cm^{-1}, attributed to ester and –OH groups, respectively), 10E, 12Z CLA (1603 cm^{-1} and ~2922 – 2852 cm^{-1}, belonging to CH_3 bending and symmetrical/asymmetrical CH_2 stretches), as well as iron oxide (FeO = 580 cm^{-1}), were evident in the spectrum of CLA-coated PTX-SPIONs (**Figure 5.3a**) (Akilo et al., 2016; Muzio et al., 2017), confirming the formation of the nanosystem. Likewise, major peaks at 1685 cm^{-1} and 2561 cm^{-1} (belonging to –C=O of the carboxyl groups and –SH of the thiol groups, respectively) (Çitoğlu et al., 2021) were present in the spectrum of DMSA (**Figure 5.3b**). A split and a shift in DMSA peak (–C=O) from 1685 cm^{-1} to around 1680 – 1675 cm^{-1} (red marker) could be seen in a DMSA-functionalized CLA-coated PTX-SPIONs spectrum (**Figure 5.3c**), attributed to carboxylate (COO^-) ions vibrations when DMSA is linked onto SPIONs surface via the carboxyl group (**Figure 5.1**) (Çitoğlu et al., 2021; Tsoukalas et al., 2018). A pure CTT peptide (**Figure 5.3d**) exhibited characteristic peaks for terminus primary amine (-NH_2 = 3280 cm^{-1}), -C=O stretches (1625, 1518 cm^{-1}), and peptide bond stretch (C-N = 1199 – 1134 cm^{-1}) (Rinawati et al., 2015; Sebben and Pendleton, 2014). A conjugation of CTT, and overall formation of CLA-coated PTX-SPIONs@CTT was confirmed (**Figure 5.3e**) by the presence of characteristic peaks of all constituents (red rectangular markers) in the spectrum, with a visible amide II bond at ~ 1570 cm^{-1} (dotted rectangular marker) emanating from CTT conjugation via –NH_2 onto activated COO^- afforded by DMSA (**Figure 5.1**), and wide peak at 3278 cm^{-1} (red dotted circle) belonging to –N-H stretching from the new amide II bond formed from CTT conjugation.

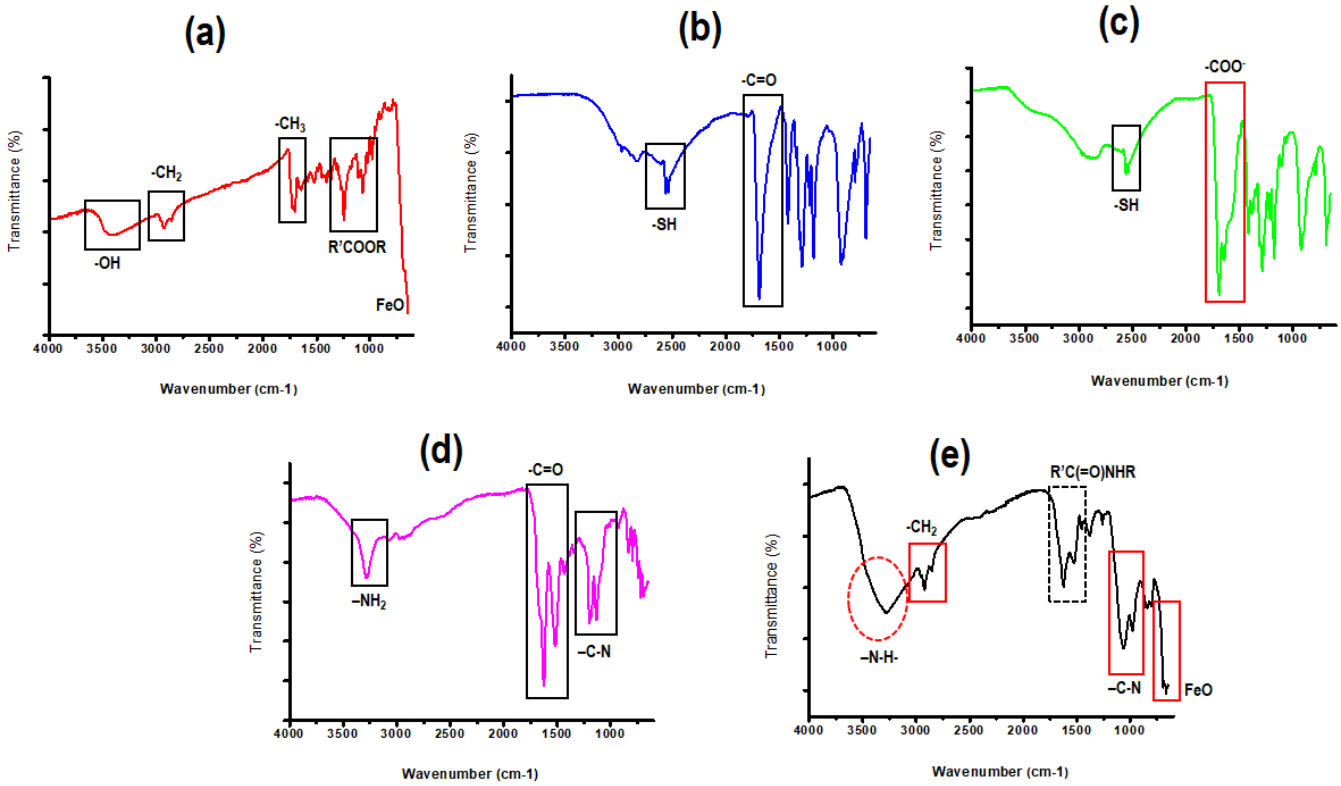

Figure 5.3. FTIR spectra showing chemical functionality mappings of (**a**) CLA-coated PTX-SPIONs, (**b**) DMSA, (**c**) carboxylated (DMSA) CLA-coated PTX-SPIONs, (**d**) CTT peptide, and (**e**) CLA-coated PTX-SPIONs@CTT.

5.3.4. *In vitro* release profile of PTX from CLA-coated PTX-SPIONs@CTT

The release of PTX from CLA-coated PTX-SPIONs was evaluated over 24 h, and the attained profile is presented in **Figure 5.4**. Varying levels of release were recorded at two different pH levels, suggesting smart pH-responsiveness of the nanoformulation. Accordingly, a high and sustained release of PTX was observed at pH 6.8, meanwhile a comparatively lower release was recorded at physiological pH 7.4. An initial release of nearly 30% (1 h) was recorded at pH 6.8, with a continuous release up to a maximum of 99.2 % at 16 h. Contrary, an initial release of only 10.4% PTX could be recorded at pH 7.4, reaching a maximal release of only 19.9% at 24 h, which was even lesser than the release at first hour at pH 6.8. Essentially, the favoured release at pH 6.8 could be associated with breaking of hydrophobic-hydrophobic interactions between CLA and PTX at acidic conditions over time. Related studies have reported similar observations when PTX was loaded onto hydrophobic oleic acid and glycerol monooleate, and found that hydrophobic interactions are not permanent and are rapidly weakened at acid pH (Dilnawaz et al., 2010; Wulandari et al., 2019).

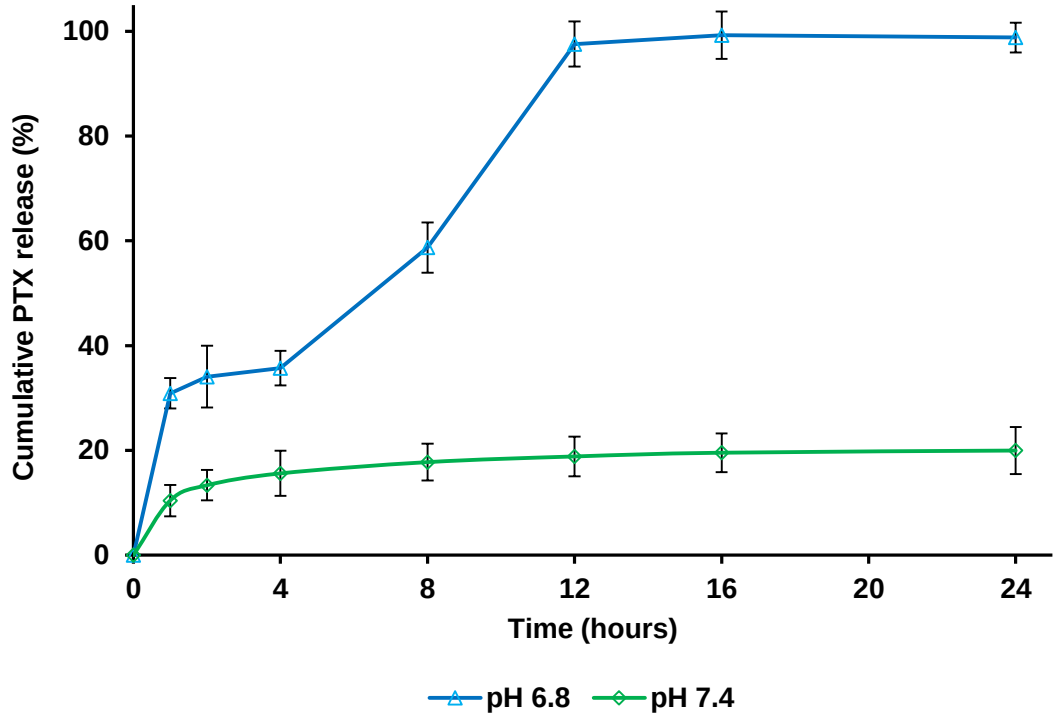

Figure 5.4. Cumulative release of PTX at pH 6.8 and pH 7.4 over 24 h. A highly favoured release at pH 6.8 could be observed compared to pH 7.4. Data presented as mean ± SD, *n* = *3*.

5.3.5. Evaluation of anti-proliferative activity of CLA-coated PTX-SPIONs@CTT from A549 cell viability

The anti-proliferative activity of CLA-coated PTX-SPIONs@CTT on A549 cells was ascertained by the determination of viable cells post treatment. **Figure 5.5** presents the viability assessment at different concentrations. A concentration-dependent anti-proliferative activity was observed, with recorded % cell viability of 18.5, 15.2, and 12.4% at 25, 50, and 100 µg/mL, respectively. A decrease in the number of viable cells with an increase in treatment concentration is representative of an effectively working formulation, and correlates to previous studies that have reported a dose dependent cellular cytotoxicity from various nanoformulations in NSCLC (Engelberg et al., 2019; Foldbjerg et al., 2011; Mohtar et al., 2021). The cell viability data obtained is comparable to the findings of our previous investigations, where CLA-coated PTX-SPIONs were shown to enhance the anti-proliferative activity of pristine PTX by almost 3 folds (**Chapter 3**).

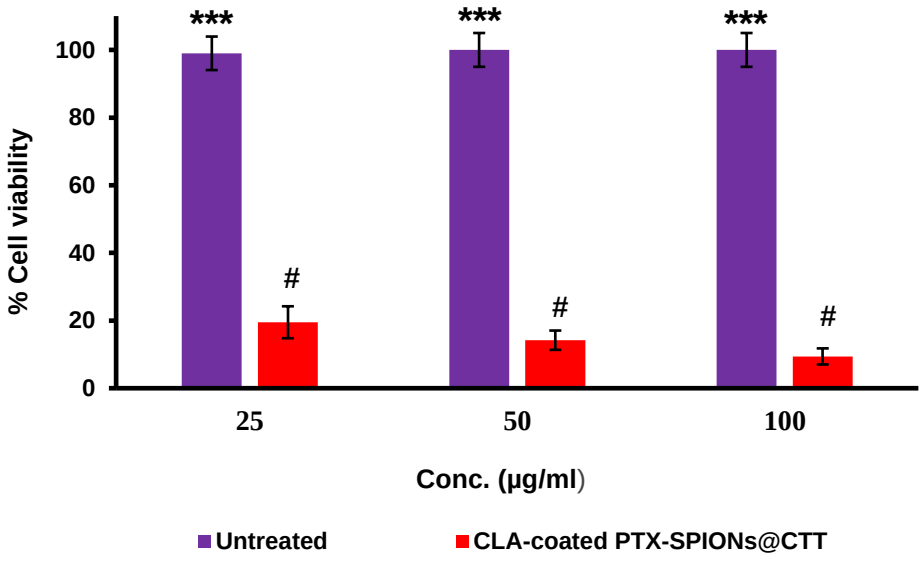

Figure 5.5. The % cell viability of A549 cells at varying pre-determined treatment concentrations of CLA-coated PTX-SPIONs@CTT. Cell viability (%) was computed after 72 h of treatment, and is presented as mean ± SD of three (*n = 3*) biological analyses. (*** denotes $p < 0.001$, statistically significant compared to CLA-coated PTX-SPIONs@CTT, and # denotes $p < 0.05$, statistically significant at each concentration).

5.3.6. Cellular uptake of CLA-coated PTX-SPIONs@CTT by A549 cells

A remarkable uptake and internalization of CLA-coated PTX-SPIONs@CTT by A549 cells was observed. The cells were identified through nuclei visualization by DAPI staining (blue fluorescence) (**Figure 5.6a**), and CLA-coated PTX-SPIONs@CTT were tracked by FITC-labelling (green fluorescence) (**Figure 5.6b**). A high accumulation of CLA-coated PTX-SPIONs@CTT (green fluorescence) closest to the nuclei (blue fluorescence) compellingly indicated the uptake of the nanosystem by the cells (**Figure 5.6c**). The high uptake and internalization of CLA-coated PTX-SPIONs@CTT by A549 cells could be presumed to emanate from various distinct physical characteristics possessed by the nanosystem, such as the presence of 10E, 12Z CLA, smaller size and quasi-spherical shape. The presence of 10E, 12Z CLA may be linked to increased selective affinity by A549 cells, since cancer cells are known for high uptake of essential fatty acids as energy source (Currie et al., 2013).

Moreover, Zhong *et al*., 2016, reported that a CLA-PTX conjugate could self-assemble to form spherical nanoparticles with enhanced cellular uptake, and the shape had direct effect on cell cytotoxicity (Zhong et al., 2016). Additionally, the high cellular uptake observed in the present study could be directly linked to enhanced anti-proliferative activity exhibited by CLA-coated PTX-SPIONs@CTT on A549 cells (**Figure 5.5**). Accordingly, a sufficient concentration of

CLA-coated PTX-SPIONs@CTT was internalized and reached the nuclei of A549 cells, eliciting cytotoxic effects on the nuclei, resulting in cellular death. Some studies report nuclei rupture as a common event when sufficient cytotoxic agents are taken up by cancerous cells and reach the nuclei (Adeyemi et al., 2019; Foldbjerg et al., 2011).

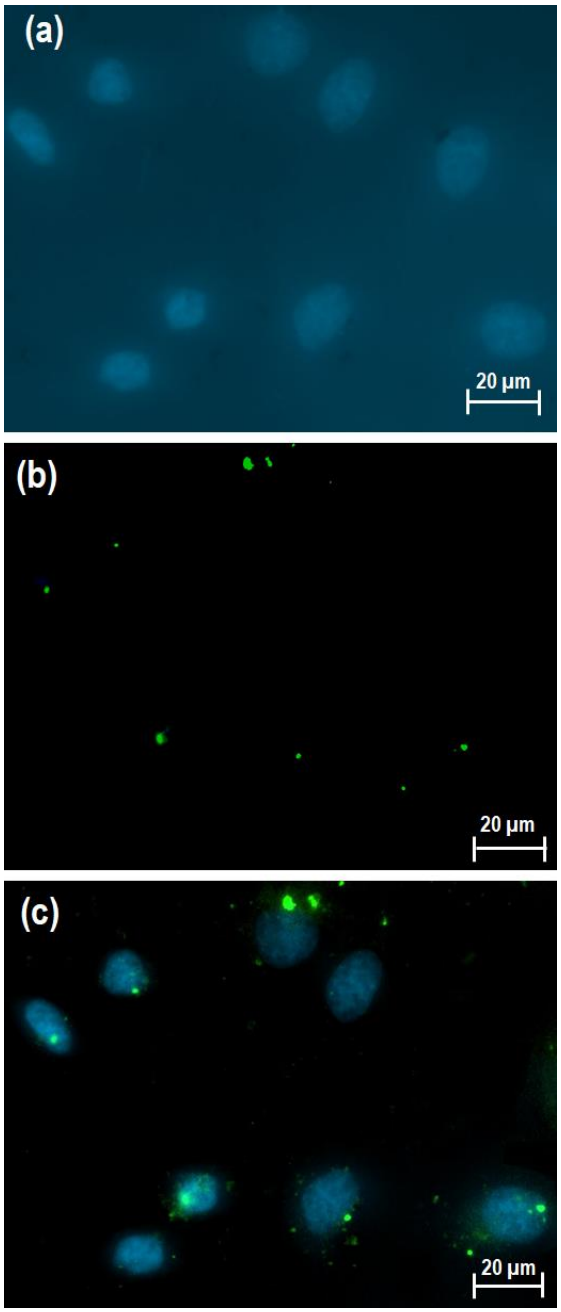

Figure 5.6. Visualization of cellular uptake and internalization of CLA-coated PTX-SPIONs@CTT by A549 cell. Micrograph (**a**) shows nuclei of A549 cells as visualized by DAPI staining, and (**b**) shows CLA-coated PTX-SPIONs@CTT (FITC-labelled) tracking, while (**c**) is the overlay of (**a**) and (**b**) showing the cellular uptake of formulated CLA-coated PTX-SPIONs@CTT.

5.3.7. Assessment of MMP-2 binding and secretion levels by ELISA

Secretion levels of MMP-2 by HMEC-1 cells were detected and quantified from the cell culture media, using human MMP-2 ELISA kit. Presented in **Figure 5.7** is the MMP-2 concentration plot from untreated cells as well as cells treated with antiangiogenic CTT-functionalized (CLA-coated PTX-SPIONs@CTT) and non-functionalized (CLA-coated PTX-SPIONs) nanosystems. A highest MMP-2 concentration (1.68 ng/mL) was recorded from untreated cells, meanwhile the lowest concentration (0.47 ng/mL) was recorded from cells treated with CLA-coated PTX-SPIONs@CTT. Treatment with CLA-coated PTX-SPIONs resulted in concentration levels of 1.55 ng/mL. Higher MMP-2 secretion levels could be expected from untreated cells, indicative of normal uninterrupted endothelial cell growth. Endothelial cells secrete MMP-2 to facilitate the removal of matrix barriers and initiate signalling pathways that promote cell growth, including angiogenesis (Quintero-Fabián et al., 2019; Shen et al., 2010).

A significant variation in MMP-2 secretion levels between cells treated with CLA-coated PTX-SPIONs@CTT and cells treated with CLA-coated PTX-SPIONs was an interesting revelation. Essentially, the non-functionalized CLA-coated PTX-SPIONs was solely employed for comparison with CLA-coated PTX-SPIONs@CTT, to discern the activity of CTT peptide on MMP-2 targeting. Accordingly, the lower MMP-2 secretion levels recorded from CLA-coated PTX-SPIONs@CTT treatments compellingly confirmed the MMP-2 targeting ability of the peptide, resulting in MMP-2 arrest at active sites and inactivation of these endopeptidases that would promote angiogenesis under normal circumstances, and tumor angiogenesis in cancers. Meanwhile, non-functionalized CLA-coated PTX-SPIONs treatments yielded elevated MMP-2 levels, which were comparable with untreated control cells, indicating that the nanosystem had negligible effect on MMP-2 secretion. However, a slight change to 1.55 ng/mL could be the result of cells experiencing a mild shock from the introduction of a foreign substance (CLA-coated PTX-SPIONs).

MMPs are largely implicated in cancer as enablers of tumor angiogenesis (Quintero-Fabián et al., 2019). Generally, inhibitors of MMPs, both endogenous and synthetic, have been studied on various cancers and shown to suppress angiogenic responses *in vitro* and *in vivo* (Cabral-Pacheco et al., 2020; Fares et al., 2020; Shen et al., 2010) However, most of these inhibitors are only selective for a general class of MMPs, and lack specificity for individual MMP family members (Cabral-Pacheco et al., 2020). Therefore, a better understanding of specific MMPs and corresponding inhibitors with precise targeting capabilities has been called for in antiangiogenic approaches. Likewise, in the present study, we have identified and confirmed CTT as a specific MMP-2 inhibitor.

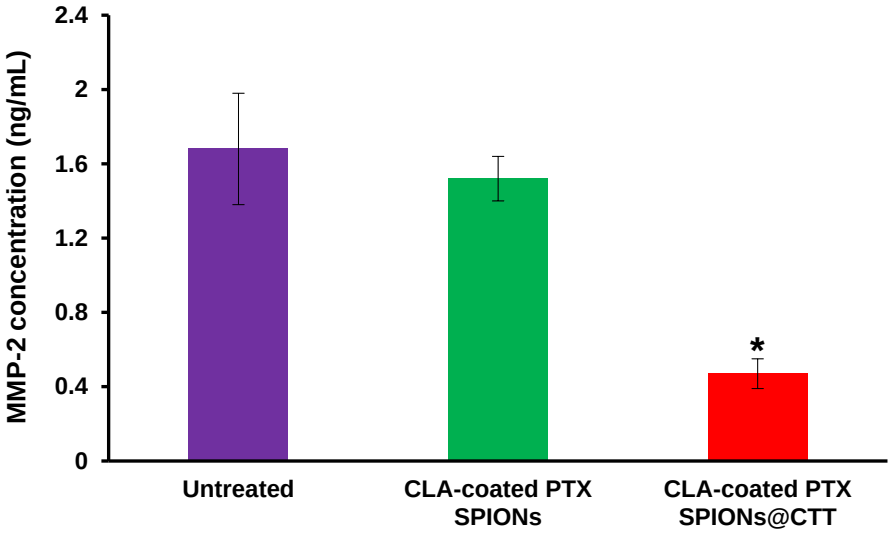

Figure 5.7. MMP-2 secretion levels from HMEC-1 incubated with CLA-coated PTX-SPIONs and CLA-coated PTX-SPIONs@CTT, as well as untreated cells, quantified by ELISA kit. Data presented as mean ± SD (* denotes $p < 0.05$, statistically significant compared to untreated and CLA-coated PTX-SPIONs).

5.3.8. Inhibition of endothelial cell migration by CLA-coated PTX-SPIONs@CTT

Evaluation of cell motility is of particular interest in the design of antiangiogenic therapeutics, as cell migration is facilitated through the angiogenesis pathway. During cell migration and invasion, cells are stimulated to degrade the extracellular matrix (ECM) in response to a gradient of angiogenesis-inducing factor, namely; MMP-2 (Quintero-Fabián et al., 2019). Thus, a decrease in overall endothelial cell motility can be a measure of limited MMP-2 activity and inhibition of angiogenesis. Accordingly, in the present study, CLA-coated PTX-SPIONs@CTT was shown to significantly inhibit the migration of HMEC-1 (**Figure 5.8**). This could be attributed to the specific binding of CLA-coated PTX-SPIONs@CTT to MMP-2 (facilitated by CTT peptide), which blocks angiogenesis signalling and subsequently halts cell proliferation and migration. The migration of cells incubated with non-functionalized CLA-coated PTX-SPIONs was not significantly affected, which indicated that even though the nanosystem confer anti-proliferative activity on cancerous cells, the involved mechanism is not associated with the inhibition of angiogenesis. A % migration of 23.6% and 78.4% was recorded from cells incubated with CLA-coated PTX-SPIONs@CTT and CLA-coated-PTX-SPIONs, respectively.

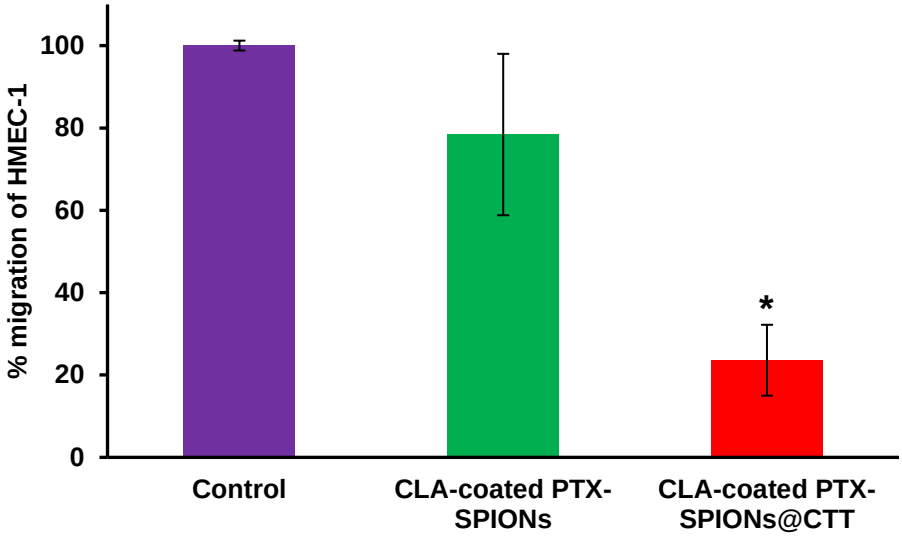

Figure 5.8. Migration (%) of HMEC-1 incubated with 50μg/mL of CLA-coated PTX-SPIONs and CLA-coated PTX-SPIONs@CTT. Control cells were left untreated. A % migration of 78.4 and 23.6 was recorded for cells incubated with CLA-coated PTX-SPIONs and CLA-coated PTX-SPIONs@CTT. (* denotes $p < 0.05$, statistically significant compared to control and CLA-coated PTX-SPIONs).

5.4. Concluding Remarks

The work presented in this chapter set to surface-functionalize the formally fabricated CLA-coated PTX-SPIONs with a distinct selective MMP-2 inhibitory peptide, CTT, using the established methodology involving DMSA-aided EDC/NHS chemistry. Accordingly, a targeted PTX delivery nanosystem with anti-MMP-2 activity was successfully formulated and exhibited highly desired characteristics, including a high drug loading capacity, site-specific sustained *in vitro* PTX release, enhanced PTX anti-proliferative activity, and excellent cellular uptake, for potential application as a nanomedicine in NSCLC therapy. The formulated CLA-coated PTX-SPIONs@CTT possess specific MMP-2 binding ability for halting angiogenesis and endothelial cell migration *in vitro*. The efficiency of the fabrication methodology is applauded in yielding a desired nanosystem, and the *in vitro* cellular analyses were found to be robust in discerning the antiangiogenic activity of the nanosystem prior to *in vivo* investigations.

Further *in vivo* studies will ascertain the antitumor activity of the nanosystem for potential application in targeted NSCLC therapy. In the next chapter, the peptide-functionalized nanosystems; CLA-coated PTX-SPIONs@HRH (presented in **Chapter 4**) and CLA-coated PTX-SPIONs@CTT are tested for tumor angiogenesis targetability and antitumor activity on a lung tumor xenograft mouse model to establish pre-clinical therapeutic efficacy.

5.5. References

Adekiya, T.A., Kumar, P., Kondiah, P.P.D., Ubanako, P., Choonara, Y.E., 2022. *In vivo* evaluation of praziquantel-loaded solid lipid nanoparticles against *S. mansoni* infection in preclinical murine models. Int. J. Mol. Sci. 23, 9485.

Adeyemi, S.A., Choonara, Y.E., 2022. *In vitro* and *in vivo* evaluation of a cyclic LyP-1-modified nanosystem for targeted endostatin delivery in a KYSE-30 cell xenograft athymic nude mice model. Pharmaceuticals 15, 353.

Adeyemi, S.A., Choonara, Y.E., Kumar, P., du Toit, L.C., Marimuthu, T., Kondiah, P.P.D., Pillay, V., 2019. Folate-decorated, endostatin-loaded, nanoparticles for anti-proliferative chemotherapy in esophaegeal squamous cell carcinoma. Biomed. Pharmacother. 119, 109450.

Adeyemi, S.A., Choonara, Y.E., Kumar, P., du Toit, L.C., Pillay, V., 2017. Design and characterization of endostatin-loaded nanoparticles for *in vitro* antiangiogenesis in squamous cell carcinoma. J. Nanomater. 2017, 2539065.

Akilo, O.D., Choonara, Y.E., Strydom, A.M., du Toit, L.C., Kumar, P., Modi, G., Pillay, V., 2016. An *in vitro* evaluation of a carmustine-loaded nano-co-plex for potential magnetic-targeted intranasal delivery to the brain. Int. J. Pharm. 500, 196-209.

Aloisio, A., Nisticò, N., Mimmi, S., Maisano, D., Vecchio, E., Fiume, G., Iaccino, E., Quinto, I., 2021. Phage-displayed peptides for targeting tyrosine kinase membrane receptors in cancer therapy. Viruses 13, 649.

Bałan, B.J., Siwicki, A.K., Pastewka, K., Demkow, U., Skopiński, P., Skopińska-Różewska, E., Lewicki, S., Zdanowski, R., 2017. Synergistic activity for natural and synthetic inhibitors of angiogenesis induced by murine sarcoma L-1 and human kidney cancer cells. Adv. Exp. Med. Biol. 1020, 91-104.

Cabral-Pacheco, G.A., Garza-Veloz, I., Castruita-De la Rosa, C., Ramirez-Acuña, J.M., Perez-Romero, B.A., Guerrero-Rodriguez, J.F., Martinez-Avila, N., Martinez-Fierro, M.L., 2020. The roles of matrix metalloproteinases and their inhibitors in human diseases. Int. J. Mol. Sci. 21, 9739.

Chen, T., Jiang, Y., Wang, C., Cai, Z., Chen, H., Zhu, J., Tao, P., Wu, M., 2021. The Ph-triggered drug release and simultaneous carrier decomposition of effervescent SiO_2–drug–Na_2CO_3 composite nanoparticles: To improve the antitumor activity of hydrophobic drugs. RSC Adv. 11, 5335-5347.

Çitoğlu, S., Coşkun, Ö.D., Tung, L.D., Onur, M.A., Thanh, N.T.K., 2021. DMSA-coated cubic iron oxide nanoparticles as potential therapeutic agents. Nanomedicine 16, 925-941.

Currie, E., Schulze, A., Zechner, R., Walther, Tobias C., Farese, Robert V., Jr., 2013. Cellular fatty acid metabolism and cancer. Cell Metab. 18, 153-161.

Dachev, M., Bryndová, J., Jakubek, M., Moučka, Z., Urban, M., 2021. The effects of conjugated linoleic acids on cancer. Processes 9, 454.

den Hartigh, L.J., 2019. Conjugated linoleic acid effects on cancer, obesity, and atherosclerosis: A review of pre-clinical and human trials with current perspectives. Nutrients 11, 370.

Dilnawaz, F., Singh, A., Mohanty, C., Sahoo, S.K., 2010. Dual drug loaded superparamagnetic iron oxide nanoparticles for targeted cancer therapy. Biomaterials 31, 3694-3706.

Engelberg, S., Netzer, E., Assaraf, Y.G., Livney, Y.D., 2019. Selective eradication of human non-small cell lung cancer cells using aptamer-decorated nanoparticles harboring a cytotoxic drug cargo. Cell Death Dis. 10, 702.

Fares, J., Fares, M.Y., Khachfe, H.H., Salhab, H.A., Fares, Y., 2020. Molecular principles of metastasis: A hallmark of cancer revisited. Sig. Trans. Target. Ther. 5, 28.

Foldbjerg, R., Dang, D.A., Autrup, H., 2011. Cytotoxicity and genotoxicity of silver nanoparticles in the human lung cancer cell line, A549. Arch. Toxicol. 85, 743-750.

Genova, C., Rossi, G., Tagliamento, M., Rijavec, E., Biello, F., Cerbone, L., Zullo, L., Grossi, F., 2020. Targeted therapy of oncogenic-driven advanced non-small cell lung cancer: Recent advances and new perspectives. Expert Rev. Respir. Med. 14, 367-383.

Gonçalves, L.C., Seabra, A.B., Pelegrino, M.T., de Araujo, D.R., Bernardes, J.S., Haddad, P.S., 2017. Superparamagnetic iron oxide nanoparticles dispersed in pluronic F127 hydrogel: Potential uses in topical applications. RSC Adv. 7, 14496-14503.

Gonzalez-Avila, G., Sommer, B., Mendoza-Posada, D.A., Ramos, C., Garcia-Hernandez, A.A., Falfan-Valencia, R., 2019. Matrix metalloproteinases participation in the metastatic process and their diagnostic and therapeutic applications in cancer. Crit. Rev. Oncol. Hematol. 137, 57-83.

Hall, R.D., Le, T.M., Haggstrom, D.E., Gentzler, R.D., 2015. Angiogenesis inhibition as a therapeutic strategy in non-small cell lung cancer (NSCLC). Transl. Lung Cancer Res. 4, 515-523.

Han, L., Sheng, B., Zeng, Q., Yao, W., Jiang, Q., 2020. Correlation between MMP2 expression in lung cancer tissues and clinical parameters: A retrospective clinical analysis. BMC Pulm. Med. 20, 283-283.

Hoshyar, N., Gray, S., Han, H., Bao, G., 2016. The effect of nanoparticle size on *in vivo* pharmacokinetics and cellular interaction. Nanomedicine (Lond.) 11, 673-692.

Kumar, P., Srivastava, R., 2018. FITC conjugated polycaprolactone-glycol-chitosan nanoparticles containing the longwave emitting fluorophore IR820 for *in vitro* tracking of hyperthermia-induced cell death. bioRxiv, 273748.

Li, W., Yu, H., Ding, D., Chen, Z., Wang, Y., Wang, S., Li, X., Keidar, M., Zhang, W., 2019. Cold atmospheric plasma and iron oxide-based magnetic nanoparticles for synergetic lung cancer therapy. Free Radic. Biol. Med. 130, 71-81.

Lu, L., Chen, H., Hao, D., Zhang, X., Wang, F., 2019. The functions and applications of A7R in anti-angiogenic therapy, imaging and drug delivery systems. Asian J. Pharm. Sci. 14, 595-608.

Lugano, R., Ramachandran, M., Dimberg, A., 2020. Tumor angiogenesis: Causes, consequences, challenges and opportunities. Cell. Mol. Life Sci. 77, 1745-1770.

Mashreghi, M., Azarpara, H., Bazaz, M.R., Jafari, A., Masoudifar, A., Mirzaei, H., 2018. Angiogenesis biomarkers and their targeting ligands as potential targets for tumor angiogenesis. J. Cell. Physiol. 233, 2949-2965.

Mohtar, N., Parumasivam, T., Gazzali, A.M., Tan, C.S., Tan, M.L., Othman, R., Fazalul Rahiman, S.S., Wahab, H.A., 2021. Advanced nanoparticle-based drug delivery systems and their cellular evaluation for non-small cell lung cancer treatment. Cancers (Basel) 13, 3539.

Muzio, G., Miola, M., Ferraris, S., Maggiora, M., Bertone, E., Puccinelli, M.P., Ricci, M., Borroni, E., Canuto, R.A., Verné, E., Follenzi, A., 2017. Innovative superparamagnetic iron-oxide nanoparticles coated with silica and conjugated with linoleic acid: Effect on tumor cell growth and viability. Mater. Sci. Eng: C 76, 439-447.

Ndinguri, M.W., Bhowmick, M., Tokmina-Roszyk, D., Robichaud, T.K., Fields, G.B., 2012. Peptide-based selective inhibitors of matrix metalloproteinase-mediated activities. Molecules (Basel, Switzerland) 17, 14230-14248.

Ngema, L.M., Adeyemi, S.A., Marimuthu, T., Choonara, Y.E., 2021. A review on engineered magnetic nanoparticles in non-small-cell lung carcinoma targeted therapy. Int. J. Pharm. 606, 120870.

Ngema, L.M., Adeyemi, S.A., Marimuthu, T., Ubanako, P., Wamwangi, D., Choonara, Y.E., 2022. Synthesis of novel conjugated linoleic acid (CLA)-coated superparamagnetic iron oxide nanoparticles (SPIONs) for the delivery of paclitaxel with enhanced *in vitro* anti-proliferative activity on A549 lung cancer cells. Pharmaceutics 14, 829.

Pugliese, R., Gelain, F., 2020. Cross-linked self-assembling peptides and their post-assembly functionalization via one-pot and in situ gelation system. Int. J. Mol. Sci. 21, 4261.

Quintero-Fabián, S., Arreola, R., Becerril-Villanueva, E., Torres-Romero, J.C., Arana-Argáez, V., Lara-Riegos, J., Ramírez-Camacho, M.A., Alvarez-Sánchez, M.E., 2019. Role of matrix metalloproteinases in angiogenesis and cancer. Front. Oncol. 9.

Rinawati, L., Nugraha, R.E., Mahdia, R., Munifa, I., Chasanah, U., Wahyuningsih, S., Ramelan, A., 2015. Increasing the effectiveness of pesticides based urea nanofertilizer encapsulated nanosilica with addition of rice husk TiO_2 additive substances. J. Chem. Pharm. Res. 2015, 85-89.

Rosca, E.V., Koskimaki, J.E., Rivera, C.G., Pandey, N.B., Tamiz, A.P., Popel, A.S., 2011. Anti-angiogenic peptides for cancer therapeutics. Curr. Pharm. Biotechnol. 12, 1101-1116.

Salehi, M., Movahedpour, A., Tayarani, A., Shabaninejad, Z., Pourhanifeh, M.H., Mortezapour, E., Nickdasti, A., Mottaghi, R., Davoodabadi, A., Khan, H., Savardashtaki, A., Mirzaei, H., 2020.

Therapeutic potentials of curcumin in the treatment of non-small-cell lung carcinoma. Phytother. Res. 34, 2557-2576.

Salgia, R., Pharaon, R., Mambetsariev, I., Nam, A., Sattler, M., 2021. The improbable targeted therapy: KRAS as an emerging target in non-small cell lung cancer (NSCLC). Cell Rep. Med. 2, 100186.

Sawisai, R., Wanchanthuek, R., Radchatawedchakoon, W., Sakee, U., 2019. Simple continuous flow synthesis of linoleic and palmitic acid-coated magnetite nanoparticles. Surf. Interfaces 17, 100344.

Sebben, D., Pendleton, P., 2014. Infrared spectrum analysis of the dissociated states of simple amino acids. Spectrochim. Acta A: Mol. Biomol. Spectrosc. 132, 706-712.

Shen, Q., Lee, E.S., Pitts, R.L., Wu, M.H., Yuan, S.Y., 2010. Tissue inhibitor of metalloproteinase-2 regulates matrix metalloproteinase-2–mediated endothelial barrier dysfunction and breast cancer cell transmigration through lung microvascular endothelial cells. Mol. Cancer Res. 8, 939-951.

Shukla, N.A., Yan, M.N., Hanna, N., 2020. The story of angiogenesis inhibitors in non–small-cell lung cancer: The past, present, and future. Clin. Lung Cancer 21, 308-313.

Slimani, S., Meneghini, C., Abdolrahimi, M., Talone, A., Murillo, J.P.M., Barucca, G., Yaacoub, N., Imperatori, P., Illés, E., Smari, M., Dhahri, E., Peddis, D., 2021. Spinel iron oxide by the co-precipitation method: Effect of the reaction atmosphere. Appl. Sci. 11, 5433.

Song, L.N., Gu, N., Zhang, Y., 2017. A moderate method for preparation DMSA coated Fe_3O_4 nanoparticles. IOP Conf. Ser.: Mater. Sci. Eng. 164, 012026.

Sun, M., Wang, J., Lu, Q., Xia, G., Zhang, Y., Song, L., Fang, Y., 2015. Novel synthesizing method of Ph-dependent doxorubicin-loaded anti-CD22-labelled drug delivery nanosystem. Drug Des. Devel. Ther. 9, 5123-5133.

Tsoukalas, C., Psimadas, D., Kastis, G.A., Koutoulidis, V., Harris, A.L., Paravatou-Petsotas, M., Karageorgou, M., Furenlid, L.R., Moulopoulos, L.A., Stamopoulos, D., Bouziotis, P., 2018. A novel metal-based imaging probe for targeted dual-modality SPECT/MR imaging of angiogenesis. Front. Chem. 6.

Wang, H., Shi, Y., Gu, J., 2020. A multitarget angiogenesis inhibitor, CTT peptide-endostatin mimic-kringle 5, prevents diet-induced obesity. J. Mol. Med. 98, 1753-1765.

Wang, H., Yang, Z., Gu, J., 2014. Therapeutic targeting of angiogenesis with a recombinant CTT peptide–endostatin mimic–kringle 5 protein. Mol. Cancer Ther. 13, 2674-2687.

Webb, A.H., Gao, B.T., Goldsmith, Z.K., Irvine, A.S., Saleh, N., Lee, R.P., Lendermon, J.B., Bheemreddy, R., Zhang, Q., Brennan, R.C., Johnson, D., Steinle, J.J., Wilson, M.W., Morales-Tirado, V.M., 2017. Inhibition of MMP-2 and MMP-9 decreases cellular migration, and angiogenesis in *in vitro* models of retinoblastoma. BMC Cancer 17, 434-434.

Winkler, J., Abisoye-Ogunniyan, A., Metcalf, K.J., Werb, Z., 2020. Concepts of extracellular matrix remodelling in tumour progression and metastasis. Nat. Commun. 11, 5120.

Wulandari, I.O., Sulistyarti, H., Safitri, A., Santjojo, D., Sabarudin, A., 2019. Development of synthesis method of magnetic nanoparticles modified by oleic acid and chitosan as a candidate for drug delivery agent. Development 9.

Ye, Z., Huang, Y., Ke, J., Zhu, X., Leng, S., Luo, H., 2021. Breakthrough in targeted therapy for non-small cell lung cancer. Biomed. Pharmacother. 133, 111079.

Zhang, K., Wang, L., Wei, A., Jia, X., Liu, X., 2020. CM082, a novel angiogenesis inhibitor, enhances the antitumor activity of gefitinib on epidermal growth factor receptor mutant non-small cell lung cancer *in vitro* and *in vivo*. Thorac. Cancer 11, 1566-1577.

Zhang, Q., Liu, Q., Du, M., Vermorken, A., Cui, Y., Zhang, L., Guo, L., Ma, L., Chen, M., 2019. Cetuximab and doxorubicin loaded dextran-coated Fe_3O_4 magnetic nanoparticles as novel targeted nanocarriers for non-small cell lung cancer. J. Magn. Magn. Mater. 481, 122-128.

Zhang, T.Y., Huang, J.T., Tian, H.B., Ma, Y., Chen, Z., Wang, J.J., Shi, H.P., Luo, J., 2018. *Trans*-10,*cis*-12 conjugated linoleic acid alters lipid metabolism of goat mammary epithelial cells by regulation of *de novo* synthesis and the AMPK signaling pathway. J. Dairy Sci. 101, 5571-5581.

Zhong, T., Yao, X., Zhang, S., Guo, Y., Duan, X.-C., Ren, W., Dan, H., Yin, Y.-F., Zhang, X., 2016. A self-assembling nanomedicine of conjugated linoleic acid-paclitaxel conjugate (CLA-PTX) with higher drug loading and carrier-free characteristic. Sci. Rep. 6, 36614.

Zhou, Y.J ., Zheng, W., Zeng, Q. H., Ye, Y., Wang, C., Fang, C., Liu, C. J., Niu, L., Wu, L. M., 2021. Targeted exome sequencing identifies mutational landscape in a cohort of 1500 Chinese patients with non-small cell lung carcinoma (NSCLC). Hum. Genomics 15, 21.

CHAPTER 6

IN VIVO EVALUATION OF NOVEL ANTIANGIOGENIC PEPTIDE-FUNCTIONALIZED PACLITAXEL DELIVERY NANOSYSTEMS ON A LUNG TUMOR XENOGRAFT MOUSE MODEL

The in vivo study received approval from the Animal Research Ethics Committee (AREC) of the University of the Witwatersrand, clearance certificate number: 2020/11/01/B (see Appendix A)

6.1. Introduction

Paclitaxel (PTX) is a primary anticancer drug currently used in first-line treatment of non-small cell lung carcinoma (NSCLC) (Gui et al., 2021). However, the available formulations of PTX for NSCLC treatment still show limited therapeutic efficacy due to non-specificity and detrimental side effects. Particularly, the commercial polyethoxylated castor oil and anhydrous alcohol (Kolliphor® EL, formerly Cremophor® EL) formulation (Taxol®) is riddled with severe side effects such as peripheral neuropathy, hyperlipidemia, and sometimes fatal hypersensitivity reactions (Gala et al., 2020). Meanwhile, a solvent free, nanoparticle albumin-bound PTX formulation (*nab*-paclitaxel; Abraxane®) available for advanced and metastatic NSCLC is speculated to comprise the quality of life for some patients due to its side effects such as pain, fatigue, hair loss, neuropathy, and anemia (Sun et al., 2020). Moreover, the intravenous (IV) route of administration currently employed in first and second-line treatment has concerning limitations, including patient discomfort, catheter failures, need for trained practitioners, and high clinical costs (Bordat et al., 2022).

Consequently, in the present study we have formulated novel targeted PTX delivery nanosystems as subcutaneously injectable nanomedicine for NSCLC management. A subcutaneous (SC) route of administration is proposed as a suitable alternative to IV, owing to its safety and ease of application, reduced discomfort, slow and sustained rate of absorption for continuous delivery, and reduced costs (Bordat et al., 2022). The formulated nanosystems comprise superparamagnetic iron oxide nanoparticles (SPIONs) as core, a natural anticancer fatty acid (*trans*10, *cis*12 conjugated linoleic acid; 10E, 12Z CLA) as a coating and PTX partitioning agent, and functionalized with antiangiogenic peptides HRH and CTT. The nanosystems; CLA-coated PTX-SPIONs@HRH and CLA-coated PTX-SPIONs@CTT show to bind and arrest vascular endothelial growth factor receptors (VEGFRs) and matrix metalloproteinase 2 (MMP 2), respectively, *in vitro*. Moreover, the nanosystems exhibit enhanced anti-proliferative activity on lung adenocarcinoma cells (A549), which coincides with the site-specific sustained release of PTX over time.

Although extensive *in vitro* evaluations have been conducted and provided valid information about the anticancer activity of CLA-coated PTX-SPIONs@HRH and CLA-coated PTX-SPIONs@CTT, further *in vivo* evaluations are required to validate the safety and therapeutic efficacy of the nanosystems. Essentially, *in vivo* analyses provide accurate and realistic pharmacodynamics (PD) and pharmacokinetics (PK) data to determine the safety and efficacy of therapeutics prior to further testing in humans (Pantaleão et al., 2022). Accordingly, animal models, such as mouse xenografts, play a pivotal role in cancer research for screening of new therapeutic candidates and understanding cancer pathophysiology (Adeyemi and Choonara, 2022). Mouse xenograft models are established from implantation of cancer cells within the animals to mimic human cancer pathophysiology, and nude mice are the most commonly used rodents for the establishment of xenografts, owing to their compromised immune system (Adeyemi and Choonara, 2022; Xie et al., 2021).

In the present study, female Athymic nude mice were employed to establish a SC lung tumor xenograft mouse model for evaluation of antitumor activity and PK profiles of CLA-coated PTX-SPIONs@HRH and CLA-coated PTX-SPIONs@CTT. Female mice were chosen over male mice to avoid the dominance phenomena, and moreover, male mice tend to be more aggressive when they develop tumors, thus increasing chances of unwanted injuries (Lee et al., 2018).

6.2. Materials and Methods

6.2.1. Materials

Lung adenocarcinoma cell line (A549) was purchased from Cellonex, Johannesburg, South Africa. Athymic (MF1-nu/nu) female nude mice (6 weeks old) weighing 22 g were sourced from the Wits Research Animal Facility (WRAF), University of the Witwatersrand, Johannesburg, South Africa. Taxol® and phosphate buffered saline tablets (PBS) were procured from Sigma-Aldrich Corp. (St. Louis, MO, USA). Docetaxel (DTX) was purchased from DLD-Scientific (Durban, South Africa). Isoflurane gas, sodium pentobarbitone, and all other related consumables were provided by WRAF. Solvents used for high pressure liquid chromatography (HPLC) analysis were of HPLC-grade, and all other reagents were of analytical grade and highest purity. All reagents were used as received, unless stated otherwise.

6.2.2. Animal housing and welfare

Mice were housed in individual cages in a temperature and humidity controlled room (**Figure 6.1**), with the provision of food and water *ad libitum* on a 12 h light/day cycle. The mice were routinely monitored at least once a day for 1 h to assess their state of well-being, and weighed at least twice a week. A qualified WRAF staff was always present to note any signs of distress displayed by the animals during the period of the study.

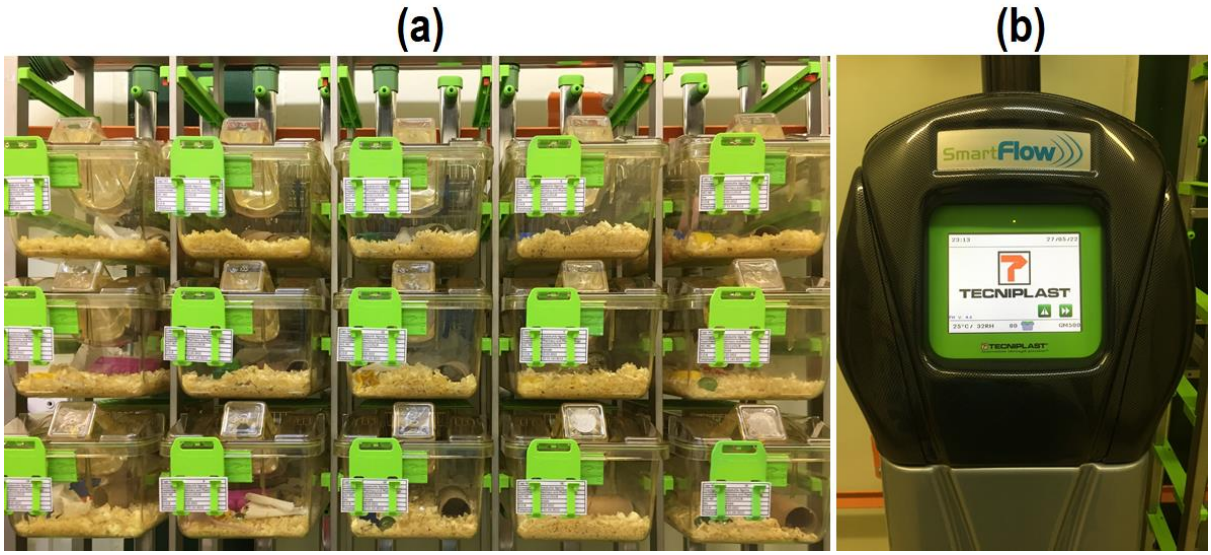

Figure 6.1. Photographic evidence of (**a**) mice housed in individual cages in a temperature and humidity controlled room, and (**b**) a device used to maintain the temperature (~25°C) and humidity (80%).

6.2.3. Development of a lung tumor xenograft mouse model

A habituation period of one (1) week was established before experimentation could commence. After habituation, all mice were anaesthetized with 2% isoflurane gas and inoculated with 3.9×10^5 A549 cells via a SC injection of 50 µL cell suspension in PBS at the right flank. Solid tumors were visible 20 days post-inoculation and allowed to grow to a treatable volume of 90 – 100 mm^3. A digital calliper was used to measure tumor dimensions (**Figure 6.2**), and tumor volume (*V*) was computed using the equation 6.1 (Sápi et al., 2015):

$$V = \frac{W^2 \times L}{2} \qquad \text{(Equation 6.1)}$$

Where *W* is the tumor width and *L* is the length in mm (as measured by a digital calliper).

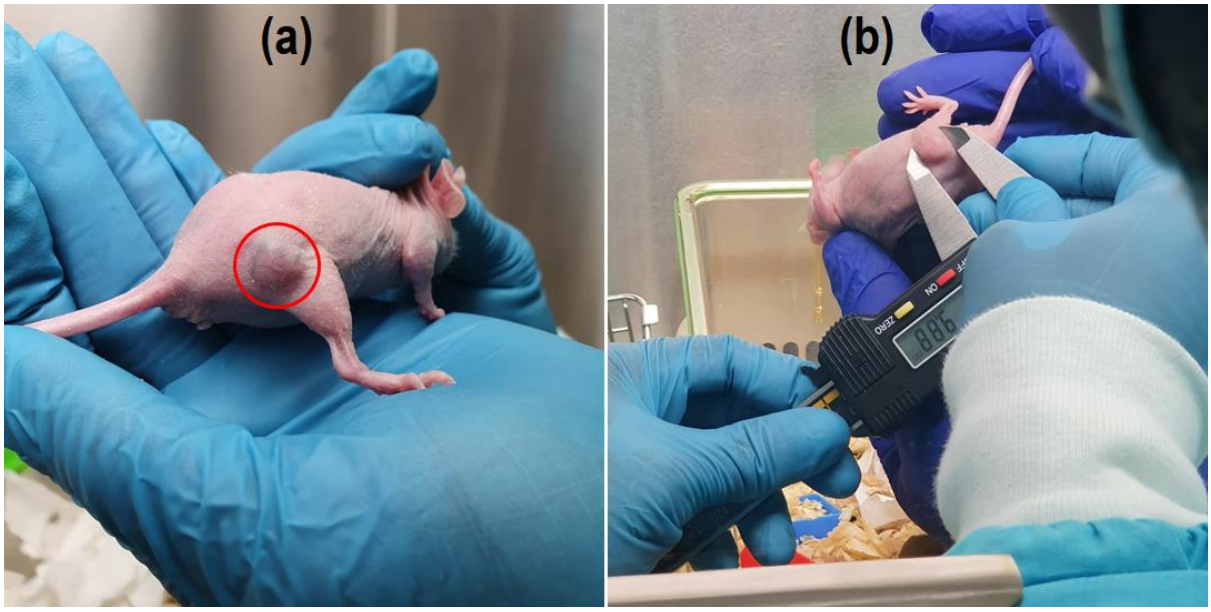

Figure 6.2. Captured images of (**a**) nude mouse with a developed solid tumor (red circle) and (**b**) measurement of tumor dimensions using a digital calliper.

6.2.4. Preparation of formulations and administration of treatment on the developed lung tumor xenograft mouse model

The novel nanosystems; CLA-coated PTX-SPIONs@HRH and CLA-coated PTX-SPIONs@CTT were formulated as described in **Chapter 4** (4.2.2) and **Chapter 5** (5.2.2), respectively. Appropriate dosage of the nanosystems and a corresponding dose of the comparator drug (Taxol®) were prepared for administration. The mice were randomly divided into 4 groups (as per the experimental design below) with each group having 3 mice (*n = 3*). The sample size (*n = 3*) was adopted to adhere to ethical regulations, and obtain reliable and statistically sound data. A 25G needle on a 1 mL syringe was employed to administer (SC, 20 mm away from tumor) 100 μL injection volume of 12 mg/kg CLA-coated PTX-SPIONs@HRH, CLA-coated PTX-SPIONs@CTT, and CLA-coated PTX-SPIONs each, and 1.2 mg/kg Taxol® (tolerated dosage equivalent to 10% PTX in the nanosystems, corresponding to 10% drug loading capacity). Meanwhile, control mice received only PBS (100 μL). A 4-cycle treatment plan was adopted in which mice received treatment at day 0, 4, 8, and 12 (Zou et al., 2018), with tumor volumes routinely measured at each treatment day before injection, and further 12 days post-treatment, until day 20, to observe growth regression. Moreover, the weight of the mice was measured after every 2 days until day 20.

6.2.5. *In vivo* antitumor experimental design

A total of 15 Athymic female nude mice (6 weeks old) were used for evaluation of *in vivo* antitumor activity of the formulated nanosystems. Tumor-bearing mice (lung tumor xenograft model) were randomly divided into 5 groups as depicted below and in **Figure 6.3**:

- **Group 1** (Control/placebo group, *n* = *3*): This group received a SC injection of 100 μL PBS at day 0, 4, 8, and 12.
- **Group 2** (Experimental, *n* = *3*): This group received a SC injection of 100 μL equivalent to 1.2 mg/kg of Taxol® (tolerated dose equivalent to 10% PTX in the nanosystems, corresponding to 10% DLC), at day 0, 4, 8, and 12.
- **Group 3** (Experimental, *n* = *3*): This group received a SC injection of 100 μL equivalent to 12 mg/kg of CLA-coated PTX-SPIONs, at day 0, 4, 8, and 12.
- **Group 4** (Experimental, *n* = *3*): This group received a SC injection of 100 μL equivalent to 12 mg/kg of CLA-coated PTX-SPIONs@CTT, at day 0, 4, 8, and 12.
- **Group 5** (Experimental, *n* = *3*): This group received a SC injection of 100 μL equivalent to 12 mg/kg of CLA-coated PTX-SPIONs@HRH, at day 0, 4, 8, and 12.

The study was concluded at day 20, and the tumor growth inhibition (%TGI) was determined from the measured tumor volumes, using equation 6.2 (Tsukihara et al., 2015):

$$\%TGI = [1 - (\frac{RTV_{treatment}}{RTV_{control}})] \times 100 \qquad \text{(Equation 6.2)}$$

where $RTV_{treatment}$ is the relative tumor volume of a specified treatment group (*calculated as tumor volume on day 20 divided by tumor volume on day 0*) and $RTV_{control}$ is the relative tumor volume of the control group.

Mice were humanely euthanized at day 20 with 200 mg/kg intraperitoneal injection of sodium pentobarbital. Tumors, lung, and liver tissues were excised from tumor-bearing mice at termination (**Figure 6.4**) for further histological analysis. Essentially, the lung and liver are amongst the most affected vital organs in NSCLC (Tamura et al., 2015). The excised tissues were kept in 10% neutral buffered formalin before being transferred into paraffin for sectioning (4 – 5 μm). The sectioned tissues were stained with haematoxylin and eosin (H&E) and examined for histological variations according to the IDEXX JB661428 protocol (IDEXX Laboratories Pty. Ltd, Johannesburg, South Africa).

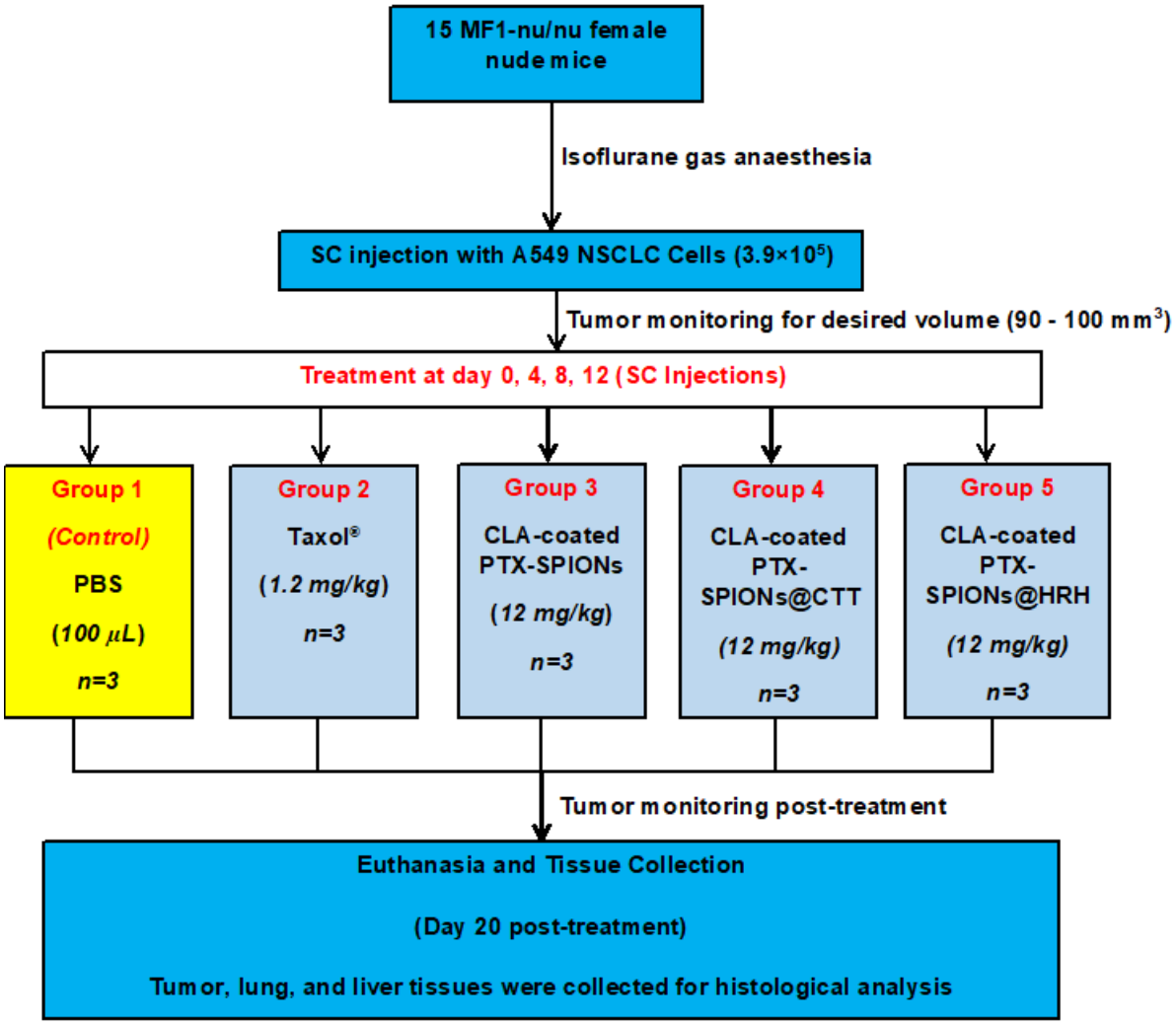

Figure 6.3. Experimental design of the *in vivo* antitumor study in mice.

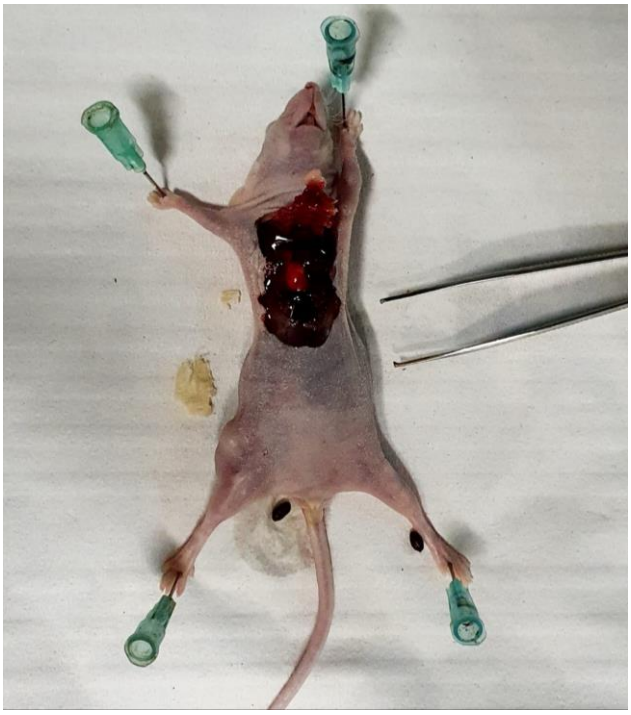

Figure 6.4. A tumor-bearing mouse fixed for excision of lung, liver, and tumor tissues after euthanasia.

6.2.6. Pharmacokinetics evaluation of PTX from plasma

A pharmacokinetics (PK) study was further conducted to evaluate the fate of PTX from the formulated delivery nanosystems, when administered subcutaneously. Essentially, PK evaluation plays a key role in the development of new therapeutics, for the assessment of the absorption and excretion profiles of the active pharmaceutical ingredient (API). Ideally, an API should achieve adequate concentration in the body over time in order to elicit a desired therapeutic action and meet safety standards (Reichel and Lienau, 2016). Herein, additional 12 female nude mice were acquired to conduct the PK study. Mice were randomly divided into 4 groups ($n = 3$) and received a single SC injection of corresponding dosage of Taxol®, CLA-coated PTX-SPIONs@CTT, and CLA-coated PTX-SPIONs@HRH. Treated mice were humanely euthanized at different time points and the blood was collected for analysis. Drug-free blood from untreated mice was used to construct a calibration curve.

6.2.6.1. Blood sample collection

Treated mice were humanely euthanized with a single intraperitoneal injection of 200 mg/kg sodium pentobarbital at varying time points, t = 0.5, 1, 4, 8, and 24 h, post-treatment, and the blood was collected at each time point via cardiac puncture (**Figure 6.5**). The blood samples were collected into heparin-flushed micro-centrifuge tubes to avoid clogging, and centrifuged at 10 000 rpm, 10°C for 10 min (TC-MiniSpin Centrifuge, TopScien, Ningbo, China). Plasma was collected and stored at -80°C for further analysis.

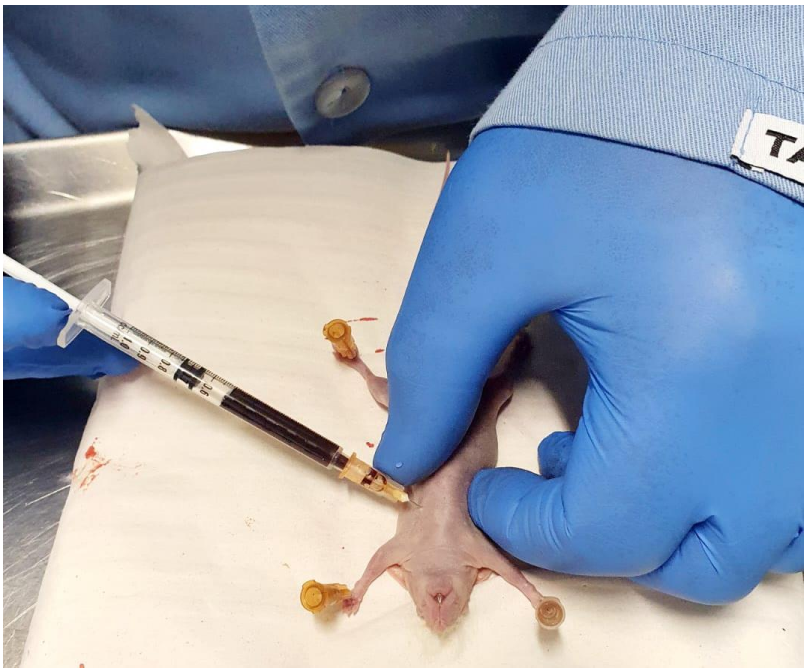

Figure 6.5. Blood collection via cardiac puncture, from a euthanized mouse.

6.2.6.2. Quantification of PTX concentration in plasma using high pressure liquid chromatography

Quantification of PTX in plasma was carried out on a Flexar LC UV/VIS HPLC (PerkinElmer Inc., Waltham, MA, USA). The separation was achieved using a Waters C_{18} column (250 × 3.9 mm, 5 μm) (Waters Chromatography Ireland Ltd, Wexford, Ireland). A validated rapid and sensitive reversed-phase HPLC method was employed for the quantification of PTX from plasma using a liquid-liquid extraction technique (Rezazadeh et al., 2015). The method comprised acetonitrile (ACN) and water as a mobile phase, with appropriate flow rate and running wavelength, as shown in **Table 6.1**. The solvents were prepared and filtered through 0.22 μm filters before usage. An internal standard (IS) of docetaxel (DTX) was carefully chosen for the quantification analysis.

Table 6.1. HPLC parameters employed for the determination of PTX concentration from plasma

Parameters	Conditions
Mobile phase	ACN and water (58:42), isocratic gradient
Flow rate	1.9 mL/min
Injection volume	20 μL
Wavelength	227 nm
Column temperature	58°C

A linear calibration curve with a range from 0.25 – 10 μg/mL was prepared from the blank (drug-free) plasma. Accordingly, stock solutions of PTX and DTX (100 μg/mL) were prepared in 70% methanol, and 100 μL of each, corresponding to the appropriate concentration was used to spike the plasma for the generation of the calibration curve. A 300 μL of 1.25% (v/v) absolute ethanol in diethyl ether was added into spiked plasma and vortexed briefly before centrifugation at 13 000 rpm, 10°C for 10 min (liquid-liquid extraction). The supernatant containing the drugs was collected into clean vials and allowed to dry. An appropriate volume of the mobile phase mixture was used to reconstitute the calibration standards, and filtered before injection into HPLC. A generated calibration curve was then used for the determination of PTX concentrations from the plasma samples collected from the mice. The plasma samples were prepared for the analysis by firstly thawing at room temperature. The thawed samples were spiked with 100 μL DTX (IS) and briefly vortexed for 30 sec. A liquid-liquid extraction procedure was performed similarly to the calibration curve standards, and the samples were filtered before running.

6.3. Results and Discussion

6.3.1. Effects of the formulated nanosystems on tumor growth

A lung tumor xenograft mouse model was successfully established and used to evaluate *in vivo* antitumor activity of the formulated CLA-coated PTX-SPIONs@CTT and CLA-coated PTX-SPIONs@HRH nanosystems. Expectedly, a rapid tumor growth was observed in the PBS (placebo) group, with tumors reaching an average volume of 1484.7 mm^3 at day 20 (**Figure 6.6a**). Tumor volumes in the similar range have been reported for SC lung tumor xenografts, owing to the robustness of A549 cancer cells (Zou et al., 2018). A significant regression in tumor volumes was observed in mice treated with the formulated nanosystems compared to the PBS, Taxol®, and CLA-coated-PTX-SPIONs groups. Accordingly, a

remarkable tumor growth inhibition rate (%TGI) of 76.6 and 69.7% was recorded from tumor-bearing mice treated with CLA-coated PTX-SPIONs@HRH and CLA-coated PTX-SPIONs@CTT, respectively (**Figure 6.6b**).

Treatment with non-functionalized CLA-coated PTX-SPIONs also showed a promising antitumor activity, with %TGI of 52.8%. Contrary, treatment with comparator Taxol® resulted in mild regression with a %TGI of only 26.3%. Such a distinction in tumor growth variations amongst the groups could be visually confirmed from excised tumors (**Figure 6.6c**). Essentially, the ability of CLA-coated PTX-SPIONs@HRH to significantly suppress tumor progression is greatly attributed to the antiangiogenic activity of HRH peptide, which is primarily involved in halting tumor angiogenesis and starving the tumor of growth nutrients and oxygen (Zhang et al., 2017). Likewise, the observed antitumor activity of CLA-coated PTX-SPIONs@CTT could be attributed to tumor targetability conferred by CTT peptide, which suppresses MMP-2 activity and halts signalling of angiogenesis, thus preventing rampant growth of tumors. Additionally, the synergy of antiangiogenic activity (peptides) and antimitotic activity (PTX) presented by CLA-coated PTX-SPIONs@HRH and CLA-coated PTX-SPIONs@CTT is responsible for the observed tumor regression.

The impact of the peptides in halting tumor growth was apparent as the non-functionalized nanosystem (CLA-coated PTX-SPIONs = 52.8% TGI) could not match the antitumor activity of CLA-coated PTX-SPIONs@HRH (76.6% TGI) and CLA-coated PTX-SPIONs@CTT (69.7% TGI), although it showed improved tumor regression compared to Taxol® (26.3% TGI). In essence, the promising antitumor activity of CLA-coated PTX-SPIONs is attributed to the enhanced PTX anticancer activity, conferred by the nanosystem. It is believed that the nanosystem allows for a sufficient therapeutic dose of PTX to be released at the tumor microenvironment and reach tumors to elicit antimitotic activity and prevent tumors from rapidly dividing. In **Chapter 3**, we reported that CLA-coated PTX-SPIONs enhance the anti-proliferative activity of PTX *in vitro*, and the current results validated that notion *in vivo* as well.

(a)

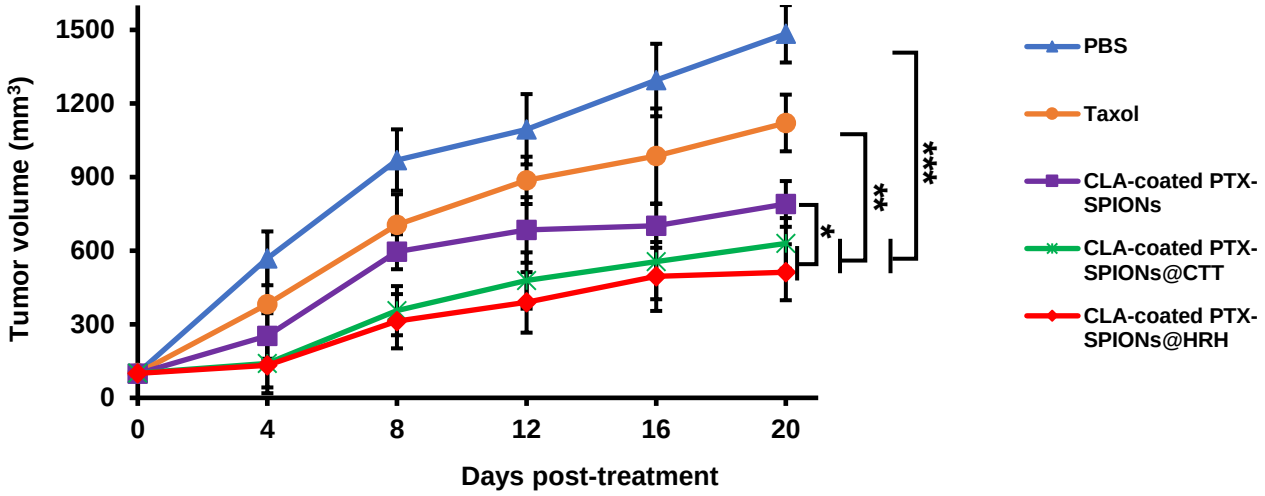
Tumor volume (mm³)
1500
1200
900
600
300
0
0
4
8
12
16
20
Days post-treatment
*
**
***
PBS
Taxol
CLA-coated PTX-SPIONs
CLA-coated PTX-SPIONs@CTT
CLA-coated PTX-SPIONs@HRH

(b)

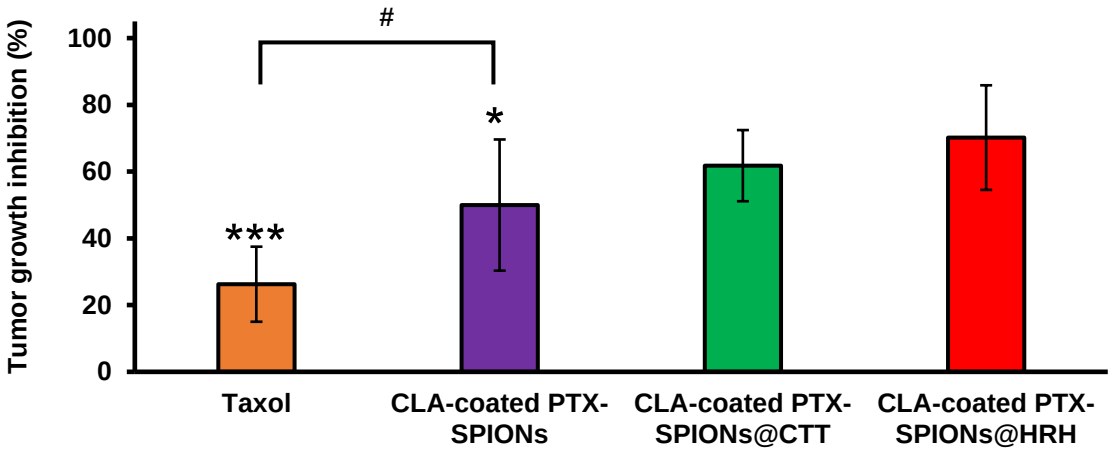
Tumor growth inhibition (%)
100
80
60
40
20
0
#
*
***
Taxol
CLA-coated PTX-SPIONs
CLA-coated PTX-SPIONs@CTT
CLA-coated PTX-SPIONs@HRH

(c)

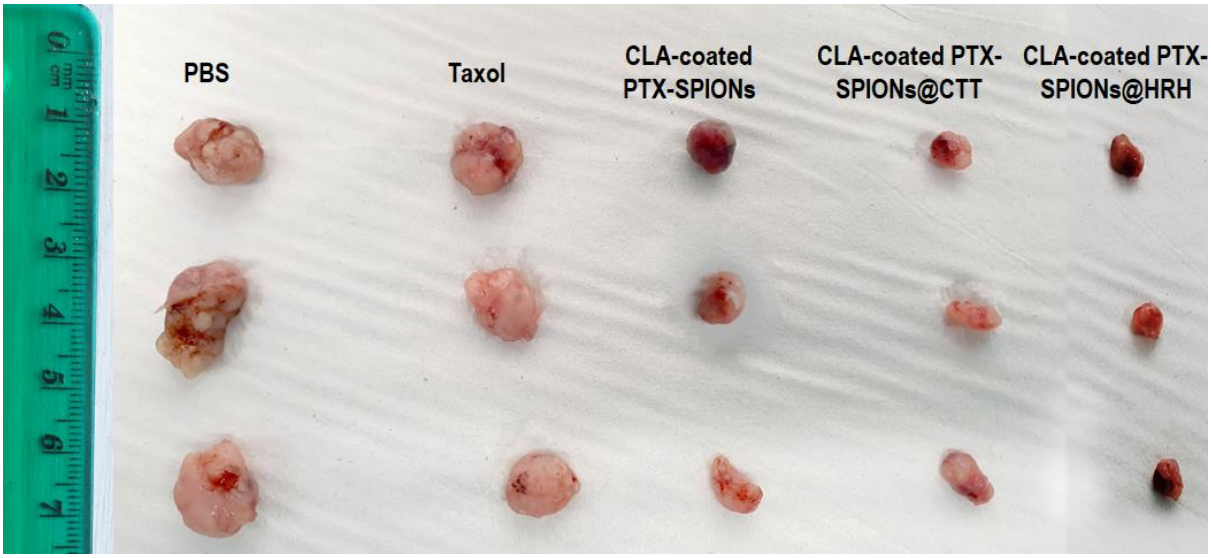
PBS
Taxol
CLA-coated PTX-SPIONs
CLA-coated PTX-SPIONs@CTT
CLA-coated PTX-SPIONs@HRH

Figure 6.6. A representation of the effects of treatment on the established SC lung tumor xenograft model, showing (**a**) variation in tumor volumes post treatment, (**b**) %TGI determined at the end of the study, and (**c**) images of excised tumors from the mice. Day 0, 4, 8, and 12 are treatment cycles 1 – 4, and days 16 to 20 are observation period. Excised tumors from different groups exhibit visibly distinct sizes, corresponding to the antitumor activity conferred by each treatment option. Data presented as mean ± SD of biological triplicates, *n=3* (* $p < 0.05$; ** $p < 0.01$; and *** $p < 0.001$, denoting statistically significant compared to CLA-coated PTX-SPIONs@CTT and CLA-coated PTX-SPIONs@HRH, and # denotes $p < 0.05$, compared to Taxol®).

Moreover, no significant loss was observed in the body weight of mice from the experimental groups, meanwhile the placebo group (mice that received only PBS) showed a notable weight loss (>5%), due to the progression of cancer over the duration of the study (**Figure 6.7**). A loss of weight in skeletal muscles and adipose tissue, known as cachexia, is fairly common in cancer and may also present as a side effect to chemotherapy (Adeyemi and Choonara, 2022; Zombeck et al., 2013). As such, the results obtained indicated the safety of CLA-coated PTX-SPIONs@HRH, CLA-coated PTX-SPIONs@CTT and CLA-coated PTX-SPIONs, with respect to limiting cachexia during treatment, and further suggest that the dosage of PTX administered could be tolerated, as no other side effects were observed.

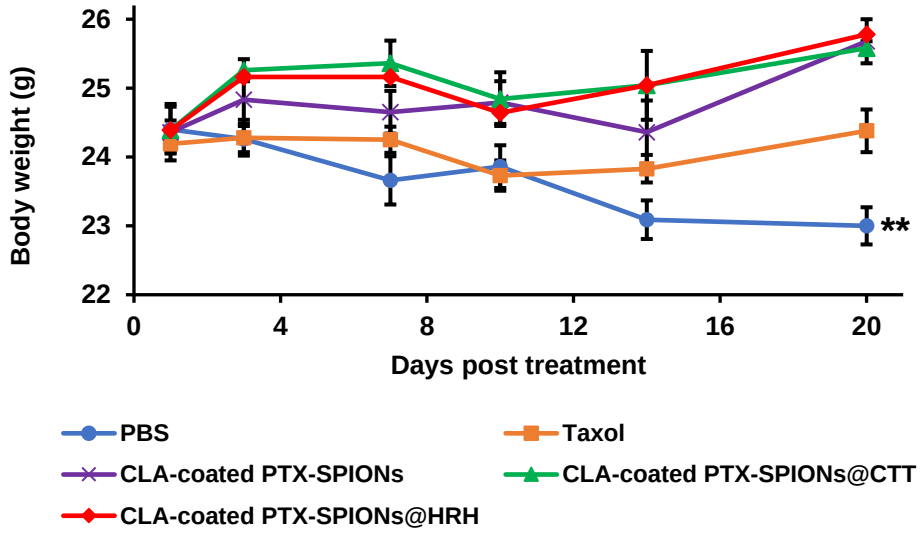

Figure 6.7. Weight measurements from tumor-bearing mice from day 1 post-treatment till the last day of the study. Mice exhibiting 10% and more weight loss would be removed from the study, as per ethical guidelines. Data presented as mean ± SD of biological triplicates, *n = 3* (** $p < 0.01$, statistically significant weight loss compared to day 1).

6.3.2. Histological analysis of selected organs and tumor tissue

A histopathological analysis of selected organs and tumors was primarily carried out to discern the effects of cancer by assessing the organelles possibly affected by the disease, and further investigate any structural variations afforded by different treatments. The histological analysis of liver, lung, and tumor tissues was conducted, and presented in **Figure 6.8** are corresponding images (H&E staining) for (**a**) normal healthy mice, (**b**) PBS group, (**c**) Taxol® group, (**d**) CLA-coated PTX-SPIONs group, (**e**) CLA-coated PTX-SPIONs@CTT group, and (**f**) CLA-coated PTX-SPIONs@HRH. A normal histological appearance was observed in the liver tissues of healthy mice, as expected, whereas livers from tumor-bearing mice in the placebo (PBS) and Taxol® groups exhibited prominent swollen hepatocytes (as depicted by arrows). Likewise, mildly swollen hepatocytes were identified in liver tissues from tumor-bearing mice in the CLA-coated PTX-SPIONs, CLA-coated PTX-SPIONs@CTT, and CLA-coated PTX-SPIONs@HRH groups, with occasional granular and finely vacuolated cytoplasm (squares). The observed swelling of hepatocytes and cytoplasmic vacuolization normally occur secondary to neoplastic-induced factors, and are characteristic of the complicating effects of cancer (Sharma et al., 2021).

Lungs from normal healthy mice provided a good reference, showing a normal histological appearance with a characteristic terminal brochiole (TB) leading to the alveolar duct (AD). Lungs from tumor-bearing mice in the PBS group exhibited a severe lobar haemorrhage (LH) and necrosis of the alveolar walls (AW), while a mild leukostasis (LKS) was present in alveolar capillaries in the lungs of Taxol® treated mice. Extensive haemorrhage could be seen throughout the disrupted pulmonary parenchyma (PP) in the lungs of tumor-bearing mice in the CLA-coated PTX-SPIONs, CLA-coated PTX-SPIONs@CTT, and CLA-coated PTX-SPIONs@HRH groups, linked with accumulation of oedema (OD) fluid, yielding a fibrillar appearance in the former. These histological appearances could be associated with neoplastic-induced changes arising from the lung cancer that was induced in mice.

Remarkable histological variations were observed in tumors of the mice amongst the groups. Tumors from mice that received only PBS showed a multifocal inflammation surrounding muscle fibres, along with oedema. There were no signs of neoplastic degeneration, with a record of 29 mitoses present in 10 high-power fields/2.37mm^2. Accordingly, the surrounding inflammation could be associated with the rapid growth of tumors, as inflammation is implicated in promoting stages of tumorigenesis (Greten and Grivennikov, 2019; Zhao et al., 2021). A cystic space was present in tumor mass of Taxol®-treated mice, with few necrotic cells and loose red blood cells scattered throughout, and 20 mitoses could be spotted in 10 high-power fields. Tumors from mice treated with CLA-coated PTX-SPIONs, CLA-coated

PTX-SPIONs@CTT, and CLA-coated PTX-SPIONs@HRH all exhibited areas of degeneration of neoplastic cells (red arrows), more present in peptide-functionalized nanosystems treatment groups (~60% of the mass), with 10, 5, and 2 mitoses presents in 10 high-power fields/2.37 mm^2, respectively. Essentially, the variation in mitotic rates between the placebo and treatment groups validated the antimitotic effect of PTX, and a further decline in mitoses recorded from the tumors of mice treated with our nanosystems supports our initial findings that CLA-coated PTX-SPIONs enhances the activity of PTX (as reported in **Chapter 3**).

Since angiogenesis promotes tumor growth, a pronounced degeneration of neoplastic cells in tumor tissues from the mice treated with CLA-coated PTX-SPIONs@CTT and CLA-coated PTX-SPIONs@HRH indicated that the nanosystems halt tumor growth through a mechanism involving angiogenesis inhibition. Primarily, CLA-coated PTX-SPIONs@CTT and CLA-coated PTX-SPIONs@HRH are believed, from the compelling evidence gathered *in vitro* and *in vivo*, to bind and arrest angiogenesis-promoting factors (i.e., MMP-2 and VEGFRs, respectively), which then halts the formation of new blood vessels, and deprive neoplastic cells of the necessary growth nutrients, resulting in their demise, since neoplasm feeds from angiogenesis (Saman et al., 2020).

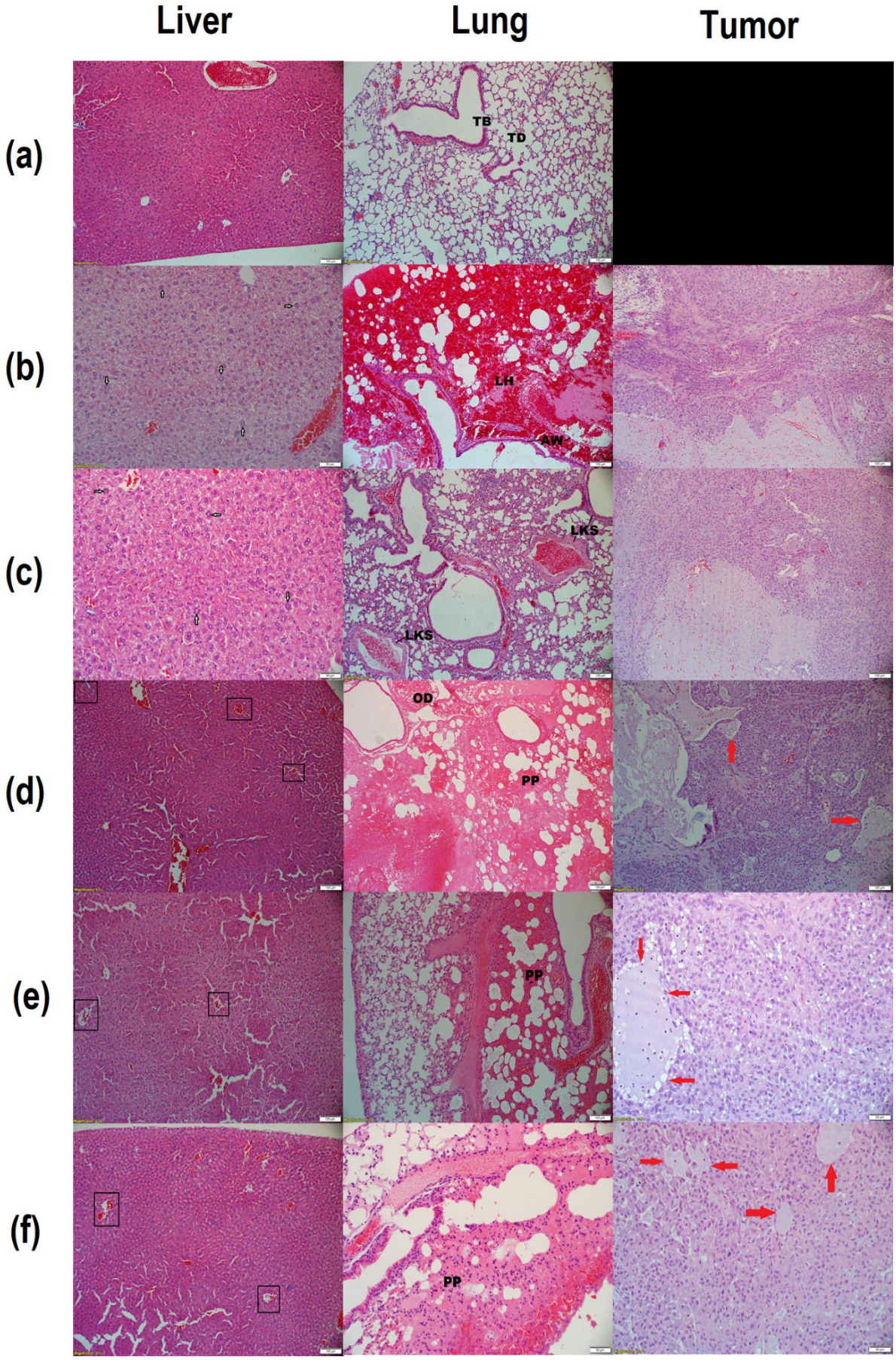
Liver
Lung
Tumor
(a)
(b)
(c)
(d)
(e)
(f)
TB
TD
LH
AW
LKS
LKS
OD
PP
PP
PP

Figure 6.8. Histological analysis of liver, lung and tumor tissues from (**a**) normal healthy mice and tumor-bearing mice treated with (**b**) PBS only, (**c**) Taxol®, (**d**) CLA-coated PTX-SPIONs, (**e**) CLA-coated PTX-SPIONs@CTT, and (**f**) CLA-coated PTX-SPIONs@HRH. The images are generated from 4 – 5 µm tissue sections, stained with H&E and captured at 100 µm, 6.3x magnification. Arrows with white fill show swollen hepatocytes identified on liver tissues, whilst red arrows show areas of degeneration of neoplastic cells, identified on tumors from CLA-coated PTX-SPIONs, CLA-coated PTX-SPIONs@CTT, and CLA-coated PTX-SPIONs@HRH treated mice. (TB: terminal bronchiole; AD: alveolar duct; LH: lobar haemorrhage; LKS: leukostasis; AW: alveolar walls; PP: pulmonary parenchyma; OD: oedema)

6.3.3. Pharmacokinetics profile of PTX in plasma

The concentration of PTX in plasma was determined following a single SC injection of equivalent PTX dosage from CLA-coated PTX-SPIONs@CTT, CLA-coated PTX-SPIONs@HRH, and Taxol® in mice. The pharmacokinetics profile is presented in **Figure 6.9** with corresponding pharmacokinetic parameters in **Table 6.2**. Notably, the plasma concentration of PTX from Taxol® was relatively higher on the onset, at 0.5 h (19.7 µg/mL) compared to that of CLA-coated PTX-SPIONs@CTT (15.2 µg/mL) and CLA-coated PTX-SPIONs@HRH (15.6 µg/mL). Moreover, commercial PTX had a maximum plasma concentration (C_{max}) of 32.5 µg/mL reached at 1 h of administration, meanwhile CLA-coated PTX-SPIONs@CTT and CLA-coated PTX-SPIONs@HRH reached C_{max} of 48.8 µg/mL and 49.2 µg/mL at 4 h, respectively. The half-life ($T_{1/2}$) of commercial PTX was estimated to be 9.0 h, which was substantially lower compared to the $T_{1/2}$ of 16.8 h and 17.1 h for CLA-coated PTX-SPIONs@CTT and CLA-coated PTX-SPIONs@HRH, respectively. The area under the concentration time curve (AUC_{0-24}) was found to be 365.4, 663.6, and 665.9 µg/mL.h for commercial PTX, CLA-coated PTX-SPIONs@CTT, and CLA-coated PTX-SPIONs@HRH, respectively.

Essentially, the pharmacokinetics data indicated that PTX from our formulated nanosystems is slowly absorbed and released into plasma following SC injection, which is consistent with the *in vitro* data which demonstrated a sustained release of PTX over time. A higher C_{max} and prolonged half-life could be attributed to the marked ability of the nanostructures to shield PTX from pre-systemic degradation and non-specific binding, as opposed to the commercial formulation which results in reduced bioavailability of PTX and subsequent rapid elimination. Primarily, PTX is known to present with non-specific protein binding, enzymatic degradation, and rapid clearance, which affect its bioavailability (Ye et al., 2021), and thus the formulated CLA-coated PTX-SPIONs@CTT and CLA-coated PTX-SPIONs@HRH present a promising PTX delivery solution and potential nanomedicine for NSCLC.

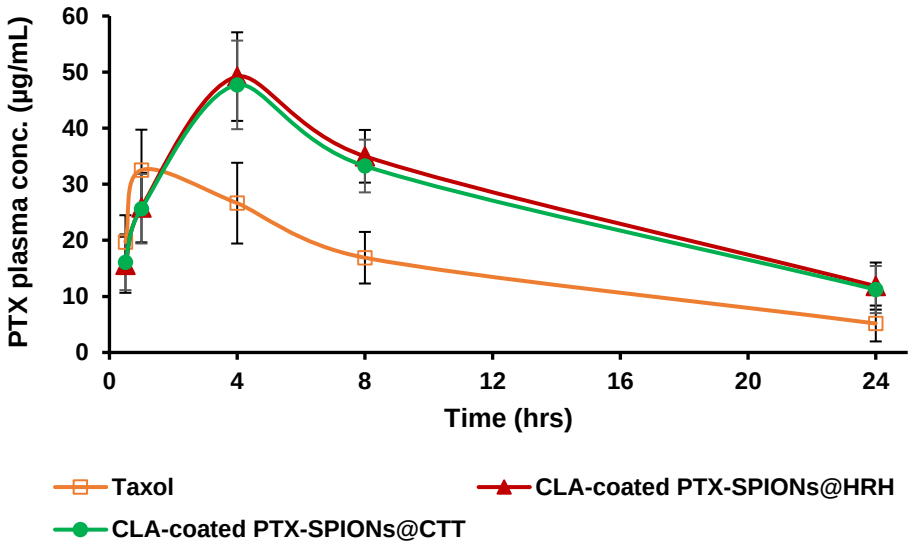

Figure 6.9. Plasma PK profile showing the concentration of PTX quantified at 0.5 h up to 24 h following SC injection of CLA-coated PTX-SPIONs@CTT, CLA-coated PTX-SPIONs@HRH, and Taxol®. Data presented as mean ± SD, *n* = *3*.

Table 6.2. Plasma PK parameters of CLA-coated PTX-SPIONs@HRH and CLA-coated PTX-SPIONs@CTT in comparison to Taxol®

	C_{max} (µg/mL)	T_{max} (h)	$T_{1/2}$ (h)	K_{el} (h^{-1})	AUC_{0-24} (µg/mL.h)
CLA-coated PTX-SPIONs@HRH	49.2 ± 5.2	4.0	17.1	0.03	665.9
CLA-coated PTX-SPIONs@CTT	48.8 ± 4.3	4.0	16.8	0.03	659.6
Taxol®	32.5 ± 3.7	1.0	9.0	0.07	365.4

C_{max}, maximum concentration; T_{max}, time taken to reach maximum concentration; $T_{1/2}$, half-life; K_{el}, elimination rate constant; AUC_{0-24}, area under the concentration-time curve.

6.4. Concluding Remarks

A lung tumor xenograft mouse model was successfully developed and afforded accurate representation of the pathophysiology of NSCLC to enable pre-clinical investigations on the therapeutic efficacy of the formulated PTX delivery nanosystems. Accordingly, the formulated CLA-coated PTX-SPIONs@CTT and CLA-coated PTX-SPIONs@HRH demonstrated active tumor targetability and antiangiogenic activity, as supported by a remarkable tumor growth regression. The marked ability of the nanosystems to halt neoplastic cell formation and tumor

mitoses validates its therapeutic efficacy as a potent targeted nanomedicine in NSCLC therapy. Moreover, the improved half-life and prolonged plasma circulation time recorded for PTX when delivered via the nanosystems substantiate the potential application of CLA-coated PTX-SPIONs@CTT and CLA-coated PTX-SPIONs@HRH as an alternative modality for the effective delivery of PTX in NSCLC.

6.5. References

Adeyemi, S.A., Choonara, Y.E., 2022. In vitro and in vivo evaluation of a cyclic LyP-1-modified nanosystem for targeted endostatin delivery in a KYSE-30 cell xenograft Athymic nude mice model. Pharmaceuticals 15, 353.

Bordat, A., Boissenot, T., Ibrahim, N., Ferrere, M., Levêque, M., Potiron, L., Denis, S., Garcia-Argote, S., Carvalho, O., Abadie, J., Cailleau, C., Pieters, G., Tsapis, N., Nicolas, J., 2022. A polymer prodrug strategy to switch from intravenous to subcutaneous cancer therapy for irritant/vesicant drugs. J. Am. Chem. Soc. 144, 18844-18860.

Gala, U.H., Miller, D.A., Williams, R.O., 2020. Harnessing the therapeutic potential of anticancer drugs through amorphous solid dispersions. Biochim. Biophys. Acta 1873, 188319.

Greten, F.R., Grivennikov, S.I., 2019. Inflammation and cancer: Triggers, mechanisms, and consequences. Immunity 51, 27-41.

Gui, G., Fan, Z., Ning, Y., Yuan, C., Zhang, B., Xu, Q., 2021. Optimization, characterization and in vivo evaluation of paclitaxel-loaded folate-conjugated superparamagnetic iron oxide nanoparticles. Int. J. Nanomed. 16, 2283-2295.

Lee, S., Kim, W.J., Jeon, Y., Lim, C.H., Sun, K., 2018. Specification of subject sex in oncology-related animal studies. Acute Crit. Care 33, 178-184.

Pantaleão, S.Q., Fernandes, P.O., Gonçalves, J.E., Maltarollo, V.G., Honorio, K.M., 2022. Recent advances in the prediction of pharmacokinetics properties in drug design studies: A review. ChemMedChem 17, e202100542.

Reichel, A., Lienau, P., 2016. Pharmacokinetics in drug discovery: An exposure-centred approach to optimising and predicting drug efficacy and safety, in: Nielsch, U., Fuhrmann, U., Jaroch, S. (Eds.), New approaches to drug discovery. Springer International Publishing, Cham, pp. 235-260.

Rezazadeh, M., Emami, J., Mostafavi, A., Rostami, M., Hassanzadeh, F., Sadeghi, H., Minaiyan, M., Lavasanifar, A., 2015. A rapid and sensitive HPLC method for quantitation of paclitaxel in biological samples using liquid-liquid extraction and UV detection: Application to pharmacokinetics and tissues distribution study of paclitaxel loaded targeted polymeric micelles. J. Pharm. Pharm. Sci. 18, 647-660.

Saman, H., Raza, S.S., Uddin, S., Rasul, K., 2020. Inducing angiogenesis, a key step in cancer vascularization, and treatment approaches. Cancers (Basel) 12, 1172.

Sápi, J., Kovács, L., Drexler, D.A., Kocsis, P., Gajári, D., Sápi, Z., 2015. Tumor volume estimation and quasi-continuous administration for most effective bevacizumab therapy. PLoS One 10, e0142190.

Sharma, S., Ghufran, S.M., Ghose, S., Biswas, S., 2021. Cytoplasmic vacuolation with endoplasmic reticulum stress directs sorafenib induced non-apoptotic cell death in hepatic stellate cells. Sci. Rep. 11, 3089.

Sun, D., Zhou, S., Gao, W., 2020. What went wrong with anticancer nanomedicine design and how to make it right. ACS Nano 14, 12281-12290.

Tamura, T., Kurishima, K., Nakazawa, K., Kagohashi, K., Ishikawa, H., Satoh, H., Hizawa, N., 2015. Specific organ metastases and survival in metastatic non-small-cell lung cancer. Mol. Clin. Oncol. 3, 217-221.

Tsukihara, H., Nakagawa, F., Sakamoto, K., Ishida, K., Tanaka, N., Okabe, H., Uchida, J., Matsuo, K., Takechi, T., 2015. Efficacy of combination chemotherapy using a novel oral chemotherapeutic agent, TAS-102, together with bevacizumab, cetuximab, or panitumumab on human colorectal cancer xenografts. Oncol. Rep. 33, 2135-2142.

Xie, W., Kordt, M., Palme, R., Grambow, E., Vollmar, B., Zechner, D., 2021. Diagnostic ability of methods depicting distress of tumor-bearing mice. Animals 11, 2155.

Ye, Z., Huang, Y., Ke, J., Zhu, X., Leng, S., Luo, H., 2021. Breakthrough in targeted therapy for non-small cell lung cancer. Biomed. Pharmacother. 133, 111079.

Zhang, Y., He, B., Liu, K., Ning, L., Luo, D., Xu, K., Zhu, W., Wu, Z., Huang, J., Xu, X., 2017. A novel peptide specifically binding to VEGF receptor suppresses angiogenesis in vitro and in vivo. Signal Transduct. Target. Ther. 2, 17010-17010.

Zhao, H., Wu, L., Yan, G., Chen, Y., Zhou, M., Wu, Y., Li, Y., 2021. Inflammation and tumor progression: Signaling pathways and targeted intervention. Signal Transduct. Target. Ther. 6, 263.

Zombeck, J.A., Fey, E.G., Lyng, G.D., Sonis, S.T., 2013. A clinically translatable mouse model for chemotherapy-related fatigue. Comp. Med. 63, 491-497.

Zou, Y., Wei, J., Xia, Y., Meng, F., Yuan, J., Zhong, Z., 2018. Targeted chemotherapy for subcutaneous and orthotopic non-small cell lung tumors with cyclic RGD-functionalized and disulfide-crosslinked polymersomal doxorubicin. Signal Transduct. Target. Ther. 3, 32.

CHAPTER 7

CONCLUSIONS AND RECOMMENDATIONS

7.1. Conclusions

Lung cancer remains a global scourge, with NSCLC continuing to affect millions of people worldwide and threatening the life expectancy. Sadly, the current conventional treatment options available for NSCLC have reached the therapeutic plateau. Particularly, combination chemotherapy, as the main therapeutic intervention for NSCLC management, is riddled with non-specificity, resulting in poor tumor reach, cytotoxicity to healthy cells, and often adverse side effects, which make the therapeutic regimen intolerable to most patients. Thus, the major focus in NSCLC therapy research has been towards the development of potent chemotherapeutics that can locate tumors and elicit therapeutic action directly at tumor sites, by targeting key molecular tumor markers. The expanding discipline of targeted nanomedicine, in which nanotechnology is employed to develop nano-based drug delivery systems that are capable of delivering therapeutics in a controlled manner to targeted sites, presents great prospects towards effective management of NSCLC.

The present study has explored targeted nanomedicine as a viable and potent therapeutic intervention in the management of NSCLC, where two tumor-targeted PTX delivery nanosystems have been successfully formulated and evaluated both *in vitro* and *in vivo*. A timely thorough review on the prospects of magnetic nanoparticles and CLA, was initially conducted to provide insights on the design and the suitability thereof, for application in NSCLC management. Using a safe-by-design approach, novel 10E, 12Z CLA-coated PTX-loaded SPIONs were formulated and characterized for pertinent physicochemical and pharmaceutical characteristics, via sophisticated cutting-edge technologies. CLA-coated PTX-SPIONs exhibited aqueous stability and a desirable size of 96.5 ± 0.6 nm, ideal for tumor penetration, with high loading capacity and a sustained site-specific release of PTX which culminated in an enhanced *in vitro* anti-proliferative activity on A549 lung cancer cells. Accordingly, it was concluded that 10E, 12Z CLA favoured maximal partitioning of hydrophobic PTX and synergistically conferred additional anticancer benefits.

An efficient methodology for surface functionalization of CLA-coated PTX-SPIONs with antiangiogenic peptides was successfully established in the study. EDC/NHS chemistry proved to be an ideal strategy to conjugate HRH and CTT peptides onto CLA-coated PTX-SPIONs to formulate anti-VEGF and anti-MMP-2 targeted nanosystems, respectively. Detailed physicochemical characterization confirmed the conjugation of the peptides as well as the morphological attributes of the nanosystems, meanwhile, *in vitro* cellular analyses showed that CLA-coated PTX-SPIONs@HRH and CLA-coated PTX-SPIONs@CTT possess

enhanced anti-proliferative activity and a marked cellular uptake and internalization by lung cancer cells. Moreover, CLA-coated PTX-SPIONs@HRH and CLA-coated-PTX-SPIONs@CTT demonstrated a remarkable ability to bind and arrest VEGFRs and MMP-2, respectively, which resulted in reduced secretion levels of VEGF-A and MMP-2 enzyme by endothelial cells *in vitro*. This was a significant revelation, and since VEGF-A and MMP-2 promote angiogenesis, a decline in secretion levels of these angiogenic biomarkers is compellingly synonymous with the inhibition of angiogenesis.

A practical S.C lung tumor Xenograft mouse model was successfully developed and employed to evaluate the antitumor activity of the formulated nanonosystems. The *in vivo* assessments revealed that a 4-cycle treatment with either CLA-coated PTX-SPIONs@HRH or CLA-coated PTX-SPIONs@CTT significantly regressed tumor growth, with %TGI of 76.6 and 69.7, respectively. Most importantly, a marked degeneration of neoplastic cells in tumors of mice treated with the nanosystems ascertained that CLA-coated PTX-SPIONs@HRH and CLA-coated PTX-SPIONs@CTT inhibit angiogenesis, meanwhile, the significant reduction in mitoses counts confirmed that the nanosystems successfully delivered PTX into tumors to elicit its anticancer activity. Moreover, from the pharmacokinetics evaluation, it was found that both CLA-coated PTX-SPIONs@HRH and CLA-coated PTX-SPIONs@CTT prolonged the half-life of PTX in plasma.

In essence, it can be concluded that two novel and robust tumor-targeted PTX delivery nanosystems have been fabricated from this study, for potential application as targeted nanomedicine in the management of NSCLC. The nanosystems present with the key desirable features (i.e., ideal size for tumor penetration, maximal drug loading capacity, site-specific release, biocompatibility, and antiangiogenic and antitumor activity) for application specifically in NSCLC targeted therapy. Fundamentally, a novel design involving 10E, 12Z CLA as a partitioning and surface directing agent is appreciated in the successful development of the nanosystems. Similarly, the flexibility of SPIONs to easily adapt to surface modifications with varying moieties is applauded, and further motivates the rationale for choosing SPIONs as an ideal nanomaterial to execute this study.

7.2. Recommendations

Although the therapeutic efficacy of CLA-coated PTX-SPIONs@HRH and CLA-coated SPIONs@CTT has been established *in vitro* and *in vivo*, more pre-clinical studies are recommended to validate the applicability of the nanosystems as alternative therapeutic interventions in NSCLC management. Additional biochemical assays including TUNEL and zymogen assays are well recommended to assess the apoptotic activity of the nanosystems and the matrix degradation as a marker of MMP-2 activity in cells treated with CLA-coated PTX-SPIONs@CTT, respectively. A zebrafish model can also be employed to study blood vessel development from the embryo, as a marker of angiogenesis, and assess any aberrations resulting from treatment with the formulated antiangiogenic nanosystems. Extreme care and caution would need to be exercised during the establishment of model embryos, as this is a delicate process and mostly performed by researchers with experience, for best desired outcomes. Moreover, an in-depth look into the theragnostic application of the formulated nanosystems is advised, where the superparamagnetism of SPIONs can be further exploited for biomedical imaging in the visualization of tumors in NSCLC subjects. The inherent magnetism and biocompatible properties of SPIONs make the nanoparticles excellent image contrast agents, and therefore can be employed in both diagnostic (MRI scan) and therapeutic interventions in NSCLC and other cancers.

CHAPTER 8

FULBRIGHT FOREIGN STUDENT PROGRAM EXPERIENCE

8.1. Overview of the Program

The South African (S.A) Fulbright Foreign Student Program is an initiative of the government of the United States of America (USA) which provides grants for S.A university graduates to pursue post-graduate studies or research activities at a U.S institution in any field of choice. Students are selected through a rigorous application and interview process, and receive high level of support from the U.S Embassy and Consulates in S.A, including visa processing, and health insurance. Accordingly, I was selected to partake in the program's 2022 – 2023 intake as a Visiting Student Researcher (VSR) at a host institution in the US, under a research advisor with research expertise in oncology, particularly in the development of smart cancer therapeutics. My U.S host institution was Johns Hopkins University, School of Medicine, and I was hosted by Professor Wilfred Ngwa, in the Department of Radiation Oncology and Molecular Radiation Sciences.

8.2. Research Focus of the Visited Research Group

Professor Ngwa's research group studies the smart radiotherapy biomaterials (SRBs) for application in radiotherapy and immunotherapy, or in combination (immuno-radiotherapy). The lab is at the forefront of the innovative research to extend the use of immuno-radiotherapy to curative platforms of both local and metastatic cancers. A key focus of the research is the use of biomaterial-derived vectors for smart sustained delivery of immunoadjuvants or drug payloads that can engender robust *in-situ* vaccination in combination with radiotherapy to cause regression of both local and metastatic tumors with minimal toxicity. The lab also focuses on collaborative global health work, aimed at catalysing high impact international collaborations to eliminate global health disparities, with main focus on cancer and related diseases. As such, I had the opportunity to partake in various projects and acquired the necessary skills in cancer research, related to my current work in anticancer drug discovery.

8.3. Abstracts from the Work Undertaken During the Fulbright Program Period

The following are the abstracts from some of the studies I was involved in during the Fulbright Foreign Exchange Program period, as a VSR. The abstracts have been submitted for conference presentations, including the 65th American Association of Physicists in Medicine (AAPM) Annual Meeting and the 65th American Society for Radiation Oncology (ASTRO) Annual Meeting, 2023.

Pre-clinical Investigations on the Toxicity of a Smart Radiotherapy Biomaterial-Derived Immunogenic Vector for Cancer Therapy and Imaging

Michele Moreau[1], **Lindokuhle M. Ngema[1, 2],** Shahinur Acter[1], Lensa S. Keno[3], Yahya E. Choonara[2], Wilfred Ngwa[1*]

[1] Johns Hopkins University, Sydney Kimmel Cancer Centre, Baltimore, MD 21218, USA
[2] Wits Advanced Drug Delivery Platform Research Unit, Department of Pharmacy and Pharmacology, School of Therapeutic Sciences, University of the Witwatersrand, Johannesburg, 7 York Road, Parktown, 2193, South Africa
[3] The University of Scranton, 800 Linden Street, Scranton, PA 18510, USA

Submission: AAPM (Early-Career Investigator Symposium)

Purpose: The application of immunogenic smart radiotherapy biomaterials (iSRBs) in radiotherapy presents an effective approach for providing image guidance and sustained drug release during treatment. This study set to evaluate the pharmacodynamics (PD) of the formulated novel multifunctional iSRB system.

Methods: iSRB seeds prepared from silicone tubing with a poly (lactic-co-glycolic) acid (PLGA) matrix fixated with titanium oxide nanoparticles (for image-contrast and radiosensitization) were loaded with an immunotherapeutic payload (anti-CD40 monoclonal antibody) to formulate iSRB_Anti-CD40. Healthy male and female mice were grouped into 3 cohorts ($n = 3$) and received single subcutaneous injection of iSRB_Anti-CD40 or empty iSRB, while control mice were left untreated. Blood sampling was done on day 1, 4, 7, 21, and 30 post treatment, for evaluation of renal and hepatic function. Accordingly, blood urea nitrogen (BUN), creatinine, and gamma-glutamyl transferase (GGT) levels were quantified. The data was processed on GraphPad Prism 9 and presented as plots (mean ± standard deviation).

Results: The BUN levels at day 1 were comparable amongst all groups, and within the normal range (9.42 – 31.53 mg/dL). Similarly, on the final day of the study (day 30), the BUN levels from the treated mice were within the normal range, and comparable to the levels from the untreated control mice. No significant deviation in creatinine levels was observed between the treatment groups and the healthy control. Creatinine levels remained within the normal range (0.12 – 0.43 mg/dL) throughout the study. Treatment with iSRB_Anti-CD40 maintained GGT levels within the normal range (3.79 – 11.62 mg/dL) in male mice, despite the elevated levels recorded from the control mice.

Conclusion: A developed iSRB_Anti-CD40 system exhibit non-toxicity to the liver and kidneys in pre-clinical testing, and the results support potential application of the system in radiotherapy for effective cancer treatment.

Patient Reported Outcomes Following Palliative Whole Brain Radiation Therapy in Patients with Brain Metastasis

Bolanle Adegboyega[1]; Adedayo Joseph[1]; Adewumi Alabi[1]; John Omomila[1]; **Lindokuhle M. Ngema[2]**; Victoria Ainsworth[2]; Jennifer Chin[2]; Wilfred Ngwa[2*]

[1]NSIA-LUTH Cancer Centre, Lagos University Teaching Hospital, Lagos, Nigeria

[2]Johns Hopkins University, Sydney Kimmel Cancer Centre, Baltimore, MD 21218, USA

Submission: ASTRO

Purpose/Objectives

Brain metastases (BM) are a common occurrence in patients with advanced cancers, and extremely challenging to treat, resulting in short survival periods. Consequently, whole brain radiation therapy (WBRT) remains the standard palliative intervention for patients with BM. The present study set to evaluate the efficacy of WBRT by assessing the quality of life (QoL) and survival outcomes in WBRT-treated patients with BM.

Materials/Methods

This was a prospective, longitudinal, hospital-based single-centre study. Consecutive sampling methodology was used to recruit 52 patients with BM undergoing WBRT. Patients were followed up on days 7, 30, 90 and 180 after WBRT. The EORTC QLQ-C15-PAL was employed to report patient responses in a likert scale. A descriptive analysis and multi-trait scaling correlation was computed using IBM SPSS Statistics 29.0, 95% confidence interval. The overall survival analysis (Kaplan-Meier) was also performed.

Results

The study cohort was predominantly females (82.7%), and accordingly, 65.4% of the respondents had a breast primary tumor. A Shapiro-Wilk test of normality revealed that the data was not normally distributed (*sig.* < 0.05), however, statistic values (*W*) closer to 1 suggested a good fit. A goodness-of-fit test ascertained the assumption, yielding non-significant Chi square Pearson ($p = 0.325$) and Deviance ($p = 1.000$) residuals. There was a significant correlation ($p < 0.001$) between physical functioning and emotional functioning. Median overall survival was 180 days (~6 months). A total of 20 patients (38%) that survived up to 180 days reported alleviated symptoms and better functioning. A significant improvement in physical functioning ($p < 0.001$) and emotional functioning ($p = 0.031$) was reported at 180 days post WBRT, compared to baseline. Similarly, a significant improvement in visual disorders ($p = 0.002$), motor dysfunction ($p = 0.031$), and communication deficit ($p = 0.001$) was also reported.

Conclusions

WBRT is an effective palliative intervention in patients with BM, resulting in improved QoL and prolonged survival. More than 50% of patients that survived 3 months reported a significant alleviation of pain, and 38% of patients that survived for 6 months reported a significantly improved functioning. This demonstrated the effectiveness of WBRT in palliative care and will add to the body of data on the efficacy of radiotherapy.

Investigation of Factors Contributing to Patient Reported Quality of Life Outcomes following whole brain radiation therapy

Victoria Ainsworth[1]; **Lindokuhle M. Ngema[1, 2]**; Jennifer Chin[1]; Alabi Adewumi[3]; John Omomila[3]; Bolanle Adegboyega[3]; Wilfred Ngwa[1*]

[1]Johns Hopkins University, Sydney Kimmel Cancer Centre, Baltimore, MD 21218, USA
[2]Wits Advanced Drug Delivery Platform Research Unit, Department of Pharmacy and Pharmacology, School of Therapeutic Sciences, University of the Witwatersrand, Johannesburg, 7 York Road, Parktown, 2193, South Africa
[3]NSIA-LUTH Cancer Centre, Lagos University Teaching Hospital, Lagos, Nigeria

Submission: AAPM (Early Career Investigator Symposium)

Purpose: Analysis of Quality of life (QoL) outcomes and efficacy of whole brain radiation therapy (WBRT) for brain metastasis at one Nigerian cancer center was carried out. Factors contributing to QoL outcomes and function/symptom status were investigated including demographic and pertinent medical history.

Methods: Patient reported outcomes along with demographic data was collected using survey questions from the EORTC standardized questionnaires. Responses were gathered at day 0, 7, 30, 90 and 180 post-treatment to inform on currently unmet needs and efficacy of interventional radiotherapy in Nigeria with a focus on contributing factors that may correspond with improving or declining patient status. Data was then divided into cohorts based on the contributing factor of interest. Averages and standard deviations were computed, and statistical analysis was performed using a student's t-test.

Results: Significant improvement in function and/or symptom severity was recorded between baseline and days 90 and/or 80 for at least one cohort in each category. Most cohorts, like government workers or patients with comorbidities, showed QoL improvement until day 90 after which QoL plateaued or worsened. This trend gives important insight to how much different factors can influence outcomes.

Conclusion: WBRT is an effective approach to improve QoL, and function/symptom severity. When investigated individually, we can see a fuller picture of how different demographic factors like sex and education status or medical history like presence of comorbidities or previous RT treatment can influence treatment outcomes and QoL. Further, it is shown that after 90 days, many patients experience decline in all three categories, indicating that further investigation into palliative symptom relief is warranted.

8.4. Concluding Remarks

My involvement in the listed studies above, was a huge learning experience which equipped me with the interdisciplinary research skills. Particularly, I acquired first-hand experience in the discovery process (i.e., screening, development, and pre-clinical testing) of the smart radiotherapy biomaterials with theranostic application in cancer therapy. Moreover, a high level skill in data handling was attained during the processing and analysis of the clinical data from the WBRT study. This collaborative work also granted me an opportunity to broaden my knowledge in an unfamiliar field of public health, with insights on the current state of research, especially in Sub-Saharan Africa, and the gaps that could be filled through interdisciplinary collaborations. In addition to academic experiences, the Fulbright Program enriched my interpersonal skills as an individual, and an aspiring researcher, to be able to interact and work with people from different backgrounds. In overall, the Fulbright experience could be summed as a life-changing, once in a lifetime opportunity I will forever be grateful for.

Appendix A: Supplementary Material

Table S1: Mean absorbance values *(n=3)* used to compute drug release presented in *Chapter 3, Figure 3.7*

Time (h)	pH 6.8	pH 7.4
1	0.278	0.103
2	0.280	0.106
4	0.282	0.113
8	0.556	0.121
12	0.736	0.134
24	0.716	0.129

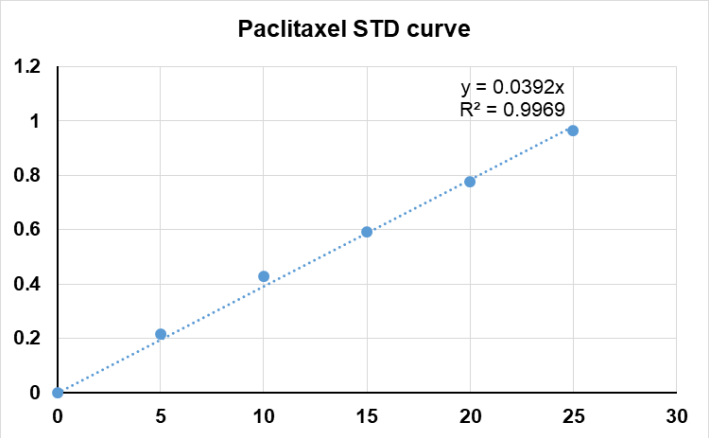

Figure S1: Paclitaxel standard curve used to compute drug adsorption efficiency (%AE) and loading capacity (%DLC).

Table S2: MTT absorbance values used to compute % cell viability (72 h) presented in *Chapter 3*, *Figure 3.8*

Conc. (µg/mL)	SPIONs			CLA			CLA-coated PTX-SPIONs			PTX		
100	1.749	1.706	1.651	1.526	1.538	1.568	0.409	0.430	0.423	0.652	0.607	0.616
50	1.687	1.774	1.673	1.628	1.627	1.635	0.493	0.483	0.489	0.661	0.620	0.621
25	1.749	1.774	1.720	1.735	1.752	1.709	0.509	0.491	0.511	0.692	0.642	0.636
12.5	1.753	1.735	1.755	1.803	1.812	1.807	0.522	0.527	0.520	0.79	0.719	0.694
6.25	1.861	1.754	1.653	1.841	1.774	1.793	0.561	0.559	0.575	0.945	0.894	0.962
3.125	1.747	1.806	1.756	1.855	1.896	1.875	0.609	0.959	0.616	1.193	1.147	1.269
BLANK	0.213	0.208	0.216	*CONT; control, UNT; untreated*								
CONT.	1.824	1.861	1.845									
UNT.	1.979	1.999	2.156									

Table S3: Mean absorbance values *(n=3)* used to compute drug release presented in *Chapter 4, Figure 4.4*

Time (h)	pH 6.8	pH 7.4
1	0.242	0.136
2	0.251	0.134
4	0.263	0.137
8	0.286	0.134
12	0.722	0.125
16	0.737	0.145
24	0.538	0.186

Table S4: MTT absorbance values used to compute % cell viability after (72 h) presented in *Chapter 4*, *Figure 4.5*

Conc. (μg/mL)	CLA-coated PTX-SPIONs			CLA-coated PTX-SPIONs@HRH		
100	0.422	0.435	0.447	0.250	0.276	0.263
50	0.492	0.477	0.486	0.324	0.335	0.320
25	0.512	0.507	0.496	0.466	0.455	0.512
BLANK	0.232	0.213	0.221			
CONTROL	1.925	1.881	1.953			
UNTREATED	1.985	1.979	1.989			

Table S5: Absorbance values *(n=3)* used to compute VEGF-A secretion levels presented in *Chapter 4, Figure 4.7*

Treatment	Absorbance @ 450nm		
CLA-coated PTX-SPIONs@HRH	0.046	0.119	0.121
CLA-coated PTX-SPIONs	0.151	0.157	0.162
Untreated	0.128	0.125	0.136

Table S6: Mean absorbance values *(n=3)* used to compute drug release presented in *Chapter 5, Figure 5.4*

Time (h)	pH 6.8	pH 7.4
1	0.236	0.129
2	0.254	0.140
4	0.259	0.139
8	0.291	0.131
12	0.751	0.129
16	0.746	0.152
24	0.539	0.173

Table S7: MTT absorbance values used to compute % cell viability after (72 h) presented in *Chapter 5*, *Figure 4.5*

Conc. (µg/mL)	CLA-coated PTX-SPIONs@CTT		
100	0.242	0.253	0.244
50	0.362	0.372	0.364
25	0.425	0.417	0.496
BLANK	0.232	0.213	0.221
CONTROL	1.925	1.881	1.953
UNTREATED	1.985	1.979	1.989

Table S8: Absorbance values *(n=3)* used to compute MMP-2 secretion levels presented in *Chapter 5, Figure 5.7*

Treatment	Absorbance @ 450nm		
CLA-coated PTX-SPIONs@CTT	0.117	0.124	0.121
CLA-coated PTX-SPIONs	0.232	0.248	0.234
Untreated	0.283	0.298	0.275

Appendix B: Animal Ethics Clearance Certificate

ANIMALS RESEARCH ETHICS COMMITTEE (AREC)

UNIVERSITY OF THE WITWATERSRAND, JOHANNESBURG

STRICTLY CONFIDENTIAL

CLEARANCE CERTIFICATE NUMBER: 2020/11/01/B

APPLICANT: Mr L Ngema
School: School of Therapeutic Sciences; Department: N/A; Location: WRAF

PROJECT TITLE: Novel Drug-Loaded Conjugated Linoleic Acid (CLA) Targeted Theragnostic Nanosystem for Non-Small-Cell Lung Carcinoma Treatment in the MF1-nu/nu Nude Mice Model.
Category: B; Species and Numbers involved: *45X 4 - 6 weeks old mice (15 for pilot study and 30 for main study), female MF1-nu/nu nude mice*

Approval is hereby given for the use of animals for the research project named above and described in the application reviewed by a quorate meeting of the AREC held on 1 Dec 2020. This approval remains valid until 31 Jan 2023 and is conditional to the following (if blank there are no special conditions):

Condition 1	Condition 2	Condition 3	Condition 4
A report following the pilot study	Liaise with WRAF for the peritoneal fluid sampling to discuss the options and if required use an abdominal incision		

All material changes to the approved research must be reported to the AREC before they are implemented. Failure to do so will invalidate this clearance certificate.

An annual progress report must be provided to the AREC.

The use of these animals is subject to AREC guidelines on the use and care of laboratory animals, is limited to the procedures described in the application and is subject to additional conditions listed below:

I, the Chair of the AREC (or my designated representative) am satisfied that the proposed research is ethical as judged by local law, international standards and University policy.

Signed: _____ _____ Date: __01/02/2021___

(Chairperson of the AREC)

CC: Student supervisor: «Title1» «Initials1» «Supervisor_surname»
Director Central Animals Service: Dr Kim Jardine

Appendix C: Publications

C1: A review on Engineered Magnetic Nanoparticles in Non-Small-Cell Lung Carcinoma Targeted Therapy. Lindokuhle M. Ngema, Samson A. Adeyemi, Thashree Marimuthu and Yahya E. Choonara. *International Journal of Pharmaceutics*, 606, 120870, 2021.

International Journal of Pharmaceutics 606 (2021) 120870

Contents lists available at ScienceDirect

International Journal of Pharmaceutics

journal homepage: www.elsevier.com/locate/ijpharm

Review

A review on engineered magnetic nanoparticles in Non-Small-Cell lung carcinoma targeted therapy

Lindokuhle M. Ngema, Samson A. Adeyemi, Thashree Marimuthu, Yahya E. Choonara *

Wits Advanced Drug Delivery Platform Research Unit, Department of Pharmacy and Pharmacology, School of Therapeutic Sciences, Faculty of Health Sciences, University of the Witwatersrand, Johannesburg, 7 York Road, Parktown 2193, South Africa

ARTICLE INFO

Keywords:
Non-small-cell lung carcinoma
Chemotherapy
Conjugated linoleic acid
Nanotechnology
Angiogenesis

ABSTRACT

There are growing appeals for the design of efficacious treatment options for non-small-cell lung carcinoma (NSCLC) as it accrues to ~ 85% cases of lung cancer. Although platinum-based doublet chemotherapy has been the main therapeutic intervention in NSCLC management, this leads to myriad of problems including intolerability to the doublet regimens and detrimental side effects due to high doses. A new approach is therefore needed and warrants the design of targeted drug delivery systems that can halt tumor proliferation and metastasis by targeting key molecules, while exhibiting minimal side effects and toxicity. This review aims to explore the rational design of magnetic nanoparticles for the development of tumor-targeting systems for NSCLC. In the review, we explore the anticancer merits of conjugated linoleic acid (CLA) and provide a concise incursion into its application for the invention of functionalized magnetic nanoparticles in the targeted treatment of NSCLC. Recent nanoparticle-based targeted chemotherapies for targeting angiogenesis biomarkers in NSCLC will also be reviewed to further highlight versatility of magnetic nanoparticles. These developments through molecular tuning at the nanoscale and supported by comprehensive pre-clinical studies could lead to the establishment of precise nanosystems for tumor-homing cancer therapy.

C2: Synthesis of Novel Conjugated Linoleic Acid (CLA)-Coated Superparamagnetic Iron Oxide Nanoparticles (SPIONs) for the Delivery of Paclitaxel with Enhanced *In Vitro* Anti-Proliferative Activity on A549 Lung Cancer Cells. Lindokuhle M. Ngema, Samson A. Adeyemi, Thashree Marimuthu, Philemon Ubanako, Daniel Wamwangi and Yahya E. Choonara. *Pharmaceutics*, 14, 8219, 2022.

pharmaceutics

MDPI

Article

Synthesis of Novel Conjugated Linoleic Acid (CLA)-Coated Superparamagnetic Iron Oxide Nanoparticles (SPIONs) for the Delivery of Paclitaxel with Enhanced In Vitro Anti-Proliferative Activity on A549 Lung Cancer Cells

Lindokuhle M. Ngema [1], Samson A. Adeyemi [1], Thashree Marimuthu [1], Philemon Ubanako [1], Daniel Wamwangi [2] and Yahya E. Choonara [1,*]

[1] Wits Advanced Drug Delivery Platform Research Unit, Department of Pharmacy and Pharmacology, School of Therapeutic Sciences, Faculty of Health Sciences, University of the Witwatersrand, 7 York Road, Parktown, Johannesburg 2193, South Africa; lindokuhle.ngema@students.wits.ac.za (L.M.N.); samson.adeyemi@wits.ac.za (S.A.A.); thashree.marimuthu@wits.ac.za (T.M.); philemon.ubanako@wits.ac.za (P.U.)

[2] School of Physics, Materials Physics Research Institute, University of the Witwatersrand, Private Bag 3, WITS, Johannesburg 2050, South Africa; daniel.wamwangi@wits.ac.za

* Correspondence: yahya.choonara@wits.ac.za; Tel.: +27-11-717-2052

check for updates

Citation: Ngema, L.M.; Adeyemi, S.A.; Marimuthu, T.; Ubanako, P.; Wamwangi, D.; Choonara, Y.E. Synthesis of Novel Conjugated Linoleic Acid (CLA)-Coated Superparamagnetic Iron Oxide Nanoparticles (SPIONs) for the Delivery of Paclitaxel with Enhanced In Vitro Anti-Proliferative Activity on A549 Lung Cancer Cells. *Pharmaceutics* **2022**, *14*, 829. https://doi.org/10.3390/pharmaceutics14040829

Academic Editor: Carlos Alonso-Moreno

Received: 15 March 2022

Abstract: The application of Superparamagnetic Iron Oxide Nanoparticles (SPIONs) as a nanomedicine for Non-Small Cell Lung Carcinoma (NSCLC) can provide effective delivery of anticancer drugs with minimal side-effects. SPIONs have the flexibility to be modified to achieve enhanced oading of hydrophobic anticancer drugs such as paclitaxel (PTX). The purpose of this study was to synthesize novel *trans*-10, *cis*-12 conjugated linoleic acid (CLA)-coated SPIONs loaded with PTX to enhance the anti-proliferative activity of PTX. CLA-coated PTX-SPIONs with a particle size and zeta potential of 96.5 ± 0.6 nm and −27.3 ± 1.9 mV, respectively, were synthesized. The superparamagnetism of the CLA-coated PTX-SPIONs was confirmed, with saturation magnetization of 60 emu/g and 29 Oe coercivity. CLA-coated PTX-SPIONs had a drug loading efficiency of 98.5% and demonstrated sustained site-specific in vitro release of PTX over 24 h (i.e., 94% at pH 6.8 mimicking the tumor microenvironment). Enhanced anti-proliferative activity was also observed with the CLA-coated PTX-SPIONs against a lung adenocarcinoma (A549) cell line after 72 h, with a recorded cell viability of 17.1%. The CLA-coated PTX-SPIONs demonstrated enhanced suppression of A549 cell proliferation compared to pristine PTX, thus suggesting potential application of the nanomedicine as an effective site-specific delivery system for enhanced therapeutic activity in NSCLC therapy.

Keywords: superparamagnetic iron oxide nanoparticles; non-small-cell lung carcinoma; A549 cell

C3. Surface Immobilization of Anti-VEGF Peptide on SPIONs for Anti-Angiogenic and Targeted Delivery of Paclitaxel in Non-Small-Cell Lung Carcinoma. Lindokuhle M. Ngema, Samson A. Adeyemi, Thashree Marimuthu, Philemon Ubanako, Wilfred Ngwa and Yahya E. Choonara. *ACS Applied Bio Materials*, 6, 2747, 2023.

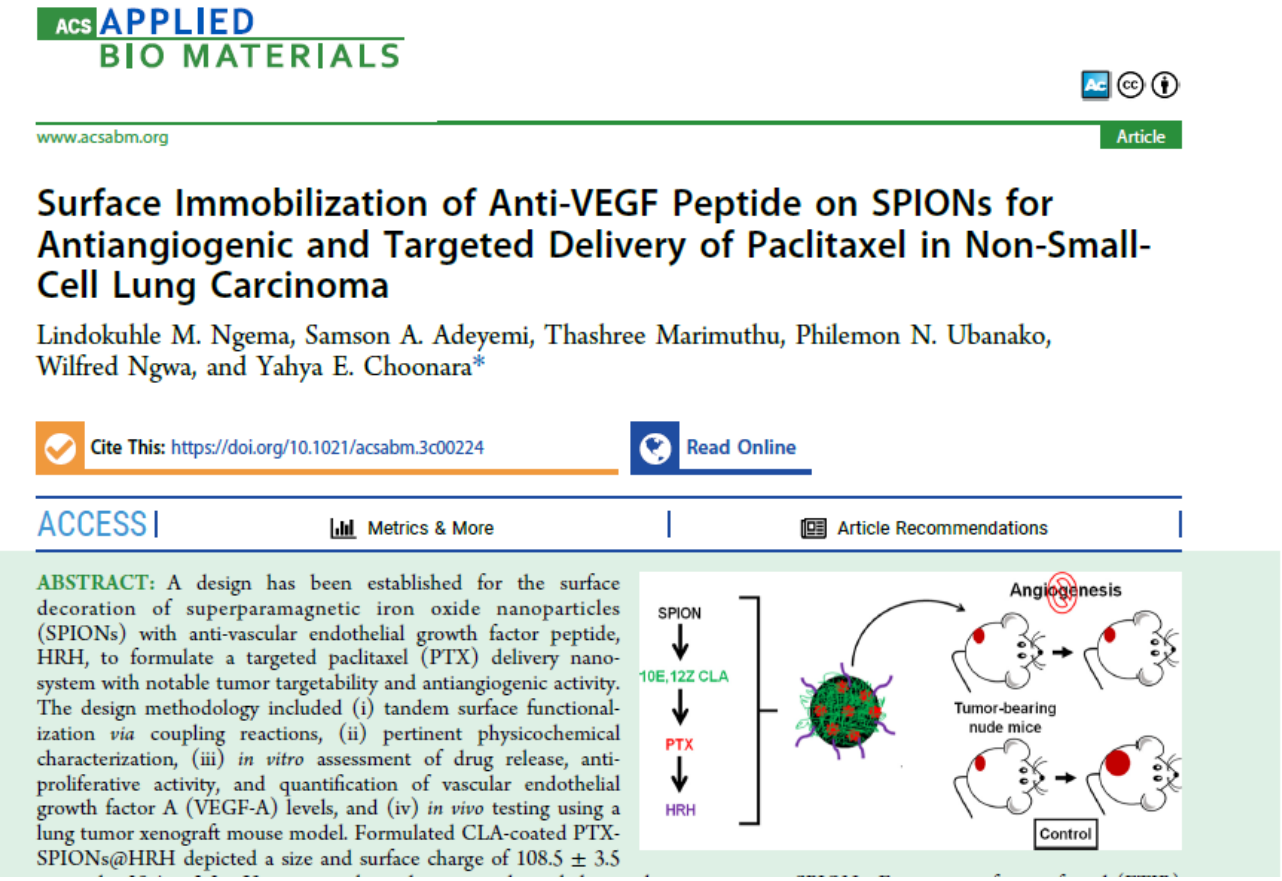

ACS APPLIED BIO MATERIALS

www.acsabm.org Article

Surface Immobilization of Anti-VEGF Peptide on SPIONs for Antiangiogenic and Targeted Delivery of Paclitaxel in Non-Small-Cell Lung Carcinoma

Lindokuhle M. Ngema, Samson A. Adeyemi, Thashree Marimuthu, Philemon N. Ubanako, Wilfred Ngwa, and Yahya E. Choonara*

Cite This: https://doi.org/10.1021/acsabm.3c00224 Read Online

ACCESS | Metrics & More | Article Recommendations

ABSTRACT: A design has been established for the surface decoration of superparamagnetic iron oxide nanoparticles (SPIONs) with anti-vascular endothelial growth factor peptide, HRH, to formulate a targeted paclitaxel (PTX) delivery nano-system with notable tumor targetability and antiangiogenic activity. The design methodology included (i) tandem surface functional-ization *via* coupling reactions, (ii) pertinent physicochemical characterization, (iii) *in vitro* assessment of drug release, anti-proliferative activity, and quantification of vascular endothelial growth factor A (VEGF-A) levels, and (iv) *in vivo* testing using a lung tumor xenograft mouse model. Formulated CLA-coated PTX-SPIONs@HRH depicted a size and surface charge of 108.5 ± 3.5

C4. Short Anti-Angiogenic MMP-2 Peptide Decorated Nanoparticles for Targeted Paclitaxel Delivery in an A549 Cell Xenograft Mouse Tumor Model. Lindokuhle M. Ngema, Samson A. Adeyemi, Thashree Marimuthu, Philemon Ubanako, Wilfred Ngwa and Yahya E. Choonara. *Submitted for review: ACS Applied Nano Materials.*

Appendix D: Research Outputs

D1: Annual Young Scientists Conference 2023 (**Oral Presentation**). University of Venda, Thohoyandou, South Africa, June 12 – 13, 2023.

1B01: Synthesis of novel CLA-coated SPIONs for the delivery of paclitaxel with enhanced *in vitro* anti-proliferative activity on A549 lung cancer cells

Lindokuhle Malibongwe Ngema, Samson Adeyemi, Philemon Ubanako, Thashree Marimuthu and Yahya E. Choonara*

Wits Advanced Drug Delivery Platform Research Unit, Department of Pharmacy and Pharmacology, School of Therapeutic Sciences, Faculty of Health Sciences, University of the Witwatersrand, 7 York Road, Parktown, 2193, Johannesburg, South Africa.
*Yahya.Choonara@wits.ac.za

Introduction: Non-Small Cell Lung Carcinoma (NSCLC) is the most prevalent type of lung cancer, constituting 85% of all diagnosed lung cancer cases. The treatment of NSCLC continues to be a daunting challenge, with combinational chemotherapy as first-line treatment reportedly at its therapeutic plateau. Thus, the application of superparamagnetic iron oxide nanoparticles (SPIONs) as a nanomedicine for NSCLC provides an alternative modality. SPIONs have the flexibility to be modified to achieve enhanced loading of hydrophobic anticancer drugs such as paclitaxel (PTX). The purpose of this study was to synthesize novel *trans*-10, *cis*-12 conjugated linoleic acid (CLA)-coated SPIONs loaded with PTX to enhance the anti-proliferative activity of PTX.

Methods: SPIONs were fabricated using a co-precipitation method and coated with *trans*-10, *cis*-12 CLA in a single-step reaction. PTX was then loaded onto the surface of *trans*-10, *cis*-12 CLA-coated SPIONs via self-assembly, to formulate CLA-coated PTX-SPIONs. CLA-coated PTX-SPIONs were characterized for all pertinent physiochemical and pharmaceutical (including anti-proliferative activity on an A549 lung cancer cell line) properties.

Results: CLA-coated PTX-SPIONs were successfully synthesized with a particle size and zeta potential of 96.5 ± 0.6 nm and −27.3 ± 1.9 mV, respectively. CLA-coated PTX-SPIONs had a drug loading efficiency of 98.5% and demonstrated sustained site-specific *in vitro* release of PTX over 24 h (i.e., 94% at pH 6.8 mimicking the tumor microenvironment). Enhanced anti-proliferative activity was observed with the CLA-coated PTX-SPIONs against a lung adenocarcinoma (A549) cell line after 72 h, with a recorded cell viability of 17.1%.

Conclusions/Impact: The CLA-coated PTX-SPIONs demonstrated enhanced suppression of A549 cell proliferation compared to pristine PTX, thus suggesting potential application of the nanomedicine as an effective site-specific delivery system for enhanced therapeutic activity in NSCLC therapy. The results of this work provide new insights into the design of nanomedicines for NSCLC.

Acknowledgements: This study was funded by the National Research Foundation (NRF) of South Africa, SARChI grant and the University of the Witwatersrand, Johannesburg: Friedel Sellschop grant.

Presenters Bibliography: Lindokuhle Malibongwe Ngema is a doctoral candidate at the University of the Witwatersrand. He carries out research in the field of pharmaceutics where he focuses on the development of targeted cancer nanomedicines.

6

D2: 13th WITS Cross Faculty Postgraduate Symposium (**Oral Presentation**), University of the Witwatersrand, Johannesburg, South Africa, July 11 – 13, 2022.

WITS UNIVERSITY

13th Wits Cross Faculty Postgraduate Symposium: Abstract

Please use this design below:

NAME: (FIRST NAME THEN SURNAME!): Lindokuhle M. Ngema
DEGREE AND YEAR OF STUDY: Doctoral (PhD); Year 03
FACULTY: Health Sciences
SCHOOL: Therapeutic Sciences
STUDENT NUMBER: 845407
STUDENT EMAIL: 845407@students.wits.ac.za
INDICATE YOUR PREFERRED CHOICE: Oral
TITLE of RESEARCH TOPIC: Synthesis of Novel CLA-Coated SPIONs for the Delivery of Paclitaxel with Enhanced *In Vitro* Antiproliferative Activity on A549 Lung Cancer Cells
SUPERVISOR NAME: Prof. Y.E Choonara

Keywords: Superparamagnetic iron oxide nanoparticles, conjugated linoleic acid, paclitaxel, lung cancer

---

The treatment of non-small-cell lung carcinoma (NSCLC) continues to be a daunting challenge, with combinational chemotherapy as first-line treatment reportedly at its therapeutic plateau [1]. The application of superparamagnetic iron oxide nanoparticles (SPIONs) as a nanomedicine for NSCLC provides an alternative modality. The purpose of this study was to synthesize novel *trans*-10, *cis*-12 conjugated linoleic acid (CLA)-coated SPIONs loaded with paclitaxel (PTX) to enhance the anti-proliferative activity of PTX. SPIONs were fabricated via co-precipitation and coated with CLA, to allow self-assembled loading of PTX, forming CLA-coated PTX-SPIONs. CLA-coated PTX-SPIONs had a particle size and zeta potential of 96.5 ± 0.6 nm and −27.3 ± 1.9 mV, respectively. CLA-coated PTX-SPIONs exhibited a drug loading efficiency of 98.5% and demonstrated sustained site-specific *in vitro* release of PTX over 24 h (i.e., 94% at pH 6.8 mimicking the tumor microenvironment). Enhanced anti-proliferative activity was also observed with the CLA-coated PTX-SPIONs against a lung adenocarcinoma (A549) cell line after 72 h, with a recorded cell viability of 17.1%. The CLA-coated PTX-SPIONs demonstrated enhanced suppression of A549 cell proliferation compared to pristine PTX, thus suggesting potential application of the nanomedicine as an effective site-specific delivery system for enhanced therapeutic activity in NSCLC therapy.

REFERENCE

1. Ngema, L.M.; Adeyemi, S.A.; Marimuthu, T.; Choonara, Y.E. A review on engineered magnetic nanoparticles in non-small-cell lung carcinoma targeted therapy. *Int. J. Pharm.* **2021**, *606*, 120870.

D3: 4th International Conference on Nanomedicine and Drug Delivery (**Oral Presentation**). Webinar, June 06 – 07, 2022.

Novel Conjugated Linoleic Acid (CLA)-Coated Superparamagnetic Iron Oxide Nanoparticles (SPIONs) for the Delivery of Paclitaxel with Superlative Anti-Proliferative Activity in Non-Small-Cell Lung Carcinoma

Lindokuhle M. Ngema, MMedSci, Wits Advanced Drug Delivery Platform Research Unit, University of the Witwatersrand, South Africa

*Prof. Yahya. E. Choonara, PhD, Wits Advanced Drug Delivery Platform Research Unit, University of the Witwatersrand, South Africa

Abstract (300 word limit)

Statement of the Problem: Non-Small Cell Lung Carcinoma (NSCLC) is the most prevalent type of lung cancer, constituting 85% of diagnosed lung cancer cases. The treatment of NSCLC continues to be a daunting challenge, with combinational chemotherapy as first-line treatment reportedly at its therapeutic plateau. Thus, the application of superparamagnetic iron oxide nanoparticles (SPIONs) as a nanomedicine for NSCLC provides an alternative modality. SPIONs have the flexibility to be modified to achieve enhanced loading of hydrophobic anticancer drugs such as paclitaxel (PTX). The purpose of this study was to synthesize novel trans-10, cis-12 conjugated linoleic acid (CLA)-coated SPIONs loaded with PTX to enhance the anti-proliferative activity of PTX. **Methodology:** SPIONs were fabricated using a co-precipitation method and coated with trans-10, cis-12 CLA in a single-step reaction. PTX was then loaded onto the surface of trans-10, cis-12 CLA-coated SPIONs via self-assembly, to formulate CLA-coated PTX-SPIONs. CLA-coated PTX-SPIONs were characterized for all pertinent physiochemical and pharmaceutical (including anti-proliferative activity on an A549 lung cancer cell line) properties. **Findings:** CLA-coated PTX-SPIONs were successfully synthesized with a particle size and zeta potential of 96.5 ± 0.6 nm and −27.3 ± 1.9 mV, respectively. CLA-coated PTX-SPIONs had a drug loading efficiency of 98.5% and demonstrated sustained site-specific *in vitro* release of PTX over 24 h (i.e., 94% at pH 6.8 mimicking the tumor microenvironment). Enhanced anti-proliferative activity was also observed with the CLA-coated PTX-SPIONs against a lung adenocarcinoma (A549) cell line after 72 h, with a recorded cell viability of 17.1%. **Conclusion & Significance:** The CLA-coated PTX-SPIONs demonstrated enhanced suppression of A549 cell proliferation compared to pristine PTX, thus suggesting potential application of the nanomedicine as an effective site-specific delivery system for enhanced therapeutic activity in NSCLC therapy. The results of this work provide new insights into the design of nanomedicines for NSCLC.

Recent Publications (minimum 5)

1. Ngema, L. M., et al. (2022). "Synthesis of Novel Conjugated Linoleic Acid (CLA)-Coated Superparamagnetic Iron Oxide Nanoparticles (SPIONs) for the Delivery of Paclitaxel with Enhanced In Vitro Anti-Proliferative Activity on A549 Lung Cancer Cells." Pharmaceutics 14(4): 829.
2. Ngema, L. M., et al. (2021). "A review on engineered magnetic nanoparticles in Non-Small-Cell lung carcinoma targeted therapy." International Journal of Pharmaceutics 606: 120870.

Photograph

D4: American Association of Pharmaceutical Sciences (AAPS) PharmSci360 (**Poster Presentation**). Boston Convention and Exhibition Center, Boston, MA, United States of America, October 16 – 19, 2022.

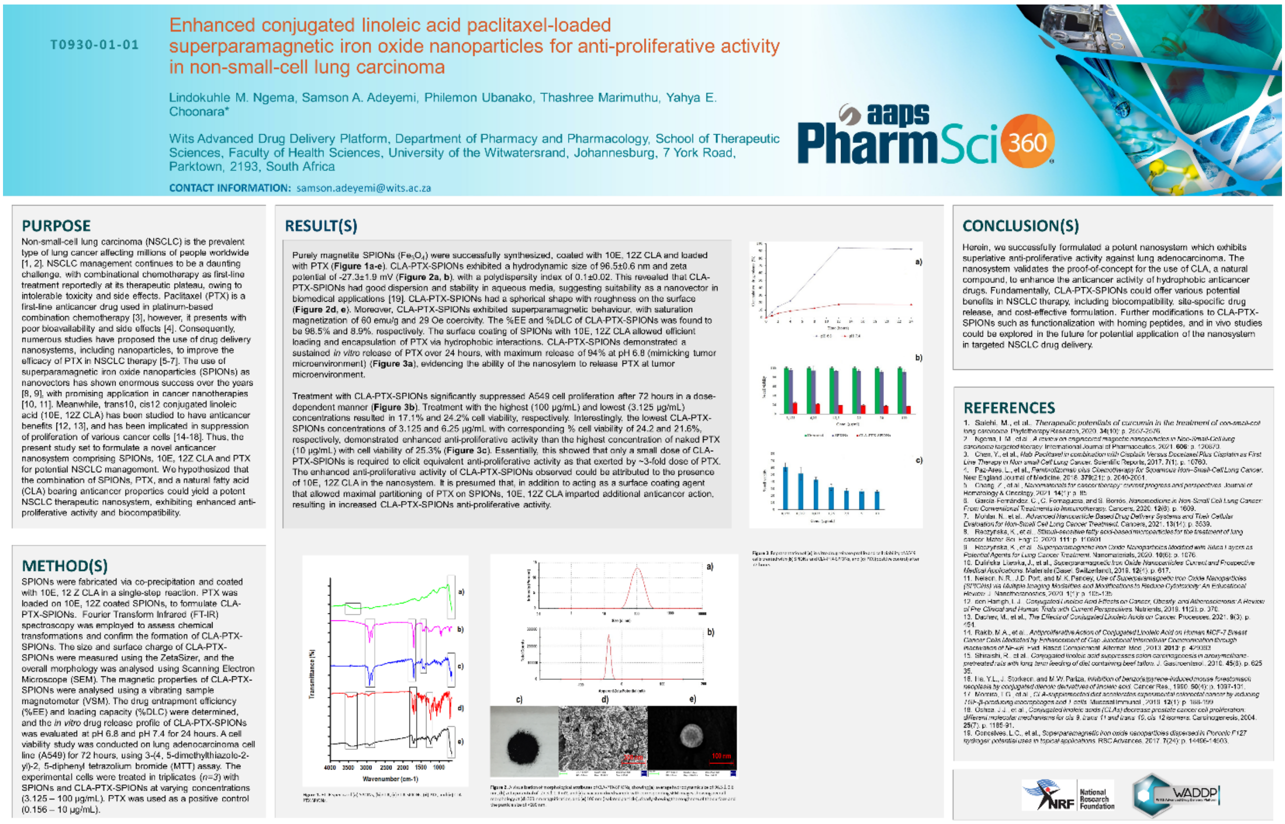

Appendix E: Originality Report

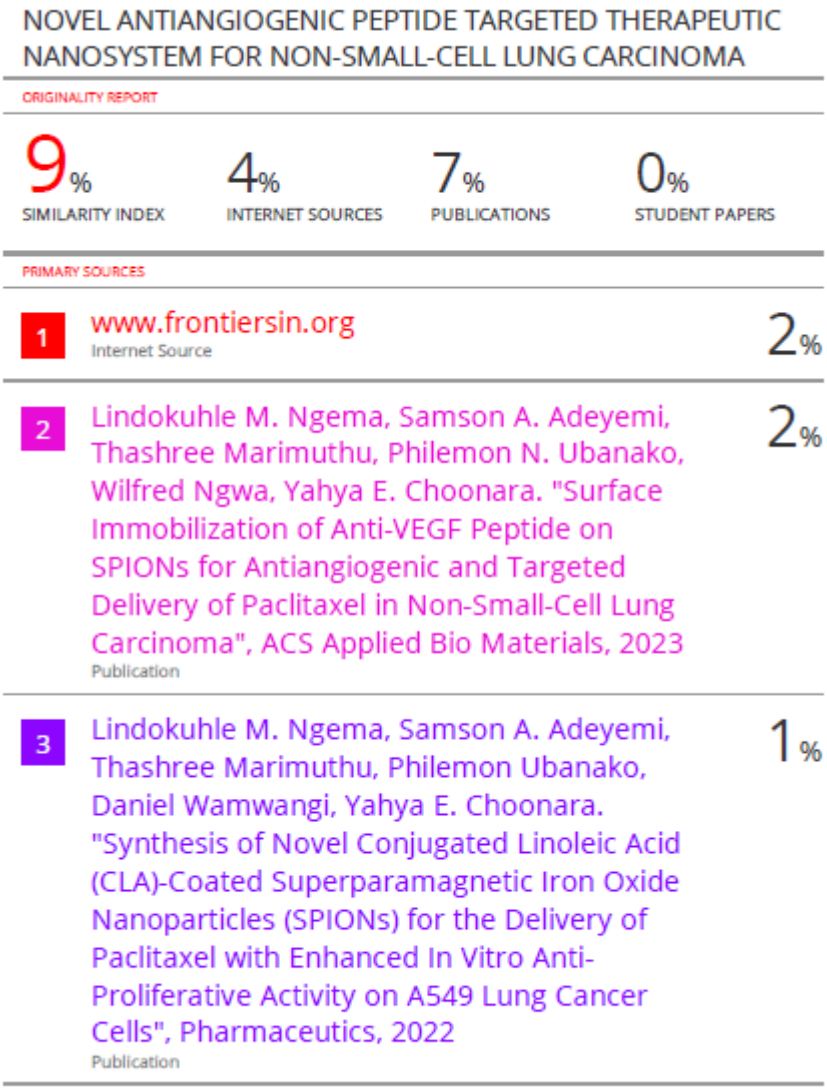

NOVEL ANTIANGIOGENIC PEPTIDE TARGETED THERAPEUTIC NANOSYSTEM FOR NON-SMALL-CELL LUNG CARCINOMA

ORIGINALITY REPORT

9%	4%	7%	0%
SIMILARITY INDEX	INTERNET SOURCES	PUBLICATIONS	STUDENT PAPERS

PRIMARY SOURCES

1	www.frontiersin.org Internet Source	2%
2	Lindokuhle M. Ngema, Samson A. Adeyemi, Thashree Marimuthu, Philemon N. Ubanako, Wilfred Ngwa, Yahya E. Choonara. "Surface Immobilization of Anti-VEGF Peptide on SPIONs for Antiangiogenic and Targeted Delivery of Paclitaxel in Non-Small-Cell Lung Carcinoma", ACS Applied Bio Materials, 2023 Publication	2%
3	Lindokuhle M. Ngema, Samson A. Adeyemi, Thashree Marimuthu, Philemon Ubanako, Daniel Wamwangi, Yahya E. Choonara. "Synthesis of Novel Conjugated Linoleic Acid (CLA)-Coated Superparamagnetic Iron Oxide Nanoparticles (SPIONs) for the Delivery of Paclitaxel with Enhanced In Vitro Anti-Proliferative Activity on A549 Lung Cancer Cells", Pharmaceutics, 2022 Publication	1%

4	Ndinguri, Margaret, Manishabrata Bhowmick, Dorota Tokmina-Roszyk, Trista Robichaud, and Gregg Fields. "Peptide-Based Selective Inhibitors of Matrix Metalloproteinase-Mediated Activities", Molecules, 2012. Publication	1 %
5	Isabel Canga, Pedro Vita, Ana Isabel Oliveira, María Ángeles Castro, Cláudia Pinho. "In Vitro Cytotoxic Activity of African Plants: A Review", Molecules, 2022 Publication	1 %
6	epdf.pub Internet Source	1 %
7	jpet.aspetjournals.org Internet Source	1 %
8	stax.strath.ac.uk Internet Source	<1 %
9	www.science.gov Internet Source	<1 %
10	Xuefei zhang, Ming Liu, Fan Yang, Li Ma. "Antiproliferative effect of cryptotanshinone against human non-small cell lung cancer cells through inactivation of lncRNA HOTAIR /p-Akt signaling pathway", Arabian Journal of Chemistry, 2021 Publication	<1 %